Thermo-mechanical behavior of soil-structure interface under monotonic and cyclic loads in the context of energy geostructures

Soheib Maghsoodi



UNIVERSITÉ DE LORRAINE

École doctorale SIMPPÉ

Science et Ingénierie des Molécules, des Produits,
des Procédés et de l'énergie

Laboratoire d'Énergétique et de
Mécanique Théorique et Appliquée

THÈSE

Présentée en vue de lobtention du grade de
Docteur de l'Université de Lorraine
Spécialité : Énergie et Mécanique

Par

Soheib MAGHSOODI

Thermo-mechanical behavior of soil-structure interface under monotonic and cyclic loads in the context of energy geostructures

Soutenance prévue le 17 juin 2020 devant la commission d'examen :

M. Hussein Mroueh	Professeur-Université de Lille	Rapporteur
M. Erdin Ibraim	Professeur-University of Bristol	Rapporteur
M. Fabrice Emeriault	Professeur-Université de Grenoble-Alpes	Examinateur
Mme. Alice Di Donna	Maître de conferences-Université de Grenoble-Alpes	Examinateur
M. Nicolas Utter	Soletanche Bachy	Invité
M. Marc Boulon	Professeur-Université de Grenoble-Alpes	Invité
M. Umur Okyay	Docteur-WSP de France	Invité
Mme. Farimah Masrouri	Professeur-Université de Lorraine	Directeur de Thèse
M. Olivier Cuisinier	Maître de conferences-Université de Lorraine	Co-directeur de Thèse

To Nahid and Masood,
To Mojdeh and Saba,
To the Homeland...

Acknowledgment

I would like to gratefully acknowledge Mr. Marcel Poinsignon, director of école Superieure dIngénieurs des Travaux de la construction (ESITC) de Metz for financing this research project and also accepting me in his engineering school warmly. Working for him was one of my greatest experiences. Je vous remercie très fortement Monsieur Poinsignon. I would like to thank my Ph.D. supervisor, Prof. Farimah Masrouri, to give me the opportunity to carry out my PhD studies and for her continuous support, motivation and academic guidance throughout this research. I would like to also thank co-supervisor of this study, Dr. Olivier Cuisinier, whom we had fruitful discussions throughout my period of studies. He always responded my questions with patience and his door was always open for me for further discussions. I owe my profound gratitude to Dr. Adel Abadallah for being a resourceful person with unfailing guidance and valuable suggestions for me to constantly fighting failures and disappointments.

I should express my thanks to the members of the jury; Prof. Fabrice Emeriault, Prof. Hussein Mroueh, Prof. Erdin Ibraim, Prof. Marc Boulon, Dr. Alice Di Donna, Mr. Nicolas Utter and Dr. Umur Okyay for their time and precious comments. I should express my gratitude to Prof. Fabrice Emeriault, Prof. Marc Boulon, Dr. Nicolas Utter, Dr. Hanène Souli and Dr. Umur Okyay to participate in the supervising committee of my thesis. Their comments and fruitful discussions that we had helped me to increases the quality of my work.

I would like also to thank the technical staff in the laboratory of soil mechanics (LEMTA) for their help and support particularly Jordane Rudolf. I can remember my first days in this laboratory when Mme. Sarah Feuillatre was helping me to advance my administrative staff. Thanks Sarah for helping me in administrative issues while always smiling. I appreciate the help of Jordane in my laboratory staff, he is a professional technician, with a lot of expertise. I also owe gratitude to all my friends and colleagues at the laboratory of my work (LEMTA).

I would like also to extend my gratitude to Moise, Zayad, Ahmed, Marvin, Nidal Jaime and Alice and all the others I met in the laboratory during my thesis. Merci Moise d'avoir corrigé mon français, qui se terminait souvent par beaucoup de rires. J'ai eu l'occasion d'avoir un collègue comme toi, toujours positif et souriant. Je tiens à remercier Marie Christelle et Angès. L'amitié avec vous m'a fait plaisir et je suis heureux d'avoir des amis comme vous à Nancy.

I stand and salute to my beloved wife, Mojdeh, who was more than a wife, she was a real

friend rather. In ups and downs of this study she was always listening to me with patience and did her best as a colleague and as a wife. Thanks for always being there for me and thanks to learn me to be self-motivated. I acknowledge her for long hours of discussions that we had about different perso-geotechnical issues.

Last but not the least, my family and my homeland to whom I owe so much. My mum and dad, Nahid and Masood, whom unconditionally supported me and encouraged me throughout my life, thanks. Their commitment and fortitude continue to influence me in all my pursuits in life. I owe my deepest gratitude to my sister, Saba, for believing in me. Despite our age difference you were and are a good friend for me whom I always can account on.

Soheib

Abstract

Incorporation of heat exchangers in conventional geostructures like piles can extract the heat from the soil for heating purposes and inject it to the soil for cooling purposes. In recent years, research has been conducted at full and laboratory scale to investigate the effect of temperature on the geotechnical behavior of these energy geostructures as well as on the surrounding soil. Indeed, these energy geostructures can be subjected to cyclic mechanical loads and thermal variations throughout their lifetime. The aim of this study was to deepen the understanding regarding the behavior of sand/clay-structure contact under complex thermo-mechanical loads. A temperature-controlled direct shear device to perform monotonic and cyclic constant normal load or constant normal stiffness tests was developed.

The response of the interface to the thermal effects on the mechanical behaviour of soils and soil-structure interface was investigated. Fontainebleau sand and kaolin clay were used as proxies for sandy and clayey soils. The results showed that the applied thermal variations have a negligible effect on the shear strength of the sand and sand-structure interface. In clay samples the temperature increase, increased the cohesion and consequently the shear strength, due to thermal contraction during heating. The adhesion of the clay-structure interface, was less than the cohesion of the clay samples.

To investigate the mechanical cyclic load effects on the clay-structure interface at different temperatures, monotonic and cyclic constant-volume equivalent-undrained direct shear tests were performed on clay-clay and clay-structure interface at different temperatures. The results showed that, the number of cycles to failure for the clay-structure interface test was lower than that for the clay-clay case in the same range of cyclic and average shear stress ratios. Increasing the temperature, decreased the rate of strain accumulation and the number of cycles to failure increased by 2-3 times. The rate of degradation (degradation parameter, t) decreased by 16% with heating from 22 to 60^{o}C for the different cyclic stress ratios tested.

A non-isothermal soil-structure interface model based on critical state theory was then developed. The non-isothermal model takes into account the effect of temperature on the void ratio of interface prior to shearing. The model is capable to capture the effect of temperature on soil-structure interface under constant normal load and constant normal stiffness conditions for both sandy and clayey interfaces. The additional parameters have physical meanings and can be determined from classical laboratory tests. The formulation is in good agreement with the experimental results and the main trends are properly reproduced.

Keywords: Soil-structure interface, energy geostructures, thermo-mechanical loads, constant normal load (CNL), constant normal stiffness (CNS), cyclic loading, constant-volume equivalent-undrained conditions, cyclic degradation, non-isothermal model, critical state theory

Résumé

L'incorporation d'échangeurs de chaleur dans des géostructures conventionnelles comme les pieux peut extraire la chaleur du sol à des fins de chauffage et l'injecter dans le sol à des fins de refroidissement. Ces dernières années, des recherches ont été menées à l'échelle réelle et en laboratoire pour étudier l'effet de la température sur le comportement géotechnique de ces géostructures énergétiques ainsi que sur le sol environnant. En effet, ces géostructures énergétiques peuvent être soumises à des charges mécaniques cycliques et à des variations thermiques tout au long de leur durée de vie. L'objectif de cette étude était d'approfondir la compréhension du comportement du contact sable/argile-structure sous des charges thermo-mécaniques complexes. Un dispositif de cisaillement direct à température contrôlée permettant d'effectuer des essais monotones et cycliques à charge normale constante ou à rigidité normale constante a été mis au point.

La réponse de l'interface aux effets thermiques sur le comportement mécanique des sols et l'interface sol-structure a été étudiée. Le sable de Fontainebleau et l'argile kaolinique ont été utilisés comme substituts pour les sols sableux et argileux. Les résultats ont montré que les variations thermiques appliquées ont un effet négligeable sur la résistance au cisaillement de l'interface entre le sable et la structure du sol. Dans les échantillons d'argile, l'augmentation de la température a augmenté la cohésion et par conséquent la résistance au cisaillement, en raison de la contraction thermique pendant le chauffage. L'adhérence de l'interface argile-structure était inférieure à la cohésion des échantillons d'argile.

Pour étudier les effets de la charge mécanique cyclique sur l'interface argile-structure à différentes températures, des essais de cisaillement direct monotone et cyclique à volume équivalent non drainé ont été réalisés sur l'interface argile-argile et argile-structure à différentes températures. Les résultats ont montré que le nombre de cycles jusqu'à la rupture pour l'essai d'interface argile-structure était inférieur à celui du cas argile-argile dans la même gamme de rapports de contraintes de cisaillement cycliques et moyennes. L'augmentation de la température a réduit le taux d'accumulation des contraintes et le nombre de cycles jusqu'à la rupture a été multiplié par 2 ou 3. Le taux de dégradation (paramètre de dégradation, t) a diminué de 16% avec un chauffage de 22 à 60^{o}C pour les différents rapports de contrainte cyclique testés.

Un modèle d'interface sol-structure non isotherme basé sur la théorie de l'état critique a ensuite été développé. Le modèle non isotherme prend en compte l'effet de la température sur

le taux de vide de l'interface avant le cisaillement. Le modèle est capable de saisir l'effet de la température sur l'interface sol-structure dans des conditions de charge normale constante et de rigidité normale constante pour les interfaces sableuses et argileuses. Les paramètres supplémentaires ont des significations physiques et peuvent être déterminés à partir d'essais classiques en laboratoire. La formulation est en bon accord avec les résultats expérimentaux et les principales tendances sont correctement reproduites.

Mots clés: Interface sol-structure, géostructures énergétiques, sollicitations thermo-mécanique, charge normale constante (CNL), rigidité normale constante (CNS), charge cyclique, conditions à volume-constant équivalent non-draineé, dégradation cyclique, modèle non isothermique, théorie de l'état critique

Publications

This study is a paper based thesis consists of 5 chapter. Chapter 1 is the literature review of the work. Chapter 2 is the materials used in this study and experimental method details. Chapter 3, 4 and 5 are published or are under review in scientific journals.

Journal papers:

• **Maghsoodi, S.**, Cuisinier, O., & Masrouri, F. (2020). Thermal effects on mechanical behaviour of soilstructure interface. *Canadian Geotechnical Journal*, 57(1), 32-47. `https://doi.org/10.1139/cgj-2018-0583` (**Chapter 3**).

• **Maghsoodi, S.**, Cuisinier, O., & Masrouri, F. (2020). Effect of temperature on cyclic behavior of clay-structure interface. *Journal of Geotechnical and Geoenvironmental Engineering*. `https://doi.org/10.1061/(ASCE)GT.1943-5606.0002360.` (**Chapter 4**).

• **Maghsoodi, S.**, Cuisinier, O., & Masrouri, F. (2020). Non-isothermal soil-structure interface constitutive model based on critical state theory. *Acta Geotechnica*, (Submitted March 2020, under review)(**Chapter 5**).

Conference papers:

• **Maghsoodi, S.**, Cuisinier, O., and Masrouri, F. 2019. Thermo-mechanical behavior of clay-structure interface. 7th International Symposium on Deformation Characteristics of Geomaterials. Glasgow, United Kingdom. Vol. 92. `https://doi.org/10.1051/e3sconf/20199210002`

• **Maghsoodi, S.**, Cuisinier, O., and Masrouri, F. 2019. Thermo-mechanical behavior of soil-structure interface. Ecsmge 2019 XVII European conference on soil mechanics and geotechnical engineering, Reykjavik, Iceland, 1st 7th September 2019. `https://doi.org/10.32075/17ECSMGE-2019-0274`

• **Maghsoodi, S.**, Cuisinier, O., and Masrouri, F. 2019. "Effet de la température sur le comportement thermo-mécanique de l'interface sol-structure." (oral presentation in French), RUGC 2019 - 37èmes Rencontres Universitaires de Génie Civil, Nice, France, 19 - 21st June 2019.

Nomenclature

CNL :	$(-)$	Constant normal load
CNS :	$(-)$	Constant normal stiffness
K :	(kPa/mm)	Imposed normal stiffness
τ :	(kPa)	Shear stress
$\sigma_n^{'}$:	(kPa)	Effective normal stress
U :	(mm)	Normal displacement
W :	(mm)	Shear displacement
R_{max} :	(mm)	Maximum surface roughness
R_n :	$(-)$	Normalized surface roughness
$\delta_p^{'}$:	$(^o)$	Peak friction angle of interface
$\delta_{res}^{'}$:	$(^o)$	Residual friction angle of interface
$\phi_p^{'}$:	$(^o)$	Peak friction angle of soil
$\phi_{res}^{'}$:	$(^o)$	Residual friction angle of soil
$C_p^{'}$:	$(^o)$	Peak cohesion of soil
$C_{i,p}^{'}$:	$(^o)$	Peak adhesion of soil-structure
D_{50} :	(mm)	mean diameter of soil particles
ρ_s :	(g/cm^3)	grain density of soil particles
γ_{dmax} :	(kN/m^3)	maximum dry density
γ_{dmin} :	(kN/m^3)	minimum dry density
e_{max} :	$(-)$	maximum void ratio
e_{min} :	$(-)$	minimum void ratio
C_u :	$(-)$	coefficient of uniformity

k :	(m/s)	hydraulic conductivity
ϵ_{cy} :	(%)	Cyclic shear strain
ϵ_p :	(%)	Permanent shear strain
S_u :	(kPa)	Undrained shear strength
S_u^{DS} :	(kPa)	Undrained shear strength of direct shear
τ :	(kPa)	Shear stress
τ_a :	(kPa)	Average shear stress
τ_{cy} :	(kPa)	Cyclic shear stress
$\sigma_n^{'}$:	(kPa)	Effective normal stress
$\sigma_{n,i}^{'}$:	(kPa)	Initial effective normal stress
τ_{cy}/S_u^{Ds} :	(-)	Cyclic stress ratio (CSR)
τ_a/S_u^{Ds} :	(-)	Average stress ratio (ASR)
ϵ :	(%)	Shear strain
u* :	(kPa)	Equivalent pore water pressure
R_n :	(-)	Normalized surface roughness
p$^{'}$:	(kPa)	Confining pressure
q_{cyc} :	(kPa)	Cyclic deviatoric stress
ρ_s	(g/cm^3)	Grain density of soil particles
LL :	(%)	Liquid limit
PL :	(%)	Plastic limit
PI :	(%)	Plasticity index
λ :	(W/mK)	Thermal conductivity
C :	(J/m^3K)	Heat capacity
k :	(m/s)	Hydraulic conductivity

e :	(%)	Void ratio
e_{in} :	(-)	Initial void ratio
$e_{in}(T)$:	(-)	Initial void ratio at temperature T
e_{cs} :	(-)	Critical state void ratio
ϵ :	$(-)$	Shear strain (in direct shear test)
ξ :	(mm^{-1})	Controls the rate of void ratio evolution
k_1^* :	$((mm^{-1}))$	intensifies the initial contraction
k_2 :	(kPa/mm)	parameter of the model
K :	(kPa/mm)	Stiffness
t :	(mm)	Interface thickness
Γ :	(-)	Initial critical void ratio
λ :	(-)	Slope of the critical void ratio reduction with normal stress
μ_0 :	(kPa)	Elastic shear modulus
k_{t0} :	(kPa/mm)	slope of the initial part of the $\tau - w$ curve
M :	(-)	Slope of the τ/σ_n
N :	(-)	Controls the peak and the strain softening
ψ :	(%)	Controls the rate of volumetric evolution
α :	$(^oC^{-1})$	Slope of the void ratio evolution with temperature
T :	(^oC)	Temperature
β :	(-)	Parameter of the model

Contents

General Introduction

The increase in emission of greenhouse gases due to the fossil fuel consumption, has raised several concerns for their negative environmental impacts. More than 80% of energy demand is provided by fossil fuels and among different sectors, buildings consume more than 40% of the whole energy consumption. In recent years, several agreements and environmental policies have been affirmed to decrease the dependency to fossil fuels and increase the tendency towards the renewable energies such as geothermal energy, wind and solar. Several techniques and technologies were developed to increase the energy efficiency and exploit new types of renewable energy. Among several types of developed technologies, recent years shallow geothermal energy has been in the center of attentions. Research has been conducted on different aspects which led to the emerge of thermally-active energy geostructures.

In earth contact geostructures like piles, diaphragm walls, tunnels and slabs, prior to concreting phase, polyethylene tubes are attached to the reinforcement cage. After concreting and start of the serviceability of the geostructure, the heat carrier fluid circulates in the tubes and consequently makes the heat exchange possible with the surrounding soil. Daily and seasonally heat flux fluctuations, between heat exchanger tubes and the adjacent soil, can affect the mechanical behavior of concrete body, soil-structure interface and the surrounding soil. Among the mentioned elements, the serviceability of embedded geostructures depends strongly on the mechanical behavior of soil-structure interface. Soil-structure interface consists of a thin layer of soil and structural material adjacent to the structural element which acts as a transmission zone to transfer the loads from the structure to the surrounding soil. Effect of thermo-mechanical solicitations on the interface can be a crucial issue for the stability of the structure which is tackled in this study.

Several thermo-mechanical aspects of soil-structure interface remain unanswered until present such as thermal effects on monotonic response of soil-structure interface under constant normal stiffness (CNS) conditions, mechanical cyclic behavior of clay and clay-structure interface under non-isothermal conditions and for design approaches the lack of a non-isothermal constitutive model of soil-structure interface. To address these issues, a temperature-controlled direct shear device is used to perform monotonic and cyclic interface shear tests on sandy and clayey interfaces. Several experimental protocols were developed to perform constant normal load and constant normal stiffness tests. In the following the thesis plan is described in detail.

Chapter I: This chapter describes the energy geostructure definition, construction and serviceability details. Afterwards, thermo-mechanical behavior of soils which consists of thermal effects on volumetric, shear behavior, microscopic and hydraulic characteristics of the soil are presented. Then, soil-structure interface definition, interface shear devices, boundary conditions and influencing parameters are discussed. Then, cyclic behavior of soils and soil-structure interfaces are discussed in detail. Finally, the concluding remarks concerning the important points that have been mentioned in the literature and also missing aspects of it are presented.

Chapter II: A detailed description of the material used in this study is presented. The temperature-controlled direct shear device is presented in detail. Sample preparation and experimental program are discussed in this chapter. Consolidation tests on kaolin to determine the shearing rate and also experimental protocol developments in the device are discussed. The experimental campaign for sand/clay-structure interface is detailed. Cyclic program details and performing methods are discussed and finally the repeatability tests are presented.

Chapter III: In this chapter, thermal effects on the mechanical behavior of the soil-structure interface is discussed. An experimental campaign is proposed to investigate the monotonic shear characteristics of sand/clay-structure interface at non-isothermal conditions under constant normal load and constant normal stiffness conditions. Soil-soil and soil-structure interface shearing characteristics at different temperatures have been investigated and discussed (22-60 ^{o}C). Soil-soil and soil-structure interface shearing differences have been demonstrated also. At the end, the effect of temperature on shear stress-displacement and volumetric behavior is discussed and conclusions are provided.

Chapter IV: this chapter is dedicated to one-way cyclic behavior of kaolin clay-structure interface at non-isothermal conditions. The objective of this chapter is to understand the cyclic behavior of clay-structure interface at different temperatures. The constant-volume equivalent-undrained (CVEU) concept is used to perform equivalent undrained interface shear tests. The experimental program based on CVEU concept is proposed. Monotonic CVEU clay-clay and clay-structure interface shear tests are compared. Then, cyclic tests at different temperatures are presented. The effect of temperature on strain accumulation, equivalent pore water pressure and degradation of the interface is discussed. Finally the conclusions of this chapter is presented.

Chapter V: In this chapter, a constitutive model to take into account the effect of temperature on mechanical behavior of sand/clay-structure interface is developed and proposed. Based on experimental observations in chapter III and literature studies, some fundamental aspects of soil-structure interface behavior under constant normal load and constant normal stiffness conditions at non-isothermal conditions are identified. Afterwards, using critical state concept for the soil-structure interface constitutive models, these features are implemented in an extended model to capture the effect of temperature on the mechanical behavior

of sand/clay-structure interface.

Chapter 1

Literature review

1.1 Introduction

The environmental impacts of fossil fuels combustion and consequent CO_2 emissions have increased in recent years due to the population growth. Today fossil fuels provide 80% of the demanded energy. The negative impacts of fossil fuel depletion and energy crisis led to new energy policies and increased the tendency towards renewable energy. Research has been conducted to propose new techniques to access to a clean, cost benefit and renewable source of energy. The energy geostructure technology provides a mean to achieve this goal.

In this chapter first, a detailed description of energy geostructures is provided. Then to better understand the fundamental behavior of soils under temperature variations, a literature review on thermo-mechanical behavior of soils especially volumetric and shear behavior is presented. Afterwards, the behaviour of soil structure interface is discussed, under isothermal and non-isothermal conditions. Then cyclic behavior of soils and involved parameters are explained, and finally an investigation on the existing constitutive models for soil and soil-structure interface is presented.

1.2 Energy geostructures

Buildings account for approximately 40% of global energy consumption among different sectors and play an important role in CO_2 emissions (Nejat et al. 2015). More than 80% of the energy consumption in households is dedicated to space and water heating. Therefore, there is a huge potential to increase the tendency towards renewable energy. The major part of this huge demand (73%) is provided by fossil fuels which have negative impacts on environment. In recent years, utilization of renewable energies due to their clean, cost benefit and environmentally friendly aspect have been in the center of attentions. The huge potential of renewable sources can compensate

a part of the energy demand of different sectors including buildings. Among different types of renewable energy, recent years, shallow geothermal energy has been used due to its simplicity for utilization, cost benefit operation and covering a part of human needs (heating, electricity, etc.). Radioactive decay of materials at the core of earth can be the origin of geothermal energy. Due to the technological achievements, exploitation of renewable sources is facing new advancements and challenges. Among these technologies, the emerge of energy geostructure, opened a new way to exploit the shallow geothermal energy. These structures exploit the heat of the soil using the heat exchanger tubes embedded inside their reinforcement cage. Low cost operations and efficiency of the thermo-active structures are the reasons for increased demands toward these structures. Experience has shown that these geothermal heating/cooling systems from energy foundations and other thermo-active ground structures may save up to two-thirds of conventional heating costs (Brandl 2006).

The constant ground temperature from a depth of 10-15 m, can be considered as a medium to exploit and inject the heat daily and seasonally (Brandl 2006) (Fig. 1.1). The exploited heat during winter is used for heating and inversely, in summer the additional heat can be injected into the soil for cooling purposes (Fig. 1.2).

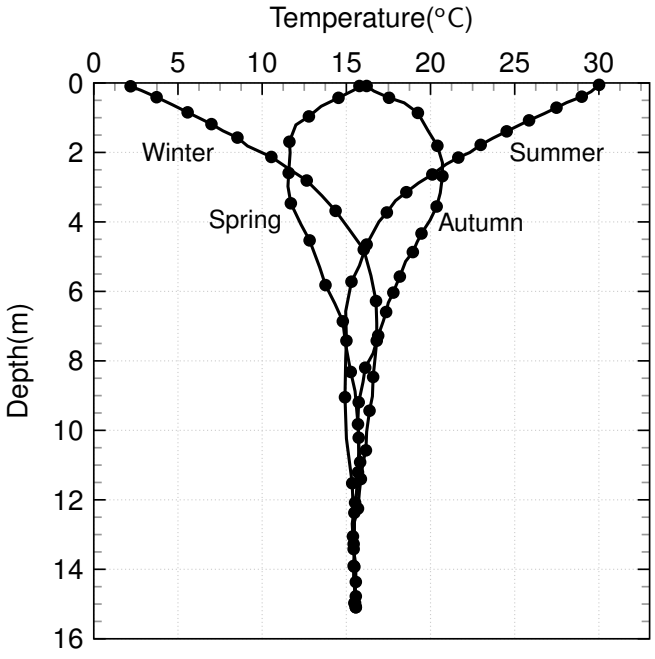

Figure 1.1: Ground temperature up to 15 m of depth for four seasons.

The conventional geostructures and foundations like piles, diaphragm walls, base slabs, retaining walls, barrettes and tunnel lining are structural elements serving to transmit the loads to the soil. Attaching heat exchanger tubes to the reinforcement cage of these conventional geostructures provides the opportunity to circulate a heat carrier fluid in the pipes (Fig. 1.3).

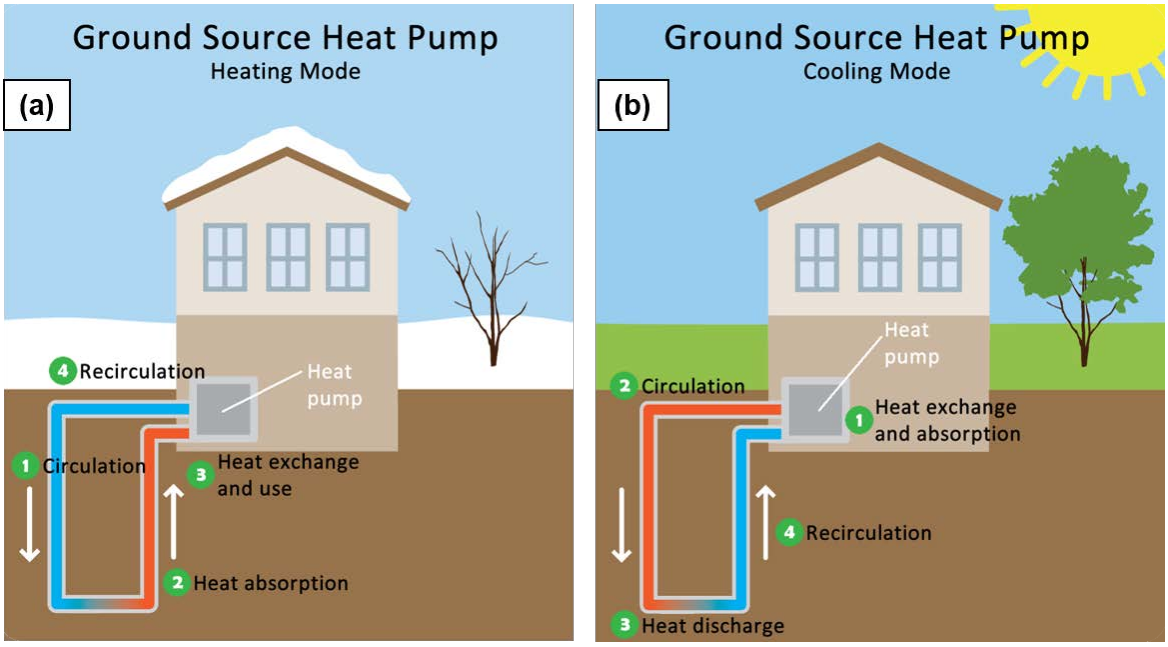

Figure 1.2: Thermal exploitation using energy geostructures. (a) Heating mode in winter; (b) Cooling mode in summer (www.geoenergymarketing.com).

After concreting, the fluid circulation makes the heat exchange possible with the surrounding soil. After the circulation, the temperature of exploited heat, is increased using a heat pump and injected into the building through the walls and roof. The cold temperature (5-7 ^{o}C) is circulated along the structural element and due to the heat exchange between the energy geostructure and the surrounding soil the temperature is increased to 10-12 ^{o}C afterwards the heat pump increases the temperature to the demanded level to be used in the building. Different types and sizes of buildings, commercial centers and metro stations can use energy geostructure technology.

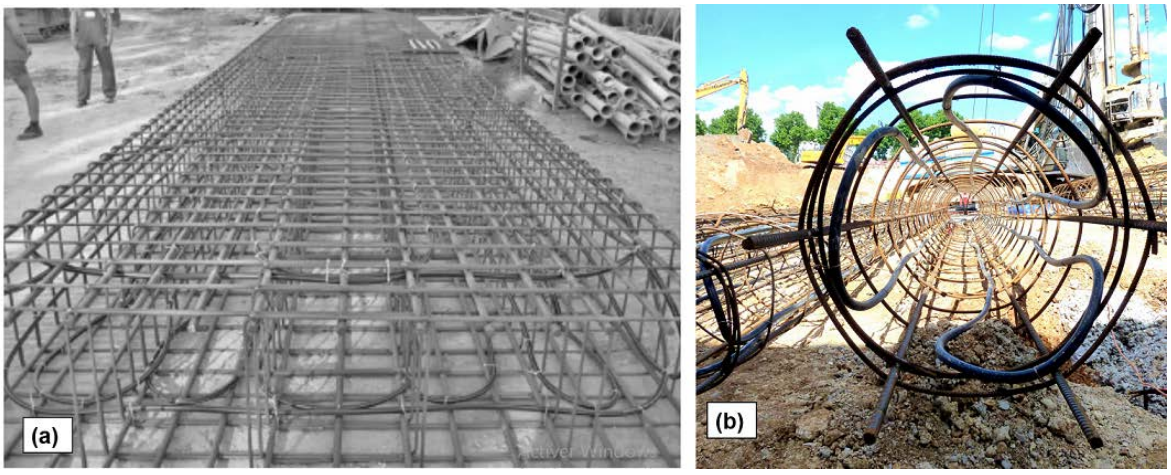

Figure 1.3: Heat exchanger tubes attached to the reinforcement cage of (a) a diaphragm wall (Brandl 2006); (b) a pile (Cfms 2017).

The efficiency of these thermo-active structures depends on, heat exchanger pipe patterns, spacing between pipes, fluid injection velocity, thermal properties of the soil and concrete, type of the structure and heating-cooling demand. For the mechanical aspect of energy geostructures, the shear characteristics of the soil and soil-structure interface, volumetric soil response should be taken into account.

The expected load distribution in the pile due to the thermo-mechanical load is illustrated in Fig. 1.4. Due to the mechanical load, the load PM decreases linearly with depth with the maximum located at the top of the pile and equal to the applied tension, T (Akrouch et al. 2014). Due to the heating process, a tension force P_T resulting from the restrained strains develops along the pile with a maximum at the NP (null point) location, $P_{T,max}$, and with a value of $P_{Bearing}$ at the bottom of the pile. The thermo-mechanical load in the pile is the sum of the mechanical and thermal load.

In Energy diaphragm walls the main issues are the variation of lateral earth pressure due to the thermal variations. After excavation, a diaphragm wall supports earth active and passive pressures (Fa and Fp) on its both sides. The evaluation of the active and passive pressures on the wall are directly related to the temperature dependent characteristics of the soil (density, cohesion and friction angle). On the other hand, the wall-soil interface stiffness parameters (kn and ks) are also temperature dependent. This shows the importance of a thermo-hydro-mechanical (THM) design of such a complex system. A key difference between diaphragm walls and more traditional types of ground heat exchanger is their exposure to the air on one side for some proportion of their depth.

In energy geostructures the mechanical loads applied to the structure on one hand, and the effect of heat exchange between structure and surrounding soil on the other hand, modify the mechanical behavior of the structure (Murphy et al. 2015; Faizal et al. 2018). These thermal variations and mechanical loads affect the bearing capacity and frictional resistance of these thermo-active structures. The applied thermo-mechanical loads are transmitted to the soil through the soil-structure interface. The interface zone plays an important role in the bearing capacity and skin friction of the structure. Therefore, the effects of temperature on the soil and soil-structure interface mechanical parameters should be investigated.

1.3 Thermo-mechanical behavior of soils

Thermal effects on the mechanical behavior of soils in recent years have been studied due to the increasing number of structures dealing with temperature. The main concern in these thermo-active structures would be the serviceability of the structure under monotonic and cyclic temperature variations in the presence of mechanical loads.

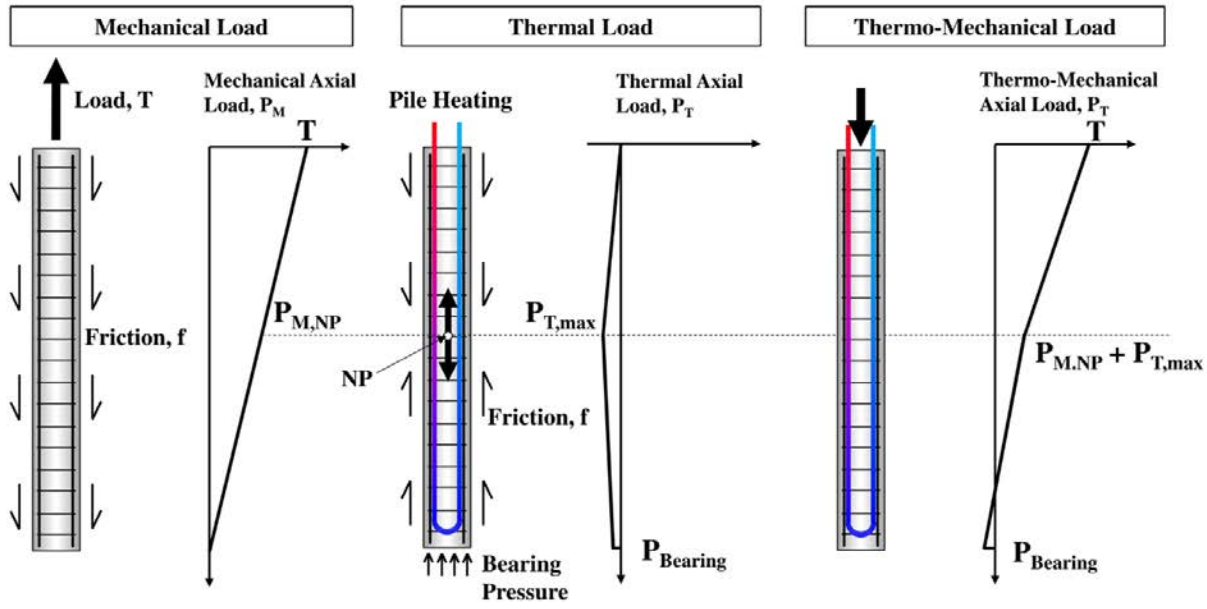

Figure 1.4: Load distribution on an energy pile (Akrouch et al. 2014).

Several studies have been performed in full or laboratory scales to investigate the effect of temperature on mechanical behavior of energy geostructures. From in-situ thermo-mechanical testing of energy piles (Laloui et al. 2006; Bourne-Webb et al. 2009; Murphy et al. 2015; Faizal et al. 2018) to advance laboratory testing of soils at non-isothermal conditions (Baldi et al. 1988; Campanella and Mitchell 1968; Ghahremannejad 2003; Burghignoli et al. 2000; Lahoori et al. 2020). The following mechanical aspects of the soils are discussed in this section:

- Temperature effects on microscopic characteristics of soils.
- Thermal volumetric behavior under drained and undrained conditions;
- The effect of the temperature variation on the shear characteristics.

1.3.1 Temperature effects on microscopic characteristics of soils

The complex macroscopic response of soils to temperature, necessitates further investigation in microscopic level. The nature, type, structure and state of the soil can change the response of the soil to temperature variations. In granular soils the interactions between particles are predominantly physical in nature and self-weight forces are dominant (Mitchell et al. 2005). Due to the complex interaction of several factors like clay particles, adsorbed layer and double diffuse layer with temperature variations, observed thermo-mechanical response of clays is controversial.

Clay minerals are allumnium silicates. The internal layer of water close to clay mineral is known as adsorbed layer and the surrounding water is double layer water (Fig 1.5).

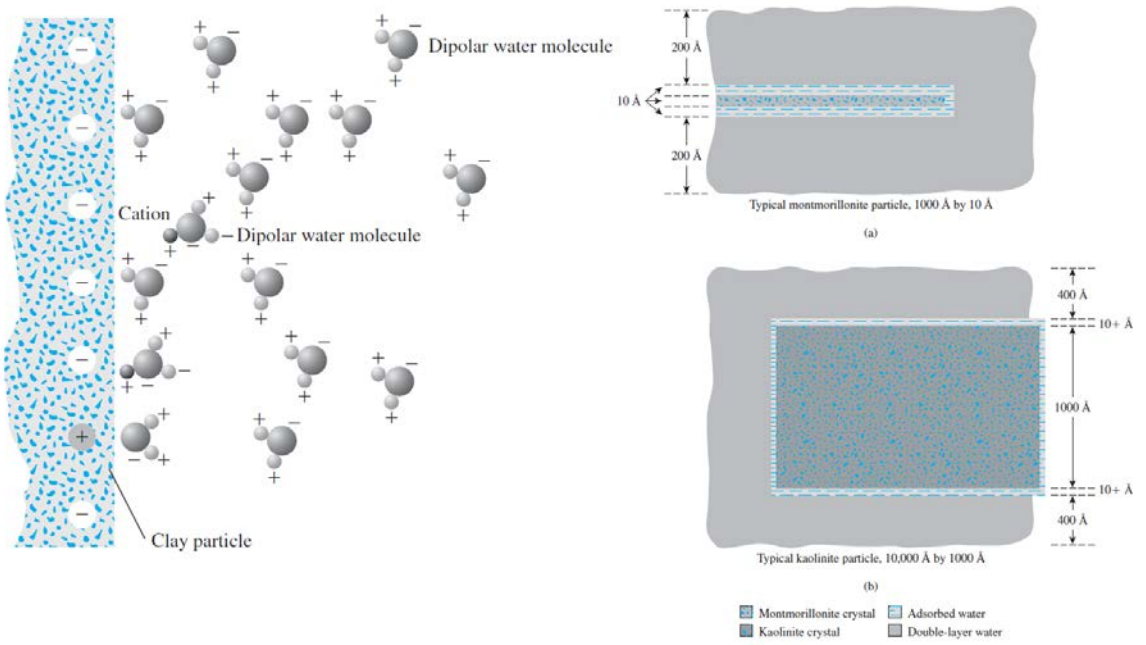

Figure 1.5: Attraction of dipolar molecules in diffuse double layer and clay-water system (Das 2015).

Thermal strains in saturated clays result from the thermal expansion of clay mineral, rearrangement of the clay skeleton structure, water behavior, and drainage conditions (Campanella and Mitchell 1968). Due to the electrochemical interactions between solid surface of minerals and surrounding water four types of pore water exists: (i). Free or bulk water which is able to flow due to hydraulic gradient. (ii). Intercluster adsorbed water, this water is restricted from flow in normal condition. (iii). Intracluster adsorbed water. (iv). Structural water in form of hydroxyl which does not leave the solid below 350^{o}C degree. Therefore investigating the behavior of different types of water upon heating may lead to better understanding the phenomena. The density and viscosity of water is found to be dependent on the temperature, therefore under complex thermo-mechanical loads, accelerated flows can be possible. For example the density of the adsorbed water may vary from 1.0 Mg/m^3 for free water to 1.4 Mg/m^3 or more for the first layers of water molecules at the solid surface (De Wit and Arens 1950; Mooney et al. 1952). Plum and Esrig 1969; Tidfors and Sällfors 1989 and Morin and Silva 1984 have reported a decrease of double layer thickness with temperature. On the contrary, Yong et al. 1962 showed a thicker double layer due to increase in temperature. Towhata, Kuntiwattanakul and Kobayashi 1993 have reported that, temperature increase, increases the kinetic energy of bound water and it would be possible to change their form to free water, consequently the thickness of the double layer water reduces and the contact between particles increases. They concluded that the decrease in water viscosity and increase in free water accelerates seepage and volume changes.

1.3.2 Thermal effects on volumetric behavior of soils

Several studies performed temperature controlled laboratory tests on different types of soils like sands and clays since 1960 (Finn 1952; Plum and Esrig 1969).

For sandy soil, Ng et al. 2016 used a temperature-controlled triaxial apparatus to investigate the thermally induced volume changes of soil skeleton of saturated Toyoura sand. The sand samples were prepared in three different state (loose, medium and dense) and two thermal cycles between 23 to 50 ^{o}C were applied. The volumetric response for loose and medium sand was contractive (0.15% and 0.05%). The authors indicated that, the observed contraction is most probably because the thermal expansion of soil particles adjusted force chains inside the specimen, inducing plastic contraction and soil hardening. With further heating from 35 to 50 ^{o}C both sand samples exhibited a dilative response (005%). On the contrary, for the dense specimen with a more stable structure, only dilation was observed during heating with a volumetric strain of approximately 01%. During the second thermal cycle, the responses of sand specimens with different densities were almost reversible with heating dilation and cooling contraction.

The thermo-mechanical behavior of soil depends on stress and thermal history (Fig. 1.6). In normally consolidated clays under drained conditions soils the thermally induced contraction during heating and subsequent cooling is irreversible. Subsequent thermal cycles, produce smaller increments of irreversible deformation (Baldi et al. 1988; Campanella and Mitchell 1968; Ghahremannejad 2003; Burghignoli et al. 2000; Cekerevac and Laloui 2004; Towhata, Kuntiwattanaku, Seko and Ohishi 1993; Abuel-Naga, Bergado, Bouazza and Ramana 2007; Delage et al. 2000). In highly overconsolidated soils (OCR>2) the heating causes an expansion and subsequent cooling causes a contraction which is totally reversible. In slightly overconsolidated clays at the beginning, heating causes an expansion but with further heating contraction is occurred while subsequent cooling causes a contraction. Therefore, thermal volume changes may be recoverable (thermo-elastic) or irrecoverable (thermo-plastic) depending on the type of soil, its degree of overconsolidation, and drainage conditions (McCartney et al. 2019). Several studies have been performed to investigate this aspect of thermo-mechanical behavior of soils (Baldi et al. 1988; Campanella and Mitchell 1968; Ghahremannejad 2003; Burghignoli et al. 2000; Cekerevac and Laloui 2004; Towhata, Kuntiwattanaku, Seko and Ohishi 1993; Abuel-Naga, Bergado, Bouazza and Ramana 2007; Delage et al. 2000). Di Donna et al. 2015 indicated that the appropriate rate of heating is 3-5^{o}C/hr in order to avoid excess pore water pressure caused by heating. Due to the low permeability of clays rapid changes in temperature can lead to pore water pressures being generated.

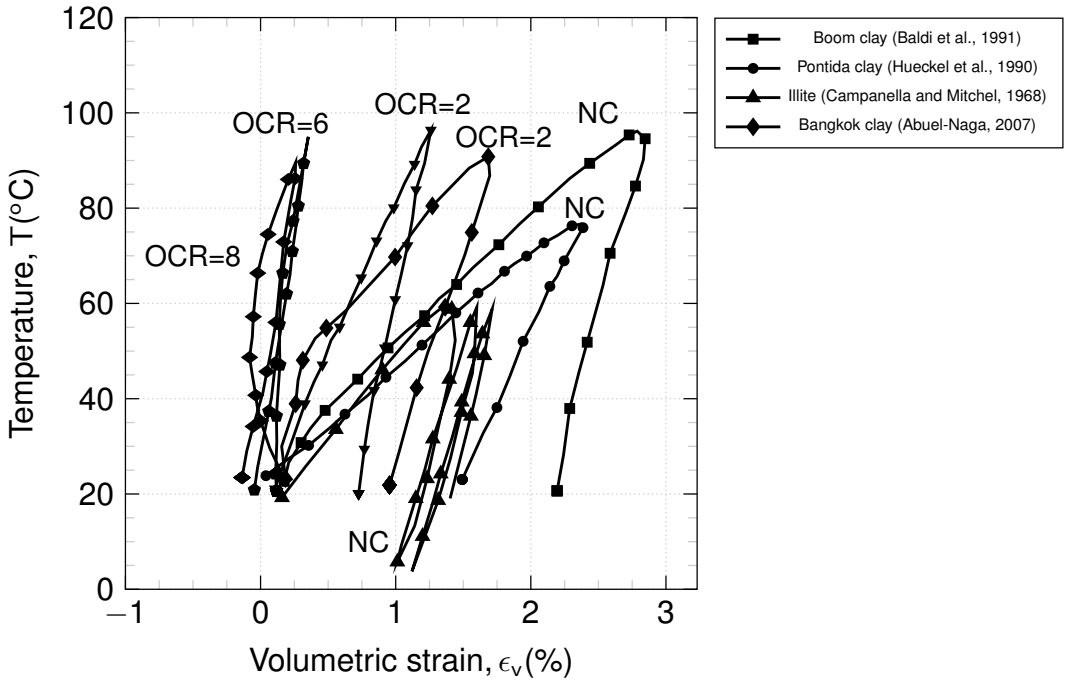

Figure 1.6: Volumetric behavior of clays during temperature changes.

For the effect of drainage, under undrained heating, in normally consolidated soils, the pore water pressure tends to increase with increasing temperature and even at constant higher temperatures the pore water pressure continues to increase (Fig. 1.7). Subsequent cooling phase generated negative pore water pressures. In overconsolidated samples, the pore water pressure increases with temperature increase under undrained heating but at constant high temperatures it tends to decrease (Burghignoli et al. 2000; Ghaaowd et al. 2015; Abuel-Naga, Bergado, Bouazza and Ramana 2007; (Graham, Tanaka, Crilly and Alfaro 2001; Monfared et al. 2011; Monfared et al. 2014).

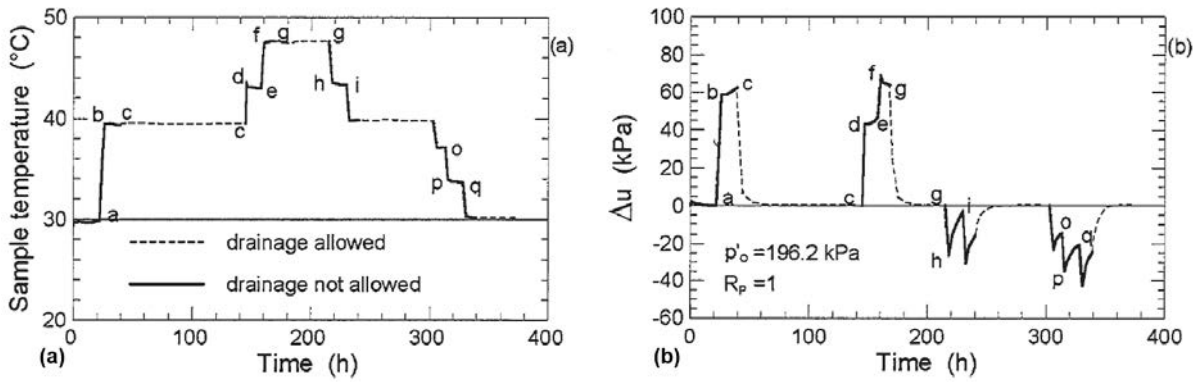

Figure 1.7: (a) Variation of sample temperature with time, and (b) pore water pressure evolution during the thermal cycle with undrained heating and cooling of normally consolidated Todi clay (Burghignoli et al. 2000).

1.3.3 Temperature effects on shear characteristics of soils

Effect of temperature on shear characteristics of soils, remains a controversial subject and needs developed answers due to conflicting results obtained by different studies (Mitchell 1964; Murayama 1969; Kuntiwattanakul et al. 1995; Di Donna et al. 2015; Cekerevac and Laloui 2004;Houston and Lin 1987; Abuel-Naga et al. 2006; Yavari 2014; Hueckel et al. 1998; Hueckel and Baldi 1990; Liu et al. 2018). Thermal and stress history are the most important factors influencing shear characteristics of soils. Therefore in the following different mechanical histories are discussed.

For sandy soils, Liu et al. 2018 conducted temperature-controlled hollow cylinder undrained shear tests on dense sands. The deviatoric peak shear stress decreased with increasing temperature on the contrary the critical shear strength and friction angle remained unchanged upon heating. During drained heating from 25 to 55 ^{o}C, the volumetric response of the sand was dilative and the soil expanded.

Heating decreases the void ratio and the soil becomes denser (A to B) (Fig. 1.8(a)). In this condition the void ratio has decreased under the same stress. In this point the soil is still normally consolidated, because point B is on the normal compression line at higher temperatures. However the void ratio of the soil can be obtained by unloading from point C (Fig. 1.8(a)).

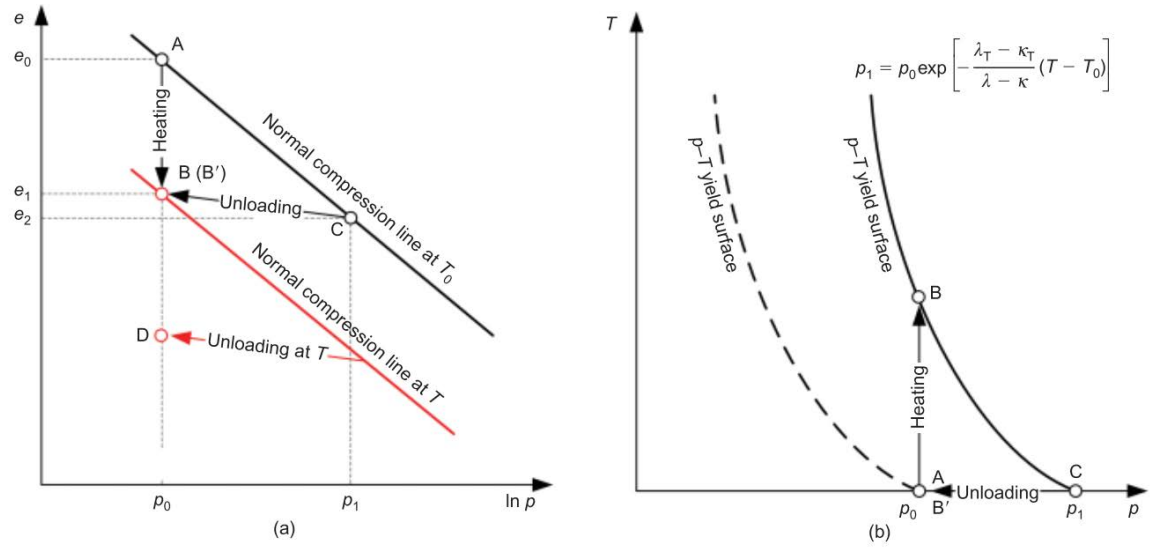

Figure 1.8: Effect of temperature on a normally consolidated soil. (a) In e-log$p$ plane; (b) In T-p plane (Yao and Zhou 2013).

The corresponding stress here is p_1 which is higher than p_0. Therefore the soil at B is slightly overconsolidated by heating which generally is known as thermally overconsolidation effect (Yao and Zhou 2013). This overconsolidation enlarges the yield surface of the soil (new p-T yield surface Fig. 1.8(b)) therefore an increase of shear strength for normally consolidated clays can be expected. For normally consolidated

(NC) soils, the elastic domain enlarges and the soil becomes denser with temperature increase under constant isotropic stress. Cekerevac and Laloui 2004 and Abuel-Naga, Bergado and Lim 2007 have found an increase of shear strength with drained heating (Fig. 1.9(a)) on kaolin clay and soft Bangkok clay respectively.

On the contrary in high OCR clays, conflicting results have been reported. Some authors have indicated that the soil during shear at higher temperatures reaches the yield limit at lower shear stresses compared to initial temperature (Hueckel et al 1988) and in high OCR clays under drained heating the shear strength tends to reduce during heating. This was observed by Hueckel et al., 1988 for Pontida clay with OCR=12. The authors have explained this behavior by ductile behavior of the soil upon heating. Temperature increase, decreases the preconsolidation pressure and consequently elastic domain shrinks. On the other hand Abuel-Naga, Bergado and Lim 2007 have found an increase in shear strength for overconsolidated clay at higher temperatures (Fig. 1.9(b)) while Cekerevac and Laloui 2004 have reported that shear strength for highly overconsolidated kaolin at higher temperature remained unchanged (Fig. 1.9(b)).

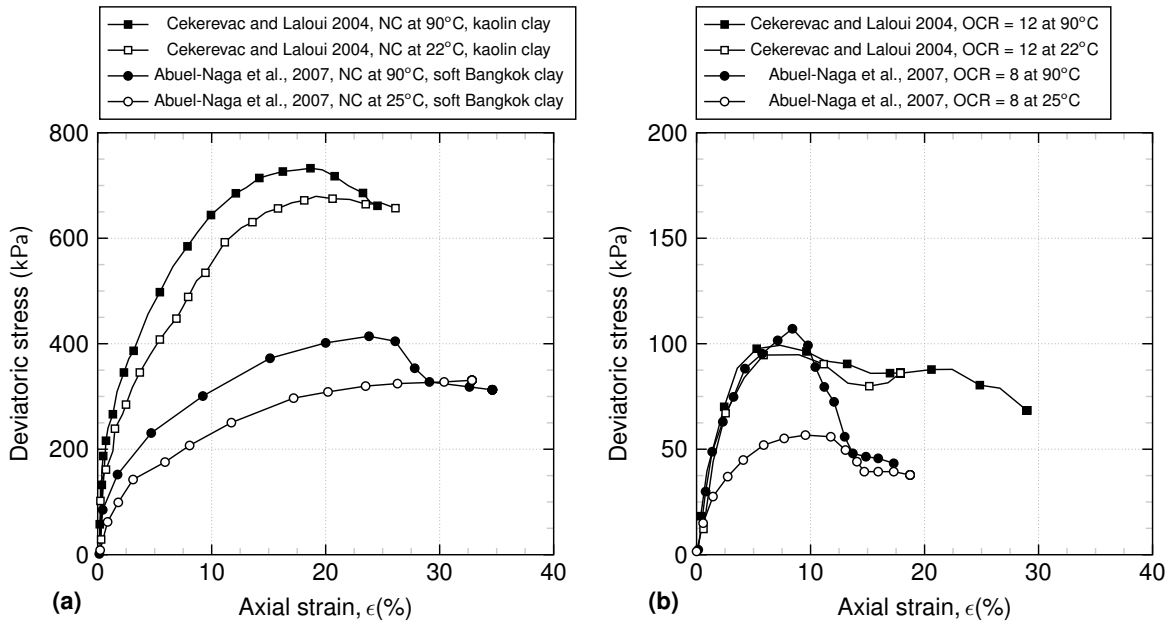

Figure 1.9: Drained triaxial tests at ambient 22 C and high 90 C temperatures. (a) normally consolidated; (b) overconsolidated (Adopted from Cekerevac and Laloui 2004 and Abuel-Naga et al. 2006).

Kuntiwattanakul et al. 1995 performed consolidated undrained triaxial tests on clays with drained heating. The authors have observed undrained shear strength increased from 20 to 90 ^{o}C while Murayama 1969; Sherif and Burrous 1969 and Laguros 1969 claimed that undrained heating caused a reduction in undrained shear strength of different clayey samples during unconfined compression tests. As can be observed controversial results are obtained concerning the shear strength of clays at different

temperature because of this confusing results Hueckel et al. 2009 have concluded that the shear characteristics of clay at higher temperature is material specific.

Thermal effects on friction angle

Several studies have been performed to investigate the effect of temperature on friction angle or critical state coefficient (M) of soils. Mitchell et al. 2005 2005 have mentioned that the change in temperature induces a change in interparticle forces, cohesion and/or friction angle of the soil. Hueckel and Baldi 1990; Houston and Lin 1987 and Graham, Tanaka, Crilly and Alfaro 2001;Cekerevac and Laloui 2004 observed that the strength envelope was independent of temperature. Hueckel et al. 2009 have showed that the friction angle can increase or decrease with temperature. The authors have explained that the variation of friction angle with temperature may be due to the physico-chemical interactions of clay particles. The thickness of adsorbed water may vary with temperature which changes the contacts between particles.

1.4 Soil-structure interface

The loads are transmitted to the soil through the foundation element. The transmission process involves the thin zone of interface between the structural element and the surrounding soil. Therefore, the soil-structure interactions at the interface are of primary importance in foundation designs. The interactions between structure and soil occurs in the thin zone adjacent to the structure surface which a shear strain localization caused by the tangential load transmission is developed. Several studies showed that the thickness of interface in granular soils is around 5-10 times D_{50} of the soil. Fig. 1.10 shows the interface shearing zone (White 2002). Several studies have shown that the mechanical behavior of the interface zone is different from the surrounding soil and it should be studied particularly. Several studies have investigated the interface behavior from different points of view (Brumund and Leonards 1973; DeJong et al. 2003; DeJong and Westgate 2009;Dejong et al. 2006; Desai and Nagaraj 1988; Evgin and Fakharian 1997; Fakharian and Evgin 1997; Fakharian and Evgin 2000; Fakharian 1996; Fioravante 2002).

One of the first studies performed to investigate the soil-structure interface behavior was done by Potyondy 1961. Potyondy 1961 mentioned that the mutual effect of soils and structures in the transmission of forces from one to the other through the contact surface is called skin friction. Grain size, grain crushability, grain roundness, soil density, initial stress state, structure roughness and shearing rate based on interface tests were addressed as the parameters influencing the soil-structure interface mechanical behaviour (Potyondy 1961; Desai et al. 1985; Boulon and Foray 1986; Ue-

sugi and Kishida 1986; Poulos and Al-Douri 1992; Jardine et al. 1993; Lehane et al. 1993; Fakharian and Evgin 1997; Mortara 2001; Pra-Ai 2013).

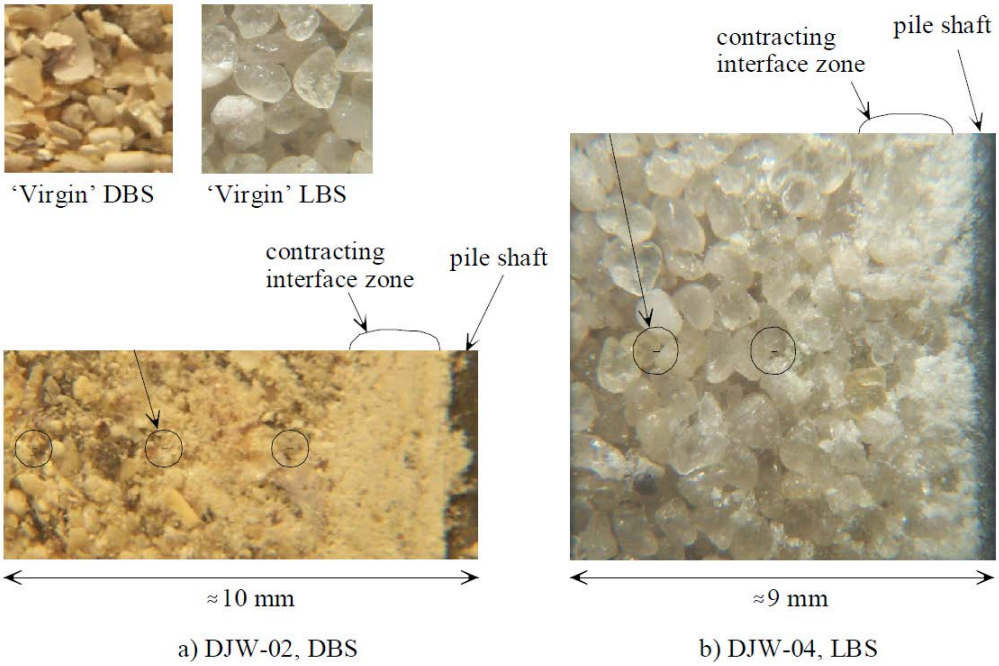

Figure 1.10: Soil-structure interface zone (White 2002).

In the following first an introduction about the interface shear testing and devices is presented then, different boundary conditions that can be applied to the interface is discussed and finally influencing parameters as shearing velocity, saturated or unsaturated state of the interface, soil density, roughness and effect of temperature are presented in detail.

1.4.1 Interface shear devices

For foundation design problems the shear parameters determination is of great importance. The shear strength along the contact surface between the soil and the foundation can be given as:

$$\tau_f = c_a^{'} + \sigma^{'} tan\delta^{'} \tag{1.1}$$

where $c_a^{'}$ is the adhesion (cohesion between soil and structure), and $\delta^{'}$ is the friction angle of interface. Due to the physical configuration of contacts between soil and structure, the direct shear device is one of the most convenient types of tests to determine the shear characteristics of the interface (Fig. 1.11(a)). The foundation material can be placed in the bottom part of the direct shear test box and then the soil can be placed above it and the shearing takes place between the shear boxes. To avoid the contact reduction during the test in classical direct shear testing, a larger structural element

can be placed in the modified lower half of the shear box (Fig. 1.11(b)). In this setup the tangential stress is applied to constant area of the sample during the test. Several studies have used the direct shear device (Potyondy 1961; Littleton 1976; Wernick 1978; Desai et al. 1985; Boulon 1989; Hoteit 1990;Poulos and Al-Douri 1992; Tabucanon et al. 1995; Shahrour and Rezaie 1997). The simplicity of test performing in direct shear test can be an advantage of the device but on the other hand the stress concentration at the shear box sides and implying the shear plane to the soil are of inconvenient. Other types of devices are modified and used to determine the shear characteristics of the interface like simple shear box (Yoshimi and Kishida 1981; Lehane and Jardine 1992; Lemos and Vaughan 2000; Eid et al. 2015; Evgin and Fakharian 1997), axial symmetric device (Coyle and Sulaiman 1967; Hebeler et al. 2016; Martinez et al. 2015) and ring shear device (Yoshimi and Kishida 1981; Lehane and Jardine 1992; Evans and Fennick 1995; Tika et al. 1996; Ho et al. 2011).

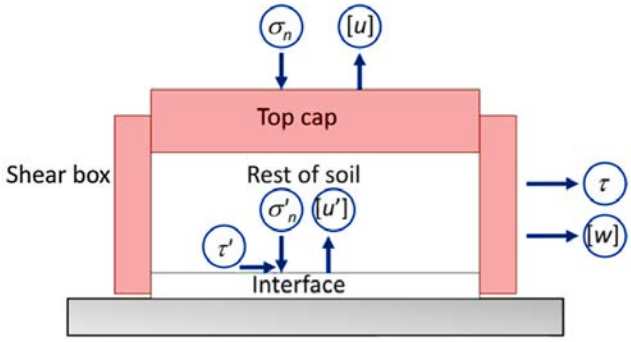

Figure 1.11: Direct interface shear apparatus Tabucanon et al. 1995.

A new interpretation has been proposed by Boulon 1989 for the interface in direct shear tests. Due to the contacts between the grains the interface zone can be distinguished clearly from the adjacent soil. Therefore, in interface tests, two zones are developed during shearing: (I) the "active" part which the tangential deformations occurs in this zone. (II) the "passive" part is the rest of the soil element on the active part, which is only subjected to normal deformations such as oedometric conditions (Fig. 1.12).

1.4.2 Boundary conditions in interface testing

Due to the different behaviors that have been observed in in-situ and laboratory testing of piles, several boundary conditions have been proposed to apply the realistic condition on soil-structure interface testing. Wernick 1978 proposed a conceptual model for the behavior of interface and surrounding soil based on observations on loads applied to the anchors. The behavior was observed in the results obtained from model pile pull-out tests (Lehane et al. 1993) and several efforts were performed to simulate the same

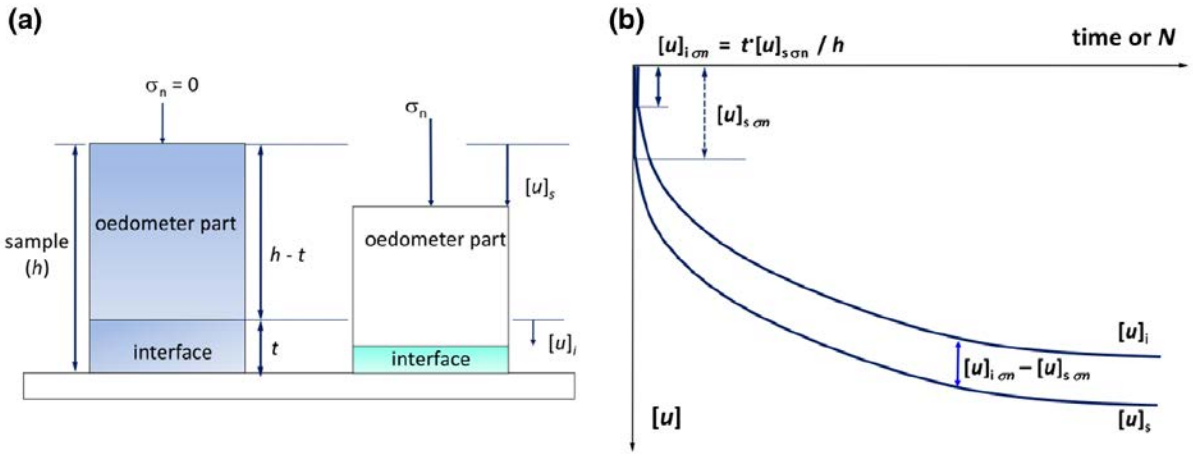

Figure 1.12: Interpretation of interface direct shear test: (a) entire sample and interface during the application of the initial normal stress; (b) full sample and interface normal relative displacement during the application of the initial normal stress and monotonic or cyclic direct shear (Boulon 1989).

behavior in laboratory tests (Foray et al. 1998; Garnier 1998). The results obtained by Lehane et al. 1993 showed that during pile pull out tests in sand, the radial stress (normal stress on the interface) changes due to the dilative response of interface. The surrounding soil of the interface was considered as a virtual spring with a certain stiffness:

$$\Delta\sigma = -K.\Delta U \tag{1.2}$$

where σ (kPa) is the stress normal to the interface, K (kPa/mm) is the stiffness of the surrounding soil and U (mm) is the normal displacement of the interface. Depending on the volumetric response of soil at the interface (contraction or dilation), the normal stress acting on the interface decreases or increases. Figure 1.13 shows the concept of constant normal stiffness in which the volumetric response of the interface is restrained by the surrounding soil stiffness. Based on this concept different boundary conditions of interface are:

Constant normal load (CNL): the normal stress is kept constant during the test and the volumetric response is free. $K = 0$, $\Delta\sigma = 0$, $\Delta U \neq 0$ (case I Fig. 1.14)
Constant volume (CV): The normal stress is varied to keep the volume of the interface constant. $K = \infty$, $\Delta\sigma \neq 0$, $\Delta U = 0$ (case II Fig. 1.14)
Constant normal stiffness (CNS): The normal stress and volumetric response are both varied with a constant ratio ($\Delta\sigma/\Delta U = K$). K = constant, $\Delta\sigma \neq 0$, $\Delta U \neq 0$ (case III Fig. 1.14). In the following an experimental description of this condition is presented.

Fioravante et al. 1999 performed interface direct shear tests on different types of sands. Three different sands (TS10, Toyoura sand and FF sand) on three steel plates

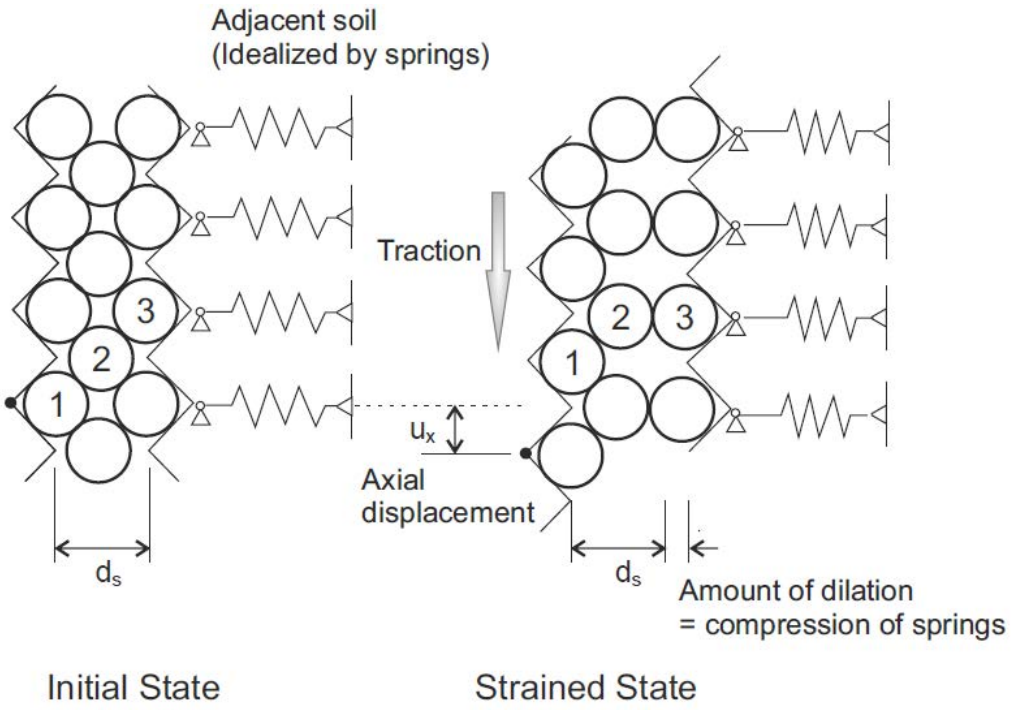

Figure 1.13: Analogy between the localized shear along pile and a direct shear test with an imposed normal stiffness (Boulon and Foray 1986 adopted from Stutz 2016).

with different roughness ranging from $0.005 < R_n < 0.33$ sheared under CNL and CNS conditions. Fig. 1.15 shows the results of CNS, tests performed on Toyoura sand (Fioravante et al. 1999). The initial normal stress was 50 kPa and different value of normal stiffness (K=0,100,1000 kPa/mm) were applied. As can be seen in Fig. 1.15(a), the shear stress behavior was totally changed before and after peak for different values of stiffness. The peak values are in larger shear displacements for higher values of stiffness. The normal stress acting on the interface for K=0 (CNL) case was constant while for other tests, due to the dilatant behavior of the soil the normal stress increased. The volumetric response Fig. 1.15(c) shows the dilatancy of the soil at the interface. By increasing the stiffness the dilation was reduced.

This effect was named confined dilatancy by Fioravante et al. 1999. The CNL and CNS tests were started from the same normal stresses but while shearing the stress states changed (Fig. 1.15(c)). They confirmed that the friction angle of the interface was not influenced by the boundary condition that was applied and in both cases (CNL and CNS) the friction angle remained unchanged.

1.4.3 Influencing parameters on soil-structure interface behavior

1.4.3.1 Effect of soil density

Di Donna et al. 2015 and Porcino et al. 2003 mentioned the effect of soil density on the

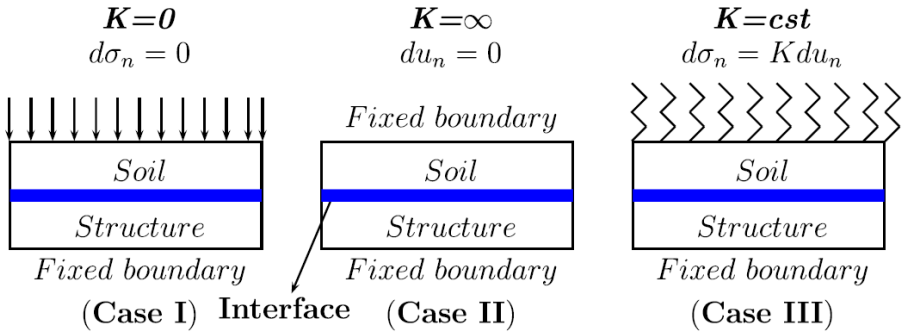

Figure 1.14: Boundary conditions in the direction normal to the interface: Case I: CNL; Case II: CV and Case III: CNS (adapted from Boulon and Foray 1986).

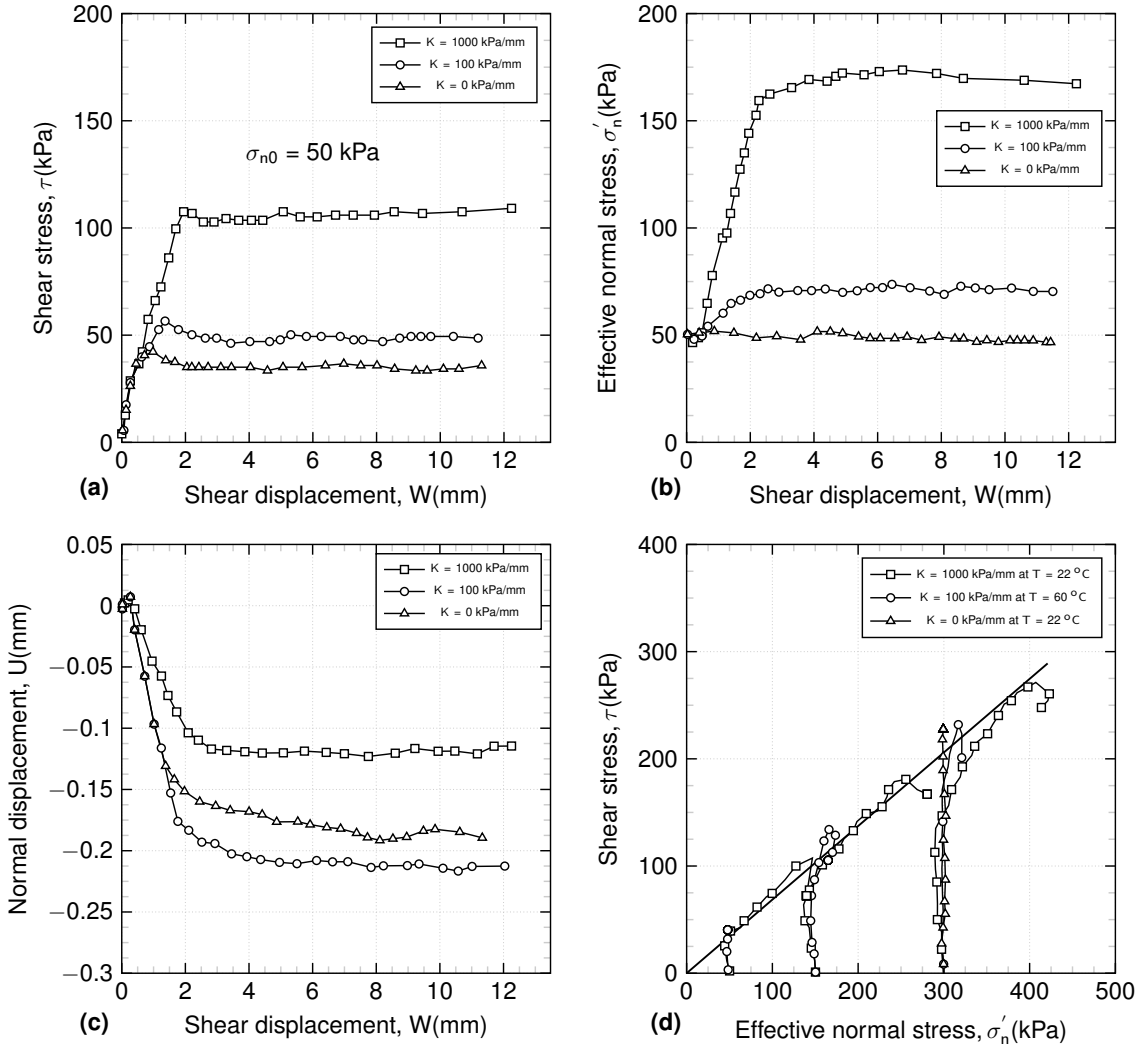

Figure 1.15: Effect of normal stiffness on shear behavior of sand-structure interface (Fioravante et al. 1999).

volumetric response of interface which can be dilative in dense sand and contractive in loose sand. In particular, dense sandy interfaces show dilatancy, while loose sandy interfaces show a contractive response. In the case of clayey interfaces, they are generally

contractive but might show dilation if subjected to highly overconsolidated conditions Shakir and Zhu 2009. When dealing with interfaces this aspect is particularly important because the volumetric response of the soil at the interface is not completely free to develop, but partially prevented by the presence of the surrounding ground.

1.4.3.2 Effect of structure roughness

Based on contact mechanics, the roughness of the structural element is of great importance in soil-structure interface behavior. The concept of interface roughness was first proposed by Yoshimi and Kishida 1981. The maximum vertical distance between the highest and lowest peak of the surface in a gauge length of L=2.5 mm was defined as maximum roughness (R_{max}) (Fig. 1.16(a)). This method was used before in mechanical engineering for evaluating the surface roughness of machine elements (Japanese Standard Association, 1976). Then Kishida and Uesugi 1987 observed that the particle diameter plays an important role in the roughness concept. It was observed that even on the same surface particles of smaller diameter have larger angle of interface (Fig. 1.16) (Kishida and Uesugi 1987). Therefore, it was proposed to consider the particle diameter:

$$R_n = \frac{R_{max}(L = D_{50})}{D_{50}} \tag{1.3}$$

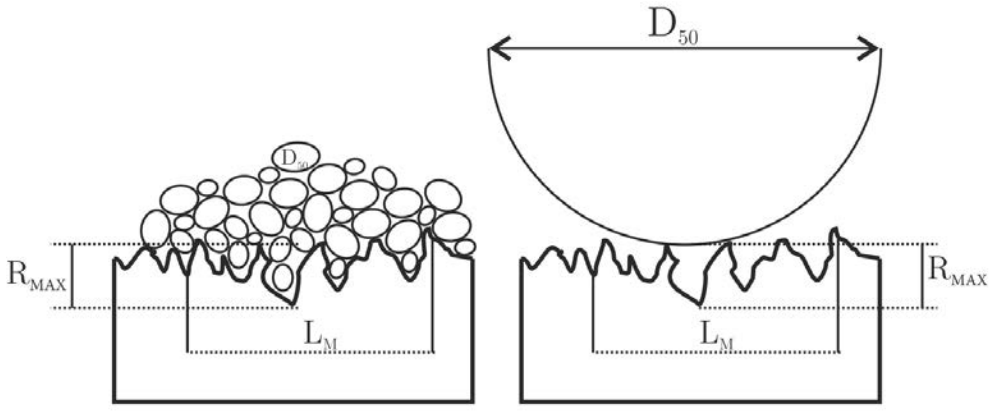

Figure 1.16: Interpretation of interface roughness; rough and smooth surface (Uesugi and Kishida 1986) adopted from Stutz 2016.

Available investigations (Uesugi and Kishida 1986; Uesugi et al. 1989; Hu and Pu 2003) indicate that the critical roughness (R_{crit}) is defined in the range of 0.1-0.13, i.e. $Rn < R_{crit}$ (smooth interface) and $Rn > R_{crit}$ (rough interface). Uesugi et al. 1989 show in microscopic and particle image velocity (PIV) measurements that the particles behave in two different patterns: rolling and sliding. The sand-steel interface showed a small amount of sliding before the peak in the frictional resistance. The sand on a smooth steel surface slide without large shear deformation. The sand particles on

a rough steel surface rolled as well as slipped along the interface. These movements caused the formation of a shear zone within the sand along a rough interface. Smooth surfaces cause only sliding of the particles along the surface, whereas rough surfaces cause both sliding and rolling of the particles. This sliding and rolling with rough surfaces increases the peak behavior of the soil-structure interface, which is coupled to the dilation behavior of the geo-structural interface. Lemos and Vaughan 2000 have indicated that In clays with a high clay content, in which residual soil-on-soil shear is in the sliding mode, the peak shear stress of clay-structure interface shear resistance is close to the soil-on-soil residual strength, and this shearing behavior is independent of roughness.

1.4.3.3 Effect of temperature

Due to the importance of soil-structure interface in energy geostructures, recently several studies have been performed on soil-structure interface under non-isothermal conditions (Di Donna et al. 2015; Yavari et al. 2016; Li et al. 2018; Yazdani et al. 2019).

Di Donna et al. 2015 have performed CNL and CNS direct shear tests on soil-soil and soil-structure interface tests on quartz sand and illite clay at different temperatures (20-60 ^{o}C). The sand-concrete interface shear tests at different temperatures are compared in Fig. 1.17. The shear stress versus shear displacement curves at different temperatures are superimposed which confirms the negligible effect of temperature on quartz sand. The volumetric behavior for both temperatures showed dilation.

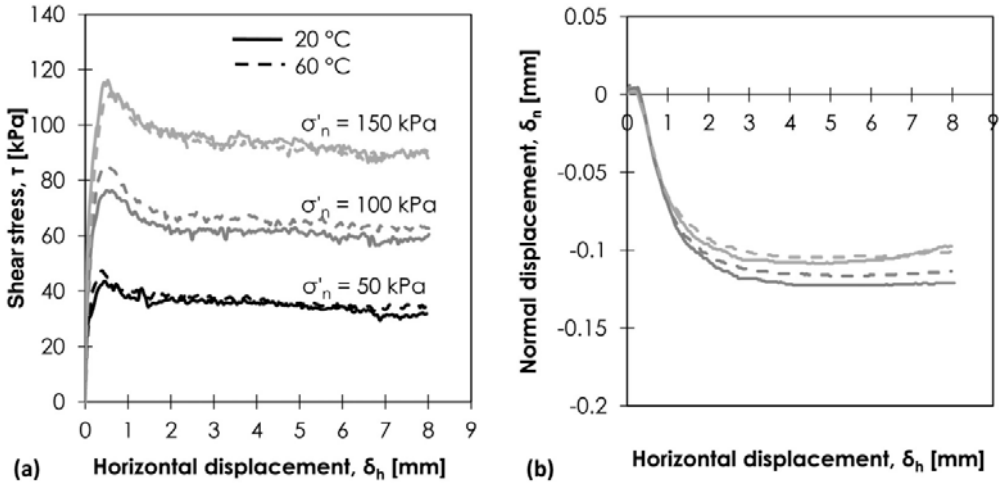

Figure 1.17: Sand-concrete interface direct shear tests at different temperatures (20-50 ^{o}C) (Di Donna et al. 2015).

Constant normal stiffness (CNS) tests were performed on sand-concrete interface. Due to the dilative response of the sand at interface, the corresponding effective stress increased. Simultaneously, the normal stiffness acts as a partial restraint for the free

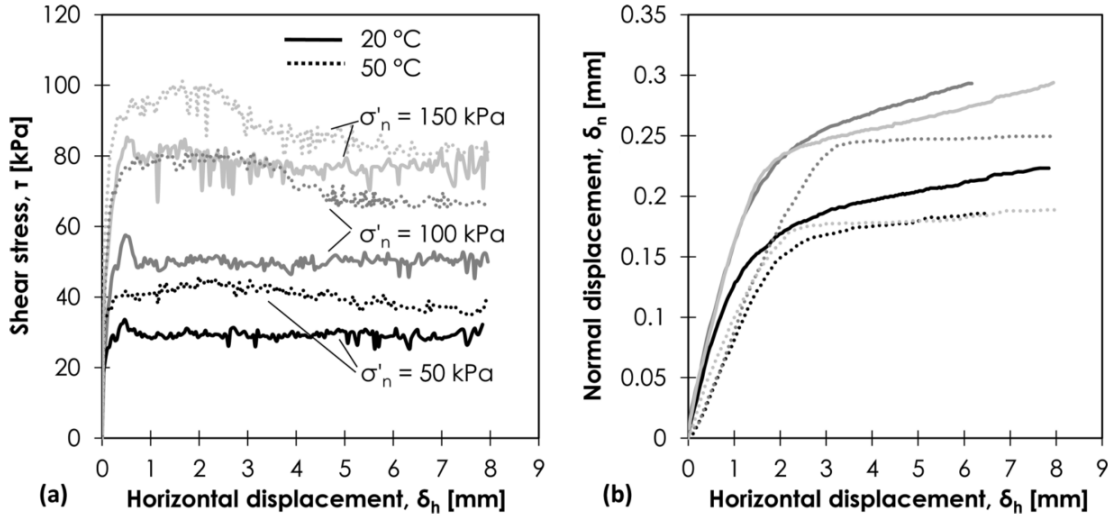

Figure 1.18: CNL clayconcrete interface tests (rough): temperature effects on (a) shear stress-horizontal displacement plane and (b) volumetric behaviour Di Donna et al. 2015.

dilation of the interface and the samples tested under CNS conditions consistently dilated less than the corresponding samples tested under CNL conditions. As it was confirmed by Porcino et al. 2003; different boundary conditions as CNL or CNS does not affect the friction angle of the interface. The stress states (shear and normal) are different in both tests but the friction angle of the interface was found to be 34^o with an adhesion of 14 kPa.

CNL results of clay-concrete at different temperature are shown in Fig. 1.18. Temperature increase, increased the shear strength of the illite clay-concrete interface, while the volumetric response for heated samples is less than unheated ones. The authors have indicated that the shear behavior under temperature, is influenced by the thermally induced overconsolidation effect. Heating the clay induced thermal contraction which made the material denser (§1.3.2) (Mitchell 1964; Cekerevac and Laloui 2004;Houston and Lin 1987; Abuel-Naga et al. 2006; Hueckel et al. 1998; Hueckel and Baldi 1990).

Di Donna et al. 2015 reported that the increase of both peak and residual shear stress of illite clay with temperature affected mainly the adhesion of the interface in the Mohr plane (Fig. 1.19). The observed adhesion of the clay to the concrete increased from approximately 7 kPa at 20 ^{o}C to approximately 20 kPa at 50 ^{o}C, while the interface friction angle changes from 25 to 23 ^{o} for the same temperature difference.

Yavari et al. 2016 have performed temperature-controlled direct shear tests on Fontainebleau sand and kaolin clay. Shear behavior of sand, clay and clay-concrete interface at various temperatures (5 ^{o}C, 20 ^{o}C, and 40 ^{o}C) was investigated through direct shear tests. To perform shear tests on the samples with the same initial condition all of the samples were consolidated up to 100 kPa and were heated to 40 ^{o}C.

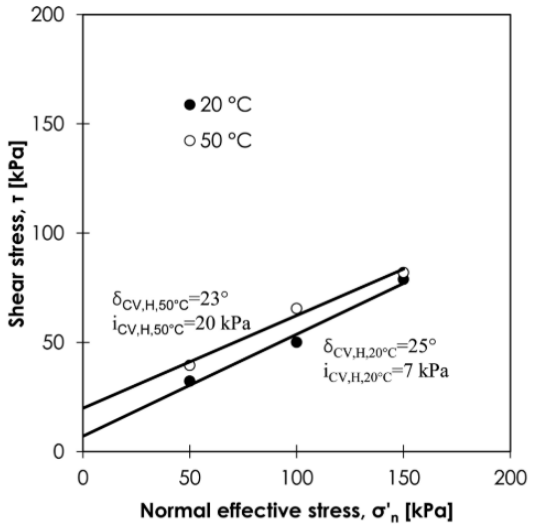

Figure 1.19: CNL clay-concrete interface tests (rough): temperature effects on (a) shear stress horizontal displacement plane and (b) volumetric behaviour Di Donna et al. 2015.

The authors concluded that the shear behavior of sand and clay tests show a hardening behavior while the clay-concrete behavior is softening. The smaller shear stress of interface tests compared to the soil-soil tests was observed. The effect of temperature in the range of 5 40 ^{o}C on the shear strength of sand, clay and clay-concrete interface was negligible (Fig. 1.20).

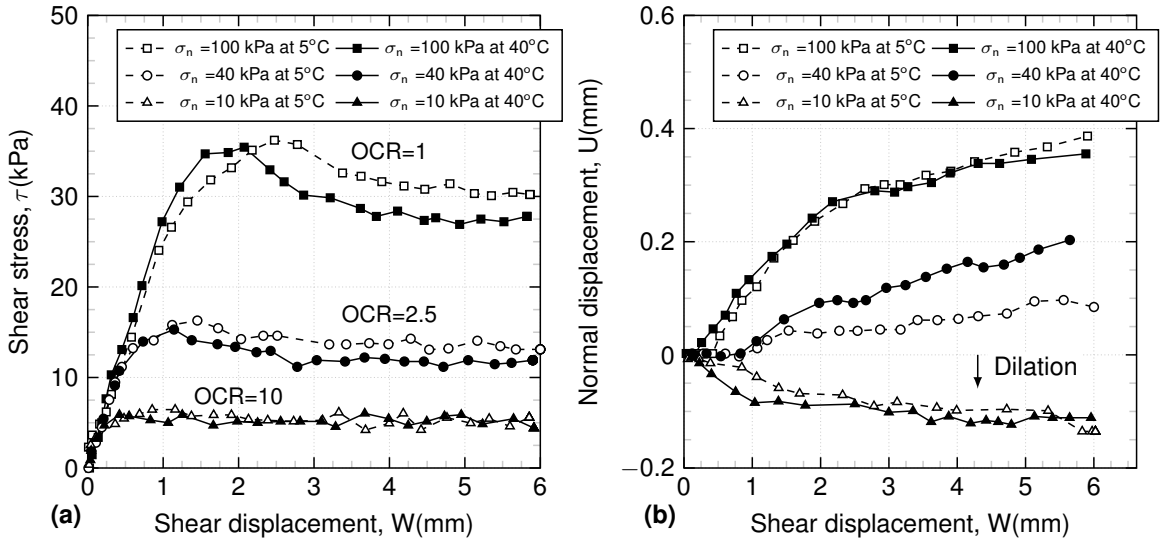

Figure 1.20: Experimental results on clay-concrete interface Shear stress at 5 and 40^{o}C (Adopted from Yavari et al. 2016).

Yazdani et al. 2019 have performed a series of direct shear tests using a temperature controlled direct shear test apparatus to evaluate the effects of heat cycles on soil-pile interface strength. The temperature cycles were between 24 and 34 ^{o}C to simulate the real thermal conditions that an energy pile may experience. The peak friction angle of

the NC clay-concrete interface increased, while the interface adhesion decreased, due to temperature increase. Thermally induced hardening of NC clay-concrete interface was found to be minor at a low normal stress (150 kPa), while it was significant at higher normal stresses (225 and 300 kPa). On the other hand, Fig. 1.22 compares the results of NC and OC (OCR=2 and 5) clay-concrete interface shear tests at different temperatures obtained by Yazdani et al. 2019. The shear stress difference between NC and OC=2 is negligible. But by increasing OCR, the shear stress increases and volumetric contraction reduces.

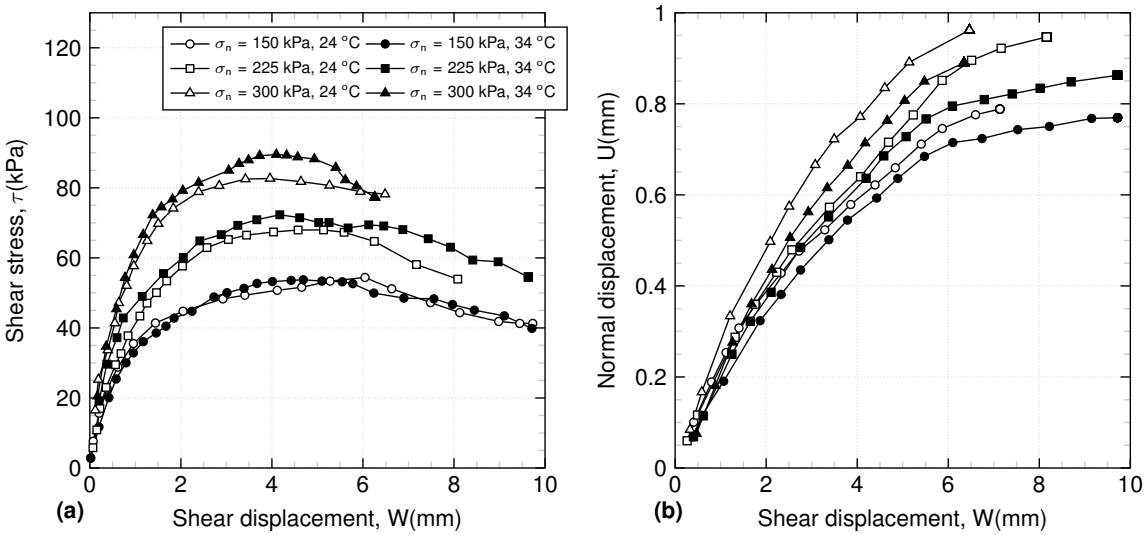

Figure 1.21: CNL NC clay-concrete interface tests at 24 and 34°C (Yazdani et al. 2019). (a) shear stress-displacement response under 150, 225 and 300 kPa; (b) volumetric response.

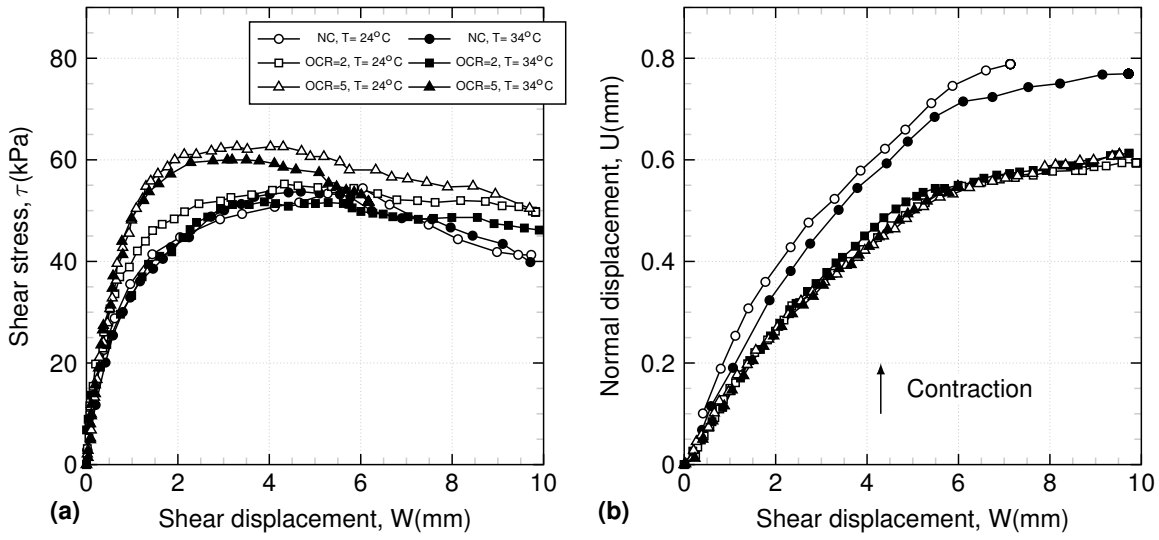

Figure 1.22: CNL NC and OC comparison clay-concrete interface tests at 24 and 34°C (Yazdani et al. 2019). (a) shear stress-displacement for NC, OCR=2, 5 under 150 kPa; (b) volumetric response.

Li et al. 2018 performed experimental investigation to assess the temperature effects on shear stress-strain behavior and shear strength parameters of red clay and its

interface with the geostructure under different normal stresses (50, 100, 200, and 400 kPa). A temperature-controlled direct shear device was used to perform red clay and red clay-structure interface tests at different temperatures (2, 15, 38 ^{o}C). Li et al. 2018 found that, the effect of temperature on friction angle and cohesion/adhesion of clay and clay-structure interface was negligible.

1.4.3.4 Shearing velocity

The effect of shear rates on the strength of clays has been investigated extensively (Lemos et al., 1985; Skempton 1985; Lemos 1986; Tika 1989; Tika and Vaughan, 1989; Lemos 1991; Tika et al. 1996; Lemos and Vaughan 2000; Martinez and Stutz 2018). Lemos and Vaughan 2000 conducted ring interface shear tests with several shearing rates. The authors reported that, shearing at a faster shear rate typically involves a new and higher peak and residual strength.

Martinez and Stutz 2018 have performed interface direct shear tests on kaolinite clay under normally consolidated and overconsolidated state with different shear rates. Fig. 1.23(a), (b) shows the shear stress-strain curve against the rough surface at a normal stress of 150 kPa (OCR=1). Increasing shearing velocity from 0.02 to 4 mm/min

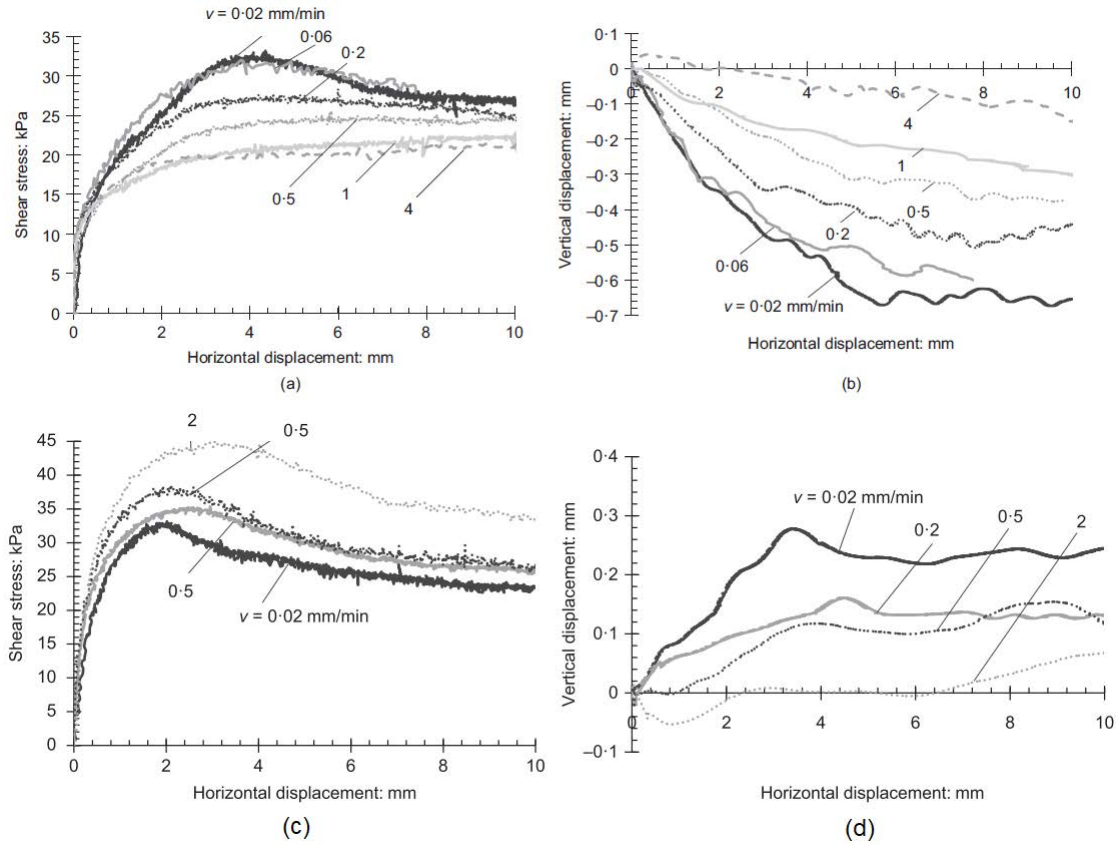

Figure 1.23: Influence of shear rate on (a)(b) normally consolidated (c)(d) overconsolidated (OCR=5) kaolinite on rough interface (Martinez and Stutz 2018).

reduced the peak and residual shear stress of the interface under normally consolidated state. On the other hand for overconsolidated tests (75 kPa OCR=5), increasing the shearing velocity increased the peak shear strength of the interface (Fig. 1.23(c), (d)). In slow tests the strain softening was observed while in faster tests it disappeared. The volumetric behavior for faster tests was close to the undrained tests. Di Donna 2014 performed direct shear tests on illite clay with different shearing rates (0.007 to 0.02 mm/min). The results showed that increasing the shearing rate decreased the peak and residual shear strength of the illite clay.

1.4.3.5 Saturated or unsaturated interface

The unsaturated soil-structure interface tests were conducted in several studies to understand the unsaturated interface behavior (Hamid and Miller 2009; Miller and Hamid 2006; Hossain and Yin 2012; Hossain and Yin 2015; Khoury and Miller 2012; Hamid and Miller 2005). Hamid and Miller 2009 modified a direct shear device to perform unsaturated interface tests using axis translation technique on a low-plasticity fine-grained soil. An air-pressure chamber, new testing cells, high air-entry porous disc (HAEPD), and a pore water pressure control system were added to the direct shear device to perform unsaturated interface tests. The Matric suction (20, 50, and 100 kPa) influenced the peak shear strength of the interface but post peak behavior was reported to be independent of the suction. It appeared that during shearing beyond the peak shear stress, the airwater menisci are completely disrupted, resulting in a negligible strength contribution due to matric suction. Increasing the matric suction, increases the dilation of the interface. Increasing the suction from 20 to 100 increased the adhesion (peak) of the interface from 10 to 40 kPa.

1.5 Cyclic behavior of soils and soil-structure interface

In this section the current knowledge about the effect of cyclic loading on mechanical behavior of soils and soil-structure interface is discussed. First, different types of cyclic loading is presented then different laboratory methods to study the cyclic behavior of soils is discussed afterwards, soil behavior under cyclic behavior is discussed and finally influencing parameters on the soil behavior under cyclic loading is presented.

1.5.1 Different types of cyclic loading

High speed trains, machine foundations, cranes, wind and waves for onshore and offshore structures can cause cyclic loads (Wichtmann 2005; Wichtmann et al. 2005). The differential settlement induced by cyclic loading can rise concerns about the structural

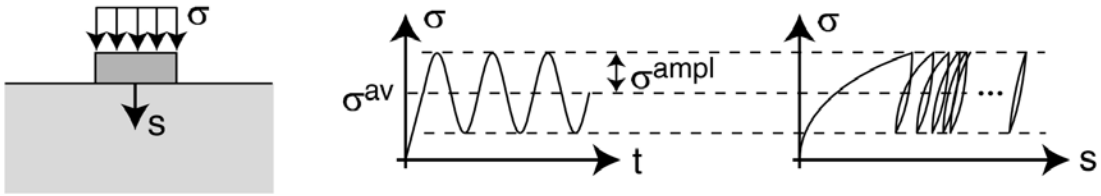

Figure 1.24: Foundations under cyclic loading (Wichtmann 2016).

stability. The repeated loads increase the residual deformation of foundations (Fig. 1.24). Deformation accumulation, excess pore water pressure and soil degradation are caused by cyclic loading. Therefore, deformation evaluation soils and interfaces under cyclic loading should be performed in design phase.

1.5.2 Laboratory cyclic testing

The behavior of soils or foundations under repeated loading can be studied in element tests in the laboratory, model tests in different scales, model tests with increased gravitation (centrifuge model tests) or field tests. Based on stress conditions on the soil element, several types of laboratory devices as direct shear, simple shear, triaxial, resonant column and torsional hollow cylinder tests can be used to perform cyclic tests. To be able to perform cyclic direct shear tests on soils and soil-structure interfaces, the concept of constant-volume equivalent-undrained is used. To apply equivalent-undrained conditions in the clay-structure interface tests, the constant-volume equivalent-undrained (CVEU) concept should be used. In the extreme case of the constant normal stiffness condition, constant volume case (K= ∞ (kPa/mm)), vertical stress is varied to keep the volume of the sample constant. In the studies using this concept, that have been conducted by Vucetic and Lacasse 1984; Dyvik et al. 1987 and Mortezaie and Vucetic 2016; during shearing, in drained condition while the pore water pressure was zero, the change in the vertical stress to keep the volume of the sample constant was equivalent to the pore water pressure generated in a truly undrained triaxial test. Several studies have confirmed this approach, using direct shear device (Takada 1993; Hanzawa et al. 2007).

1.5.3 Soil behavior under cyclic loading

The closed stress loops cause unclosed strain loops during cyclic loading. Strain accumulation and excess pore water pressure in cyclic loading reduces and consequently the strength degrades. Therefore, the bearing capacity of structures under cyclic loading is less than monotonic loading. In drained cyclic loading e.g. sand-structure interfaces, the volumetric reduction induced by cycles, decreases the normal stress acting on the

interface and therefore shear stress at each cycle decreases (CNS conditions). If the conditions are undrained, volumetric changes will be prevented by the low volumetric compressibility of the water. The normal stresses that were carried by the soil will then be transferred to the pore water and the effective stresses in the soil will decrease accordingly (Andersen et al. 1980). The shear stress-strain curve of a soil under cyclic loading can be decomposed in an average (τ_a) and a cyclic shear stress (τ_{cy}) component, while the deformation can be seen as the combination of a permanent shear strain (ϵ_p) and a cyclic shear strain (ϵ_{cy}) (Fig. 1.25(a)).

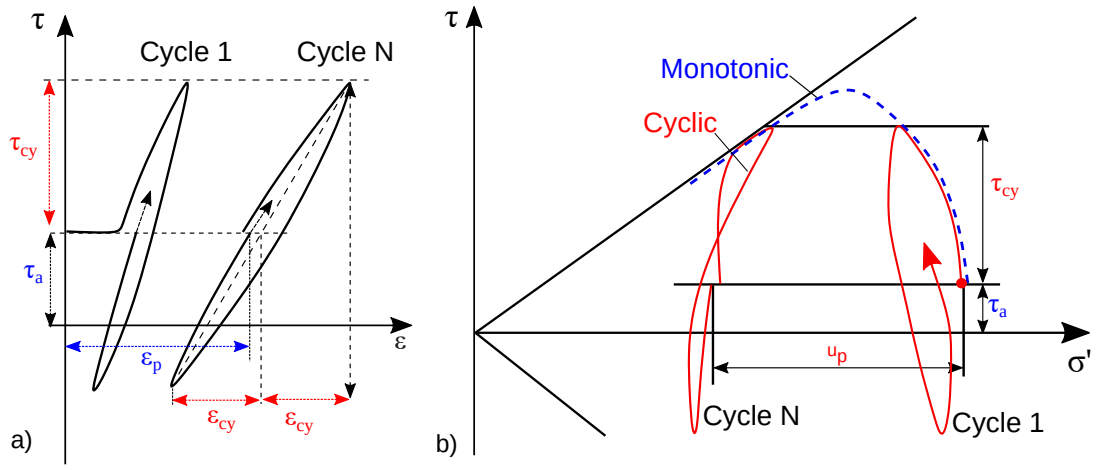

Figure 1.25: Stress-strain behavior of soils under cyclic loading Andersen (2009).

The development of pore water pressure and shear strain with cycles for a soil element subjected to undrained cyclic loading with a constant cyclic shear stress is illustrated in Fig. 1.25(b). The load cycles with a single-amplitude shear stress, τ_{cy}, around a constant shear stress, τ_a. The cyclic loading generates a pore water pressure characterized by a permanent pore water pressure component, u_p, and a cyclic pore water pressure component, u_{cy}. The increased pore water pressure reduces the effective stresses in the soil, resulting in increased permanent, ϵ_p, and cyclic, ϵ_{cy}, shear strains with time (Fig. 1.26(a)).

Due to the various stress conditions on a soil or soil-structure element of a foundation, several types of loading are possible (e.g., triaxial versus direct simple shear, DSS) from one point to another which is illustrated in Fig. 1.26(b) that shows a simplified image of the stress conditions along a potential failure surface beneath a gravity structure under cyclic loading.

To quantify the rate of degradation Idriss et al. 1976 and Idriss et al. 1978 introduced the degradation index (δ) and the degradation parameter (t), that for the stress-controlled tests can be determined as follows:

$$\delta = \frac{G_{SN}}{G_{S1}} = \frac{\tau_c/\epsilon_{cyN}}{\tau_c/\epsilon_{cy1}} = \frac{\epsilon_{cy1}}{\epsilon_{cyN}} \tag{1.4}$$

$$t = -\frac{log\delta(N)}{logN} \tag{1.5}$$

where G_{S1} and G_{SN} are the secant moduli at cycles 1 and N, τ_c is the shear stress value, ϵ_{cy1} and ϵ_{cyN} are the cyclic shear strains at cycles 1 and N, respectively. The degradation index can be seen as a mean to evaluate the rate of strain accumulation and the ratio of the cyclic strain at cycles 1 and N. Soil with a high δ value will have a low degree of degradation (Zhou and Gong 2001). The average degradation parameter, t, is the slope of the δ vs N line in a log-log scale, which describes the rate of cyclic degradation with N. Studies showed that the degradation parameter depends on plasticity index and OCR of soil (Vucetic and Dobry 1988; Tan and Vucetic 1989). The degradation parameter, t, consistently decreases with an increase of the OCR (Soralump and Prasomsri 2015). Soltani and Soroush 2010 showed that there was an increase in the degree of degradation as the number of loading cycles and cyclic shear strain amplitude increased. In cyclic strain-controlled tests carried out on kaolinite in simple shear device Mortezaie and Vucetic 2013 found that in larger cyclic shear strain amplitudes, frequency (f) increase, accelerates the degradation but in higher vertical stresses ($\sigma_{vc}^{'}$) the degradation decreases.

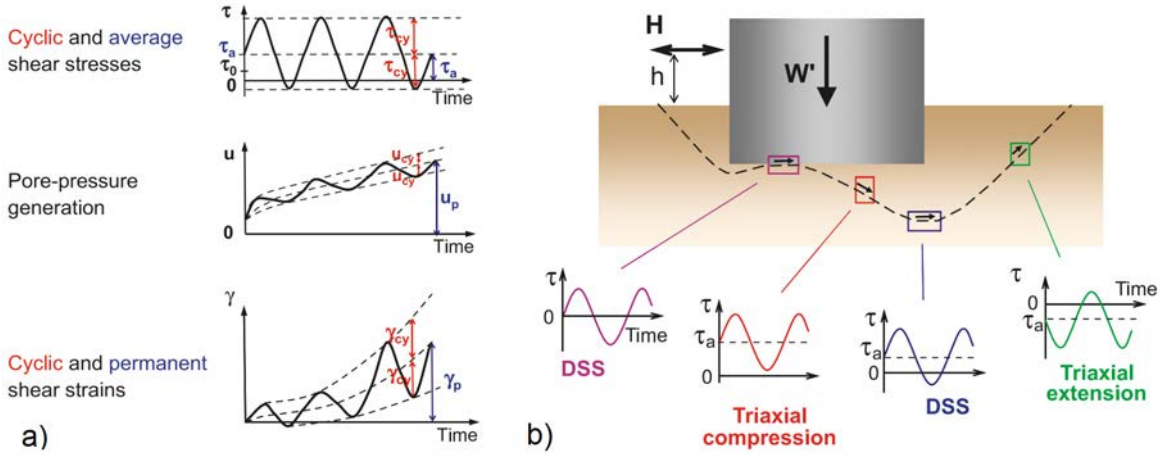

Figure 1.26: a) Pore water pressure and shear strain as function of time under undrained cyclic loading. u, pore water pressure; γ, shear strain; τ_0, initial consolidation shear stress. b)Simplified stress conditions along a potential failure surface in the soil beneath a gravity structure under cyclic loading. H, resultant horizontal load; h, height above seafloor of resultant horizontal load (Andersen 2009).

1.5.4 Influencing parameters

Several parameters as average shear stress (τ_a), cyclic shear stress (τ_{cy}), loading frequency (f), number of cycles (N), normal stress (σ_n), temperature (T^o) and initial state of the soil (normally consolidated or overconsolidated) are mentioned as influencing factors on cyclic response of soils (Andersen et al. 1980; Yasuhara et al. 1982;

Matasović and Vucetic 1995; Zhou and Gong 2001; Moses et al. 2003; Lackenby et al. 2007; Andersen 2009; Li et al. 2011; Wichtmann et al. 2013). In the following the effect of these parameters are discussed.

1.5.4.1 Effect of Cyclic stress ratio (CSR)

Thian and Lee 2017 conducted a series of cyclic constant-volume simple shear (CDSS) loading tests on a offshore clay to investigate the effect of cyclic loading on degradation behavior of the clay. They performed stress-controlled cyclic tests with cyclic stress ratios between 0.34 to 0.83 at different overconsolidation ratios (OCRs). They found that the accumulated cyclic strain and pore water pressure increases with number of cycles. With increasing overconsolidation ratio, at the beginning negative cyclic pore water pressure generated while with increasing number of cycles the pore water pressure increased. One-way cyclic strain and pore water pressure is presented in Fig. 1.27. Based on the investigation of soft clay under one-way undrained cyclic triaxial tests. Increasing the CSR value decreases the number of cycles to failure (Andersen et al. 1980; Yasuhara et al. 1982; Matasović and Vucetic 1995; Zhou and Gong 2001; Moses et al. 2003; Lackenby et al. 2007; Andersen 2009; Li et al. 2011; Wichtmann et al. 2013).

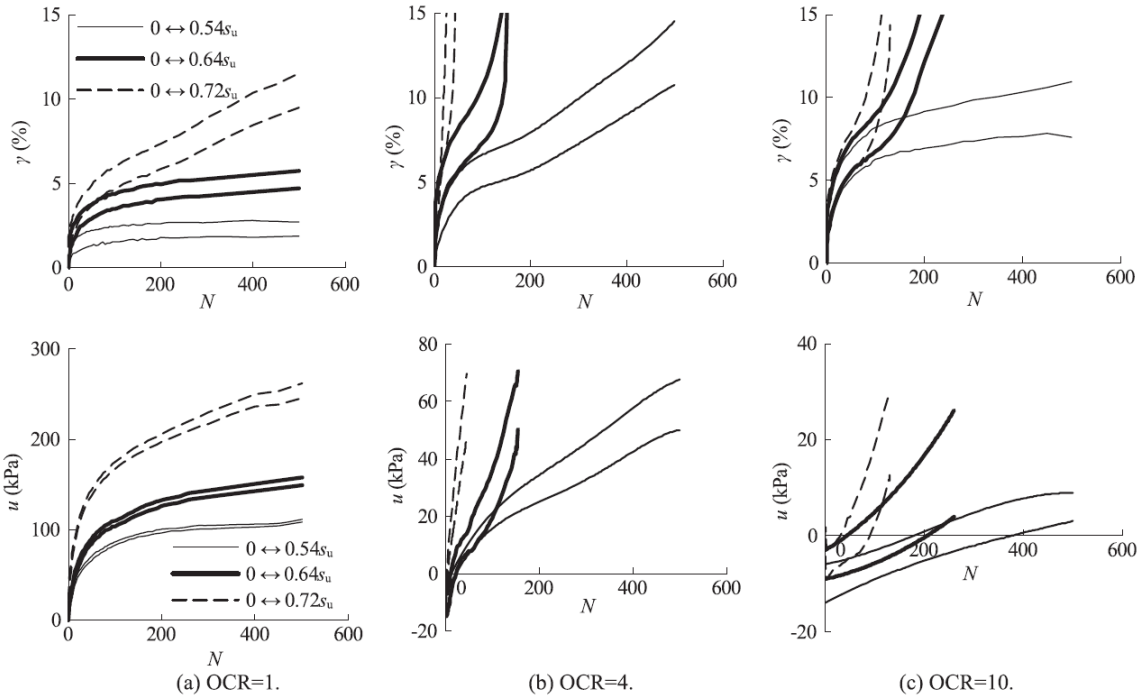

Figure 1.27: Developments of cyclic shear strain and pore water pressure in one-way simple shear cyclic loading at various values of CSR and OCR (Thian and Lee 2017).

1.5.4.2 Effect of OCR

Several studies in the literature reported that, for lightly overconsolidated soils, the pore water pressure trend is increasing with increasing number of cycles. on the contrary for highly overconsolidated soils, at the beginning the negative pore water pressure is generated while with further cycling the pore water pressure increases.

Brown et al. 1975 conducted undrained cyclic triaxial tests on samples of Keuper marl reconstituted from a slurry with OCRs from 2 to 20 with a frequency of 10 Hz (Fig. 1.28(a)). Matsui et al. 1980 performed cyclic tests on specimens with different OCR values between 1 and 4. The specimens were isotropically consolidated under different preloading stresses. After isotropic unloading the cycles were started from the same stress $p_0 = 200$ kPa. The data in Fig. 1.28(b) reveal that the dilatant phase during the first cycles gets larger with increasing OCR.

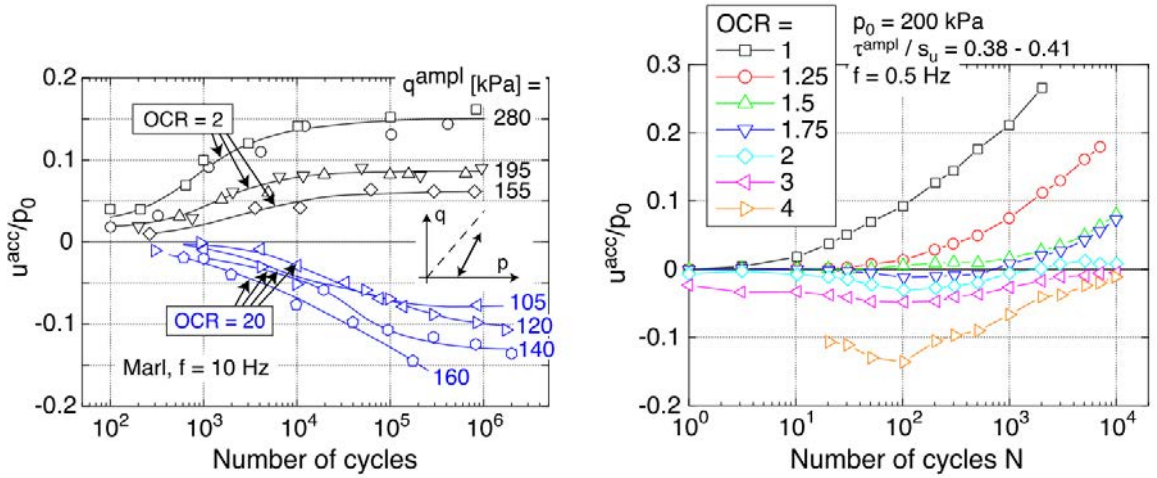

Figure 1.28: Effect of overconsolidation ratio on cyclic behavior. (a) OCR=2-20 (Brown et al. 1975); (b) OCR=1-4 (Matsui et al. 1980). adopted from (Wichtmann et al. 2013).

1.5.4.3 Effect of temperature

Very few studies have been carried out on the effect of temperature on cyclic behavior of soils. Cekerevac and Laloui 2010 performed temperature-controlled cyclic triaxial tests on kaolin samples (LL=45 %, PL=21 %). The samples were consolidated to 600 kPa and heated (90 ^{o}C) in drained conditions and were cyclically sheared under undrained conditions. The shear stress cycled between 0 and 300 kPa with a frequency of 1 cycle/hr. They found that the initial cycle imposed at either ambient or high temperature produced almost the same axial strain and pore water pressure. However later shear cycles of the heated sample induced smaller strain and smaller pore water pressure per cycle. The number of cycles to failure increased for heated samples due to the densification of clay under drained heating and also the pore water pressure of

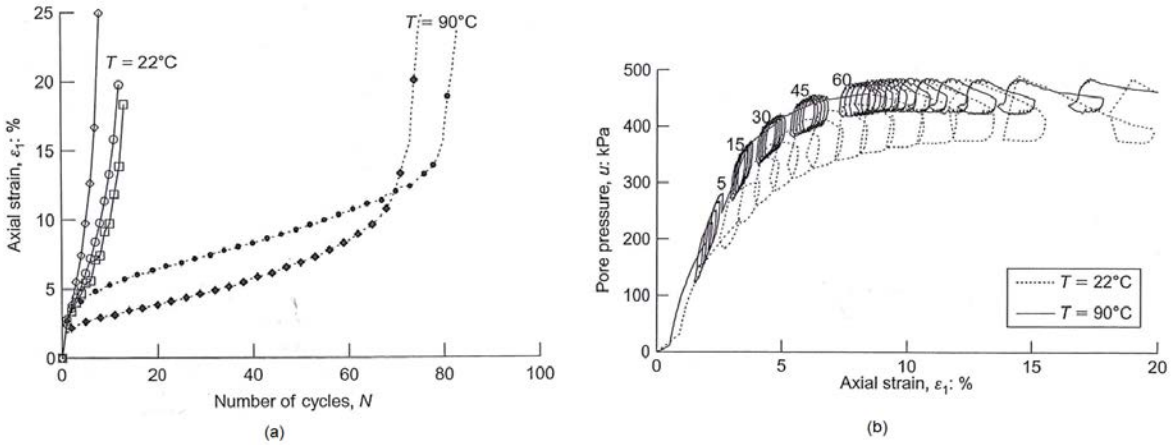

Figure 1.29: Effect of temperature on cyclic behavior of kaolin (Cekerevac and Laloui 2010).

heated samples was slightly less than unheated ones. The initial state of the samples was not the same before shearing due to the heating but the critical state line of the remained constant with temperature. The number of cycles to failure for unheated sample was ten cycles while for heated samples were failed after 70-80 cycles.

Xiong et al. 2018 performed cyclic triaxial tests at different temperatures on saturated soft clay in Ningbo city, China. They showed that the cumulative plastic strain, pore water pressure and dynamic damping ratio of saturated clay decreased with the increase of temperature, while the dynamic modulus increased with the increase of temperature and the soft clay showed a thermal hardening behavior. Cyclic stress-strain hysteresis loops at different temperatures are presented in Fig. 1.30. Xiong et al. 2018explained that the thermal hardening behavior can be explained that the absorbed water around soft clay particles acted as a barrier against the formation of the solid-solid inter-particle contacts would weaken as the temperature increases according to the kinetic theory.

1.5.4.4 Effect of frequency

Loading frequency has been mentioned as one of the important issues in cyclic loading of soils and soil-structure interfaces but its effects are poorly understood. Some studies in the literature have reported that the frequency decrease, rises the strain accumulation and excess pore water pressure (Matsui et al. 1980; Procter and Khaffaf 1984; Wang et al. 1998). However, other researchers have reported different results that the frequency has a little or no influence on the cyclic strength and deformation of soils (Ansal and Erken 1989; Hyde et al. 1993). Actually, clay behavior under undrained cyclic loading is complex for time-dependent creep and rate dependent characteristics.

The loading frequency has a distinct influence on the undrained cyclic behavior of natural clays. For a given number of cycles, larger shear strains and pore water pres-

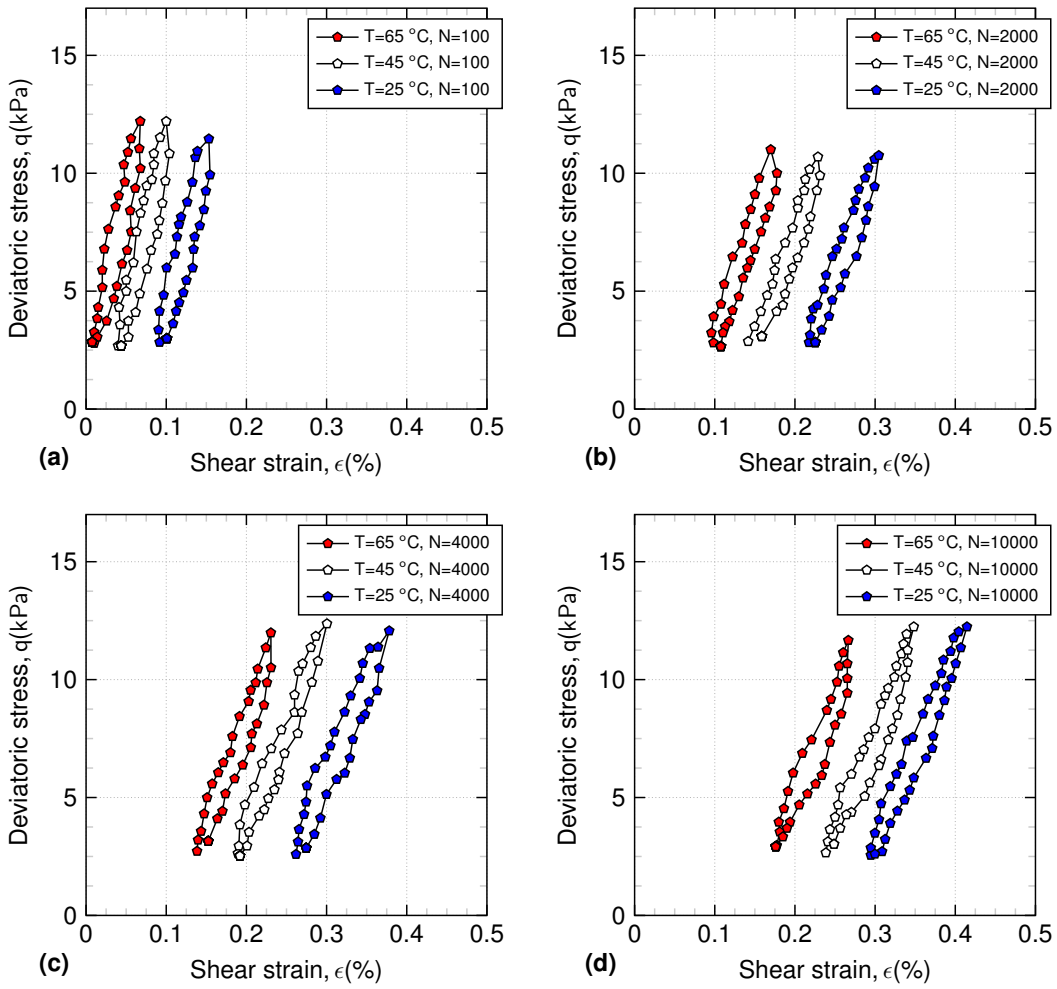

Figure 1.30: cyclic loops at different temperatures (Xiong et al. 2018).

sures are generated at lower frequency. In reality, the loading duration t plays a crucial role in controlling the undrained cyclic behavior (Li et al. 2011). When the applied cyclic stress is large and results in cyclic failure, the relationships of accumulative strain and pore water pressure versus time are nearly the same for different frequencies.

Mortezaie and Vucetic 2013 performed cyclic NGI-DSS constant-volume equivalent-undrained test on kaolinite clay. The tests were performed at three different cyclic shear strain (γc), 0.1, 0.25, and 0.5% under two normal stresses (σ) of 220 and 680 kPa, and three frequencies, 0.001, 0.01, and 0.1 Hz (Fig. 1.31). The cyclic shear stress decreased with further cycling which indicates the degradation behavior. The degradation parameter t, increased with increasing cyclic shear strains from 0.1 to 0.5% at f=0.01 and 0.1 (Fig. 1.32). Increasing the frequency from 0.01 to 0.1 increased the degradation parameter under both 216 and 680 kPa. However under the mentioned conditions, the degradation parameter decreased with increasing stress. The authors have explained that this behavior may be due to the higher void ratio at lower stresses which cause higher excess pore water pressures.

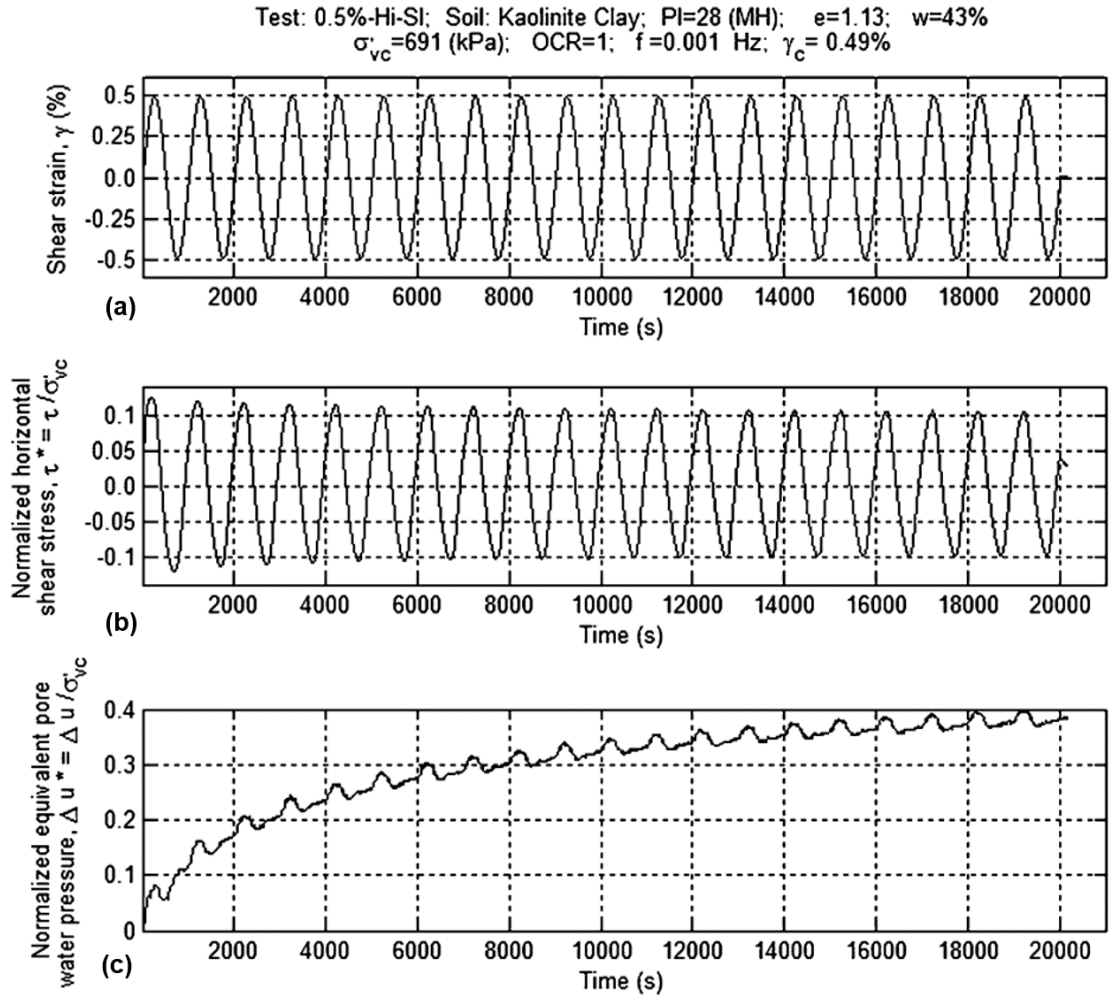

Figure 1.31: Cyclic constant-volume equivalent-undrained simple shear tests (Mortezaie and Vucetic 2013). (a) shear strain cycling between $\pm\gamma_c$ vs. time ; (b) shear stress fluctuations during cycles vs. time; (c) equivalent pore water pressure vs time.

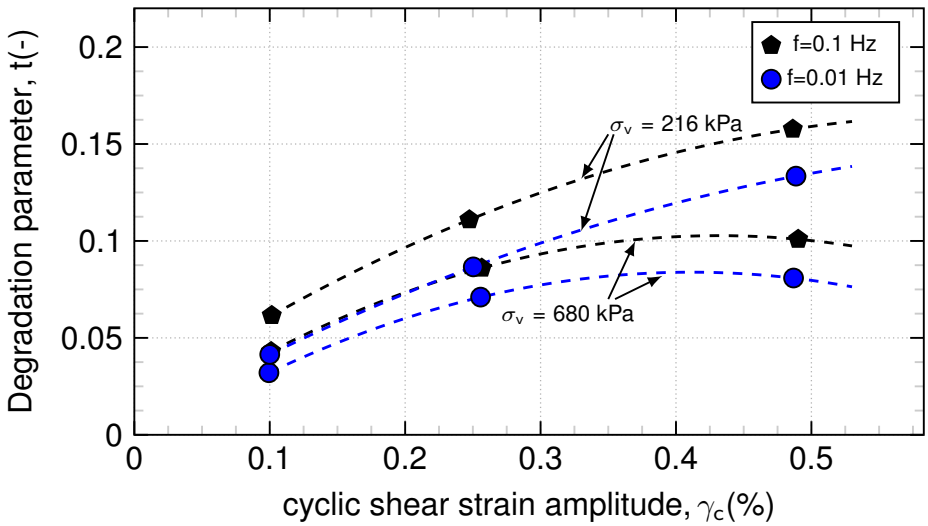

Figure 1.32: Effect of frequency on shear stress degradation vs. cyclic shear strain amplitudes of kaolinite clay under two-way cyclic loading (adopted from Mortezaie and Vucetic 2013).

1.6 Constitutive models

In this section, existing constitutive models on soils and soil-structure interface are discussed. To summarize the important aspects of constitutive modeling in soil structure interface two approaches are discussed: (I) thermo-mechanical constitutive models for soils (II) interface constitutive models at isothermal conditions. The aim of the first part is to present the important features of effect of temperature on mechanical behavior of soils that should be captured by constitutive models and discuss some thermo-mechanical constitutive model proposed for soils. The second part is dedicated to interface constitutive model mostly proposed for granular soil-structure interface at isothermal conditions. The experimental observations on the sand-structure contact behavior has been used to develop constitutive equations for granular-structure interface behavior.

1.6.1 Thermo-mechanical constitutive model for soils

Several constitutive models were proposed to take into account the effect of temperature on mechanical behavior of soils (Hueckel and Borsetto 1990; Graham, Tanaka, Crilly and Alfaro 2001; Hueckel et al. 2009; Laloui and François 2009; Hamidi and Khazaei 2010; Yao and Zhou 2013). Most of these models are based on the critical state theory. Some of these studies have considered the thermal expansions of the soil particles compressibility of the soil skeleton, and physico-chemical effects while they are not capable to take into account the effect of thermal and stress history (OCR) (Campanella and Mitchell 1968; Robinet et al. 1994; Zhou et al. 1998). One of the inconvenience of these models is the determination of numerous number of parameters. Baldi et al. 1988 introduced an improved model that could calculate volume changes for clays having low porosities. The expressions ignore nonlinear changes in soil compressibility with temperature, the effects of secondary compression, or initial effective stress. Booker and Smith 1989 and Britto et al. 1989 proposed non-isothermal models based on thermo-elasticity. These models focused just on the reversible part of thermal effects. Agar et al. (1987) showed that empirical, hypoelastic models could be developed for modeling nonlinear stress-strain behaviour of oil sand at elevated temperatures.

Laloui and Cekerevac 2003 in their proposed model discussed several features of thermo-mechanical behavior of soils that should be captured by the model. Several studies in the literature have shown that the main effect of temperature is thermally induced deformations which is directly the void ratio changes. To reproduce the effect of temperature in constitutive models, Laloui and Cekerevac 2003 considered thermal effects on preconsolidation pressure and plastic thermal strain. They reported a decrease of 4 kPa/10 ^{o}C for preconsolidation pressure. Based on several studies in the

literature, (Fig. 1.33(a)) shows the reductive trend of preconsolidation pressure with temperature. Based on the observed trend, Laloui and Cekerevac 2003 proposed the following equation:

$$\sigma_c^{'}(T) = \sigma_c^{'}(T_0)(1 - \gamma log[T/T_0]) \tag{1.6}$$

$\sigma_c^{'}(T)$ is the preconsolidation pressure at temperature T, for each material, a unique value for the parameter γ should be determined. The reduction of preconsolidation pressure with temperature has been depicted in Fig. 1.33(b) (dashed line). Based on the soil state (NC or OC) several scenarios can be expected. For highly overconsolidated soils (unloading from A to C), the stress states remains within the yield limit with heating (C to C_1). Therefore, the volumetric response is dilatant and totally thermo-elastic. For slightly overconsolidated soils, the response upon heating up to $B_1^{'}$ is thermo-elastic and dilatant while, afterwards the thermo-mechanical point reaches the yield limit ($B_1^{'}$) and with further heating a thermo-plastic strain is generated. For normally consolidated soils, the response is totally irreversible upon heating (A to A_1) and induces thermal hardening or thermal overconsolidation phenomena.

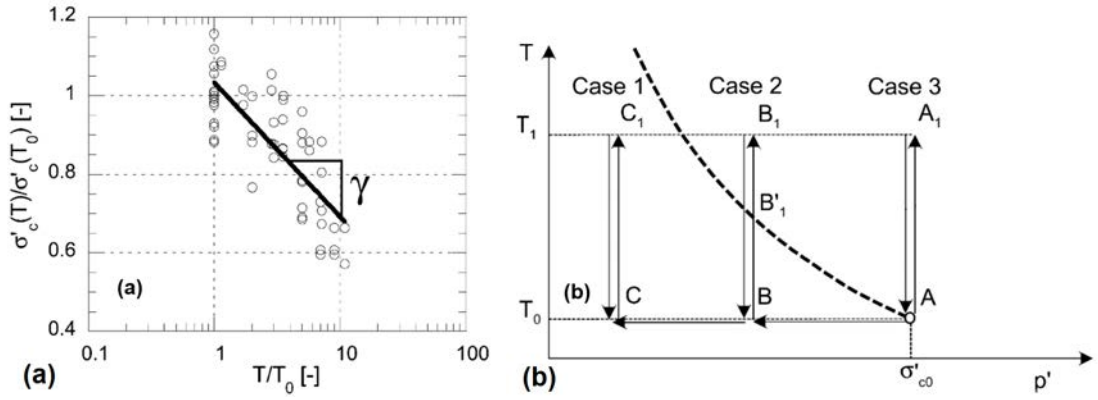

Figure 1.33: Effects of temperature on overconsolidated and normally consolidated clay (Laloui and Cekerevac 2003).

Based on the evolution of preconsolidation pressure with temperature, the size of yield surface evolves. For overconsolidated clays the thermal strains are dilatant upon heating and the preconsolidation pressure decreases with temperature increase which decreases the deviatoric elastic limit. For the normally consolidated soils, a volumetric plastic strain occurs upon heating. The plastic strain induced by thermal solicitations induces contraction which is independent of effective stress consequently the shear strength of the soil evolves due to the void ratio changes. The void ratio reduction upon heating for normally consolidated soils is known as thermally induced overconsolidation effect. Laloui and Cekerevac 2003 used an elasto-plastic approach. In this approach the strains are divided into two parts; thermo- elastic and thermo-plastic:

$$\epsilon_v^{Te} = \beta(T - T_0) + \frac{p^{'} - p_0^{'}}{K} \tag{1.7}$$

the volumetric thermo-elastic strain is ϵ_v^{Te}. the volumetric thermal dilation coefficient is β and $(T - T_0)$ is the temperature difference. $p^{'}$ and $p_0^{'}$ are the current and the initial effective mean stress, respectively. K is the bulk elastic modulus. When the stress reaches the yield limit (preconsolidation pressure) the thermo-plastic strain is generated. The relation between preconsolidation pressure and volumetric plastic strain (ϵ_v^p) can be expressed as:

$$\sigma_c^{'} = \sigma_c^{'}(T) exp(\beta \epsilon_v^p) \tag{1.8}$$

where $\sigma_c^{'}(T)$ is the value of preconsolidation pressure at temperature T and β is the plastic compressibility (the slope of the plastic part of the ϵ_v log$\sigma^{'}$). The complete expression of the isotropic thermo-plastic yield limit is thus given by:

$$f = p^{'} - \sigma_c^{'}(T_0) exp(\beta \epsilon_v^p)(1 - \gamma log[T/T_0]) \tag{1.9}$$

1.6.2 Interface constitutive model at isothermal conditions

Various constitutive models have been developed for interfaces in the literature (Boulon et al. 2003; Liu et al. 2006; DAguiar et al. 2011; Lashkari 2013; Saberi et al. 2016; Saberi et al. 2017; Saberi et al. 2019; Stutz, Mašín and Wuttke 2016) These models are Mohr-Coulomb-type models, non-linear elastic models, a directional-type model, and elasto-plastic models. The interface material has been assumed to be linear elastic (Bfer 1985) or non-linear elastic with a stress-strain relationship of the hyperbolic type in the normal and tangential directions of deformation (Clough and Duncan 1971; Desai and Ma 1992; Boulon et al. 1995). Other studies refer to the theoretical framework of elasto-plasticity. The general formulation of the elasto-plastic type models for interface behavior is similar to that of the continuum materials (Desai and Ma 1992; Shahrour and Rezaie 1997; Ghionna and Mortara 2002a; Fakharian and Evgin 2000; De Gennaro and Frank 2002; Boulon et al. 2003; Liu et al. 2006). These models incorporate one or more of the following phenomena: strain hardening, softening, contraction, dilation and damage. On the contrary Suryatriyastuti et al. 2014 and Suryatriyastuti et al. 2016 presented a numerical attempt based on load transfer approach to investigate the effect of thermal cycles on mechanical response of soil-structure interface. They proposed t-z cyclic function which takes into account the degradation of interface under temperature cycles. At the end they observed the axial stress and skin friction evolution in thermo-active piles while cycling temperature.

The interface generally separates the surface of the structure from the soil. These surfaces are generally represented by parallel planes. The interface thickness t, can be identified experimentally by direct observation, the definition of its thickness is highly variable depending on soil characteristics and inclusion, which significantly modifies the characteristics of the observed behavior. As a result, the researchers avoid formulating interface laws as a function of deformation (shear deformation: $\epsilon_t = u_t/t$ or normal deformation: $\epsilon_n = u_n/t$) as they depend on the thickness of the interface, whereas the measurable kinematic quantities are the relative normal displacement, u_n or relative tangential, u_t of the interface. Two-dimensional modeling thus imposes the use of the following four variables: τ, σ_n, u_t, u_n.

1.6.2.1 Elasto perfectly plastic model

The first use of interface models has involved rock joint analyses. To reproduce the behavior of rock joints and interfaces, most authors have considered elastic perfectly plastic linear models using the Mohr-Coulomb shear failure criterion as the loading surface. The authors who have studied rock fractures (Patton 1966; Goodman and Dubois 1972; Goodman 1989) considered the influence of joint roughness. The failure criterion is therefore defined by a bilinear envelope. Other authors such as (Goodman et al. 1968; Pande and Sharma 1979; Lee et al. 1992; Day and Potts 1994; Day and Potts 1998) have adopted a simpler Mohr-Coulomb failure criterion with an associated flow rule that defines the load function F :

$$F = |\tau| + \sigma_n tan\phi^{'} - c^{'} \tag{1.10}$$

In this case, when the shear stress reaches the breaking limit of Mohr- Coulomb, the value of the tangential stiffness becomes zero; the normal stiffness remains the same. In addition, a non-associated flow rule has also been used to avoid overestimating the plastic dilation by considering an angle of dilation different from the angle of friction (Van Langen and Vermeer 1991). In this case, the plastic potential is written as

$$Q = |\tau| + \sigma_n tan\psi \tag{1.11}$$

with ψ : angle of dilation. Slip between soil and structure occurs when the criterion is met. In this case, only the movements at the interface become discontinuous. One can also introduce a disband criterion between the structure and the ground reached when the normal stress at the interface is equal to a limit value. Perfect elasto-plastic models cannot adequately reproduce the typical mechanical responses of the interface observed

experimentally, such as progressive strain hardening and phase change (contraction-dilation).

1.6.2.2 Elastoplastic models with strain hardening

Various elasto-plastic models with strain hardening have been presented in the literature. First, the soil-structure interface models are considered within the framework of classical elasto-plasticity. In this case, the analyses of the experimental results derived from the triaxial test and the direct shear box show strong similarities. As a consequence of these analogies, Boulon and Nova 1990 adapted for the interfaces an elasto-plastic model that was previously formulated for the triaxial behavior of sands (Nova and Wood 1979).

Desai et al. 1985 suggested an elasto-plastic interface model based on the disturbed state concept. Boulon and Jarzebowski 1991 formulated an elastoplastic model based on the boundary surface concept using an elliptic plastic function. The same approach was used by Shahrour and Rezaie 1997 to study the behavior of the interface under cyclic loading.

Zeghal and Edil 2002 have developed an interface model based on the Mohr Coulomb model, on a plasticity not associated with a strain-hardening that depends on the plastic work. However, the model has the originality to consider the interface as a sinusoidal surface, and to take into account the degradation of the interface grains through a correlation between the friction coefficient and the plastic work (work hardening variable). Gómez et al. 2003 propose an extension of the hyperbolic model for sand-concrete interfaces that was developed on the basis of the model of Clough and Duncan (1971) with consideration of strain-hardening, loading-unloading-reloading and with accommodation to all stress paths.

In addition, many damage models have been developed (Navayogarajah et al. 1992; Hu and Pu 2003; Hu and Pu 2004). These authors assume that the response of the interface is the sum of an intact and a critically damaged part, based on the DSC: Disturbed State Concept (Desai and Ma 1992; Desai and Zhang 1998; Liu et al. 2006). Indeed, during the shearing of the grains, the intact part gradually transforms into a damaged part due to the accumulation of plastic deformations. The shear stress is nil in the damaged part while the normal stress is not influenced by the damage. For this purpose a damage function has been introduced to reproduce the softening and expansion phenomenon.

Navayogarajah et al. 1992 also considered the effect of roughness in the model by making the coefficient of friction as well as the value of plastic tangential displacement at the shear peak depend on the relative roughness. Table 1.1 summarizes the load functions, plastic potentials and strain-hardening variables used in some elasto-plastic

interface models. De Gennaro and Frank 2002 proposed a model in the general framework of an elasto-plastic constitutive model on purpose for describing the interface behaviour. The model was based on a Mohr-Coulomb failure criterion, including deviatoric hardening/softening, phase transformation state (compaction and dilatancy) and ultimate state. Hu and Pu 2004 took the disturbed state theory for proper simulation of hardening, softening and dilation of rough interfaces. Recently, Liu et al. 2006 suggested that the critical state soil mechanics concepts can be applied to interfaces within the framework of generalized plasticity. Lashkari 2013 by adopting the thin interface layer as a load transfer mechanism, proposed a simple but accurate critical state compatible interface constitutive model. Lashkari 2012 formulated an interface model within the context of the bounding surface plasticity is presented. New state dependent elements were employed to enhance the model predictive capability over the wide ranges of states. In addition, a novel mechanism was introduced which enables the model for proper prediction of the intense tendency to contraction that occurs immediately after the application of tangential stress. Stutz, Mašín and Wuttke 2016 introduced an interface constitutive model in the hypoplasticity frame. Stutz, Mašín, Wuttke and Prädel 2016 proposed a model which was an adaption of the thermo-mechanical hypoplastic model from Masin & Khalili (2011) and Masn & Khalili (2012). The reformulation is done by redefined tensorial definitions for the special case of soil-structure interfaces.

To discuss different aspects of one of the elasto-plastic models, the sand-structure interface model proposed by Ghionna and Mortara 2002b is presented in the following.

Ghionna and Mortara 2002b proposed an elasto-plastic model for sand-structure interface. The basic assumption of this model is to consider the interface as a zero thickness bidimensional element. The authors have used the results of CNL and CNS tests of sand-structure interface to calibrate their model. The flow rule of the model was proposed on the basis of incremental plastic vertical deformation to the incremental plastic horizontal deformation (Eq 1.15):

$$d = \frac{\dot{\upsilon}^p}{\dot{\omega}^p} \tag{1.12}$$

d here is dilatancy rate. The plastic potential represents the link between the components of the plastic incremental displacement and the components of stress. The plastic potential, plastic function, hardening law and elastic behavior of material should be introduced in inside a model.

The model curves that derived from CNL tests are calibrated with α and β values that are as follows:

$$\alpha(w_n) = \alpha_c[(\omega w_n + 1)^{\psi} - 2]exp[-Lw_n^M] + \alpha_c \tag{1.13}$$

The equations of the yield surface can be specialized for peak failure and critical conditions (large displacements) as follows:

$$\tau_p = \alpha_p \sigma_n^{\beta} \tag{1.14}$$

The plastic potential was determined using the observed trend in Fig. 1.34(a). The parameters μ and v can be determined using the linear regression of experimental CNL data at failure for d_{max} versus σ_n curve.

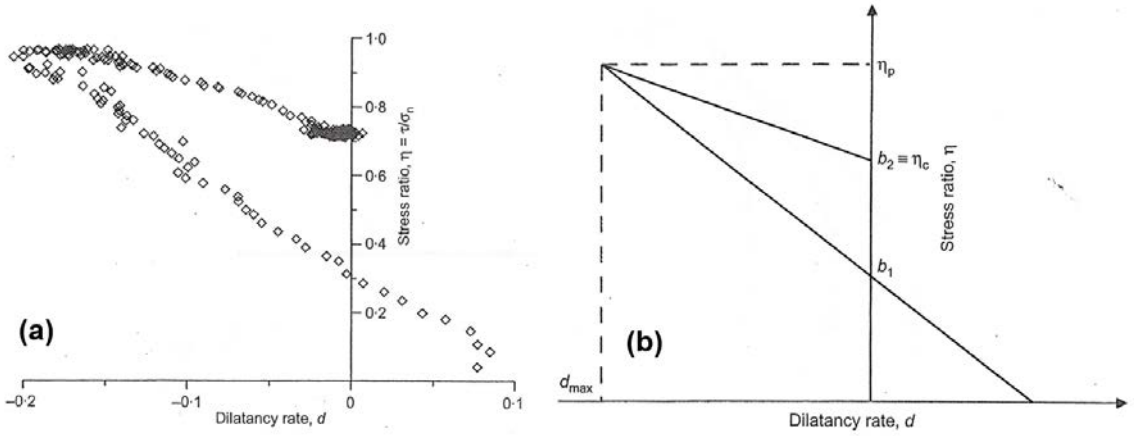

Figure 1.34: (a) Flow rule of the elastoplastic model. (b) Maximum dilatancy rates from CNL and CNS tests (Ghionna and Mortara 2002b).

To determine the yield loci, the peak plastic shear displacement w_p should be evaluated from the experimental tests. The plastic shear displacement corresponding to the peak shear stress, increases with normal stress increase according to the following relationship:

$$w_p = \xi \sigma_n + \zeta \tag{1.15}$$

1.6.2.3 Critical state models

Lashkari 2017 proposed an isothermal interface constitutive model based on critical state theory.

Among the presented models for soil structure interface in the literature, the critical state interface model proposed by Lashkari 2017 is based on void ratio evolution during shear. The model is straightforward in application and has parameters that all have physical meanings. The concept of the critical state is based on the theory that at large shear deformations, soil continues to shear without any changes in volumetric and stress conditions (Been et al. 1991). The void ratio at this large shear deformation

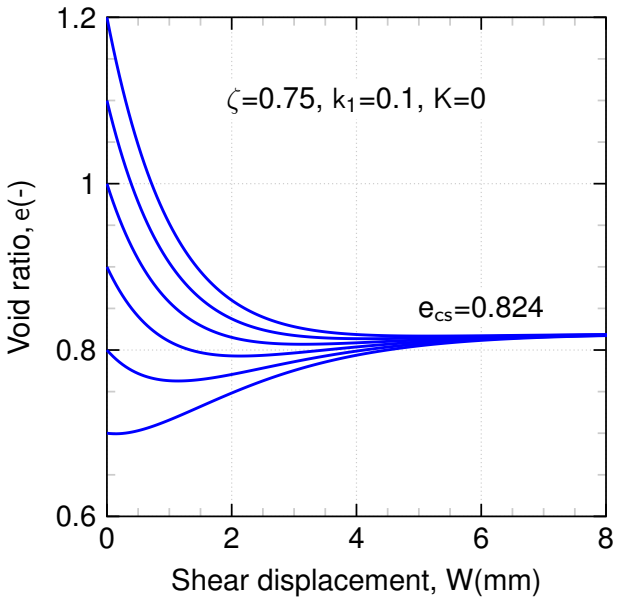

Figure 1.35: Evolution of void ratio during shearing using Eq. 1: (a) different initial void ratios (e_{in} = 0.70, 0.9, 1.0, 1.1, and 1.2) evolution towards the critical state void ratio (e_{cs} = 0.824).

is the critical state void ratio (e_{cs}). The critical state void ratio tends to decrease with increasing the normal stress. Therefore, the shear and volumetric behavior of the soil/soil-structure interface depends on the difference between current and critical state. This difference is defined as the state parameter (Been et al. 1991). Lashkari 2017 proposed the following function for the evolution of the interface void ratio with shear strain:

$$e = e(e_{in}, e_{cs}, \epsilon) = e_{cs}[1 - exp(-\xi\epsilon)] + e_{in}exp(-\xi\epsilon) - \frac{k_1}{1 + K/k_2}(\epsilon)exp(-\xi\epsilon) \quad (1.16)$$

The current void ratio (e) is a function of initial (e_{in}), critical state void ratio (e_{cs}) and shear strain (ϵ). The deformation (ϵ) is defined as the shear displacement divided by the interface thickness ($\Delta w/t$). The parameter ξ controls the rate of void ratio evolution with shear strain (ϵ). K is the normal stiffness acting on the interface. The parameters k_1 and k_2 are interface parameters. Fig. 1.35 shows Eq. 1.16 for different initial void ratios (0.7-1.2). For dense samples, $e_{in} < e_{cs}$, and for loose samples, $e_{in} > e_{cs}$. The dense sample with e_{in} = 0.70 exhibits an initial contraction upon shearing followed by dilation after phase transformation. In the sample with e_{in} = 0.8, a larger initial contraction phase is obtained, followed by dilation. Finally, the soils with e_{in} = 0.9, 1.0, 1.1, and 1.2 exhibit contraction until the shearing ceases. As can be observed, independent of initial void ratio, the curves converge towards a single state which is the critical state void ratio.

Table 1.1: Summary of recent elastoplastic interface constituent models.

Reference	**Yield function Plastic potential**	**Hardening parameter**	**Interface type**	**Num of para**
Desai et Fishman (1991)	$F = \tau^2 + \alpha\sigma_n^n - \gamma\sigma_n^2$ $Q = F + h(\sigma_n, \xi)$	$\xi = \int((du_n^p)^2+(du_t^p)^2)^{1/2}$	rock joints	7
Navayogarajah et al. (1992)	$F = \tau^2 + \alpha\sigma_n^n - \gamma\sigma_n^2$ $Q = \tau^2 + \alpha_Q\sigma_n^n - \gamma\sigma_n^2$	$\xi_D = \int \lvert du_t^p \rvert$ $\xi_V = \int \lvert du_n^p \rvert$	sand-steel	15
Desai et Ma (1992)	$F = Q = \tau^2+\alpha\sigma_n^n-\gamma\sigma_n^q$	$\zeta = \int(du_n^p du_n^p + du_t^p du_t^p)^{1/2}$	rock joints and rock-concrete interface	15
De Gennaro et Frank (2002a)	$F = \tau - \mu(u_t^p)\sigma_n$ $Q = \tau + \mu_c(u_t^p)\sigma_n ln(\frac{\sigma_n}{\sigma_0})$	$\mu(u_t^p) = \mu_0 + (\mu_f - \mu_0)\frac{u_t^p}{A(\frac{\sigma_{ni}}{p_0})t+u_t^p}$	sand-steel	10
Ghionna et Mortara (2002)	$F = \tau_p - \alpha_p\sigma_n^\beta$ $Q = \tau - \frac{b}{1+a}\sigma_n[1 + a(\frac{\sigma_n}{\sigma_c}) - \frac{1-a}{a}]$	$\dot{\omega_n} = \int \frac{\dot{\omega^p}}{\omega_p}$	sand-steel	12
Zeghal et Edil (2002)	$F = \lvert T \rvert + \mu\Sigma$ $T = (\sigma_n sin\alpha_k + \tau cos\alpha_k)$ $\Sigma = (\sigma_n cos\alpha_k - \tau sin\alpha_k)$ $Q = \lvert T \rvert$	W^p	sand-structure	6
Hu et Pu (2003)	$F = \frac{\tau}{D_s} + \epsilon_s^p(\tau^i - \sigma_n tan\delta_0)$ $F = \tau^c - \sigma_n tan\delta_r$ $Q = \tau^i$	ϵ_t^p	sand-steel	9

1.7 Conclusions

In this chapter a review of the energy geostructure definition, its technology, construction methods and probable problematics around these structures are discussed. As it was observed, in thermo-mechanical behavior of soils thermal and stress history plays a major role in the mechanical behavior of soils at different temperatures. In spite of numerous amount of research that have been conducted on the thermo-mechanical behavior of soils, conflicting results can be found on the effect of temperature on the shear characteristics of the soils.

Soil-structure interface role in serviceability of thermally-active energy geostructures is discussed. The influencing parameters on the mechanical behavior of soil-structure were discussed and based on several in-situ pile testings, the more realistic behavior of the interface (constant normal stiffness conditions) was reproduced in interface testing. Finally the effect of temperature on mechanical characteritics of interface was discussed. Despite existing literature on the thermal effects on the shear behavior of interface, conflicting results give rise to several questions that should be answered. For monotonic

behavior of soil structure interface following aspects should be addressed:

- Effect of temperature on shear characteristics of sand/clay-structure interface under constant normal load and constant normal stiffness conditions
- Thermal volumetric response of sand/clay-structure interface

In the cyclic behavior of soils and interfaces, strain accumulation, pore water pressure increase and strength degradation was observed to be dependent on frequency, cyclic strain and stress amplitudes, normal stress, number of cycles, density or state of the soil (NC or OC) and temperature. There is almost no study in the literature on the effect of temperature on cyclic behavior of soil-structure interface. The following aspects are addressed:

- Monotonic behavior of clay and clay-structure interface differences under constant-volume equivalent-undrained conditions
- Effect of temperature on strain accumulation, pore water pressure generation and strength degradation of clay-structure interface

For constitutive modeling of interfaces, two important aspect of existing constitutive model were discussed. On one hand, the important features of thermo-mechanical behavior of soils that were captured by the models were discussed. On the other hand sand-structure interface constitutive models, their constitutive formulation and prediction capacities were presented. Due to the lack of interface constitutive models to take into account the effect of temperature, in this study the questions concerning the non-isothermal interface modeling are presented as follow:

- Implementing the effect of temperature in an isothermal interface constitutive model
- Develop the non-isothermal model to reproduce clay-structure interface behavior

The literature survey allowed to understand important fundamentals of thermo-mechanical behavior of soils and soil-structure interfaces under monotonic or cyclic loads as well as its constitutive behavior. Moreover, the missing puzzles of the non-isothermal behavior of interface were identified to focus on them in the next chapters.

Chapter 2

Materials and methods

Temperature effects on the mechanical behavior of energy foundations and particularly soil-structure interface have been investigated in this study. As discussed in the first chapter, temperature variations can cause significant changes in mechanical properties of the surrounding soil and shearing characteristics of energy geostructures. In order to study the effect of temperature in laboratory, in-situ initial conditions of the geostructures should be reproduced as close as possible. The classical laboratory devices should be equipped with special configurations to be able to control the temperature of the soil samples. The heating/cooling systems should be capable to control the temperature of the sample independently from other parts of the device. The temperature should be applied in manner that no thermal gradients be generated in the soil sample.

In the current chapter the detailed description of materials used in this study, the sample preparation methods, measurements, calibrations and device details are discussed. To investigate the effect of temperature on mechanical properties of soil-structure interface, two reference soils (sandy and clayey soils) were selected. The sandy soil is Fontainebleau sand and the clayey one is kaolin clay. A structural surface with a specific roughness was fabricated to be used for the soil-structure interface tests. The techniques and devices to measure the roughness of the surface are presented. Then sample preparation for both sand and clay samples is discussed. In coherence with the study's problematic, the different methods and techniques for imposing and measuring temperature are then exposed. The temperature-controlled direct shear device is detailed afterwards, calibration results and repeatability tests are discussed.

2.1 Temperature-controlled direct shear device

In this section the experimental setup, thermal calibration of the direct shear device, and the methods to determine the roughness of the structural surface are discussed.

2.1.1 Experimental setup

Fig. 2.1 shows the temperature-controlled direct shear device, shear box and steel plate to model the interface used in this study. The shear device consisted of a loading frame which applied the normal stress, a system to apply the shear stress (in deformation or stress controlled mode), vertical and horizontal displacement transducers (Fig. 2.1(a)). The load frame was capable to apply the normal forces up to 20 kN. The range of shear displacement was 0-+25 mm. The device was capable to apply a shear rate comprised between 0.000001 to 30 mm/min.

This assemblage was connected to a heating/cooling system which controlled the temperature of a fluid. This fluid circulated in the lower part of the shear box container (Fig. 2.1(b) and (c), fluid circulation part). Several thermal sensors were placed in different parts of the device to measure the imposed and obtained temperatures. The shear box was a stainless steel (60 x 60 x 35 mm) which consisted of upper and lower halves of the shear box (Fig. 2.1(d)). A porous stone placed in the bottom of the lower half of the shear box. The upper porous stone placed inside the loading panel directly, in direct contact with the sample when the normal stress is applied. After sample preparation in the shear box, it was placed inside the shear box container filled with water (Fig. 2.1(b)). The water temperature in the container reached the same temperature that is imposed to the circulating fluid. Three thermal sensors, one in the lower half, another on the upper half of the shear box, and the last in the container, controlled the applied temperature.

In this direct shear device, normal stress σ_n (kPa), shear displacement W (mm), circulating fluid temperature T (^oC) and stiffness value K (kPa/mm) were applied, and normal displacement U (mm), shear stress τ (kPa), and sample temperature T (^oC) were measured. The system was operated by the commanding software of the shear box which was able to save whole of the data generated by the device. To perform soil-structure interface, the soil in the upper half of the shear box should be sheared against a structural surface which is placed in the lower half of the shear box. To do so, an interface mold was designed which a structural surface with a length of 80 mm could be placed inside it (Fig. 2.1(e)). The soil samples were prepared directly in the upper half of the shear box. Different types of structural surfaces as concrete or steel with different roughness can be placed inside the interface mold.

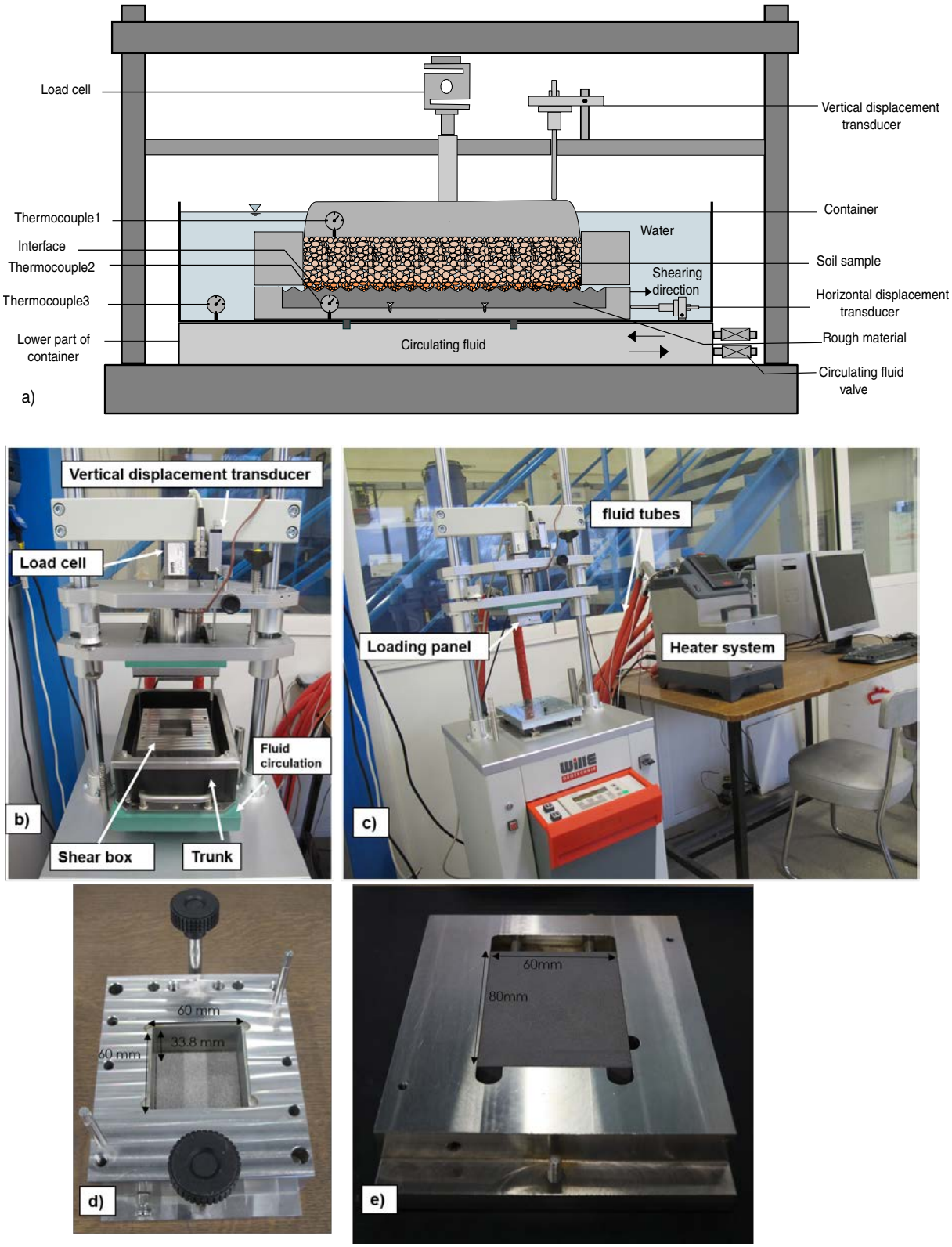

Figure 2.1: Experimental setup of the direct shear temperature-controlled device. (a) Schematic view of the device; (b) different parts of the device; (c) heating and logging system; (d) shear box; (e) structural surface placed in the designed lower half shear box.

2.1.2 Thermal calibration of the direct shear device

In order to take into account the effect of temperature on different parts of the device, the thermal calibration of the device was performed (Fig. 2.2). A cylindrical incompressible stainless steel was placed inside the shear box and the normal stress was applied. Afterwards the heating phase with a rate of 5 ^{o}C/hr was applied till 60 ^{o}C and then it reduced to 5 ^{o}C.

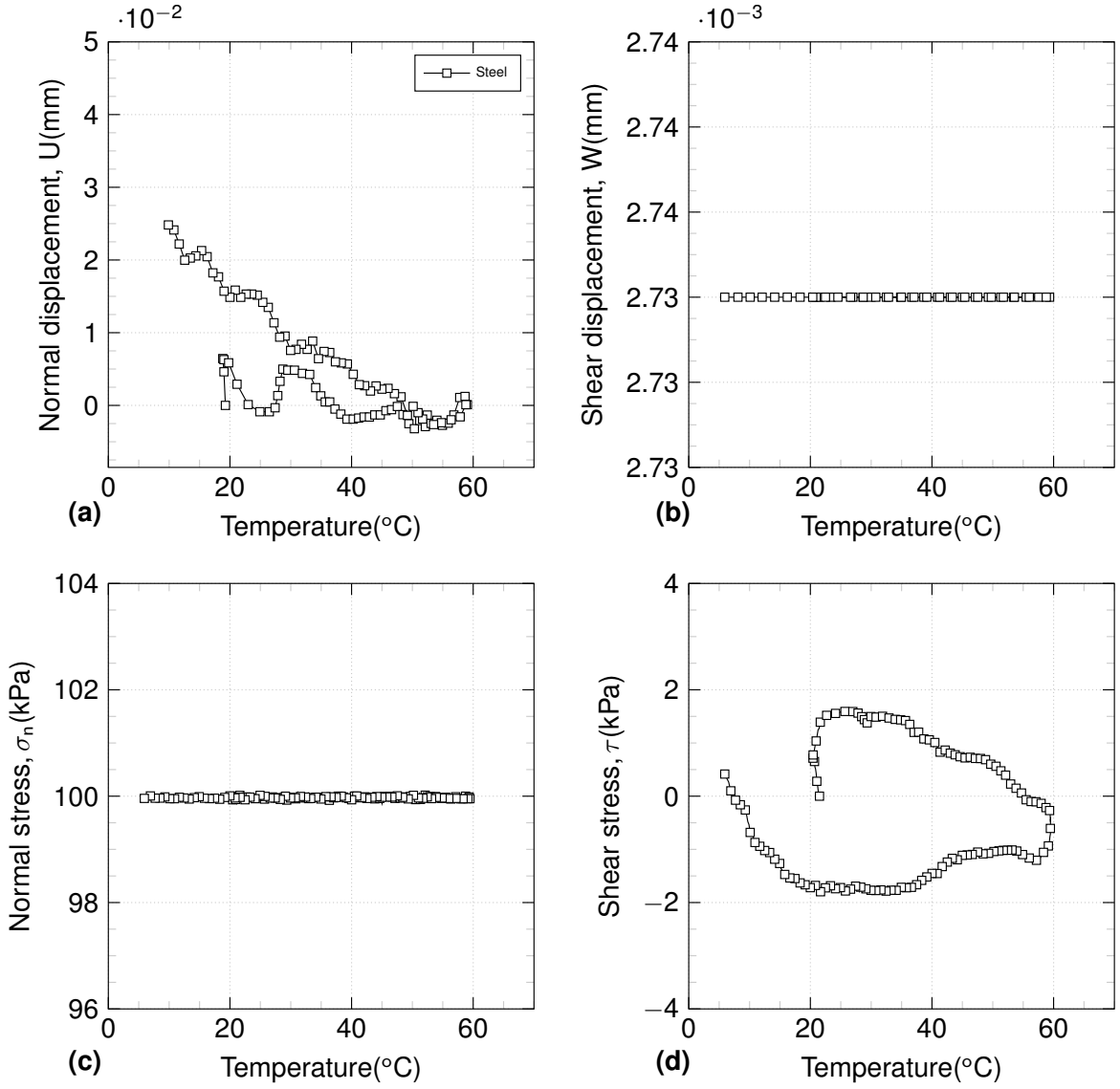

Figure 2.2: Thermal calibration of the device. (a) Normal displacement vs. temperature; (b) shear displacement vs. temperature; (c) Normal stress vs. temperature; (d) shear stress vs. temperature.

The normal displacement measurements up to 60 ^{o}C is negligible, on the contrary after cooling to 5 ^{o}C, the device showed a small contraction (Fig. 2.2(a)). The temperature cycle 20-60-5 ^{o}C had a negligible effect on the horizontal displacement transducer (Fig. 2.2(b)). The vertical stress variation upon temperature variation is negligible (Fig. 2.2(c)). The shear stress evolution with heating from 20-60 ^{o}C is negligible and

cooling from 60 to 5 ^{o}C caused an increase of shear stress which is negligible (Fig. 2.2(d)). These calibration values have been taken into account in the experimental results.

2.1.3 Roughness determination

To perform soil-structure interface direct shear tests, a stainless steel plate (80 x 60 x 10 mm) with the desired roughness was designed and used to model the structure. This steel plate was used to, avoid abrasion of the surface due to test repetition. The roughness of the steel plate was measured with a laser profilometer (Fig. 2.3(a)). The similarity between height of the roughness measurements indicated the surface homogeneity of the interface. The zoomed profile is presented in Fig. 2.3(b). Four profiles with lengths of 32 mm (Fig. 2.3(b)) parallel to the shear direction were measured. The heights of these four profiles obtained with the laser are presented in Fig. 2.4(a).

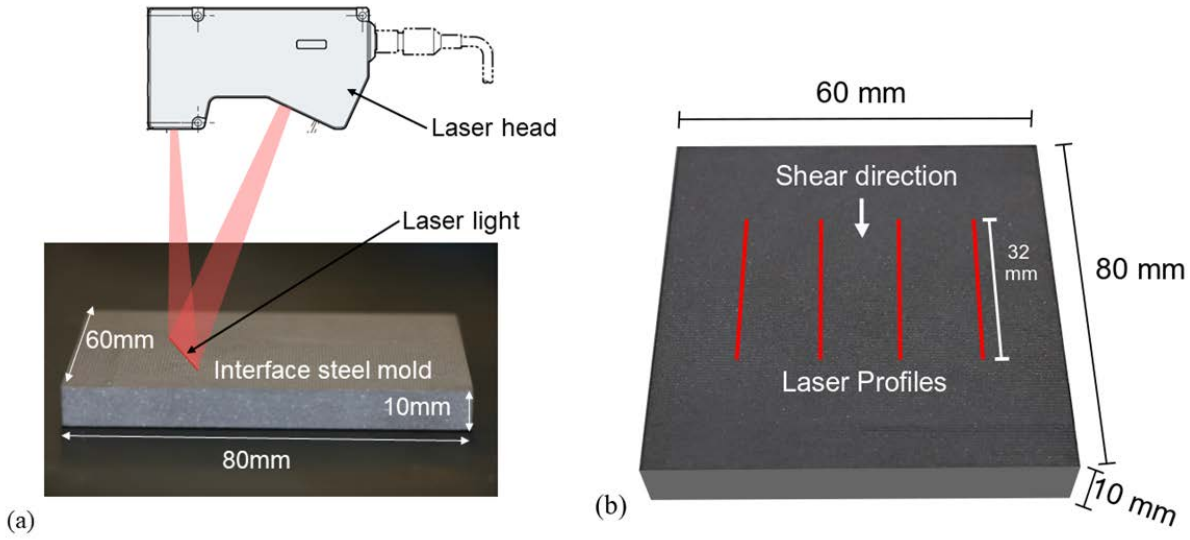

Figure 2.3: (a) Steel mould dimensions and, laser setup (b) direction and dimensions of laser profiles.

As it was explained in chapter 1 section (1.4.3.4), to determine the roughness of the interface, each profile was divided into the D_{50} of Fontainebleau sand (0.23 mm) and at each D_{50}, the R_{max} was measured . The values of R_{max} were divided by D_{50} to obtain the normalized roughness (R_n). For Fontainebleau sand, the normalized roughness R_n is presented in Fig. 2.4(c). Fig. 2.4(d) shows the normalized roughness values in a ascending order. Most of the normalized values were between 0.02 and 0.3. The largest value of normalized roughness R_n (0.32) was determined; therefore, the stainless steel plate is considered as a rough and very rough surface for Fontainebleau sand and kaolin clay.

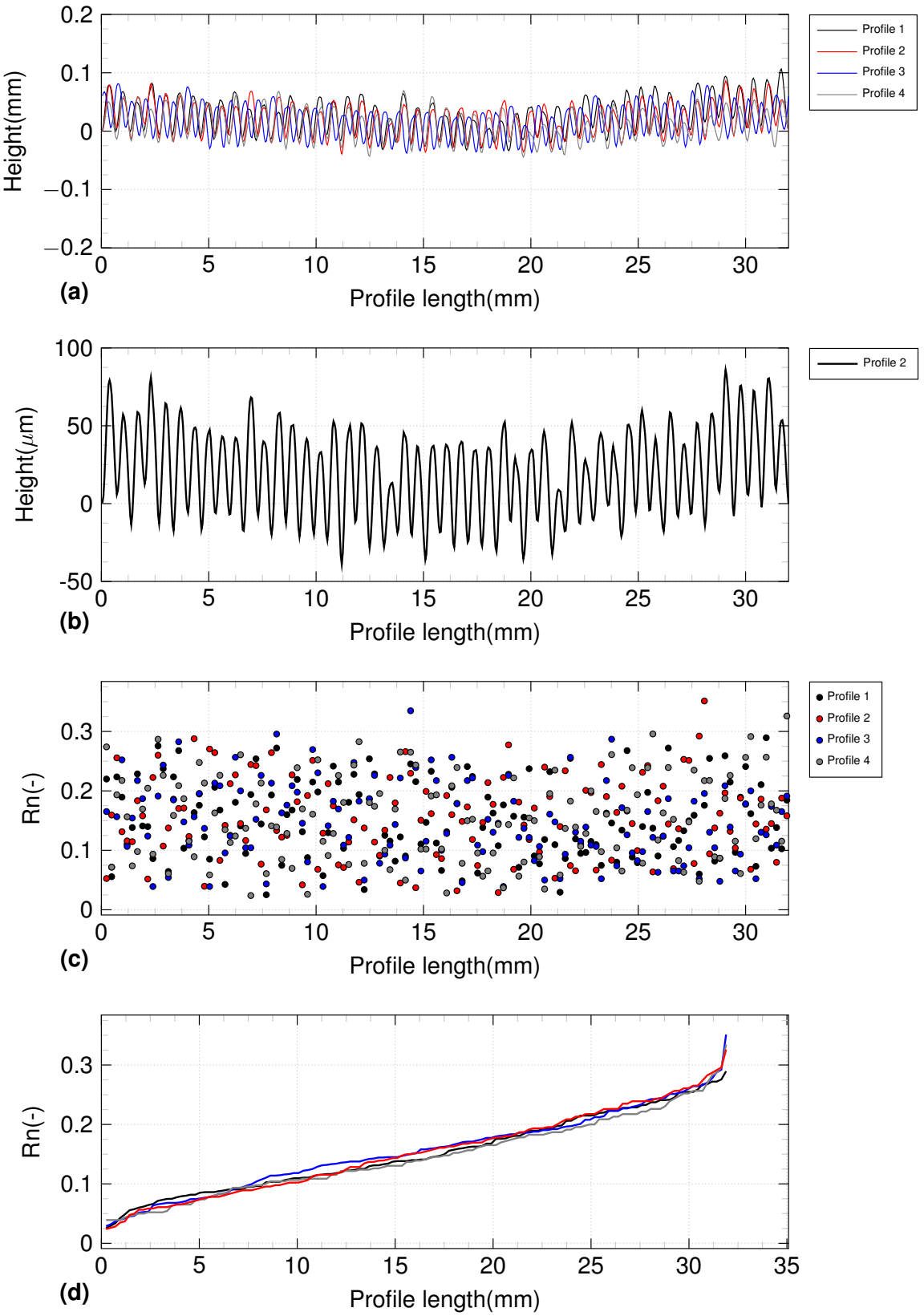

Figure 2.4: (a) Measured profiles; (b) Height of the profile N ^{o}2; (c) normalized roughness measurements for each profile length ($L = D_{50}$); (d) sorted calculated normalized roughnesses.

2.2 Materials

2.2.1 Material properties

The grain size distributions of Fontainebleau sand (siliceous) and kaolin clay used, in this study are presented in Fig. 2.5. For Fontainebleau sand the particle size distribution curve was obtained by sieving method, but for kaolin clay laser diffraction was used.

Kaolin appears as odorless white to yellowish powder (Fig. 2.6(a)). Contains mainly the clay mineral kaolinite ($Al_2O_3(SiO_2)2(H_2O)2$), a hydrous aluminosilicate. The activity is between 0.3-0.5. Due to its low activity, it is considered as non-expansive soil. Physical and geotechnical characteristics of kaolin clay are presented in Table 2.1. Yavari et al. 2016 has reported that kaolin clay has a liquid limit $LL = 57\%$, a plastic limit $PL = 33\%$; and a particle density $\rho_s = 2.60\ Mg/m^3$. Regarding its plasticity index of 24, the soil could be classified as MH or OH according to the Unified Soil Classification Standard. Thermal conductivity and volumetric specific heat capacity, measured by KD2 Pro thermal Properties analyzer device, were equal to 1.5 W/(mK) and 3.3 J/(m^{3}K) respectively.

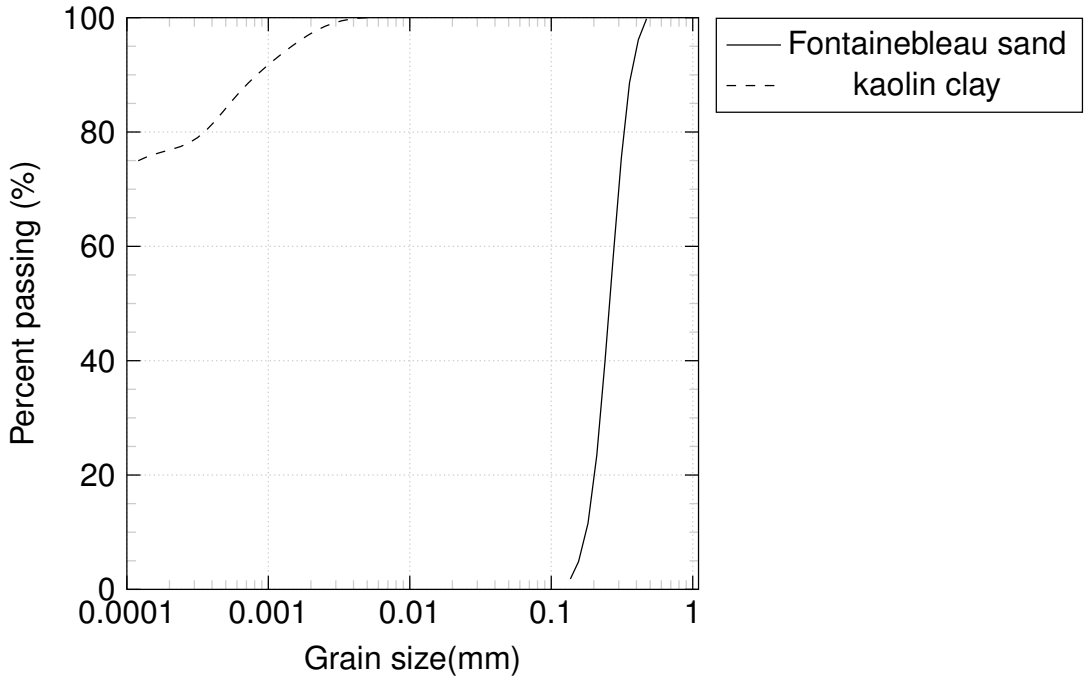

Figure 2.5: Grain size distribution of Fontainebleau sand and kaolin clay.

Table 2.1: Kaolin clay physical and thermal properties (Yavari et al. 2016)

LL (%)	PL (%)	I_p (%)	ρ_s (Mg/m^3)	λ (W/mK)	C (J/m^3K)	k (m/s)
57	33	24	2.60	1.5	3.3	10^{-8}

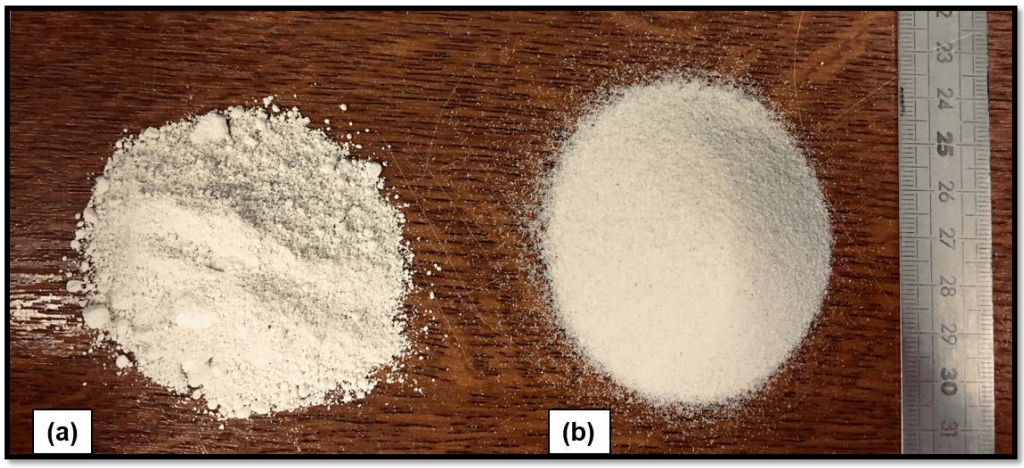

Figure 2.6: (a) kaolin clay powder (b) Fontainebleau sand.

The physical properties of Fontainebleau sand are presented in Table 2.2. The particle density is, $\rho s = 2.67\ Mg/m^3$; maximal void ratio $e_{max} = 0.94$; minimal void ratio $e_{min} = 0.54$ (De Gennaro et al., 2008); and median grain size $D_{50} = 0.23$ mm. Thermal conductivity and volumetric specific heat capacity, measured by KD2 Pro thermal Properties analyzer device, were equal to 0.2 $W/(mK)$ and 1.2 $J/(m^3.K)$, respectively.

Table 2.2: Fontainebleau sand physical properties (Pra-Ai 2013)

D_{50} (mm)	ρ_s (g/cm^3)	γ_{dmax} (kN/m^3)	γ_{dmin} (kN/m^3)	e_{max}	e_{min}	$C_u = D_{60}/D_{10}$
0.23	2.65	17.2	14.2	0.866	0.545	1.72

This sand is a siliceous sand. It has a color that ranges between grey and white (Fig. 2.6(b)). For For Fontainebleau sand NE34, Pra-Ai 2013 have reported, the values of $e_{min} = 0.545$ and $e_{max} = 0.866$, to define three states (loose ($I_{D0} = 40\%$), medium ($I_{D0} = 65$-70%) and dense ($I_{D0} = 90\%$)). These values correspond to maximum and minimum dry densities of 1.72 gr/cm^3 and 1.42 gr/cm^3 respectively (the specific gravity of the material G is taken equal to 2.65 gr/cm^3, practically pure silica). The mean grain size D_{50} is identified to be 0.23 mm for sieving method and 0.25 mm for laser granulometry. With the uniformity coefficient, from sieving method Cu ($Cu = D_{60}/D_{10}$), this sand can be considered poorly graded or uniform.

2.2.2 Sample preparation

To prepare the sand samples for the shear tests, the Fontainebleau sand with a target dry density of 1.67 Mg/m^3 was poured into the shear box and compacted using a tamper (Fig. 2.7(b)). This dry density corresponded to 90% of the relative density (D_r), and the sample was considered to be a dense sand (Table 2.2).

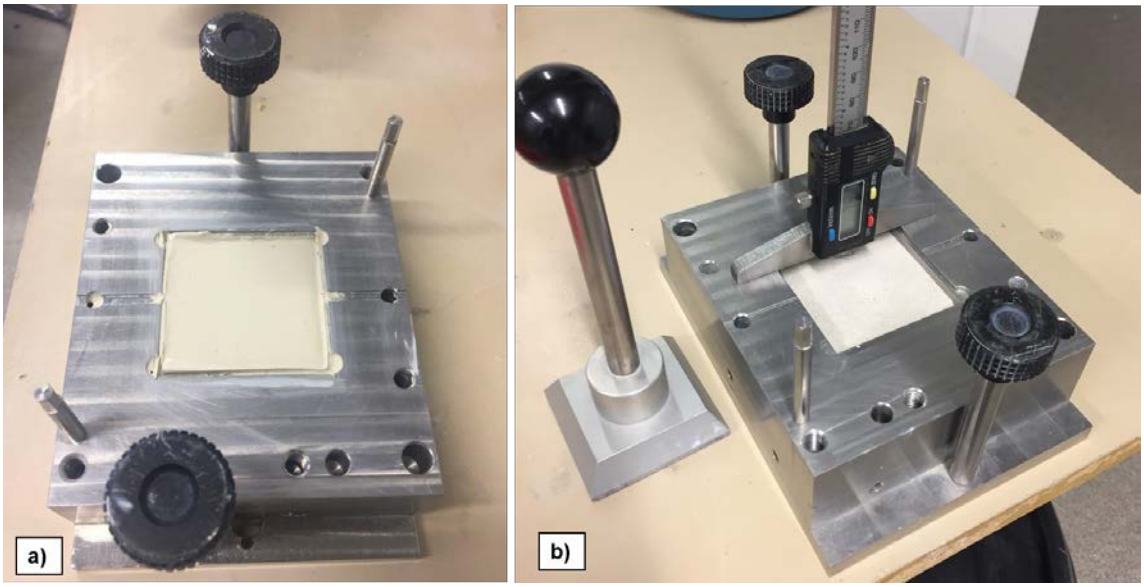

Figure 2.7: Kaolin clay and Fontainebleau sand sample preparation.

To perform the clay and clay-structure shear tests, kaolin clay was prepared with a water content of 63%, slightly higher than its liquid limit ($LL = 57\%$). The slurry was poured in a plastic film and was kept in temperature-controlled rooms (20^oC) at least for 24 hours for homogenization. Subsequently, the clay was poured into the shear box using special spoons and special attention was paid to avoid any air trap. The water content and the amount of clay that was poured in the shear box at the same time were measured. Afterwards, the surface of the clay samples were cleaned and smoothed using a special steel spatula. This part allowed to have clay samples which all have the same density (Fig. 2.7(a)).

2.3 Monotonic program procedure

This section contains the kaolin clay consolidation results, shearing rate determination methods, constant normal stiffness condition application method and verification of its adequate application. The monotonic experimental program for both sandy and clayey soil is also presented.

2.3.1 Kaolin compressibility

To perform all the clay-clay and clay-structure interface tests on kaolin clay samples with the same initial conditions, an oedometric test was performed in the direct shear device to determine the target void ratios for different normal stresses. The normal stress was applied incrementally to the clay sample till 400 kPa (Fig. 2.8). The target void ratios for 100 and 300 kPa were $e = 1$ and 0.85, respectively. The compression

index for the tested kaolin was found to be $C_c = 0.23$.

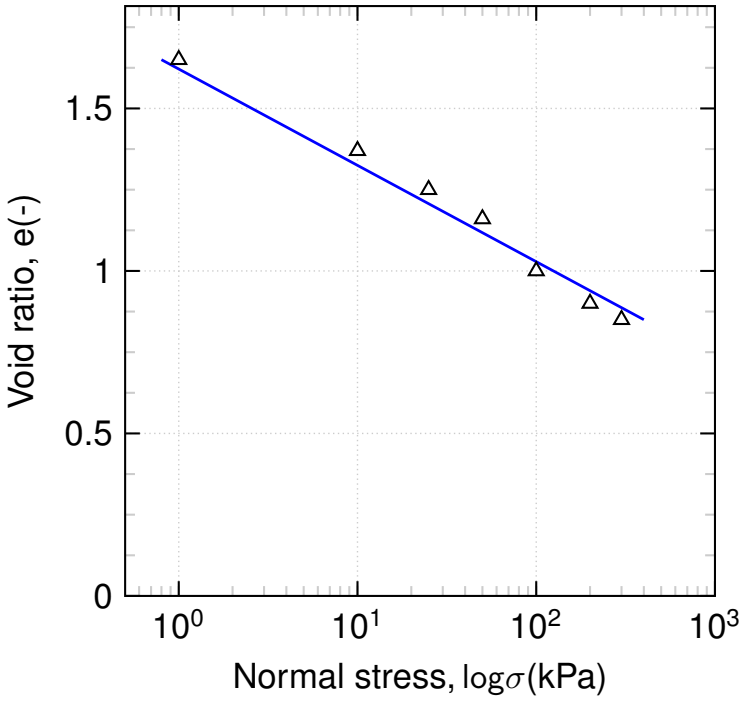

Figure 2.8: kaolin compression.

2.3.2 Shearing rate determination

To determine the appropriate shearing rate for clay-clay and clay-structure interface tests and to avoid excess pore water pressure generation, several methods that have been proposed in the literature were used (ASTM 1998; Head et al. 1998 and Gibson and Henkel 1954). The rate of displacement at which the specimen should be sheared in a drained test depends upon the drainage characteristics, i.e. the permeability of the soil and the thickness of the sample. Since the permeability is related to the coefficient of consolidation, the consolidation stage of the test can provide the data for estimating a suitable time to failure (Head et al. 1998). The rate of shearing should be determined in a way that no excess pore water pressure be generated due to the shear.

In the method proposed by Taylor 1948 to find t_{90} from the settlement versus square root of the time, first a line is traced for the beginning part of the curve AB and then draw AC in a such way that OC=1.15 OB. The abscissa of point, which is the intersection of AC and the consolidation curve, gives the square root of time for 90% consolidation (Fig. 2.9(a)). Based on the obtained t_{90}, ASTM 1998 proposed the following equation:

$$t_f = 11.6 \times (t_{90}) \tag{2.1}$$

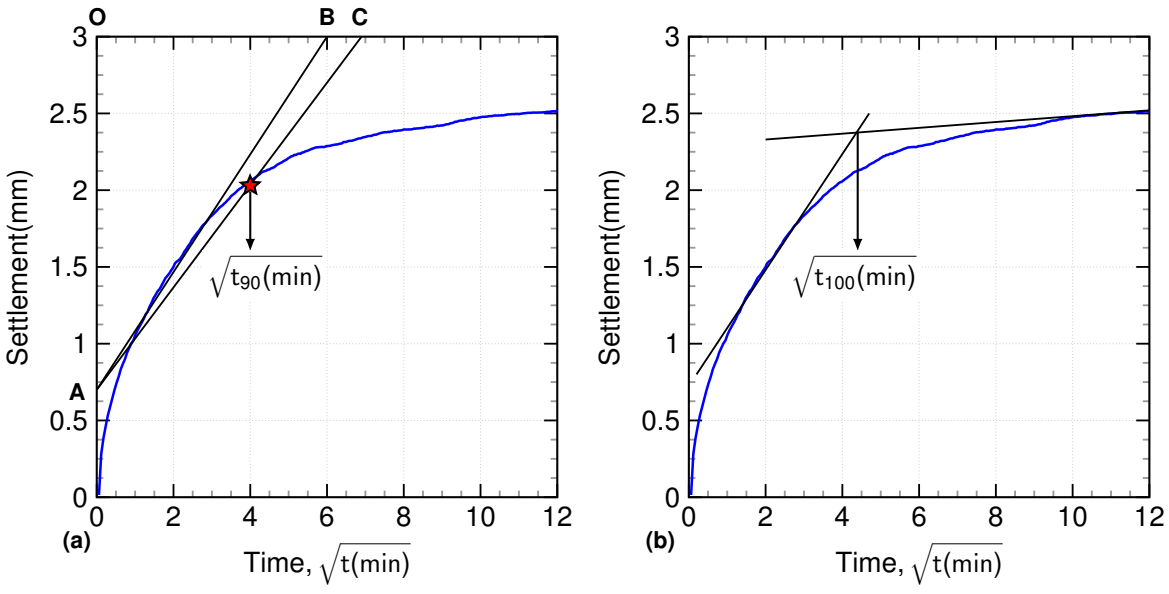

Figure 2.9: kaolin consolidation.

The method that have been proposed by Gibson and Henkel 1954; first the t_{100} of the consolidation curve should be determined (Fig. 2.9(b)) afterwards using the following equation the total time of shearing can be calculated.

$$t_f = 12.7 \times (t_{100}) \tag{2.2}$$

According to the French standards on direct shear testing (AFNOR, 1994), the corresponding equation, which gives the shear rate, is as follows:

$$\dot{\epsilon} = 125(\mu m)/t_{100}(min) \tag{2.3}$$

Several shearing rates have been calculated based on the proposed equations, but in order to avoid the excess pore water pressure generation during shearing, the rate of 0.006 mm/min was applied.

2.3.3 Constant normal stiffness application

Under constant normal stiffness (CNS) conditions, two general behaviors are observed in soils: dilative (dense or overconsolidated soils) and contractive (loose or normally consolidated soils). In the first case, with starting the shear the soil at the interface starts to contract slightly ($\Delta u > 0$) at the beginning of the test, and the amount of normal stress decreases (due to the stiffness of the soil in contact with the interface (virtual springs)). After this slight compression, the soil starts to dilate ($\Delta U < 0$), and this dilation acts on the surrounding soil. Due to the compression of the surrounding soil, the amount of the normal stress increases ($\Delta \sigma > 0$). This normal stress rise,

consequently increases the shear strength of the soil at the interface. Conversely, in the second case (loose or normally consolidated soils), the soil at the interface contracts ($\Delta U > 0$), and the normal stress decreases ($\Delta\sigma < 0$) until the shear ceases.

To apply CNS conditions to the samples tested in the temperature-controlled direct shear device, the following procedure was implemented in the command software:

1. The total desired shear displacement, W(8 mm) was divided into 100 segments ($w/100 = 0.08$ mm).
2. In order to reach the desired W(8 mm) value: $(W/100) \times i \qquad i = [1, 2, 3, ..., 100]$ where i is the number of segments.
3. At the end of each segment, the device measures the vertical displacement difference between the beginning of the segment and the end of the segment ($\Delta U = \Delta U_{i_2} - \Delta U_{i_1}$).
4. Then, according to Eq. 1.2, this difference ($\Delta U(mm)$) is multiplied by the value of stiffness (K (kPa/mm)), and the consequent normal stress ($\Delta\sigma_n$) that should be applied is calculated.
5. This process is repeated for all segments i(100) until the total shear displacement is reached.

To verify the device for the stiffness application, the variations of normal stress ($\Delta\sigma$) with normal displacement (ΔU) are presented in Fig. 2.10. The slope of these curves represents the stiffness value ($\Delta\sigma/\Delta U = -K$). Fig. 2.10(a) shows the verification results for $K = 5000$ kPa/mm. Tests at different temperatures with same stiffness were compared to verify the normal stiffness application with temperature variations. For all of the performed tests, the starting point is the initial normal stress (100 kPa). Fig. 2.10(b) shows the verification results for $K = 1000$ kPa/mm. The difference between the applied and obtained stiffness values is around 2%.

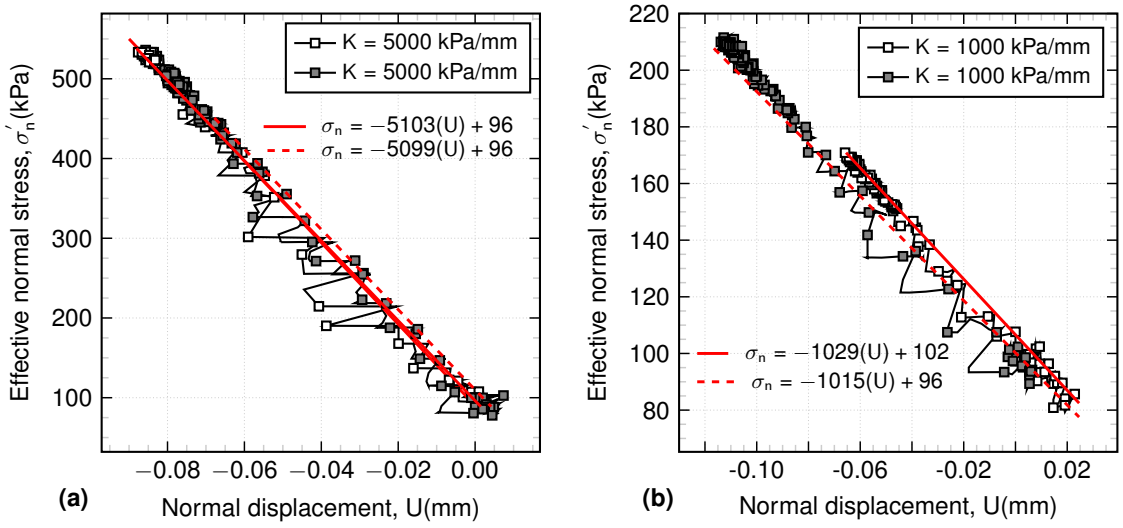

Figure 2.10: Imposed stiffness verification. (a) $K = 5000$ kPa/mm; (b) $K = 1000$ kPa/mm. $\sigma'_{n0} = 100$ kPa.

2.3.4 Experimental program

2.3.4.1 Sand program

The soil-soil and soil-structure interface experimental program and stress path are detailed in Table 2.3 and Fig. 2.11, respectively. As it was discussed, the Fontainebleau sand with a target dry density of 1.67 Mg/m^3 was poured into the shear box which corresponded to 90% of the relative density (D_r), and the sample was considered to be a dense sand (Table 2.2).

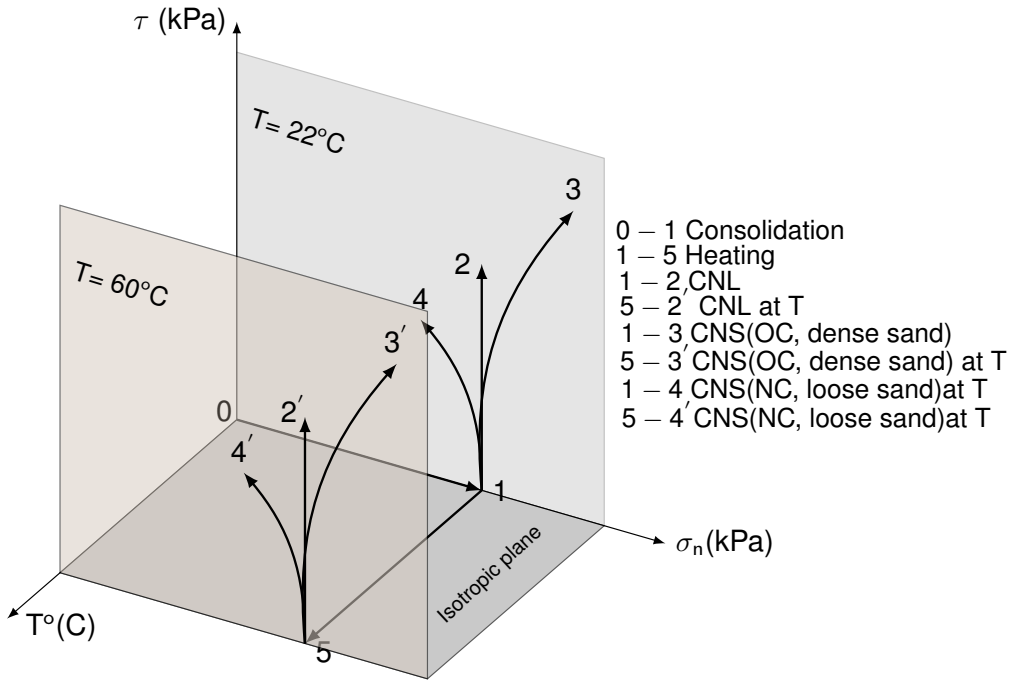

Figure 2.11: Thermo-mechanical path in this study.

Then, the normal stress was applied to the sand sample (path 0-1 in Fig. 2.11). After applying the normal stress, to shear the samples in CNL condition at 22 ^oC, a shear rate of 0.1 mm/min was applied (path 1-2).For the CNL tests at 60 ^oC, the heating phase (path 1-5, Fig. 2.11) was applied with a rate of 10 $^oC/hr$ then, the shearing phase (path 5-2$'$) started. For the sand-structure tests, the above-mentioned procedure was performed. For the sand-structure CNS tests, due to the dense state of the soil, path 1-3 at 22 ^oC and path 5-3$'$ at 60 ^oC were observed (Fig. 2.11). In sand-structure tests, CNL and CNS tests were performed at 22 and 60 ^oC. For CNS tests, different stiffness values were chosen (K = 500, 1000, and 5000 kPa/mm), that were used in previous studies (Boulon and Foray 1986; Mortara 2001; Pra-Ai 2013). Increasing the stiffness value restrains the volumetric response of the interface until a certain case of constant normal stiffness which is called the constant volume condition (CV). These values were chosen to cover the entire range of constant normal stiffness conditions, from very small ranges close to CNL, up to very high values close to CV.

Table 2.3: Experimental programme of soil and soil-structure interface tests.

	$\sigma_n(kPa)$	K (kPa/mm)	$T^o(C)$	Type of test
Sand	100, 200, 300	0	22^o	CNL
			60^o	CNL
Sand-structure	100, 200, 300	0	22^o	CNL
			60^o	CNL
Sand-structure	100	500, 1000, 5000	22^o	CNS
			60^o	CNS
	100, 200, 300	1000	22^o	CNS
Clay	100, 300	0	5^o	CNL
			22^o	CNL
			60^o	CNL
Clay-structure	100, 300	0	5^o	CNL
			22^o	CNL
			60^o	CNL
		1000	22^o	CNS
			60^o	CNS

To perform the CNS tests, two scenarios were considered. First, shear tests with different stiffness values (K = 500, 1000, and 5000 kPa/mm) and constant effective normal stress (σ'_{n0} = 100 kPa) were performed at 22 and 60 ^oC. The aim of this part was to determine the effect of different stiffness values at 22 and 60 ^oC on sand-structure interface. The second scenario, was interface shear tests at three different effective normal stress values (σ'_{n0} =100, 200 and 300 kPa) with a constant stiffness value (K = 1000 kPa/mm). This scenario was performed to determine the friction angle of the interface and also compare the CNS and CNL tests.

2.3.4.2 Clay program

Two values of initial effective normal stresses (σ'_{n0} = 100, 300 kPa) were chosen for the clay-clay and clay-structure interface program. Based on the consolidation tests performed on this kaolin clay (Fig. 2.8), the target void ratios after consolidation for σ'_n = 100 and 300 kPa were e = 1 and 0.85, respectively. Therefore,the normal stress was applied incrementally to achieve the desired target void ratio for each normal stress. After the consolidation phase for the CNL tests at 22 ^oC, a displacement rate of 0.006 mm/min was applied. This slow rate ensured drained conditions inside the shear box during shearing. The initial heating or cooling phase started at ambient temperature (22 ^oC). After the consolidation phase, heating or cooling was applied to the samples at a rate of 5 $^oC/hr$. This slow rate avoids a pore water pressure increase during the heating phase as demonstrated by Cekerevac and Laloui 2004 and Di Donna et al. 2015.

During the heating or cooling phase in the shear box, thermal vertical deformation of the soil and the soil-structure interface was measured. After these heating or cooling phases, the samples were sheared. For the CNL tests of the clay and clay-structure interface, paths 1-2 and 5-2′ were applied, as can be seen in Fig. 2.11, but for the CNS clay-structure interface tests, paths 1-4 and 5-4′ were observed due to the normally consolidated state of the kaolin samples.

2.4 Cyclic program procedure

The device is able to control both deformation and stress modes. To perform stress-controlled cyclic tests, the cyclic shear stress should fluctuate between two values of shear stress ($\pm\tau_{cy}$). To develop the device to perform correct and pertinent cyclic shear tests several protocols were developed in the commanding software of the device and consequently were tested. The device was programmed to vary the cyclic shear stress between two values (Fig. 2.12(a) and (b)). The shear strain curve consisted of a total shear strain and plastic shear strain that is presented in (Fig. 2.12(c)). The objective was to record the plastic strain at the end of each cycle. Therefore, the device was programmed to save the last shear strain at the end of each cycle (line A-B in Fig. 2.12(c)). to keep the volume of samples constant during the tests, the vertical stress varied and its evolution is presented in Fig. 2.12(d).

The shear failure was defined to the 10% of shear strain. After cycling between two shear stress values, the strain accumulation drives the interface to a point that it is no more capable to support any further cycles between two cyclic shear values, in this condition, the device starts the monotonic shearing till 10% of shear strain. The point which no longer the interface is capable of supporting further cycles can be defined as the failure point (Fig. 2.12(b)). One of the differences between cyclic triaxial and direct shear tests is the difference between the stress conditions in both tests. In triaxial tests, after certain cycles, the cross section of the sample evolves and therefore the cyclic shear stress and average shear stress that is applied to the samples is not the same as it was applied at the beginning of the test. On the contrary in the direct shear test, the same cyclic and average shear stress is applied to the sample till the failure point, which in this point the soil the cyclic solicitations goes beyond the interface shear capacity and the interface fails. To apply equivalent-undrained conditions in the clay-structure interface tests, the constant-volume equivalent-undrained concept is used in this study. As in the extreme case of constant normal stiffness condition (K= ∞), the vertical stress is varied to keep the volume of the sample constant. Mortezaie and Vucetic 2016; Dyvik et al. 1987; Vucetic and Lacasse (1984) have performed constant volume shear tests in simple shear device. They have shown that in drained conditions

while the pore water pressure is zero, the change in the vertical stress to keep the volume of the sample constant is equivalent to the pore water pressure generated in a truly undrained triaxial test. Several studies have confirmed this approach, using direct shear device (Takada 1993; Hanzawa et al. 2007), therefore, the experimental program proposed in this study is on the basis of constant-volume equivalent-undrained (CVEU) tests.

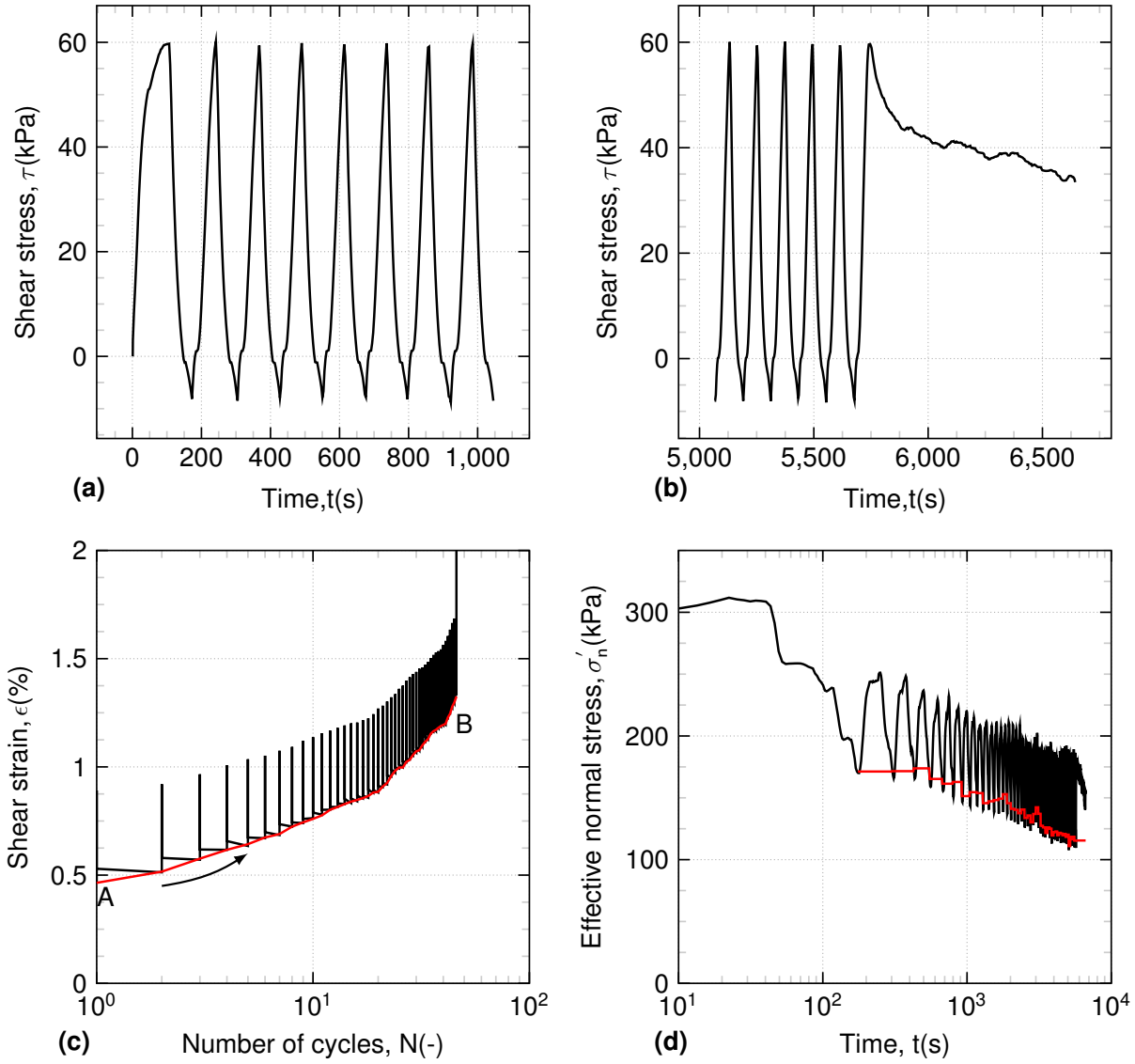

Figure 2.12: Typical one cyclic clay-structure interface results. (a) the shear stress fluctuations between $\pm\tau_{cy}$; (b) the failure point and post cyclic failure; (c) total and plastic shear strain at each cycle; (d) the normal stress resuction upon cycling.

The experimental program consisted of monotonic and cyclic constant volume equivalent undrained (CVEU) clay-clay and clay-structure interface direct shear tests at different temperatures (Table 2.4 and Table 2.5). Monotonic tests consisted of clay-clay and clay-structure interface tests to determine essential parameters for cyclic experimental program such as S_u^{Ds} (undrained shear strength in direct shear), also to be as a

Table 2.4: Monotonic experimental program.

N^o	$\sigma_{n0}^{'}(kPa)$	S_u^{Ds} (kPa)	$T^o(C)$	$w_i\%$	$w_f\%$	$\dot{\epsilon}(\%/min)$	Tt
1	300	56.4	22^o	62.3	37.2	0.01	clay-clay
2		56.4		63.3	43.2	0.02	
3		63.1		59.6	36.0	0.01	clay-structure
4		63.2		60.5	36.2	0.02	

Table 2.5: Cyclic experimental program.

N^o	$\sigma_{n0}^{'}$ (kPa)	τ_a (kPa)	τ_{cy} (kPa)	S_u^{Ds} (kPa)	τ_a/S_u^{Ds} (-)	τ_{cy}/S_u^{Ds} (-)	T $^o(C)$	N_f (-)	w_i %	w_f %
6*	300	23	27	56.4	0.41	0.47	22^o	370	63.0	36.6
7	300	26	36	63.1	0.41	0.57	22^o	39	63.0	36.6
8			36			0.57	60^o	165	61.4	39.3
9			34			0.54	22^o	46	60.9	36.4
10			34			0.54	60^o	137	61.7	35.7
11			30			0.47	22^o	185	60.7	42.5
12			30			0.47	60^o	645	63.0	35.1
13			22			0.35	22^o	4138	63.0	35.1
14			22			0.35	60^o	>10000	63.0	35.1
15	300	28	34	63.1	0.44	0.54	22^o	65	62.4	37.8
16			34			0.54	60^o	111	61.7	38.0
17	300	30	30	63.1	0.47	0.47	22^o	230	62.2	36.5
18			30			0.47	22^o	246	61.3	(-)
19			30			0.47	60^o	991	61.2	35.0
20		24	30			0.38	22^o	57	62.5	37.3
21			30			0.38	60^o	355	61.4	35.6
22	300	30	22	63.1	0.47	0.35	22^o	>1000	60.6	37.3
23							60^o	>1000	61.3	40.4

*: clay-clay test. $w_i(\%)$: initial water content, $w_f(\%)$: final water content

reference to better understand their cyclic behavior. The cyclic program consisted of two parts, the first one, cyclic clay-clay tests were performed to investigate the difference between clay-clay and clay-structure interface cyclic behavior. The second part was dedicated to the cyclic clay-structure interface tests.

For cyclic tests, the shear stress was increased to the mean value (τ_a) and then the shear cycles were applied between $\tau_a + \tau_{cy}$ and $\tau_a - \tau_{cy}$ with a frequency of 0.005 Hz. The cycles were continued till a shear strain of 10% reached. Failure was defined when the shear strain reached 10%. When the sample do not support any further cycles between maximum and minimum values of the shear stress, the post-cycle shear (after failure point) starts automatically. The volume of the sample was kept constant during whole of the test.

Two types of tests were performed, the first one consisted of a constant average shear stress ratio τ_a/S_u^{Ds} (ASR) while varying the cyclic shear stress ratio τ_{cy}/S_u^{Ds}

(CSR). The second type was performed with a constant cyclic stress ratio τ_{cy}/S_u^{Ds} but the average stress ratio τ_a/S_u^{Ds} was changed. The cyclic stress ratio τ_{cy}/S_u^{Ds} between 0.35 to 0.57 and the average stress ratio τ_a/S_u^{Ds} between 0.38 to 0.47 was chosen in order to cover a wide range of stress ratios effects on the interface behavior. The same range of values can be found in the literature for clays (Wichtmann et al. 2013; Thian and Lee 2017; Zhou and Gong 2001).

2.5 Repeatability tests

To check the repeatability of the tests several monotonic and cyclic direct shear interface tests were performed on sand/clay-structure interface at 22 and 60 ^{o}C (Fig. 2.13 and Fig. 2.14). Fig. 2.13 shows the tests conducted under 100 and 300 kPa of normal stress. Fig. 2.13(a) shows the repeatability tests for sand-structure interface at 22^{o}C under 100 kPa. The shear stress-displacement curves and volumetric responses are perfectly superimposed (Fig. 2.13(a) and (b)). Fig. 2.13(c) shows the repeatability tests for clay-structure interface at 22^{o}C under 300 kPa. The difference between peak shear stresses is 3-4 kPa. In terms of volumetric response (Fig. 2.13(d)) is around 0.15 mm at large shear displacements. Fig. 2.13(e) shows the clay-clay tests at 60 ^{o}C under 300 kPa. The difference of peak shear stresses is around 4 kPa but at larger shear displacements the shear stress curves are identical. The volumetric behavior shows a difference of 0.1 mm (Fig. 2.13(f)). One of the most determinant factors in direct shear results in terms of shear and volumetric is the volumetric evolution of shear band during shear. The repeatability in terms of shear stress-displacement shows a reasonable agreement on the contrary due to the strong dependence of volumetric behavior of samples to the shear band thickness between two shear box halves, the volumetric behavior in direct shear tests is one of the most difficult parameters to be repeated.

Fig. 2.14 shows the cyclic CVEU clay-structure interface at 22 ^{o}C that has been performed twice to check its repeatability. The average and cyclic stress values are both 30 kPa (τ_a/S_u^{Ds} and τ_{cy}/S_u^{Ds} =0.47). The repeatability in terms of stress-strain response is illustrated in Fig. 2.14(a). The reduction of effective normal stress to keep the volume of the sample constant for both tests is presented in Fig. 2.14(b). The undrained shear strength of clay-structure interface was S_u^{Ds} = 63 kPa therefore both τ_a and τ_{cy} are 30 kPa. Fig. 2.14(c) shows the shear strain versus number of cycles for both tests. The number cycles to failure for both tests is around 283 cycles. Fig. 2.14(d) shows the permanent shear strain versus number of cycles which for both tests, satisfactory repetition is observed. Fig. 2.14(e) and (f) are equivalent pore water pressure and degradation index with number of cycles.

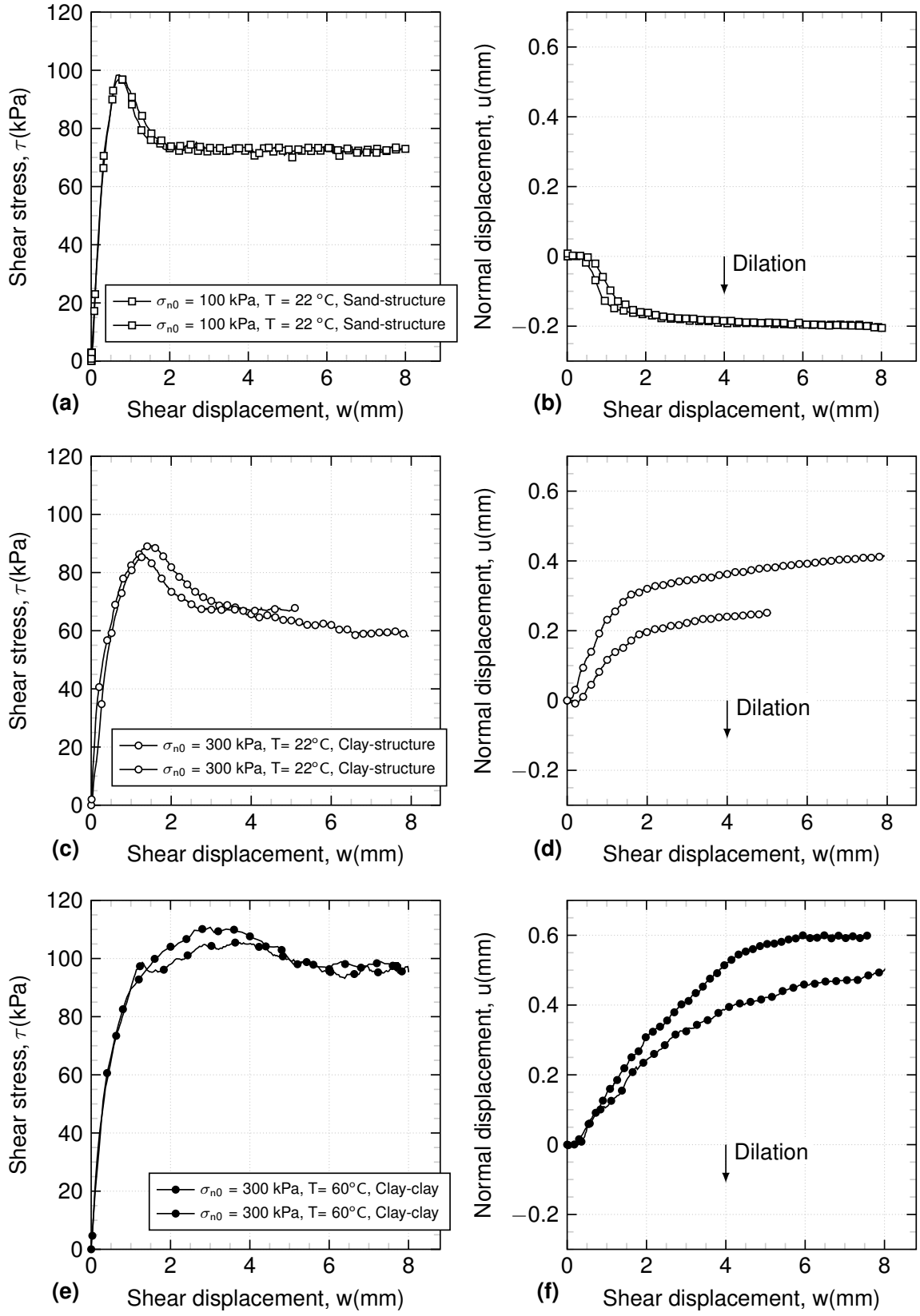

Figure 2.13: Soil-structure interface repeatability tests.

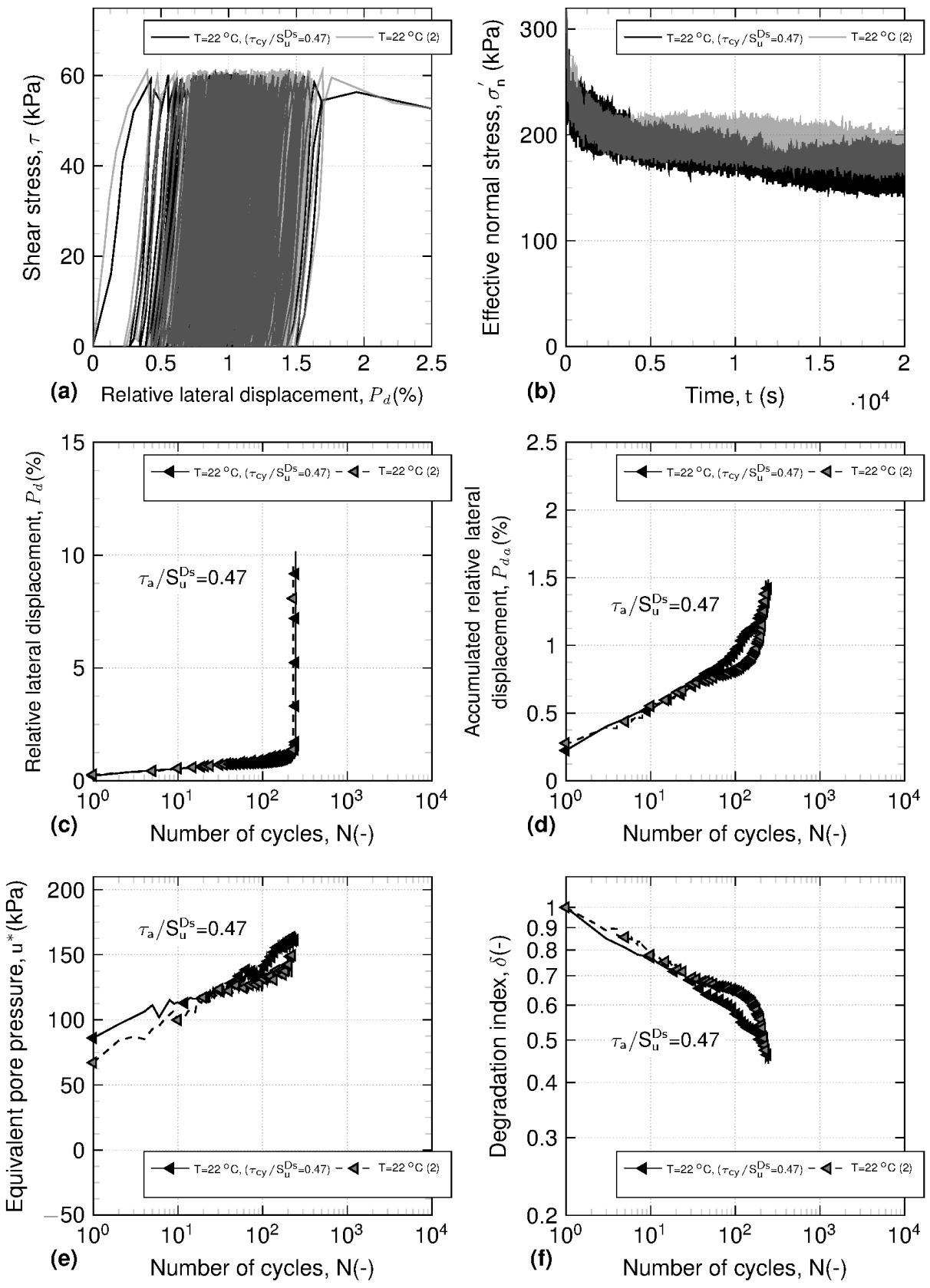

Figure 2.14: Soil-structure interface repeatability tests.

2.6 Conclusions

In this chapter the detailed description of materials used in this study was provided. The temperature-controlled direct shear device details and thermal calibration of the device was discussed. The different methods for sample preparation for sand-structure interface and clay-structure interface was presented. The experimental program for monotonic and cyclic chapter were presented. The methods for shearing rate calculations and constant normal stiffness application in the device were detailed. At the end the repeatability tests were presented. Fontainebleau sand and kaolin clay were chosen as reference soils for direct shear tests. The particle size distribution analysis were performed on both kaolin and Fontainebleau sand. The stainless steel with a certain roughness was designed and fabricated. Detailed methods for surface roughness measurements are described and calculated roughness measurements are presented. The heating system, commanding and data logging system in temperature-controlled direct shear device is presented.

Detailed description of experimental protocols developed in the direct shear device to perform constant normal stiffness conditions (CNS) was explained and validation results were presented.

Chapter 3

Thermal effects on the mechanical behavior of soil-structure interface

Abstract

The mechanical behaviour of the soil-structure interface plays a major role in the shear characteristics and bearing capacity of foundations. In thermo-active structures, due to non-isothermal conditions, the interface behaviour becomes more complex. The objective of this study is to investigate the effects of temperature variations on the mechanical behaviour of soils and soil-structure interface. Constant normal load (CNL) and constant normal stiffness (CNS) tests were performed on soil and soil-structure interface in a direct shear device at temperatures of 5, 22 and 60 ^{o}C. Fontainebleau sand and kaolin clay were used as proxies for sandy and clayey soils. The sandy soil was prepared in a dense state, and the clayey soil was prepared in a normally consolidated state. The results showed that the applied thermal variations have a negligible effect on the shear strength of the sand and sand-structure interface under CNL and CNS conditions, and the soil and soil-structure interface behaviour could be considered thermally independent. In clay samples the temperature increase, increased the cohesion and consequently the shear strength, due to thermal contraction during heating. The temperature rise had less impact on the shear strength in the case of the clay-structure interface than in the clay samples. The adhesion of the clay-structure interface, is less than the cohesion of the clay samples.

Keywords: Shear strength, Constant normal stiffness (CNS), Soil-structure interface, Temperature, Thermo-active structures.

Résumé

Le comportement mécanique de l'interface sol-structure est d'une grande importance en raison du rôle de l'interface dans la résistance due au frottement et la capacité portante des structures. Dans les structures thermo-actives du fait de la variation

de la température, le comportement de l'interface devient plus complexe. L'objectif de ce travail est d'étudier l'effet des variations de température sur le comportement mécanique de l'interface sol-structure. Des essais avec des conditions de charge normale constante (CNL) et de rigidité normale constante (CNS) ont été réalisées dans une boîte de cisaillement direct à différentes températures, 5 ^{o}, 22 ^{o} et 60 ^{o} C sur des éprouvettes sol-sol et sol-structure. Le sable de Fontainebleau et le kaolin ont été utilisés comme materiaux de référence pour les sols sableux et argileux. Les résultats ont montré que les variations thermiques appliquées ont un effet négligeable sur la résistance au cisaillement des interfaces sable-sable et sable-structure dans les conditions CNL et CNS et que le comportement du sable peut être considéré comme étant indépendent de la température. Dans l'argile étudiée, l'augmentation de la température augmente la résistance au cisaillement en raison de la contraction thermique pendant le chauffage, ce qui augmente la cohésion du sol. L'augmentation de température a eu moins d'impact sur la résistance au cisaillement dans le cas de l'interface argile-structure que dans les échantillons argile. L'adhésion de l'interface argile-structure est inférieure à la cohésion de les échantillons d'argile.
Mots clés: Resistance au cisaillement, rigidité normale constante, interface sol-structure, température, geostructures thermo-actives.

3.1 Introduction

The bearing capacity of foundations is highly dependent on the mechanical behaviour of the soil-structure interface. Therefore, the soil-structure interactions at the interface are of primary importance in foundation designs. Due to the recent developments of clean energy, traditional geostructures such as piles and diaphragm walls have been converted to energy geostructures by installing heat exchanger tubes inside the concrete element (Brandl 2006). In energy geostructures the mechanical loads applied to the structure on one hand, and the effect of heat exchange between structure and surrounding soil on the other hand, modify the behaviour of the soil-structure interface. These thermal variations and mechanical loads affect the bearing capacity and frictional resistance of these thermo-active structures. Therefore, the effects of temperature on the soil-structure interface mechanical parameters should be investigated. In this section, a state of the art about the behaviour of the soil-structure interface and its influencing parameters under isothermal conditions are presented. Then, existing studies on the effects of temperature on the mechanical behaviour of soils and soil-structure interfaces are discussed.

Grain size, grain crushability, grain roundness, soil density, initial stress state, structure roughness and shearing rate based on interface tests were addressed as the pa-

rameters influencing the soil-structure interface mechanical behaviour (Potyondy 1961; Desai et al. 1985; Boulon and Foray 1986; Uesugi and Kishida 1986; Poulos and Al-Douri 1992; Jardine et al. 1993; Lehane et al. 1993; Fakharian and Evgin 1997; Mortara 2001; Pra-Ai 2013).

An important concept to aid in understanding the interface behaviour is the constant normal stiffness (CNS) conditions, which explains the real shear behaviour of embedded foundations; as discussed in the following. The physical concept of constant normal stiffness (CNS) conditions at the soil-structure interface, was introduced by Wernick 1978 (Fig. 3.1). Depending on the volumetric response of the soil at the interface during shearing (dilative or contractive), the surrounding soil stiffness constrains the volumetric response of the interface and acts as a virtual spring with a given stiffness (Eq. 3.1).

$$\Delta\sigma = -K.\Delta U \tag{3.1}$$

Where $\Delta\sigma$(kPa) is the normal stress difference, K(kPa/mm) is the stiffness of the adjacent soil (stiffness of the spring) and ΔU(mm) is the normal displacement difference of the interface.

The tendency of the interface to dilate is counteracted by the elastic reaction of the adjacent soil (Hoteit 1990; Tabucanon et al. 1995 Fioravante et al. 1999). Porcino et al. 2003 performed constant normal load (CNL) and constant normal stiffness (CNS) tests on sand-steel interface and showed that the effect of the normal stiffness (K) on the mobilized shear resistance of the interfaces in CNS tests depends on the volumetric response exhibited by the interfaces in the CNL tests. They showed that in dilative regimes, the increase in the current normal stress (σ_n) when sheared in the CNS tests causes an increase in the current shear stress (τ). On the other hand, in the contractive regimes (smooth interface or loose soil), a decrease in the normal and shear stresses is observed. They also concluded that the increase or decrease in the mobilized shear resistance during the CNS tests are a consequence of the current normal stress evolution, and these changes in mobilized shear resistance are not an effect of the mobilized sand-structure friction angle modification, which remains unchanged.

Another important factor that influences the soil-structure interactions is the structure surface roughness (Kishida and Uesugi 1987; Porcino et al. 2003; Hu and Pu 2003). Normalized roughness (R_n), as reported by Uesugi and Kishida 1986; was defined by measuring R_{max} (vertical distance between the highest peak and lowest valley) along a profile length L equal to the mean grain size D_{50} and then normalized by D_{50}:

$$R_n = \frac{R_{max}(L = D_{50})}{D_{50}} \tag{3.2}$$

Previous investigations (Uesugi and Kishida 1986; Uesugi et al. 1989; Hu and Pu

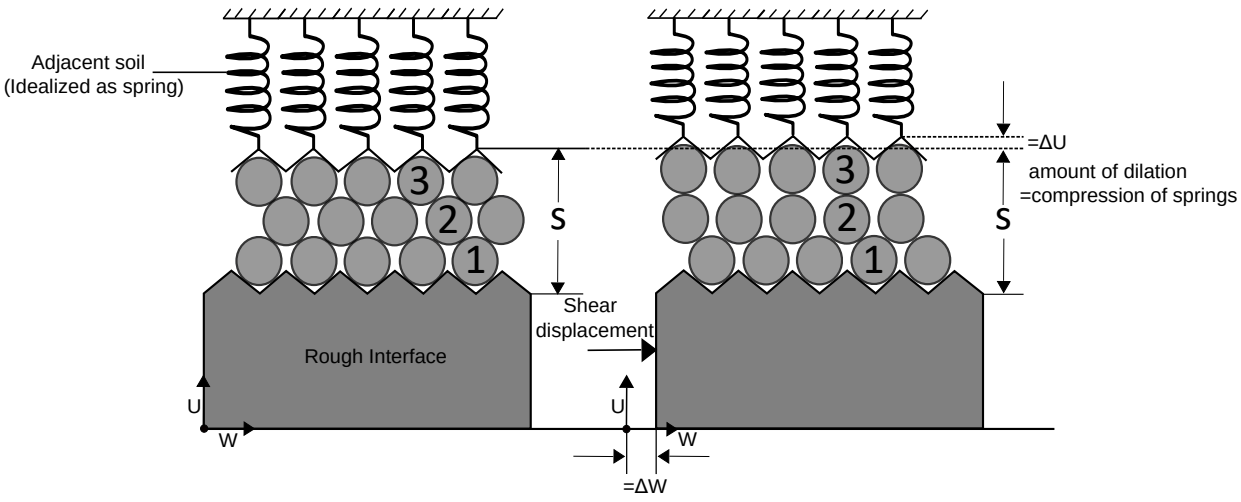

Figure 3.1: CNS concept of the soil-structure interface (after Wernick 1978).

2003) indicate a range for the smooth and rough surfaces. The critical roughness ($R_{crit} = 0.1 - 0.13$) was chosen as a range that ($R_n > R_{crit}$) is a rough surface and ($R_n < R_{crit}$) is considered as a smooth one.

The interface behaviour under non-isothermal conditions is a coupling between the above-mentioned parameters and temperature variations. In the following section, the thermal effects on the mechanical parameters of soils and the soil-structure interface are discussed. Different studies have been performed on the effects of temperature on the mechanical parameters of soils (Campanella and Mitchell 1968; Hueckel and Baldi 1990; Kuntiwattanakul et al. 1995; Burghignoli et al. 2000; Cui et al. 2000; Delage et al. 2000; Cekerevac and Laloui 2004; Abuel-Naga et al. 2006; Boukelia et al. 2017; Eslami et al. 2017; Jarad et al. 2017), and these studies indicated that the thermo-mechanical behaviour of soils is highly dependent on the stress and thermal history of the material. However, only a few studies have been performed on the soil-structure interactions under non-isothermal conditions (Di Donna et al. 2015; Yavari et al. 2016). Di Donna et al. 2015 performed interface direct shear tests on quartz sand and illite clay at different temperatures (22, 50 and 60 ^oC). These tests showed that the sand-concrete interface behaviour was not directly affected by temperature changes, but the clay-concrete interface showed higher shear strength at higher temperatures. The residual interface friction angle of the clay-concrete decreased slightly at high temperatures, but the adhesion (cohesion between soil and structure) increased with increasing temperature. The authors suggested that this result is related to the thermal consolidation of the clay, which results in an increase of the contact surface between the clay and concrete. Yavari et al. 2016 conducted soil-structure interface direct shear tests on Fontainebleau sand and kaolin clay samples at 5, 20 and 40 ^oC. The shear strength of the clay samples was higher than that of the clay-concrete interface, and the

effects of temperature (in the range of 5-40 ^oC) on the shear strength and friction angle were negligible in the sand, clay and clay-concrete interface. They pre-consolidated all the samples to 100 kPa of vertical stress and heated to 40 ^oC prior to the application of the initial conditions. Therefore, they found that the effect of temperature on the clayconcrete interface, which was mainly related to thermal consolidation, was negligible.

According to the literature, the effects of temperature on the friction angle and adhesion of the soil-structure interface, are poorly understood under both CNL and CNS conditions. In this study, a temperature-controlled direct shear device was used to perform interface tests on Fontainebleau sand and kaolin clay on a rough surface under CNL and CNS conditions, to better understand the following:

• The effects of temperature on the shear strength (friction angle, cohesion and adhesion) of soil and soil-structure interface under CNL and CNS conditions.

• The effect of surrounding soil stiffness on the soil-structure interface mechanical behaviour at different temperatures.

• The soil and soil-structure interface volumetric changes during heating (from 22 to 60 ^oC) and cooling (from 22 to 5 ^oC) under constant isotropic stress.

3.2 Material properties, device and experimental programme

In this section first, the materials used in this study are presented. Then, the details of the temperature-controlled direct shear device, CNL and CNS tests with the device, and calibration are discussed. Finally, the experimental programme is presented.

3.2.1 Material properties

The grain size distributions and physical properties of Fontainebleau sand (siliceous) and kaolin clay used, in this study are presented in Fig. 3.2, Table 3.1 and Table 3.2.

Table 3.1: Fontainebleau sand physical properties (Pra-Ai 2013)

D_{50} (mm)	ρ_s (g/cm^3)	γ_{dmax} (kN/m^3)	γ_{dmin} (kN/m^3)	e_{max}	e_{min}	$C_u = D_{60}/D_{10}$
0.23	2.65	17.2	14.2	0.866	0.545	1.72

Table 3.2: Kaolin clay physical and thermal properties (Yavari et al. 2016)

LL (%)	PL (%)	I_p (%)	ρ_s (Mg/m^3)	λ (W/mK)	C (J/m^3K)	k (m/s)
57	33	24	2.60	1.5	3.3	10^{-8}

To perform soil-structure interface direct shear tests, a stainless steel plate (80 x 60

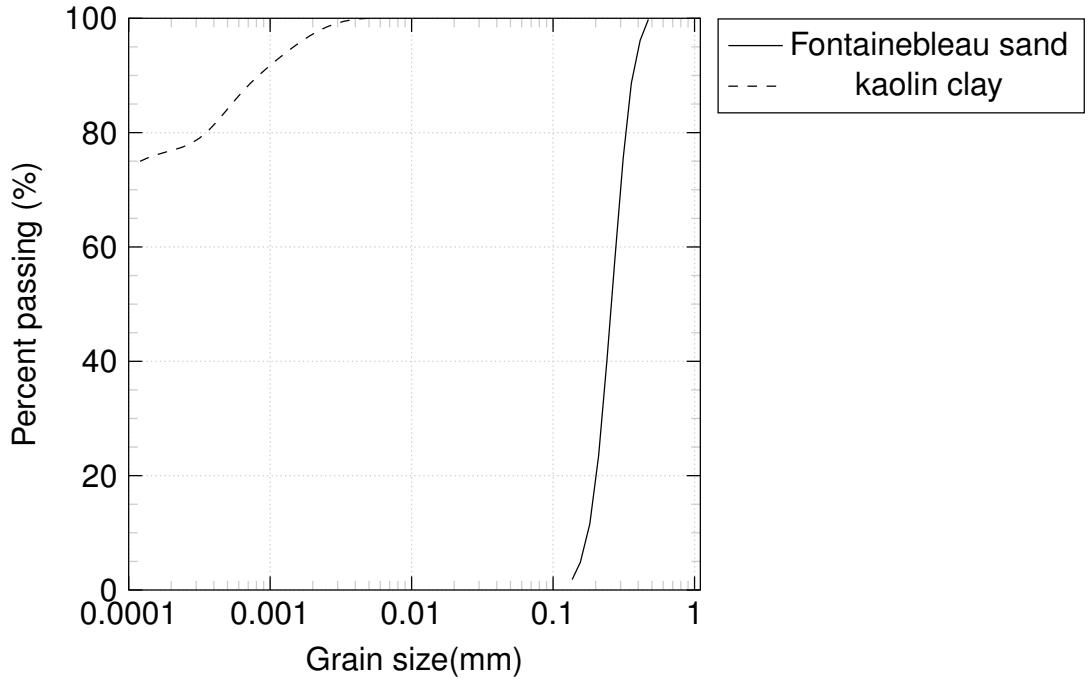

Figure 3.2: Grain size distribution of Fontainebleau sand and kaolin clay.

x 10 mm) with the desired roughness was designed and used as the structure. This steel plate is used to, avoid abrasion of the surface due to test repetition. The roughness of the steel plate was measured with a laser profilometer (Fig. 3.3(a)).

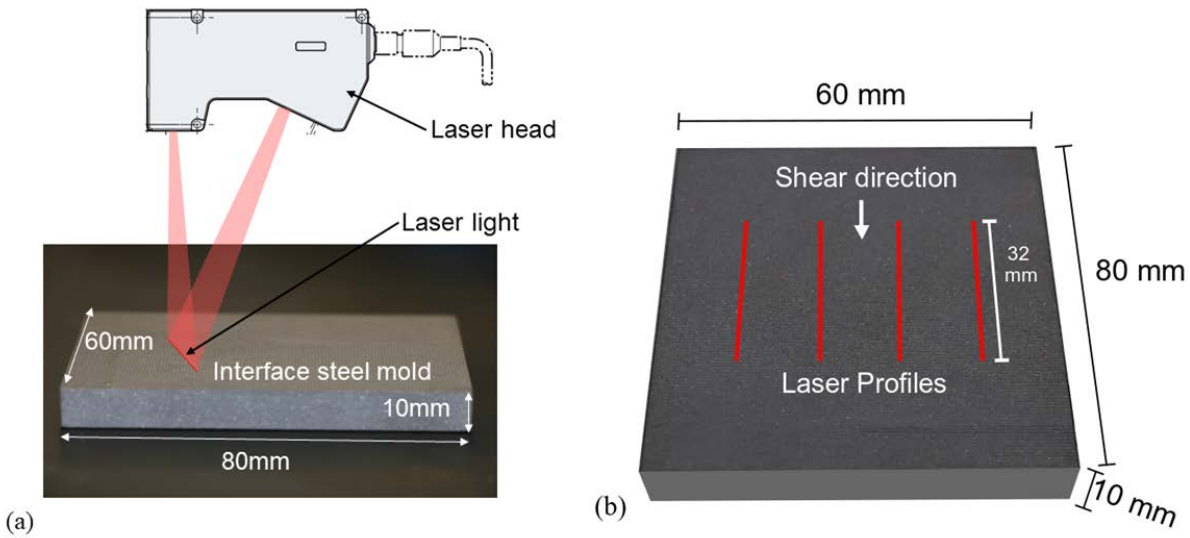

Figure 3.3: (a) Steel mould dimensions and, laser setup (b) direction and dimensions of laser profiles.

Four profiles with lengths of 32 mm (Fig. 3.3(b)) parallel to the shear direction were measured. The heights of these four profiles were obtained with the laser are presented in Fig. 3.4(a). To determine the roughness of the interface, each profile was divided

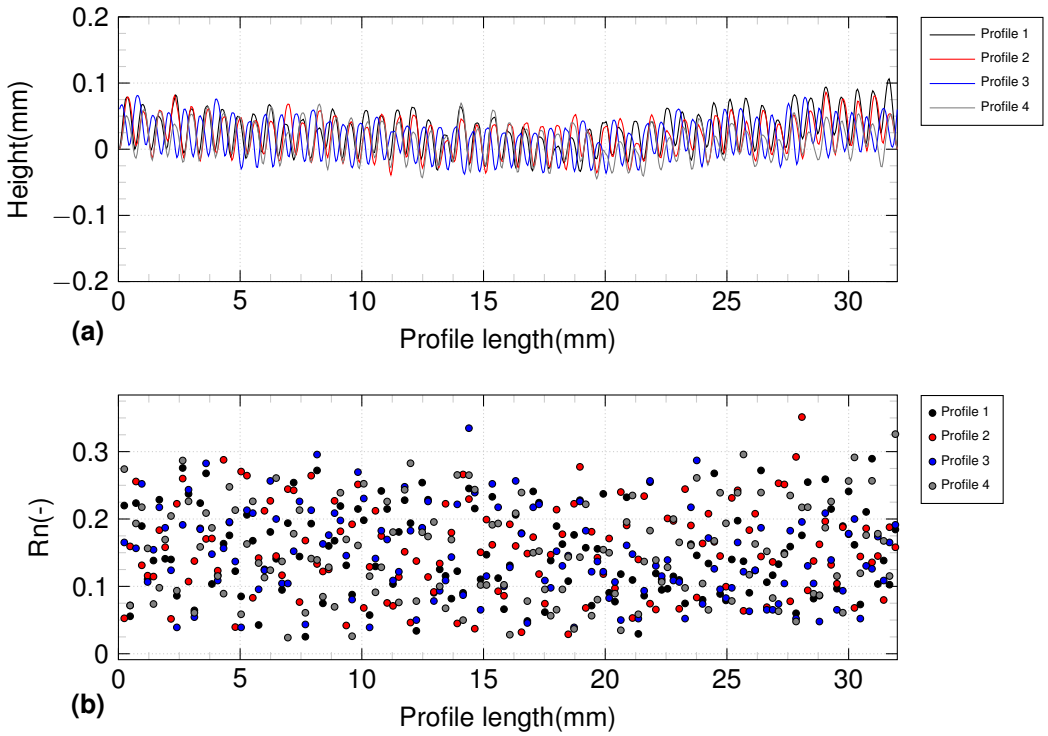

Figure 3.4: (a) Measured profiles (b) normalized roughness measurements for each profile length ($L = D_{50}$).

into the D_{50} of Fontainebleau sand (0.23 mm) and at each D_{50}, the R_{max} was measured. The values of R_{max} were divided by D_{50} to obtain the normalized roughness (R_n). For Fontainebleau sand, the normalized roughness R_n is presented in Fig. 3.4(b). Most of the normalized values are between 0.02 and 0.3. The largest value of normalized roughness R_n (0.32) was determined; therefore, the stainless steel plate is considered as a rough and very rough surface for Fontainebleau sand and kaolin clay.

3.2.2 Temperature-controlled direct shear device

Fig. 3.5 shows the temperature-controlled direct shear device. The shear box (60 x 60 x 35 mm) was placed inside a container filled with water to reach saturated conditions (Fig. 3.5). The heating system consisted of a heater that controlled the fluid temperature circulating in the lower part of the container. Therefore, the water temperature in the container reached the same temperature as the circulating fluid. Three thermocouples, one in the lower half of the shear box, another on the upper half of the shear box and the last in the container, controlled the applied temperature. In this direct shear device, normal stress σ_n (kPa), shear displacement W (mm), circulating fluid temperature T (^oC) and stiffness value K (kPa/mm) were applied, and normal displacement U (mm), shear stress τ (kPa), and sample temperature T (^oC) were measured (Fig. 3.5).

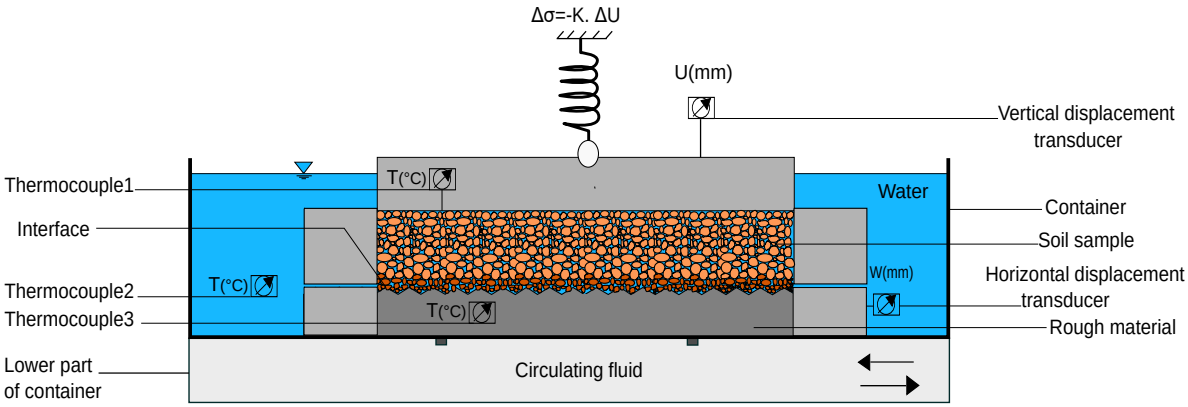

Figure 3.5: Experimental setup of the direct shear temperature-controlled device.

3.2.2.1 Constant normal load application

To perform CNL tests, the normal load was applied with a loading frame and kept constant during the tests. To start the shear, a shear displacement rate (mm/min) was applied to the lower half of the shear box and the shear stress was measured. The different parts of the device were connected to a data logger and a commanding system, which enabled the operator to apply different thermo-mechanical paths. Calibrations were performed to account for any temperature effects on different parts of the device.

Constant normal stiffness application

Under CNS conditions, two general behaviours are observed in soils: dilative (dense or overconsolidated soils) and contractive (loose or normally consolidated soils). In the first case, with starting the shear the soil at the interface starts to contract slightly ($\Delta U > 0$) at the beginning of the test, and the amount of normal stress decreases (due to the stiffness of the surrounding soil (virtual springs)) (Eq. 3.1). After this slight compression, the soil starts to dilate ($\Delta U < 0$), and this dilation acts on the surrounding soil. Due to the compression of the surrounding soil, the amount of the normal stress increases ($\Delta\sigma > 0$). This normal stress rise, consequently increases the shear strength of the soil at the interface. Conversely, in the second case (loose or normally consolidated soils), the soil at the interface contracts ($\Delta U > 0$), and the normal stress decreases ($\Delta\sigma < 0$) until the shear ceases.

To apply CNS condition to the temperature-controlled direct shear device, the following procedure was implemented in the command software:

1. The total desired shear displacement, $W(8$ mm) was divided into 100 segments ($W/100 = 0.08$ mm).

2. In order to reach the desired $W(8$ mm) value: $(W/100) \times i \qquad i = [1, 2, 3, ..., 100]$ where i is the number of segments.

3. At the end of each segment, the device measures the vertical displacement difference between the beginning of the segment and the end of the segment ($\Delta U = \Delta U_{i_2} - \Delta U_{i_1}$).
4. Then, according to Eq. 3.1, this difference ($\Delta U(mm)$) is multiplied by the value of stiffness (K (kPa/mm)), and the consequent normal stress ($\Delta\sigma_n$) that should be applied is calculated.
5. This process is repeated for all segments $i(100)$ until the total shear displacement is reached.

3.2.2.2 Normal stiffness verification

To calibrate the device for the stiffness application, the variations of normal stress ($\Delta\sigma$) with normal displacement (ΔU) are presented in Fig. 3.6. The slope of these curves represents the stiffness value. For tested values of stiffness, a satisfactory correlation is obtained (1-2% precision). Fig. 3.6(a) shows the verification results for $K = 500$

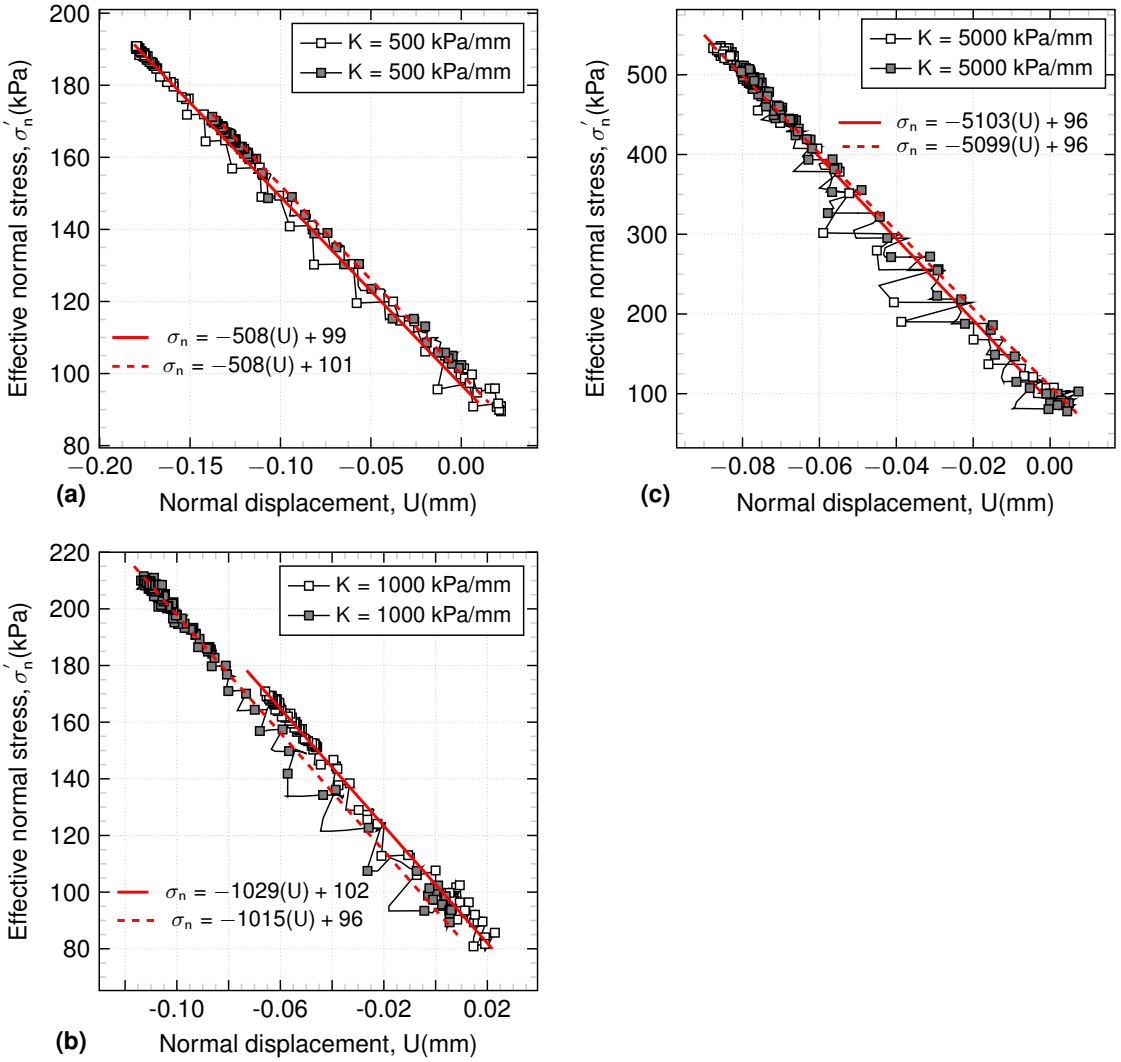

Figure 3.6: Imposed stiffness verification. (a) $K = 500$ kPa/mm; (b) $K = 1000$ kPa/mm; (c) $K = 5000$ kPa/mm. $\sigma'_{n0} = 100$ kPa.

kPa/mm. Due to the dilation of the sand at the interface, the normal stress increased in a linear manner. The slope of the curve represents the stiffness value (K). Tests at different temperatures with same stiffness were compared to verify the normal stiffness application with temperature variations. As it can observed for all of the performed tests at different stiffness values, the starting point is the initial normal stress (100 kPa) and the experimental fluctuations are due to the constant normal stiffness application method.

3.2.3 Experimental program

To answer the important aspects that was mentioned in the introduction a comprehensive experimental program was proposed to investigate the effect of temperature on the mechanical properties of the sand/clay-structure interface under constant normal load and constant normal stiffness conditions. The experimental programme consisted

Table 3.3: Experimental programme of soil and soil-structure interface tests

	$\sigma_n(kPa)$	K (kPa/mm)	$T^o(C)$	Type of test
Sand	100, 200, 300	0	22^o	CNL
Sand	100, 200, 300	0	60^o	CNL
Sand-structure	100, 200, 300	0	22^o	CNL
Sand-structure	100, 200, 300	0	60^o	CNL
Sand-structure	100	500, 1000, 5000	22^o	CNS
Sand-structure	100	500, 1000, 5000	60^o	CNS
Sand-structure	100, 200, 300	1000	22^o	CNS
Clay	100, 300	0	5^o	CNL
Clay	100, 300	0	22^o	CNL
Clay	100, 300	0	60^o	CNL
Clay-structure	100, 300	0	5^o	CNL
Clay-structure	100, 300	0	22^o	CNL
Clay-structure	100, 300	0	60^o	CNL
Clay-structure	100, 300	1000	22^o	CNS
Clay-structure	100, 300	1000	60^o	CNS

of soil and soil-structure direct shear tests at different temperatures (Table 3.3). Soil tests were performed as reference cases for comparison with soil-structure interface tests to better clarify the role of interface. Soil-soil shear tests permits to understand the mode of shearing in interface tests due to its fundamental shearing difference with the interface.

The sand programme consisted of a series of constant normal load (CNL) tests at different temperatures to investigate the effects of temperature on the mechanical characteristics. In sand-structure tests, CNL and CNS tests were performed at 22 and 60 ^oC. For CNS tests, different stiffness values (K = 500, 1000, and 5000 kPa/mm) were chosen, that were used in previous studies (Boulon and Foray 1986; Mortara 2001; Pra-Ai 2013). Increasing the stiffness value restrains the volumetric response of the interface until a certain case of constant normal stiffness which is called the constant volume condition (CV). These values were chosen to cover the entire range of constant normal stiffness conditions, from very small ranges close to CNL and up to very high values close to CV. To perform the CNS tests, two scenarios were considered. First, shear tests with different stiffness values (K = 500, 1000, and 5000 kPa/mm) and constant effective normal stress ($\sigma^{'}_{n0}$ = 100 kPa) were performed at 22 and 60 ^oC. The aim of this part was to determine the effect of different stiffness values at 22 and 60 ^oC on sand-structure interface. The second scenario, included interface shear tests at three different effective normal stress values ($\sigma^{'}_{n0}$ =100, 200 and 300 kPa) with a constant stiffness value (K = 1000 kPa/mm). This scenario was performed to determine the friction angle of the interface and also compare the CNS and CNL tests.

3.2.3.1 Sand program

To prepare the sand samples for the shear tests, the Fontainebleau sand with a target dry density of 1.67 Mg/m^3 was poured into the shear box and compacted using a tamper. This dry density corresponded to 90% of the relative density (D_r), and the sample was considered to be a dense sand (Table 3.1). Then, the normal stress was applied to the sand sample (path 0-1 in Fig. 3.7). After applying the normal stress, to shear the samples in CNL condition at 22 ^oC, a shear rate of 0.1 mm/min was applied (path 1-2). For the CNL tests at 60 ^oC, the heating phase (path 1-5, Fig. 3.7) was applied with a rate of 10 $^oC/hr$, and the shearing phase (path 5-2$^{'}$) started. For the sand-structure tests, the same procedure was performed, except the interface was placed at the lower half of the shear box.

For the sand-structure CNS tests, due to the dense state of the soil, path 1-3 at 22 ^oC and path 5-3$^{'}$ at 60 ^oC were observed (Fig. 3.7).

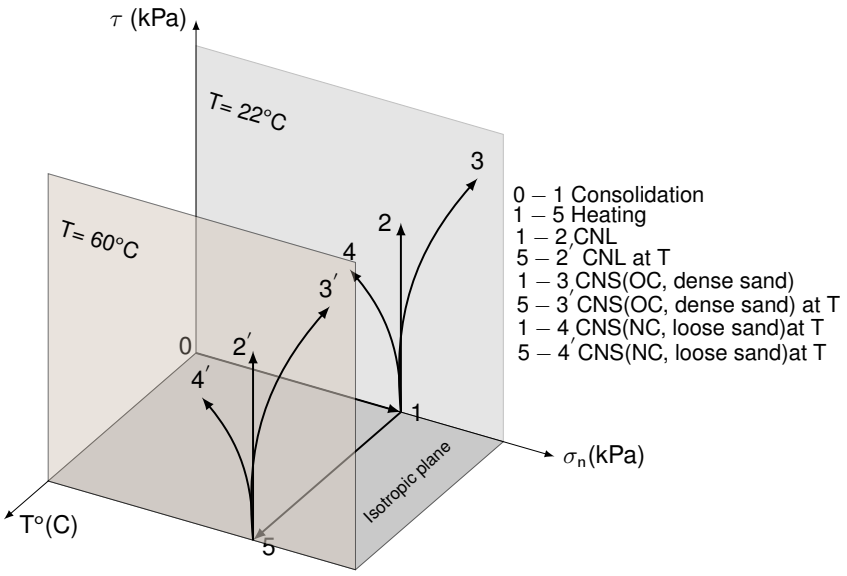

Figure 3.7: Thermo-mechanical path in this study.

3.2.3.2 Clay program

To perform the clay and clay-structure shear tests, kaolin clay was prepared with a water content of 63%, which was slightly higher than its liquid limit ($LL = 57\%$) and the sample was left for 24 hours for homogenization. Subsequently, the clay was poured into the shear box and special attention was paid to avoid any air trap. To perform the CNL tests at 22 ^oC,, the normal stress was applied slowly and incrementally during the consolidation phase, and each load increment lasted 2 hours, to ensure full consolidation at each step (Mortezaie and Vucetic 2013). Two values of initial effective normal stresses ($\sigma_{n0}^{'} = 100, 300$ kPa) were chosen for the clay programme. Based on the consolidation tests performed on this kaolin clay, the target void ratios after consolidation for $\sigma_n^{'} = 100$ and 300 kPa were $e = 1$ and 0.85, respectively.

After the consolidation phase for the CNL tests at 22 ^oC, a displacement rate of 0.006 mm/min that was calculated from the settlement curve and t_{50} (time required for the specimen to achieve 50 percent consolidation under the maximum normal stress) of the kaolin, was applied (ASTM 1998). This slow rate ensured drained conditions inside the shear box during shearing. The initial heating or cooling phase started at ambient temperature (22 ^oC). After the consolidation phase, heating or cooling was applied to the samples at a rate of 5 $^oC/hr$. This slow rate avoids a pore water pressure increase during the heating phase and was verified by Cekerevac and Laloui 2004 and Di Donna et al. 2015. During the heating or cooling phase in the shear box, thermal vertical deformation of the soil and the soil-structure interface was measured. After these heating or cooling phases, the samples were sheared. For the CNL tests of the clay and clay-structure interface, paths 1-2 and 5-2$^{'}$ were applied, as seen in Fig. 3.7,

but for the CNS clay-structure interface tests, paths 1-4 and 5-4$'$ were observed due to the normally consolidated state of the kaolin samples.

3.3 Experimental results for sand

In the following sections, first the CNL sand shear test results, and then, the CNL and CNS sand-structure interface tests are discussed.

3.3.1 Sand

Fig. 3.8(a) presents the results of the sand CNL tests at 22 and 60 ^oC, which will be used as a reference for the sand-structure tests. The dense sand samples show a peak shear stress at a small shear displacement, and then, with a decrease, reach a critical state at both 22 and 60 ^oC.

In Fig. 3.8(c), the volumetric behaviour of the sand is presented. The amount of contraction ($\Delta U > 0$) is around 0.06 mm; then, at 1.2 mm of shear displacement, the dilation ($\Delta U < 0$) phase starts and continues until $U = -0.4$ mm, and finally, a constant value corresponding to the critical state of the soil is reached. Fig. 3.8(b) shows the stress ratio ($\eta = \tau/\sigma_n^{'}$) variations with shear displacement, and the peak shear strengths are reached at similar shear displacements ($W = 1.5 - 1.6$ mm) for different normal stresses. Fig. 3.8(d) shows the Mohr-Coulomb plane for the sand samples. The peak friction angle for the tests is 41.6^o at 22 and 60 ^oC, while the residual friction angle is 34^o. The same peak and residual friction angles at both temperatures show the negligible effect of thermal variations on the shearing behaviour of the studied sand.

3.3.2 Sand-structure

3.3.2.1 Constant normal load (CNL)

Fig. 3.9(a) shows the CNL results of the sand-structure tests with different initial effective normal stresses ($\sigma_{n0}^{'} = 100, 200, 300$ kPa) at 22 and 60 ^oC. The shear stress-shear displacement curves reach peaks at approximately 1 mm of shear displacement, and then, a sharp decrease of τ is observed. The peak and residual values of the shear stress at different temperatures are almost the same. The contraction (0.01 mm) and dilation (-0.2 mm) amounts in the volumetric response are approximately half that of the sand case due to the thickness of the soil sample in the sand-structure tests (Fig. 3.9(b)). In terms of the temperature effects on the volumetric response, at both 22

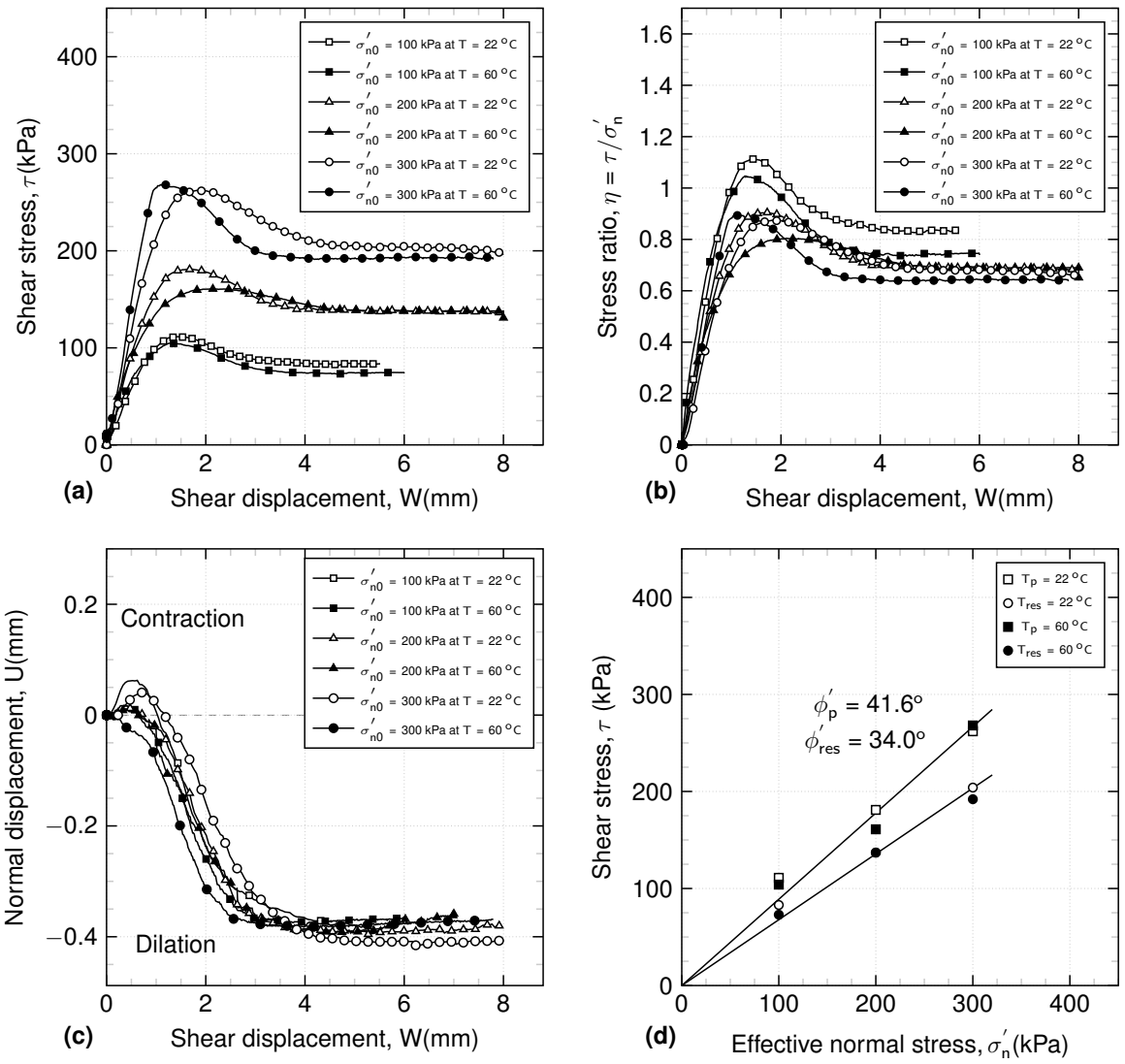

Figure 3.8: CNL results for sand samples at $T = 22^oC$ and $T = 60^oC$. (a) Shear stress vs. shear displacement; (b) normal displacement vs. shear displacement; (c) stress ratio vs. shear displacement; (d) shear stress vs. effective normal stress

and 60 ^oC, the volumetric responses follow the same trend. The stress ratio curves for different temperatures vary between 0.8-1 (Fig. 3.9(c)). The Mohr-Coulomb plane of the sand-structure tests under the CNL condition is presented in Fig. 3.9(d). The peak friction angle of the sand-structure interface is 40.4^o and the residual friction angle is 32.7^o.

3.3.2.2 Constant normal stiffness

Fig. 3.10 shows the sand-structure interface CNS results for the first case ($\sigma'_{n0} = cte$ and $K = 500, 1000, 5000$ kPa/mm). With increasing stiffness, the maximum shear strength for CNS tests was increased due to the increase in normal stress (Fig. 3.10(a)). The CNS peak shear stress obtained for larger shear displacements and the post-peak soft-

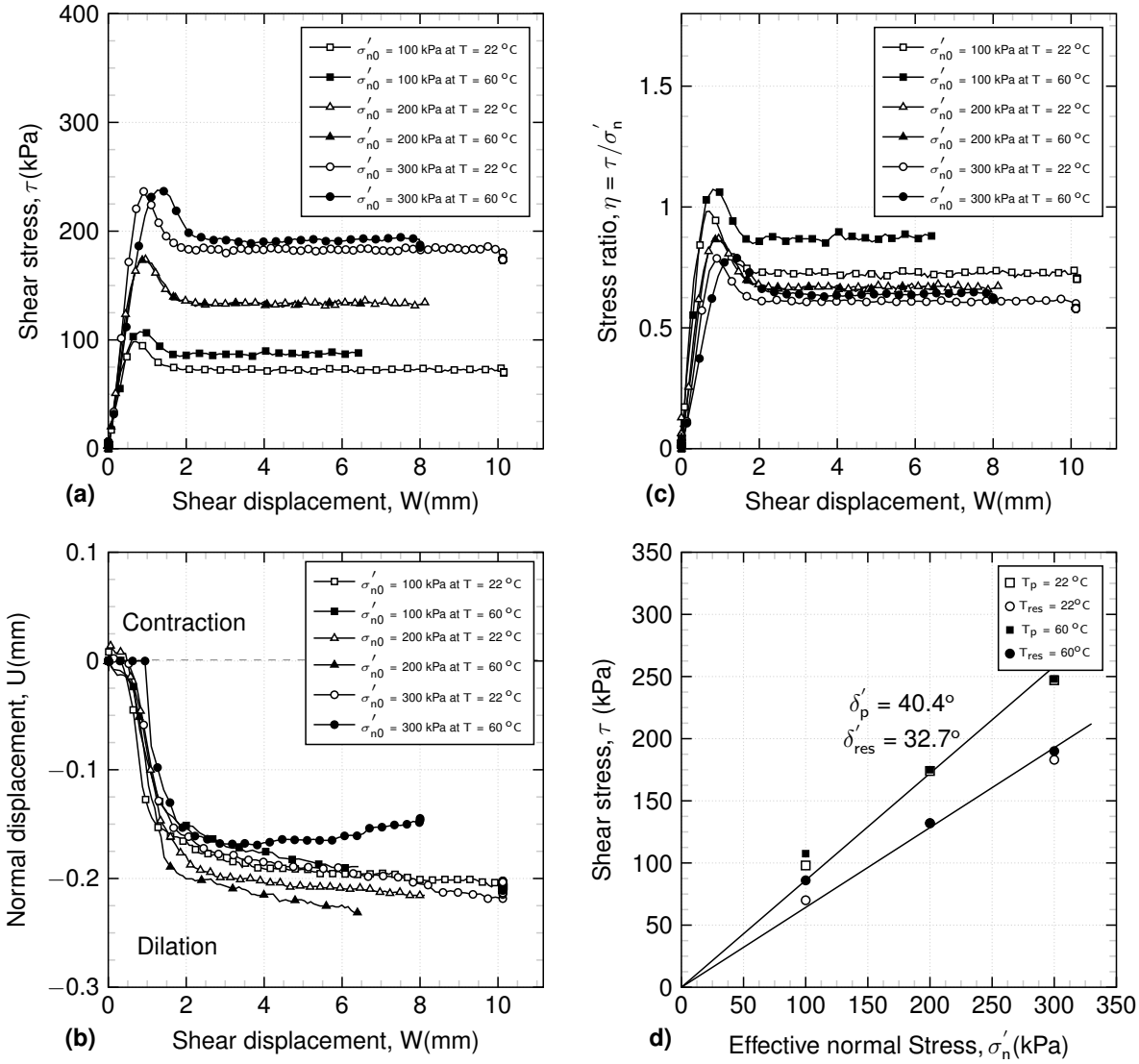

Figure 3.9: CNL results for sand-structure inerface at $T = 22^oC$ and $T = 60^oC$. (a) Shear stress vs. shear displacement; (b) normal displacement vs. shear displacement; (c) stress ratio vs. shear displacement; (d) shear stress vs. effective normal stress

ening behaviour was less evident than in the CNL sand-structure tests. The decrease of shear stress after peak or post-peak softening behavior under CNS conditions can confirm the grain breakage phenomena in the interface zone, which has not been observed in this study. In Fig. 3.10(b), at the beginning of shearing, the interface contracted slightly and then started to dilate. For $K = 500$ kPa/mm, the soil in the interface dilated approximately -0.2 mm, and by increasing the stiffness to 5000 kPa/mm, the dilation was reduced to -0.08 mm (Fig. 3.10(b)). Increasing the stiffness restrained the volumetric response of the soil at the interface. These restrained dilations, increased the normal stress (Fig. 3.10(c)). The normal stress increased from the initial value (100 kPa) to 180 kPa for K =500 and 1000 kPa/mm. For $K = 5000$ kPa/mm the normal stress increased to 510 kPa. Therefore, the normal stress variation during shear

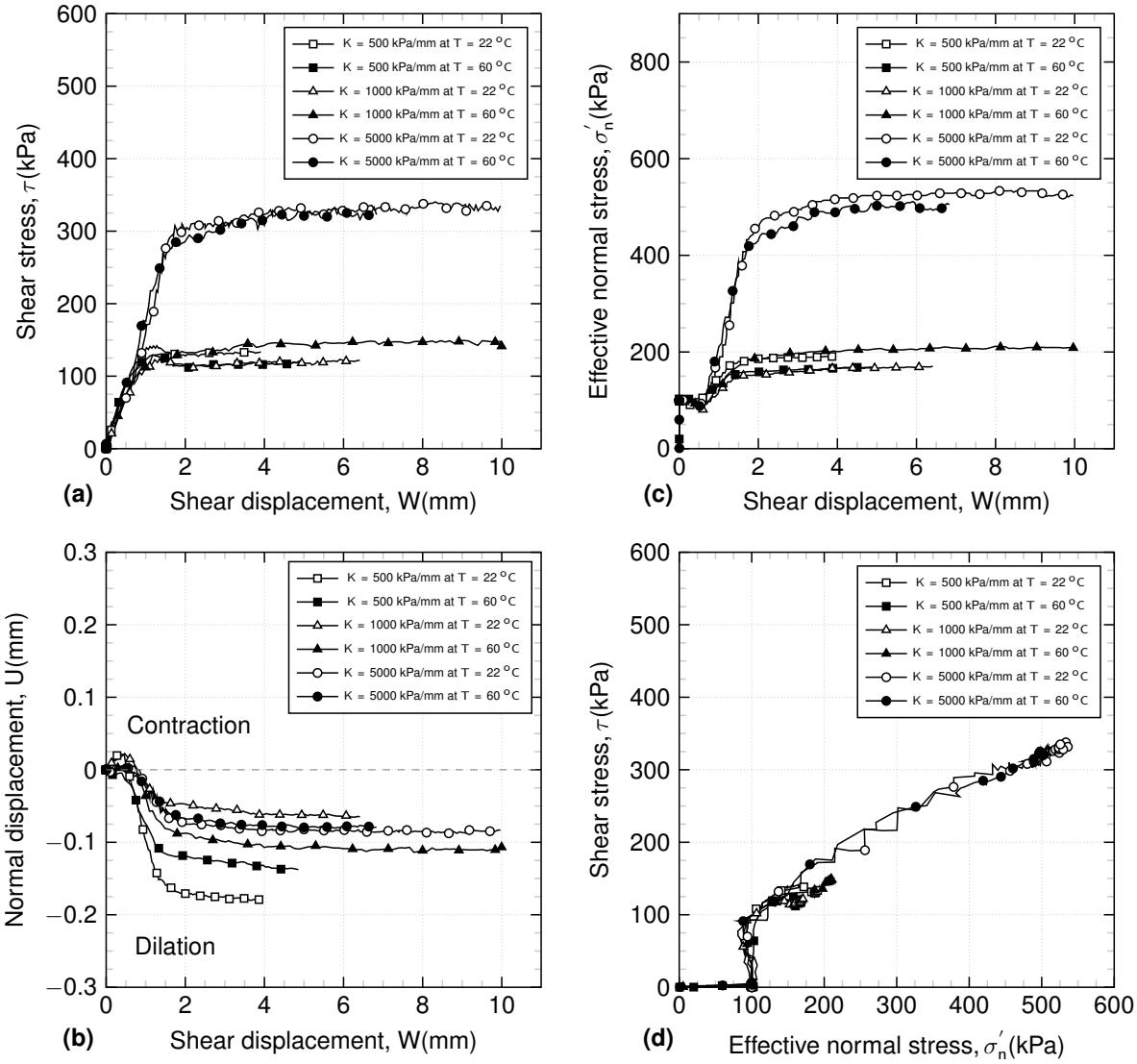

Figure 3.10: CNS results for sand-structure interface at $T = 22^oC$ and $T = 60^oC$ for same initial normal stress (100 kPa). (a) Shear stress vs. shear displacement; (b) normal displacement vs. shear displacement; (c) normal stress vs. shear displacement; (d) shear stress vs. effective normal stress

depended on the volumetric response, and these normal stress increases, consequently increase the shear stress acting on the interface. Fig. 3.10(d) shows the Mohr-Coulomb plane of the sand-structure interface. All tests showed, with shear increase, the effective normal stress decreased slightly at the beginning, then followed by an increase until the end of shear. The comparison of curves at 22 and 60 ^oC shows that the temperature has a negligible effect on the shearing behaviour of Fontainebleau sand-structure interface under CNS conditions.

The second scenario ($\sigma'_{n0} = 100, 200, 300$ kPa, $K = cte$ and T= 22 ^oC) results are reported in Fig. 3.11 and are compared with the results of the CNL case ($K = 0$ kPa/mm). The peak shear stress for CNS tests were obtained for larger shear displacements (1.3 mm), compare to CNL tests (0.8 mm). The increase in peak shear stress for

$\sigma'_{n0} = 100, 200$, and 300 kPa in the CNS tests were 20, 60 and 80 kPa respectively (Fig. 3.11(a)), compared to the values on the CNL tests. The volumetric responses in the

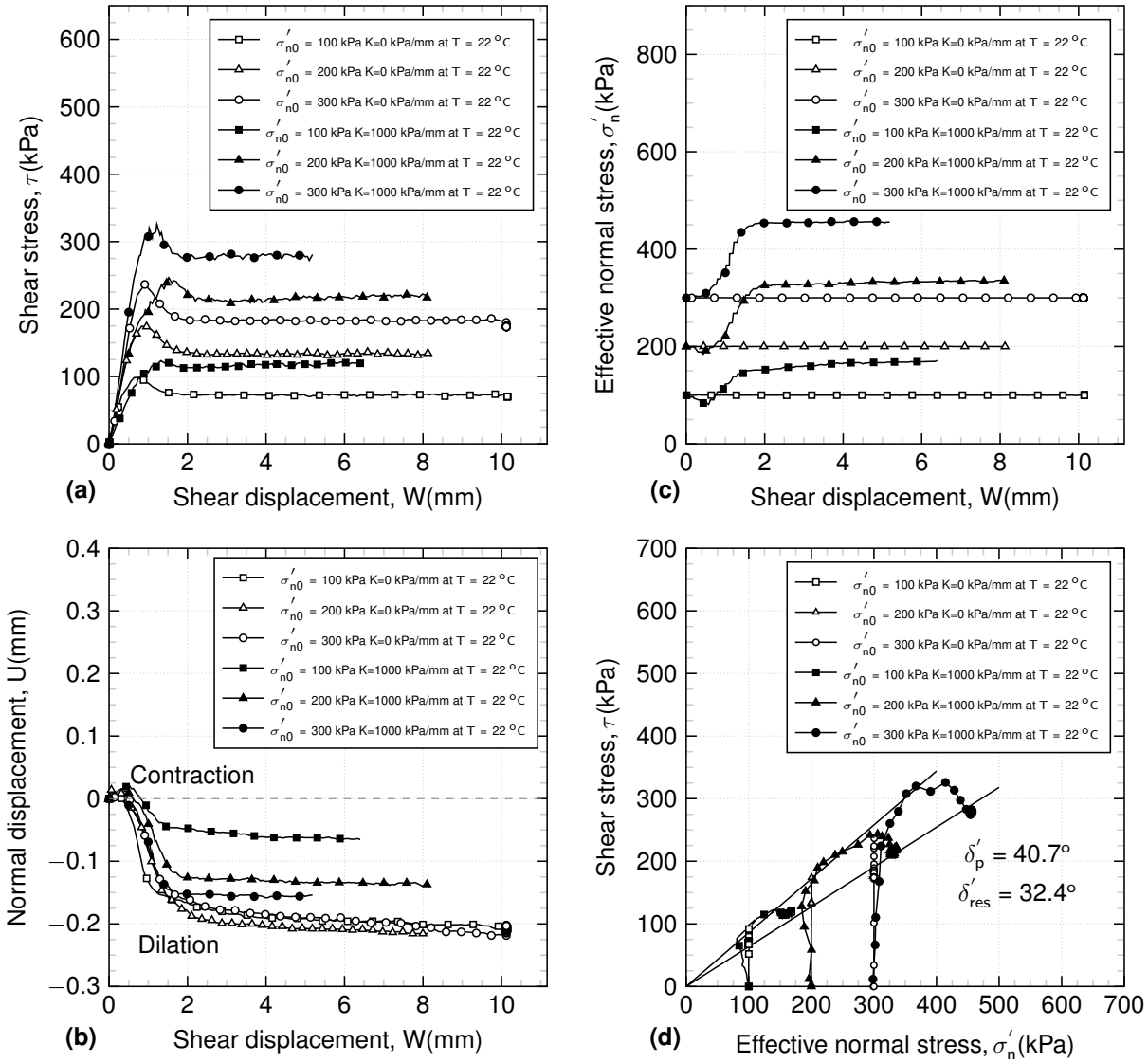

Figure 3.11: Comparison of CNS and CNL ($K = 0$ kPa/mm) results for sand-structure interface at $T = 22^oC$ for different initial normal stresses (100,200,300 kPa) and $K = 1000$ kPa/mm. (a) Shear stress vs. shear displacement; (b) normal displacement vs. shear displacement; (c) effective normal stress vs. shear displacement; (d) shear stress vs. effective normal stress

CNS tests are more restrained than in CNL tests (Fig. 3.11(b)). In Fig. 3.11(c), the normal stress variation during the CNS tests is presented. The normal stress showed a slight decrease until 0.5 mm of $W(mm)$ and then increased. This increase continued until 1.4 mm of $W(mm)$, which corresponds to the peak shear stress; after this peak was reached, the normal stress remained unchanged. The peak and residual friction angles of the interface in Fig. 3.11(d) are $\delta'_p = 40.7^o$ and $\delta'_{res} = 32.4^o$ which are smaller than the friction angles obtained in the sand tests (Fig. 3.8(d)). This point confirms that the shear occurred exactly in the interface zone, and not in the soil mass. Pra-Ai

2013 conducted interface direct shear tests on dense Fontainebleau sand samples on a rough steel plate under isothermal conditions, and they found 38^o and 29^o for the peak and residual friction angles of the interface respectively. In the CNS sand-structure interface tests, the peak and residual friction angle of the interface (40.7^o and 32.4^o) are close to those in the CNL sand-structure tests (40.4^o and 32.7^o). The friction angle of the sand-structure interface is not affected by the CNS condition, which was also observed by Porcino et al. 2003.

3.3.3 Sand vs. sand-structure interface

In this section, the CNL test results for the sand and sand-structure interface are compared to better understand the interface behaviour. The shear stress and volumetric response in the CNL sand and sand-structure tests for $\sigma_{n0}^{'}$=100 and 300 kPa at T=22 ^oC are compared in Fig. 3.12.

In the sand-structure tests, the post-peak softening behaviour is more pronounced than in the sand tests (Fig. 3.8). The peak shear stress is higher (7-15%) in the sand samples than in the sand-structure tests, which confirms the shear failure occurs in the interface zone. The peak shear stresses of the sand-structure tests are obtained at smaller shear displacements (0.7-1 mm) than in the sand (1.6-1.8 mm) case, which could be due to the rearrangement of grains in the interface zone (Hoteit 1990; Tabucanon et al. 1995; Porcino et al. 2003).). The dilation phase began at smaller shear displacements in the sand-structure interface tests (0.7 mm) than in the sand samples (1.2 mm), and the amount of dilation (0.2 mm) was almost half that of the sand samples (0.4 mm).

3.4 Experimental results for clay

This experimental section is divided into the clay and clay-structure results. For the clay tests, the CNL test results and for clay-structure interface tests, the CNL and CNS test results are discussed.

3.4.1 Clay

In this part first, thermal vertical strain of clay samples is presented. Second, the shear curves and volumetric responses for $\sigma_{n0}^{'}$=100 and 300 kPa at 5, 22 and 60 ^oC are presented. To verify the repeatability of the results, the test with $\sigma_{n0}^{'}$=300 kPa at 60 ^oC was repeated.

After consolidation and reaching the desired void ratio, a heating or cooling phase at a rate of 5 $^oC/hr$, was applied to the clay samples. This heating and cooling caused

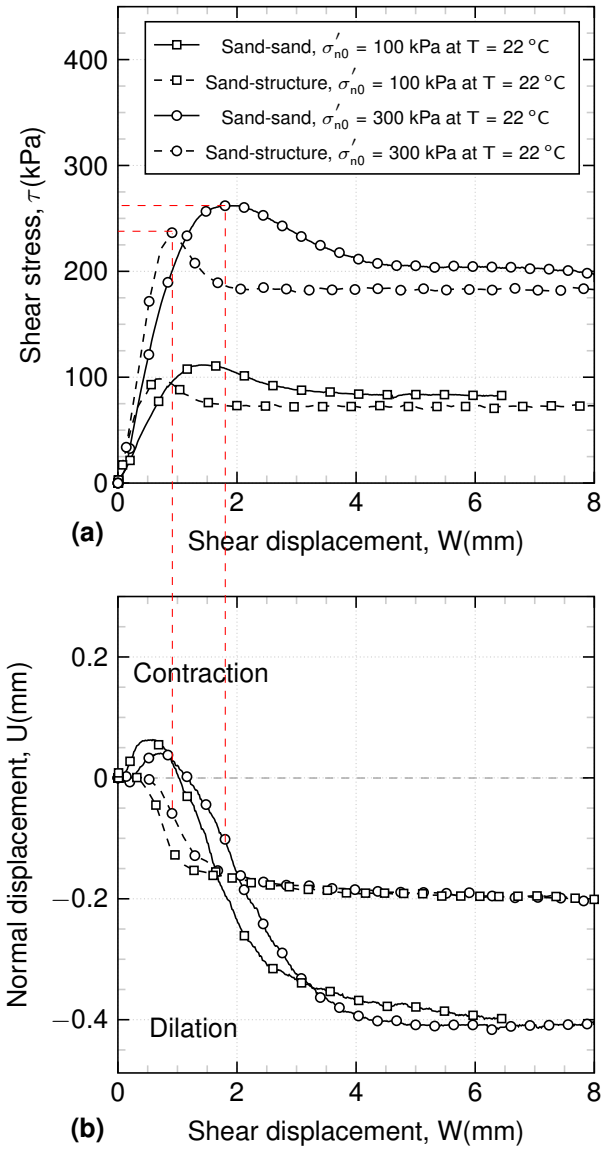

Figure 3.12: Comparison of CNL results for sand and sand-structure with $\sigma'_{n0} = 100$ and 300 kPa at $T = 22\ ^oC$.

a thermal vertical deformation under constant effective normal stresses of 100 and 300 kPa (Fig. 3.13).

The heating phase started from 22 to 60 ^oC and cooling phase was from 22 to 5 ^oC. The thermal vertical strain was higher for heating cases $(0.6 - 0.64\%)$ than cooling cases $(0.18 - 0.2\%)$. Therefore, the slope of heating curves was less than the cooling curves, and heating caused more contraction than cooling.

After heating or cooling, normally consolidated kaolin clay samples were sheared at two different effective normal stresses (σ'_{n0}=100, 300 kPa) at 5, 22 and 60 ^oC (Fig. 3.14). In Fig. 3.14(a) and (c), the shear stress-shear displacement curves for 100 kPa and 300 kPa at 5, 22 and 60 ^oC are presented. As observed for both effective normal stresses, the shear stress increased with increasing temperature, until the peak values, then it

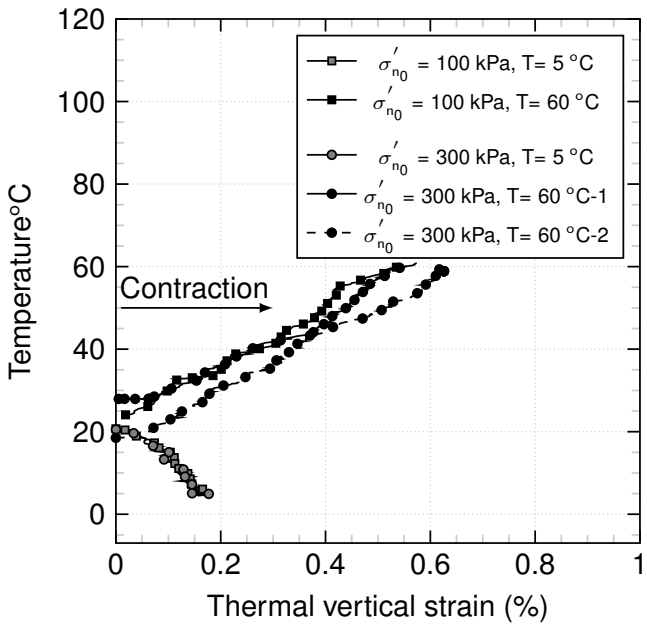

Figure 3.13: Thermal vertical strain of clay samples during heating and cooling phase. Heating or cooling rate: 5 $^oC/hr$

decreased towards the critical state. The residual shear stresses at 5, 22 and 60 ^oC for σ'_{n0}=100 kPa became convergent after a shear displacement of 5 mm. For σ'_{n0}=300 kPa at 5 and 22 ^oC the shear stress increased in the same manner, but after a shear displacement of W=3.5 mm, the stress values diverged. In the volumetric response, the samples that were exposed to higher temperatures showed less contraction during shear (Fig. 3.14(b) and Fig. 3.14(d). For example in 100 kPa of effective normal stress, the test at 5 ^oC showed a contraction approximately 0.89 mm, but for the tests at 22 and 60 ^oC, this amount decreased to approximately 0.68 mm and 0.38 mm respectively. For 300 kPa, the same trend was observed for the volumetric response (Fig. 3.14(d)). The Mohr-Coulomb plane for the clay tests at different temperatures is presented in Fig. 3.15. The internal friction angle of the clay soil obtained at different temperatures, shows a slight increase with temperature increase (14.4^o to 15.3^o) which can be considered negligible, but the main difference was the cohesion increase from 11 to 17 kPa and then to 23 kPa for tests at 5, 22 and 60 ^oC, which could be due to thermal hardening during the heating phase.

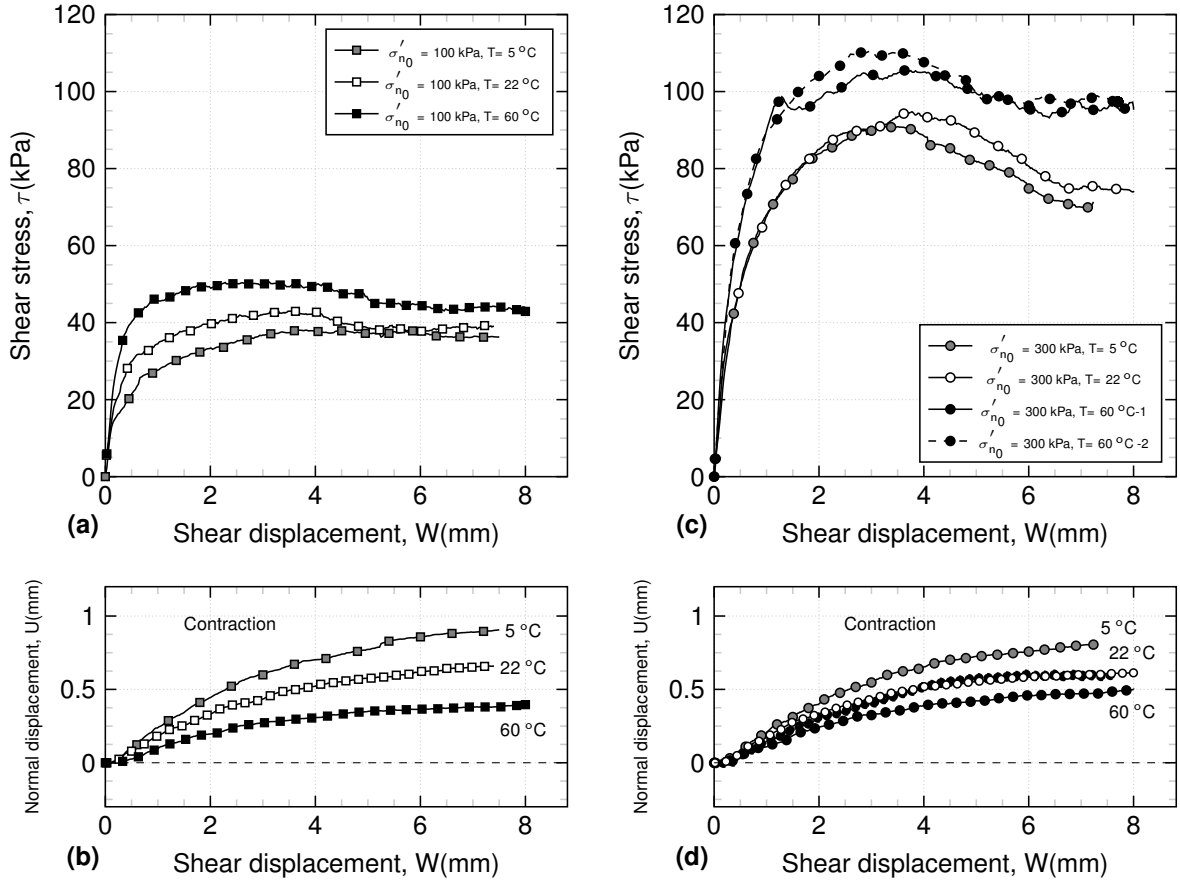

Figure 3.14: CNL results for clay samples at $T = 22\ ^oC$, $T = 60\ ^oC$ and $T = 5\ ^oC$. (a) Shear stress vs. shear displacement ($\sigma_{n0}^{'} = 100$ kPa); (b) normal displacement vs. shear displacement ($\sigma_{n0}^{'} = 100$ kPa); (c) shear stress vs. shear displacement ($\sigma_{n0}^{'} = 300$ kPa); (d) normal displacement vs. shear displacement ($\sigma_{n0}^{'} = 300$ kPa)

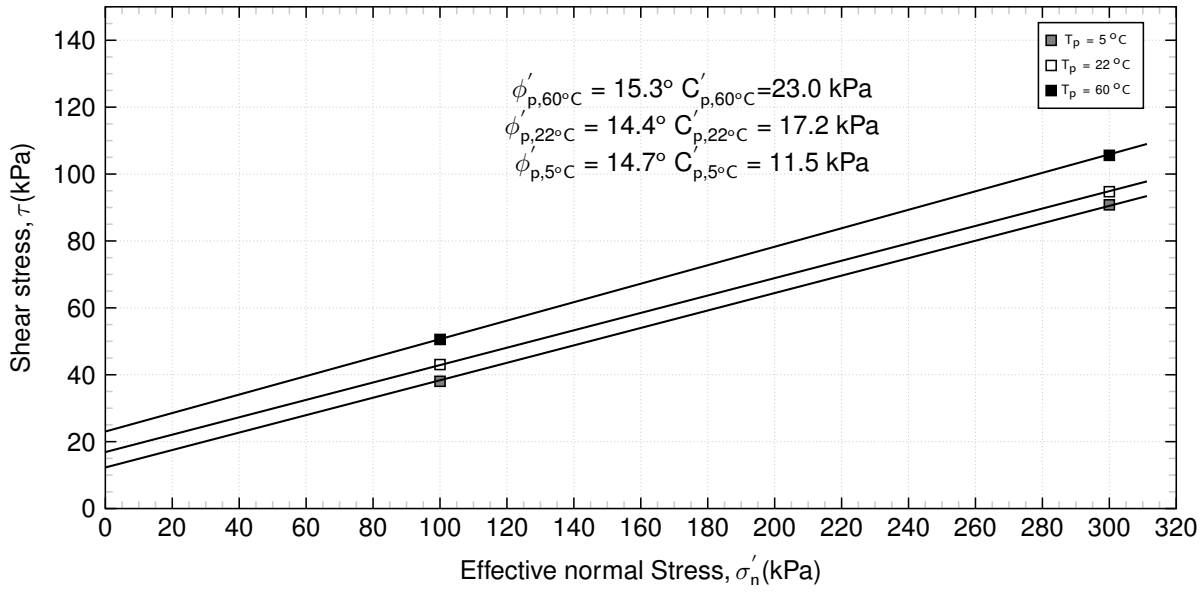

Figure 3.15: Shear stress vs. effective normal stress of CNL clay tests at $T = 5\ ^oC$, $T = 22\ ^oC$ and $T = 60\ ^oC$

3.4.2 Clay-structure

In the following sections, the CNL and CNS results for the clay-structure are presented.

3.4.2.1 Constant normal load (CNL)

Fig. 3.16 shows the thermal vertical strain for σ'_{n0}=300 kPa during the heating phase and after consolidation. The thermal vertical strain caused by the temperature increase from 22 to 60 ^oC was approximately 0.85%, and for a temperature decrease from 22 to 5 ^oC in the cooling case, the thermal vertical strain was approximately 0.2% for the clay-structure interface tests.

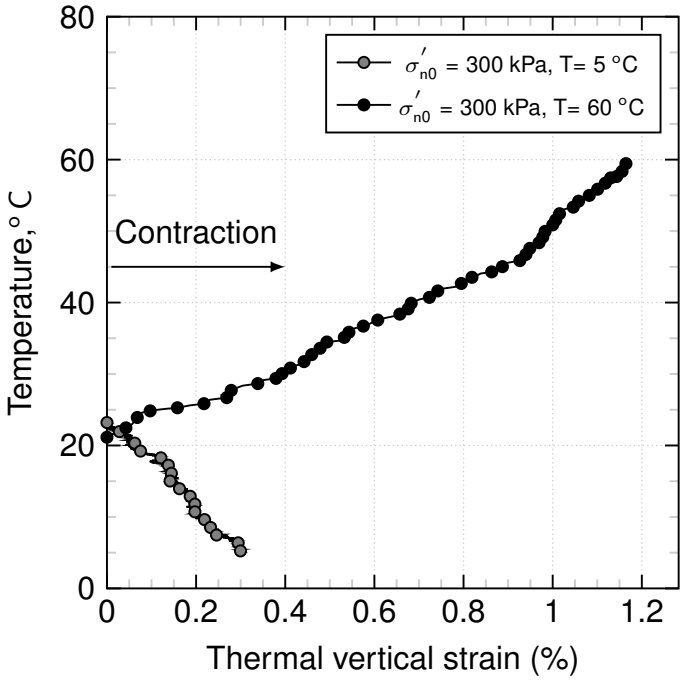

Figure 3.16: Thermal vertical strain of clay-structure interface during heating and cooling phase. Heating or cooling rate: 5 $^oC/hr$

The thermal volume deformation depends on the volume of the sample (Campanella and Mitchell 1968 and Baldi et al. 1988), and the thermal vertical strain is higher in the clay-structure interface than in the clay samples due to the volume of the clay specimen in the clay-structure tests.

In Fig. 3.17 the results of the clay-structure interface CNL tests are presented. Fig. 3.17(a) shows the shear stress versus shear displacement for σ'_{n0}=100 kPa. The peak shear strength curve was slightly higher at 60 ^oC than at 5 and 22 ^oC ($\Delta\tau$ = 8 kPa), but at the critical state, all curves at different temperatures were superimposed. For σ'_{n0}=300 kPa (Fig. 3.17(c)), the $\Delta\tau$ = 10 kPa of difference at the peak was evident for 60 ^oC compared to 5 and 22 ^oC. In the critical state, the same behaviour as σ'_{n0}=100 kPa was observed. In Fig. 3.17(b) and d the volumetric behaviours of the

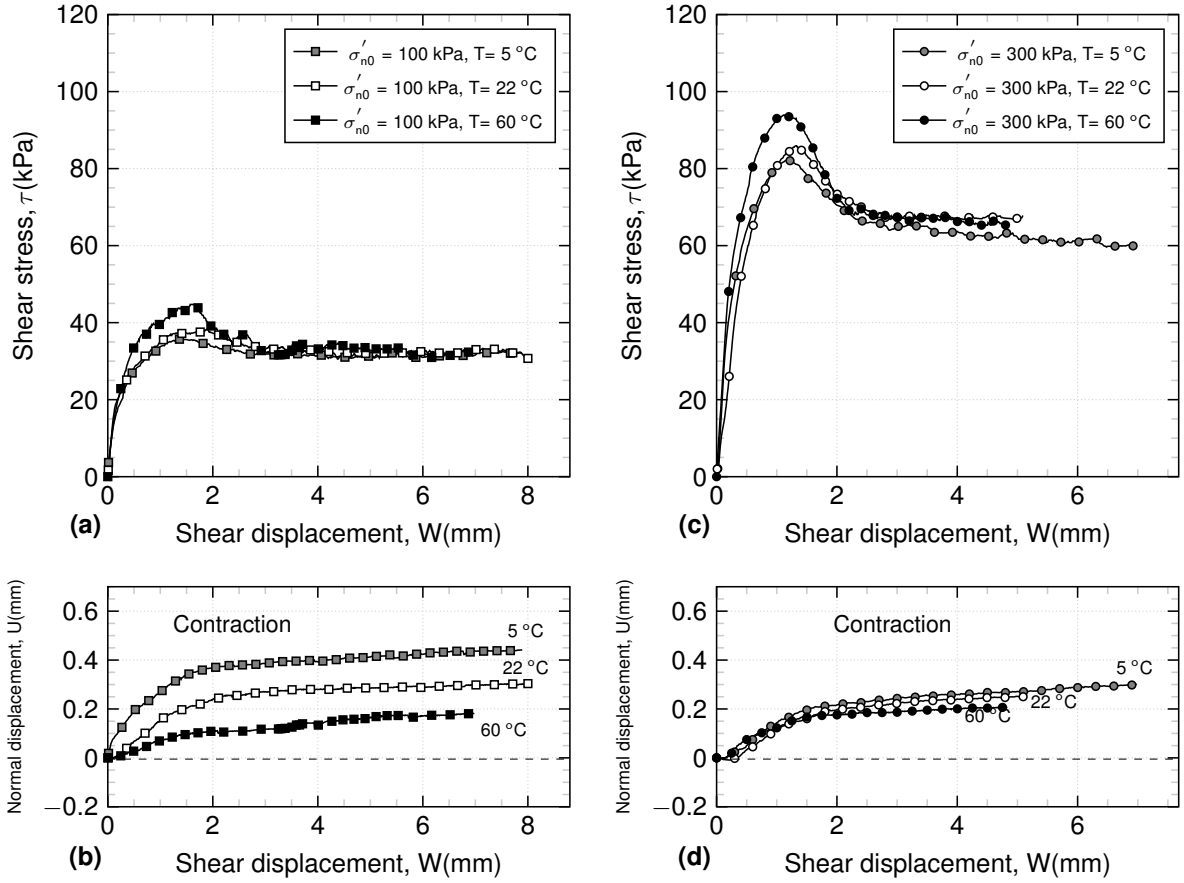

Figure 3.17: CNL results for clay-structure interface at $T = 5\ ^oC$, $T = 22\ ^oC$ and $T = 60\ ^oC$.(a) Shear stress vs. shear displacement ($\sigma^{'}_{n0} = 100$ kPa); (b) normal displacement vs. shear displacement ($\sigma^{'}_{n0} = 100$ kPa); (c) shear stress vs. shear displacement ($\sigma^{'}_{n0} = 300$ kPa); (d) normal displacement vs. shear displacement ($\sigma^{'}_{n0} = 300$ kPa)

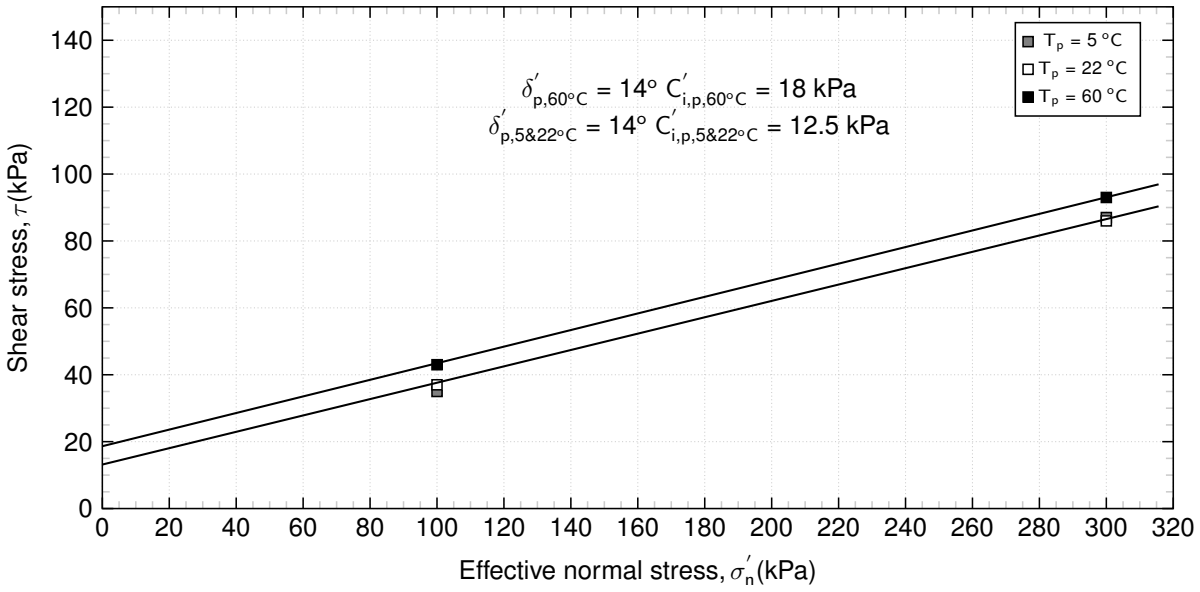

Figure 3.18: Shear stress vs. effective normal stress of CNL tests of clay-structure interface at $T = 5\ ^oC$, $T = 22\ ^oC$ and $T = 60\ ^oC$.

clay-structure interface are presented for σ'_{n0}=100 and 300 kPa. For σ'_{n0}=100 kPa (Fig. 3.17(b)), the amount of contraction was 0.4 mm for the test at 5 ^oC, while it was 0.28 mm and 0.12 mm for the tests at 22 and 60 ^oC, respectively. For σ'_{n0}=300 kPa (Fig. 3.17(d)), the same behaviour was observed, and the contraction at 5 ^oC was higher than those obtained at 22 and 60 ^oC.

Fig. 3.18 shows the Mohr-Coulomb plane for the clay-structure interface CNL tests at different temperatures. The peak friction angle for all studied temperatures was 14^o. The main difference between the Mohr-Coulomb envelopes for different temperatures was the adhesion. The increase in temperature, increased the peak adhesion (cohesion between soil and structure) from 12.5 kPa to 18 kPa while the residual adhesion remained constant (16.5 kPa).

3.4.2.2 Constant normal stiffness (CNS)

To investigate the shear characteristics of the clay-structure interface, constant normal stiffness (CNS) conditions were applied. The results for K = 1000 kPa/mm that is intermediate value between K = 500 (CNL) and 5000 kPa/mm (CV) are presented (Fig. 3.19).

The shear stress versus shear displacement for two initial normal stresses (σ'_{n0}=100 and 300 kPa) at 22 and 60 ^oC are presented in Fig. 3.19(a). At σ'_{n0}=100 kPa, the shear stress increased with increasing shear displacement until reaching a value of 1 mm (τ = 33 kPa) then, with a slight decrease, the shear stress continued towards the critical state (τ = 28 kPa). The curves for both 22 and 60 ^oC followed the same trend. Tests at σ'_{n0}=300 kPa showed a very clear peak and then decreased towards a constant value. As mentioned for 100 kPa, under σ'_{n0}=300 kPa, the shear stresses at 22 and 60 ^oC are similar. For both initial normal stresses, kaolin contracted until the end of the shear (Fig. 3.19(b)). For σ'_{n0}=100 kPa at 22 ^oC, the amount of normal displacement in the critical state was around 0.035 mm. This value was approximately 0.02 mm for tests at 60 ^oC, and the heated samples showed less contraction. For σ'_{n0}=300 kPa at 22 and 60 ^oC, the amount of normal displacement in the critical state was 0.9 and 0.6 mm, respectively. In Fig. 3.19(c) the variation of normal stress during CNS tests of clay-structure interface is presented. For both σ'_{n0}=100 and 300 kPa the normal stresses decreased during shearing process. For samples exposed to higher temperatures the amount of reduction was less than samples at 22 ^oC. For tests at σ'_{n0}=100 kPa at 22 and 60 ^oC the normal stress decrease was about 42 and 30 kPa respectively.

In Fig. 3.19(d), the normal stress vs. shear stress planes for the clay-structure interface CNS and CNL tests are presented. For σ'_{n0}=100 and 300 kPa in the CNS tests, the shear stress increased with decreasing normal stress, and the shear reached a peak value and then decreased. The heated samples showed less decrease in the normal

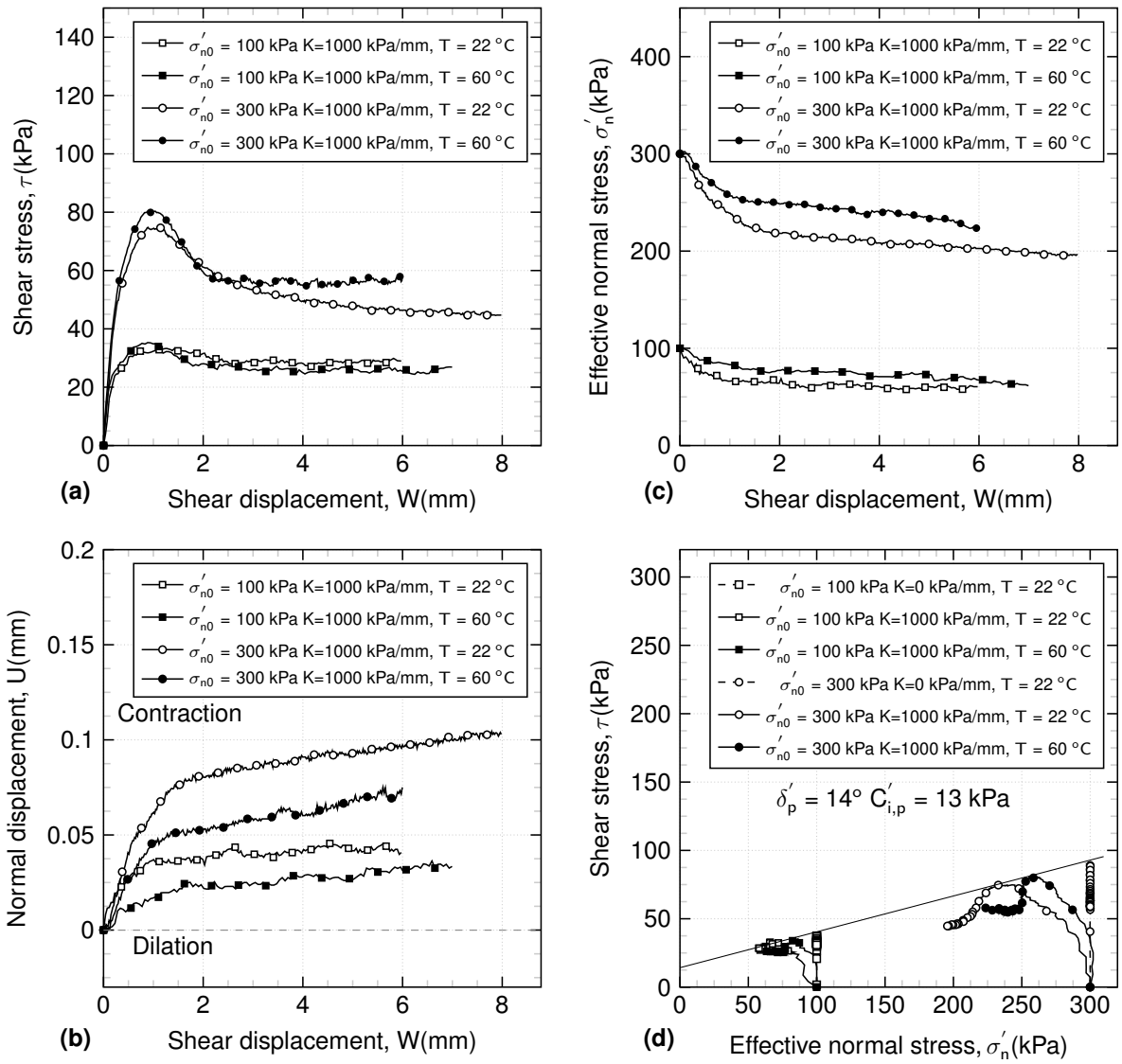

Figure 3.19: CNS results for clay-structure interface at $T = 22\ ^oC$, $T = 60\ ^oC$. (a) shear stress vs. shear displacement; (b) Normal displacement vs. shear displacement; (c) Normal stress vs. shear displacement; (d) shear stress vs. effective normal stress

stress. For example, for σ'_{n0}=300 kPa, the peak shear strength for heated samples was slightly higher than 22 ^oC, and the normal stress decrease in the heated sample was also less than that at 22 ^oC. The peak friction angle and adhesion of the CNS tests were 14^o and 13 kPa respectively.

3.4.3 Clay vs. clay-structure interface

In Fig. 3.20 the CNL tests of clay and clay-structure for σ'_{n0}=100 kPa are compared.

The peak shear stress in the clay-structure tests is obtained with smaller shear displacements (1.2-1.6 mm), while for the clay, the peak shear stress is around (2.8-3.2 mm), and the softening behaviour after the peak is more pronounced for the clay-structure interface. The peak shear stress difference of 6 kPa for clay vs clay-structure

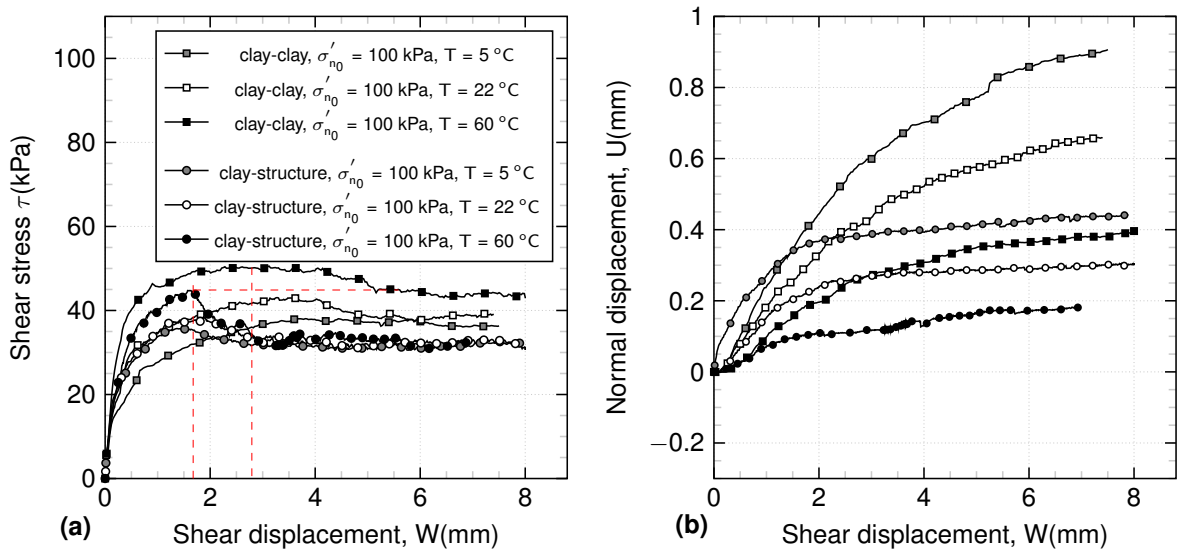

Figure 3.20: Comparison of CNL results for clay and clay-structure interface with σ'_{n0} = 100 kPa at $T = 5\ ^oC$, $T = 22\ ^oC$ and $T = 60\ ^oC$.

at 22 ^oC and 7.5 kPa at 60 ^oC for σ'_{n0}=100 kPa confirms that the shear occurs in the interface zone and not in the soil mass.

In terms of volumetric behaviour, the clay tests are completely different with clay-structure tests (Fig. 3.20(b)). In clay tests the contraction increases until the end of test but in the clay-structure tests the contraction increases more rapidly compare to the clay tests, and then remains constant. Tsubakihara and Kishida 1993 have performed direct shear tests on Kawasaki clay and mild steel. They found that, the reason for the volumetric behaviour difference between clay and clay-structure tests, can be the sliding shear mode that occurs in the interface.

3.5 Discussion

In the following section, the discussion about the effects of temperature on sand and clay interface shear strength is presented.

3.5.1 Effect of temperature on sand

Fig. 3.21 shows the effect of temperature on cohesion, adhesion and friction angle of different soils that have been studied for interface direct shear tests at different temperature variations in the literature, which is compared to results obtained in this study. As can be seen, the effect of temperature on the peak and residual friction angle of sand and sand-structure interface are negligible (Fig. 3.21(b)). The similar shear curves, volumetric behaviour and Mohr-Coulomb plane at different temperatures (Fig. 3.8) for sand samples also confirm that, the effect of temperature on the shear

strength of sand is negligible. These observations are in line with existing studies (Di Donna et al. 2015; Yavari et al. 2016). For sand-structure interface tests with different stiffness and temperatures, it was observed that, the interface behaviour in CNS condition does not change at different temperatures. For sandy soil used in this study, in the context of energy foundations, heating a sand-structure interface in this range of temperatures does not change the mechanical properties of the interface, and in the design calculations no further precautions should be considered for thermal effects.

3.5.2 Effect of temperature on clay

In clay tests, heating under drained conditions led to a contraction of the samples, and consequently the shear strength increased due to thermal hardening (Fig. 3.14). Several authors observed this thermally induced contraction and shear strength increase during drained heating of normally consolidated clays (Campanella and Mitchell 1968; Hueckel and Baldi 1990; Kuntiwattanakul et al. 1995; Chiu 1996; Cekerevac and Laloui 2004; Abuel-Naga et al. 2006). Baldi et al. 1988 have explained, the reason of this thermo-plastic strain may be in the micro-structural changes as the tendency of clay flakes to group together which increases the mineral-to-mineral contact and generates irreversible strain.

Fig. 3.20 shows that the peak and residual shear strength in the clay-structure tests, were always less than those obtained during clay tests. This showed that the shearing occurred at the interface zone. Moreover, the peak shear stresses of the clay-structure tests are close to the residual shear stress values of clay tests at all tested temperatures. This may be due to the sliding, or partially sliding, shear mode along the interface. Indeed, Lemos and Vaughan 2000 showed that, in clays with high clay content in which residual soil shear is in the sliding mode, peak interface shear strength normally is close to the soil residual strength and is independent of roughness (Fig. 3.20). Therefore, in the clay-structure interface tests performed in this study, the sliding or partially sliding shear mode at interface occurred for all tested temperatures.

The peak cohesion of clay samples increases from 17 to 23 kPa while the peak adhesion of clay-structure increases from 12 to 18 kPa with temperature increase from 22 to 60 ^oC while the residual adhesion remained stable (Fig. 3.21(a)). Therefore, it can be concluded that cohesion is more affected by temperature modification. This reflects the interaction between the structure and the clay. For kaolin clay, heating the interface tend to slightly increase the shear strength of the interface. Therefore, in terms of structural safety of energy geostructures, temperature increase in normally consolidated kaolin clay can be considered as a positive aspect.

In isothermal conditions, Potyondy 1961 have performed direct shear tests on dif-

ferent soils and different structural materials like steel, concrete and wood. He found that the friction angle and adhesion of a smooth steel interface is less than a smooth concrete interface. Therefore, it can be concluded that the nature of the structural material plays a major role in the interface behaviour and further works should be carried out to investigate the nature the interface behaviour on different construction materials.

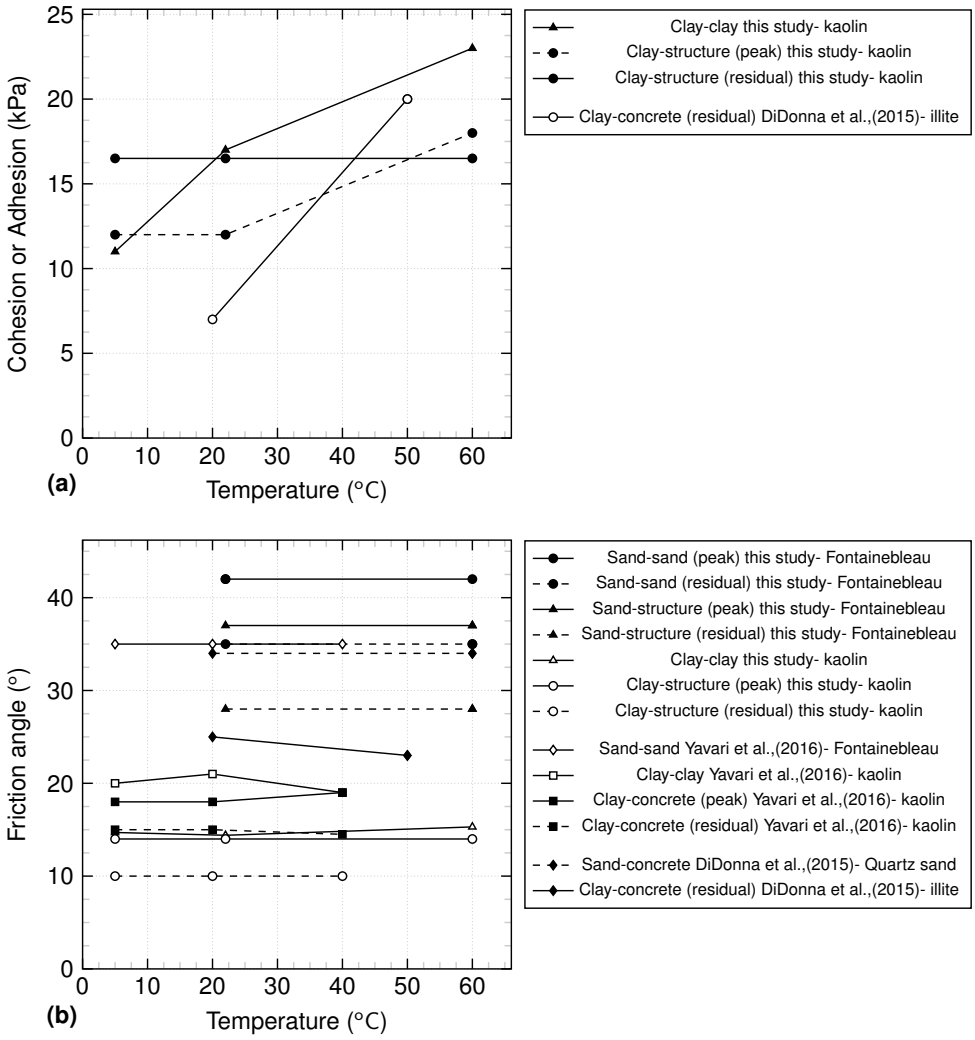

Figure 3.21: Effect of temperature on (a) cohesion and (b) friction angle.

3.6 Conclusions

Constant normal load (CNL) and constant normal stiffness (CNS) interface tests were conducted on soil and soil-structure samples at different temperatures (5,22 and 60 ^oC). The results showed that the mechanical properties of sand are independent of temperature (22 and 60 ^oC) for both sand and sand-structure tests. Different stiffness values were applied under CNS conditions at different temperatures, and it was

observed that such as the CNL tests, the temperature does not change the interface behaviour under the CNS condition. Additionally the same interface friction angle was obtained in both CNL and CNS tests for sand-structure interface tests.

In kaolin clay, temperature does not affect the friction angle and the main effect is the increase of the cohesion or adhesion. For clay tests, due to thermal contraction of kaolin during heating, the soil becomes denser and shows a higher shear strength. It was found that temperature increases the cohesion of clay samples. In clay-structure contact, due to difference in the nature of materials (clay vs. metal) the adhesion is not as much as clay case, therefore the shear strength increase with temperature increase, is not as much as clay case. In CNS tests on clay-structure interface, the soil exposed to higher temperatures, showed less contraction during shearing, and consequently less normal stress decrease due to the denser state of the heated clay-structure samples prior to shearing. Therefore, in the interface the soil becomes denser with heating and the shear strength increases slightly.

Further work will be carried out to investigate the effects of thermo-mechanical cycling on the mechanical behaviour of soil-structure interface.

Chapter 4

Effect of temperature on cyclic behavior of clay-structure interface

Abstract

The shaft capacity of foundations highly depends on the monotonic and cyclic loads applied to the soil-structure interface. In energy geostructures which exploit the heat of soil using earth-contact elements, the interface is subjected to cyclic thermo-mechanical loads. Monotonic and cyclic constant-volume equivalent-undrained (CVEU) direct shear tests were performed on clay-clay and clay-structure interface at different temperatures (22 and 60 ^{o}C). An effective vertical stress of 300 kPa was applied to the samples and the cyclic and average shear stress ratios (τ_{cy}/S_u^{Ds} and τ_a/S_u^{Ds}, respectively) were varied between 0.35 and 0.57. The tested soil was a kaolin clay (PI=24) prepared in a normally consolidated state. The results showed that, the number of cycles to failure for the clay-structure interface test was lower than that for the clay-clay case in the same range of cyclic and average shear stress ratios. In cyclic clay-structure tests, decreasing the cyclic stress ratio, increased the number of cycles to failure; however decreasing the average shear stress ratio decreased the number of cycles to failure. Increasing the temperature, decreased the rate of strain accumulation and the number of cycles to failure increased by 2-3 times. The rate of degradation (degradation parameter, t) decreased by 16% with heating from 22 to 60 ^{o}C for the different cyclic stress ratios tested.

Keywords: energy geostructures, soil-structure interface, temperature, cyclic loads, strain accumulation

Résumé

La capacité portant des fondations dépend fortement des charges monotones et cycliques appliquées à l'interface sol-structure. Dans les géostructures énergétiques qui exploitent la chaleur du sol, l'interface est soumise à des charges thermomécaniques

cycliques. Des essais de cisaillement direct monotones et cycliques à volume-constant équivalent-nondrainé (CVEU) ont été réalisés sur l'argile et l'interface argile-structure à différentes températures (22 et 60 ^{o}C). Une contrainte verticale effective de 300 kPa a été appliquée aux échantillons et les rapports des contraintes de cisaillement cycliques et moyennes (respectivement τ_{cy}/S_u^{Ds} et τ_a/S_u^{Ds}) ont varié entre 0,35 et 0,57. Le sol testé était un kaolin (PI=24) préparé dans un état normalement consolidé. Les résultats ont montré que le nombre de cycles jusqu'à la rupture pour l'essai d'interface argile-structure était inférieur à l'argile dans la même gamme de contraintes cycliques. Dans les essais cycliques sur l'interface argile-structur, la diminution du rapport de contrainte cyclique (CSR) a augmenté le nombre de cycles jusqu'à la rupture; cependant, la diminution du rapport moyen de contrainte de cisaillement (ASR) a diminué le nombre de cycles jusqu'à la rupture. L'augmentation de la température, a diminué du taux d'accumulation de la déformaiton et le nombre de cycles jusqu'à la rupture ont augmenté de 2 à 3 fois. Le taux de dégradation (paramètre de dégradation, t) a diminué de 16% avec un chauffage de 22 à 60 ^{o}C pour les différents rapports de contrainte cyclique testés.

Mots clés: géostructures énergétiques, l'interface sol-structure, température, charges cycliques, accumulation de déformation.

4.1 Introduction

Incorporation of heat exchangers in conventional geostructures like piles can extract the heat from the soil for heating purposes and inject it to the soil for cooling purposes. The heat exchanger absorber pipes are attached to the reinforcement cage of geostructures (Brandl 2006). In recent years, research has been conducted at full and laboratory scale to investigate the effect of temperature on the geotechnical behavior of these energy geostructures as well as on the surrounding soil (e.g. Laloui et al. 2006; Bourne-Webb et al. 2009; Murphy et al. 2015; Faizal et al. 2018). These energy geostructures can be subjected to cyclic mechanical loads and thermal variations throughout their lifetime. The soil-structure interface, plays a key role in the transmission of the loads to the ground. According to the observations in experimental results, soil-structure interface is a composite of the structural surface and a thin-layer soil nearby which develops a strain localization caused by the transmission of shear force of structure to the soil (Pra-ai and Boulon 2017). Mechanical behavior of interface, which differs from the surrounding soil, depends on the stress state, roughness of the structural surface, density, state of the soil and constant normal stiffness conditions. It is known that cyclic loads evolve the shear resistance of the soil-structure interface and thus the shaft capacity of the structure. Several studies have been performed on the cyclic behavior

of sand-structure interface (Potyondy 1961; Desai et al. 1985; Boulon and Foray 1986; Uesugi and Kishida 1986; Poulos and Al-Douri 1992; Jardine et al. 1993; Lehane et al. 1993; Fakharian and Evgin 1997; Mortara et al. 2007; Pra-ai and Boulon 2017), while less is known about the behavior of clay-structure interface (Lemos and Vaughan 2000; Di Donna et al. 2015). In this context, the objective of this study is to investigate the effect of temperature on the cyclic behavior of clay-structure interface. In the following the current knowledge of the influencing parameters on the cyclic behavior of soil and soil-structure interface is discussed.

Saturated clays under cyclic loading in undrained and isothermal conditions, develop accumulation of deformation and generation of excess pore water pressure with increase in number of cycles, which cause shear strength reduction and induce failure (Mortezaie and Vucetic 2013). The shear stress-strain curve of a soil under cyclic loading can be decomposed into average (τ_a) and cyclic shear stress (τ_{cy}) components, while the deformation can be seen as the combination of permanent shear strain (ϵ_p) and cyclic shear strain (ϵ_{cy}) (Fig. 4.1(a)). Several parameters, such as the average shear stress, cyclic shear stress, loading frequency (f), strain rate ($\dot{\epsilon}$), number of cycles (N), normal stress (σ_n), temperature (T^o) and initial state of the soil (normally consolidated or overconsolidated) are mentioned as influencing factors on cyclic response of soils (Andersen et al. 1980; Yasuhara et al. 1982; Matasović and Vucetic 1995; Zhou and Gong 2001; Moses et al. 2003; Lackenby et al. 2007; Andersen 2009; Li et al. 2011; Wichtmann et al. 2013).

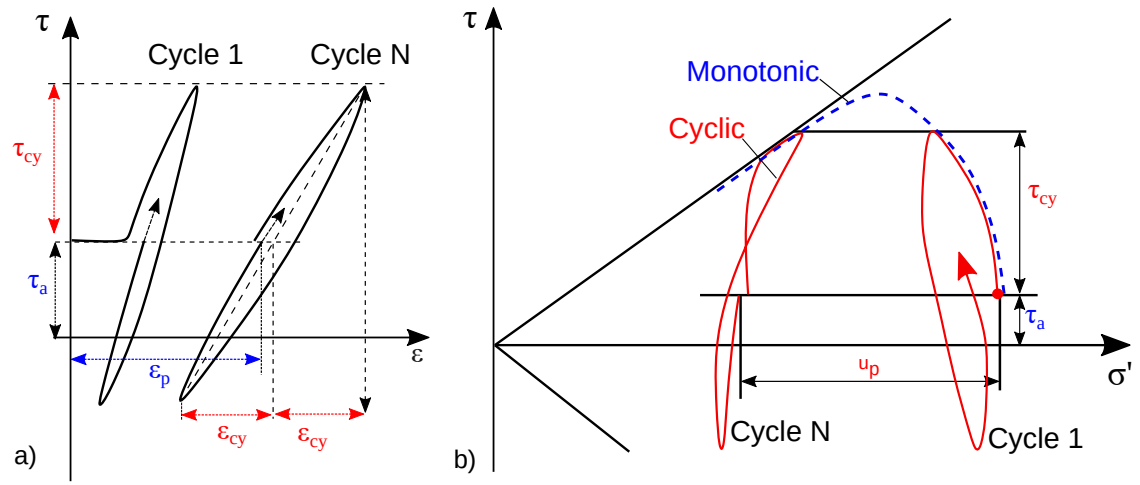

Figure 4.1: Stress-strain behavior of soils under cyclic loading.

Several studies showed that the number of cycles to failure, N_f, decreases with increasing cyclic shear stress (τ_{cy}), but for a given cyclic shear stress (τ_{cy}), a cyclic loading with a lower average shear stress (τ_a) causes failure in fewer cycles than a cyclic loading applied at higher average shear stress (τ_a) (Wichtmann et al. 2013). In undrained conditions, volumetric changes are prevented and the effective stresses in

the soil decrease with pore water pressure buildup (u_p) (Fig. 4.1(b)). The excess pore water pressure generated during cyclic loading depends on the amplitude of the cyclic shear strain or stress, the number of cycles, the frequency of cyclic loading and the overconsolidation ratio (Yasuhara et al. 1982; Ohara and Matsuda 1988). Cyclic stress or strain induced deformation accumulation and excess pore water pressure lead to soil degradation and can induce failure (Seed and Chan 1966; Andersen et al. 1980; Thian and Lee 2017). Idriss et al. 1976 and Idriss et al. 1978 introduced the degradation index (δ) and the degradation parameter (t), that for the stress-controlled tests can be determined as follows:

$$\delta = \frac{G_{SN}}{G_{S1}} = \frac{\tau_c/\epsilon_{cyN}}{\tau_c/\epsilon_{cy1}} = \frac{\epsilon_{cy1}}{\epsilon_{cyN}} \tag{4.1}$$

$$t = -\frac{log\delta(N)}{logN} \tag{4.2}$$

where G_{S1} and G_{SN} are the secant moduli at cycles 1 and N, τ_c is the shear stress value, ϵ_{cy1} and ϵ_{cyN} are the cyclic shear strains at cycles 1 and N, respectively. The degradation index can be seen as a mean to evaluate the rate of strain accumulation and the ratio of the cyclic strain at cycles 1 and N. Soil with a high δ value will have a low degree of degradation (Zhou and Gong 2001). The average degradation parameter, t, is the slope of the δ vs N line in a log-log scale, which describes the rate of cyclic degradation with N. Studies have shown that the degradation parameter depends on the plasticity index and OCR of the soil (Vucetic and Dobry 1988; Tan and Vucetic 1989). The degradation parameter, t, consistently decreases with an increase in the OCR (Soralump and Prasomsri 2015). Soltani and Soroush 2010 showed that there was an increase in the degree of degradation as the number of loading cycles and cyclic shear strain amplitude increased. In cyclic strain-controlled tests carried out on kaolinite in simple shear device, Mortezaie and Vucetic 2013 found that in larger cyclic shear strain amplitudes, increase of frequency (f), accelerates the degradation but in higher vertical stresses ($\sigma_{vc}^{'}$) the degradation decreases. Frequency is influenced by the strain rate in cyclic simple and direct shear tests and the strain rate can have crucial impacts on the shear strength and volumetric behavior during shearing. Martinez and Stutz 2018 have performed interface monotonic direct shear tests on kaolin clay-steel interface with different strain rates to investigate the interface behavior under drained and undrained conditions. They found by increasing the shearing velocity, the undrained behavior was observed by smaller interface strength and volumetric changes.

Very few studies have been carried out on the effect of temperature on cyclic behavior of soils. Cekerevac and Laloui 2010 performed temperature-controlled cyclic triaxial tests on kaolin samples. The samples were consolidated under 600 kPa and

heated up to 90 ^{o}C in drained conditions and were cyclically sheared under undrained conditions. They found that the initial cycle imposed at either ambient or high temperature produced almost the same axial strain and pore water pressure. However later shear cycles of the heated sample induced smaller strain and smaller pore water pressure per cycle. The number of cycles to failure increased for heated samples due to the densification of clay under drained heating and also the pore water pressure of heated samples was slightly less than unheated ones. Xiong et al. 2018 performed cyclic triaxial tests at different temperatures on a saturated soft clay. They showed that the cumulative plastic strain, pore water pressure and dynamic damping ratio of saturated clay decreased with increasing temperature, while the dynamic modulus increased with increasing temperature, and the soft clay showed thermal hardening behavior.

Regarding the impact of temperature on the soil-structure interface, some experimental studies have been performed (Di Donna et al. 2015; Yavari et al. 2016; Li et al. 2018; Maghsoodi et al. 2020; Yazdani et al. 2019) on direct shear device and concerning the in-situ behavior; Murphy and McCartney 2014 have developed a thermal borehole shear device to study effect of temperature on the in-situ shear behavior of soil-concrete interfaces, but to the knowledge of the authors very few studies have been carried out on the thermal effects on the cyclic behavior of clay-structure interface. Di Donna et al. 2015 performed cyclic constant normal stiffness (CNS) two-way strain controlled tests at different temperatures on illite clay. They revealed that testing clay-concrete samples under CNS conditions at higher temperatures, reduces the volumetric contraction during cyclic shearing and the material becomes denser therefore, more cycles are required to degrade the interface strength.

In this context, this study was focused on the one-way cyclic behavior of clay-structure interface under isothermal or non-isothermal conditions. The effects of two parameters on strain accumulation, excess pore water pressure and cyclic degradation were more specifically considered. The first one is the average shear stress (τ_a) that represents the allowable shear stress that is mobilized in the structures once the serviceability starts. The second one is the cyclic shear stress (τ_{cy}) that corresponds to the mechanical solicitations that are imposed to the structure during its lifetime once the average shear stress is reached.

The following aspects that influence the cyclic behavior of clay-structure interface are addressed:

• The mechanical monotonic and cyclic behavior differences between clay-clay and clay-structure interface.

• The effect of average and cyclic shear stress variations (τ_a/S_u^{Ds} and τ_{cy}/S_u^{Ds}) on clay-structure interface cyclic behavior at different temperatures.

• The effect of temperature on the strain accumulation, equivalent pore water pressure,

cyclic loop shape and degradation behavior of the clay-structure interface.

4.2 The shear device, sample preparation and the experimental program

4.2.1 Material properties

The physical and thermal properties of kaolin clay used in this study are presented in Table 4.1. To perform clay-structure interface direct shear tests, a stainless steel plate (80 x 60 x 10 mm) with the desired roughness was designed and used as the structure to avoid the surface abrasion due to test repetition. The roughness of the steel plate was measured with a laser profilometer. Several profiles parallel to the shear direction were measured. The heights of these four profiles that were obtained with the laser are presented in (Fig. 4.2(a)). Fig. 4.2(b) shows the height of the one of the profiles in a closer view. The measured average roughness R_a for the profiles was 20 μm, therefore, the plate was considered as a rough surface for clay-structure interface (Maghsoodi et al. 2019a; Maghsoodi et al. 2019b).

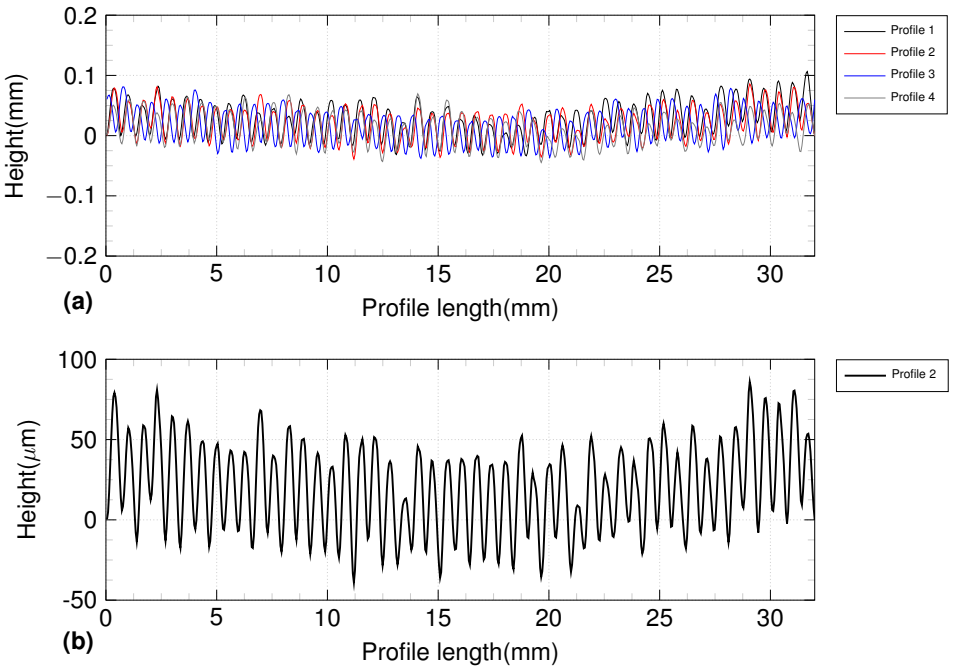

Figure 4.2: Surface roughness profiles; (a) Measured profiles (b) Surface profile 2.

4.2.2 The temperature-controlled direct shear device

Fig. 4.3 shows the configuration of the temperature-controlled direct shear device. The shear box (60 x 60 x 35 mm) was placed inside a container filled with water

Table 4.1: Kaolin clay physical and thermal properties.

Liquid limit, LL (%)	57%
Plastic limit, PL (%)	33%
Plasticity index, PI (%)	24%
Particle specific gravity, ρ_s (Mg/cm^3)	2.60
Thermal conductivity, λ (W/mK)	1.5
Heat capacity, C (J/m^3K)	3.3
Hydraulic conductivity, k (m/s)	1×10^{-8}

to reach saturated conditions (Fig. 4.3). The circulating fluid at the bottom of the shear box container was connected to a thermal regulation system. In such a setup, the temperature of the fully saturated shear box container can be controlled by three thermocouples, one in the lower half of the shear box, another on the upper half of the shear box and the last one in the container. The device can be programmed either in stress or deformation controlled tests (Maghsoodi et al. 2020). The lower half shear box is displaced horizontally to apply the shear.

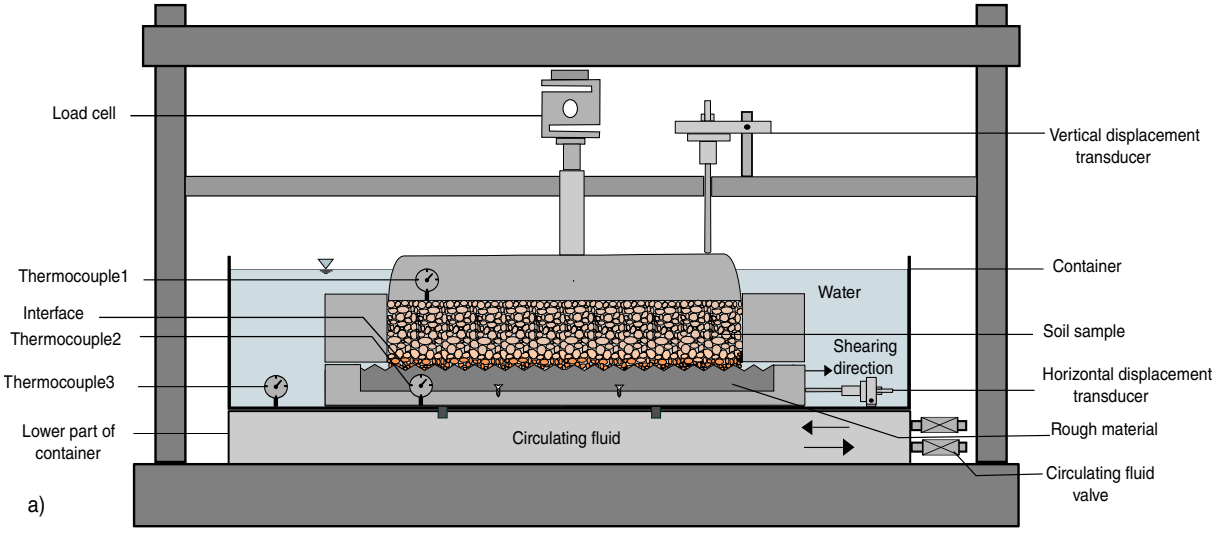

Figure 4.3: Experimental setup of the direct shear temperature-controlled device.

4.2.3 Sample preparation

To perform the clay-clay and clay-structure shear tests, a slurry of kaolin clay with a water content of 63%, which was slightly higher than its liquid limit ($LL = 57\%$) was prepared and left for 24 hours for homogenization. Subsequently, the clay was poured into the shear box and special attention was paid to avoid trapping any air. Then, the shear box was placed inside the fully saturated shear box container. Afterwards, the normal stress was applied incrementally during the consolidation phase, each load increment lasted 2 hours and the last step (300 kPa) was left 8 hours to ensure full consolidation. The consolidation phase took 24 hours. Based on the consolidation tests

performed on this kaolin clay, the final void ratio after consolidation for $\sigma'_{n0} = 300$ kPa was $e = 0.85$. For tests at 60 ^oC, a heating rate of 5 $^oC/hr$ was applied and left for 4 hours to ensure the fully thermal consolidation of the clay under constant normal stress conditions (300 kPa).

4.2.4 Experimental program

To apply equivalent-undrained conditions in the clay-structure interface tests, the constant-volume equivalent-undrained (CVEU) concept was used in this study. In the extreme case of the constant normal stiffness condition, constant volume case (K= ∞ (kPa/mm)), the vertical stress is varied to keep the volume of the sample constant. In the studies using this concept, as conducted by Vucetic and Lacasse 1984; Dyvik et al. 1987 and Mortezaie and Vucetic 2016; during shearing, in drained conditions while the pore water pressure was zero, the change in the vertical stress to keep the volume of the sample constant was equivalent to the pore water pressure generated in a truly undrained triaxial test. Several studies have confirmed this approach, using direct shear device (Takada 1993; Hanzawa et al. 2007). Takada 1993 have introduced the direct shear device that is capable to perform constant volume equivalent undrained tests and they have confirmed the capability of the direct shear device to perform CVEU tests. Hanzawa et al. 2007 have performed a comparative study of the NGI Direct Simple Shear Test (DSST) and the Direct Shear Test (DST). Samples from Norwegian Drammen clay and Japanese Ariake clay were subjected to both types of test. They found that the DST test gave generally higher stiffness and strength than the DSST. They explained these differences that can mainly be accounted for by the different shearing mechanisms and shearing rates.

The experimental program proposed in this study is based on constant-volume equivalent-undrained (CVEU) concept. As it was shown in Fig. 4.1, the shear cycles consisted of average and cyclic shear stresses. The objective of this study is to vary these two components of the shear stress in a way that reproduces probable cases of interfaces in energy geostructures under cyclic loading. Therefore, in order to cover a wide range of stress ratios and also apply diverse cyclic paths that can be subjected to the structure, different ranges of cyclic and stress ratios that are mentioned in literature were chosen (Wichtmann et al. 2013; Thian and Lee 2017; Zhou and Gong 2001). The experimental program consisted of monotonic and cyclic CVEU clay-clay and clay-structure interface direct shear tests at different temperatures (Table 4.2 and Table 4.3) and it is presented in Fig. 4.4.

The monotonic program consisted of clay-clay and clay-structure interface tests to determine the essential parameters for cyclic experimental program such as S_u^{Ds}

Table 4.2: Monotonic experimental program for a $\sigma'_{n0} = 300$ kPa and T= 22 ^{o} C .

N^o	S_u^{Ds} (kPa)	w$_i$%	w$_f$%	$\dot{P}_d(\%/min)$	e_0	Tt
1	56.4	62.3	37.2	0.01	0.835	clay-clay
2	56.4	63.3	43.2	0.02	0.828	clay-clay
3	63.1	59.6	36.0	0.01	0.844	clay-structure
4	63.2	60.5	36.2	0.02	0.836	clay-structure

w$_i$(%): initial water content at the beginning of consolidation, w$_f$(%): final water content at the end of shearing, e_0(-): void ratio before shearing, Tt: test type.

Table 4.3: Cyclic experimental program for a $\sigma'_{n0} = 300$ kPa.

N^o	τ_a (kPa)	τ_{cy} (kPa)	S_u^{Ds} (kPa)	τ_a/S_u^{Ds} (-)	τ_{cy}/S_u^{Ds} (-)	T $^o(C)$	N_f (-)	w$_i$ %	w$_f$ %	e_0 (-)
6*	23	27	56.4	0.41	0.47	22^o	370	63.0	36.6	
7	26	36	63.1	0.41	0.57	22^o	39	63.0	36.6	0.870
8	26	36	63.1	0.41	0.57	60^o	165	61.4	39.3	0.832
9	26	34	63.1	0.41	0.54	22^o	46	60.9	36.4	0.812
10	26	34	63.1	0.41	0.54	60^o	137	61.7	35.7	0.868
11	26	30	63.1	0.41	0.47	22^o	185	60.7	42.5	0.852
12	26	30	63.1	0.41	0.47	60^o	645	63.0	35.1	0.784
13	26	22	63.1	0.41	0.35	22^o	4138	63.0	35.1	0.855
14	26	22	63.1	0.41	0.35	60^o	> 10000	61.6	35.1	0.804
15	28	34	63.1	0.44	0.54	22^o	65	62.4	37.8	0.825
16	28	34	63.1	0.44	0.54	60^o	111	61.7	38.0	0.793
17	30	30	63.1	0.47	0.47	22^o	230	62.2	36.5	0.840
18	30	30	63.1	0.47	0.47	22^o	246	61.3	(-)	(-)
19	30	30	63.1	0.47	0.47	60^o	991	61.2	35.0	0.788
20	24	30	63.1	0.47	0.38	22^o	57	62.5	37.3	0.833
21	24	30	63.1	0.47	0.38	60^o	355	61.4	35.6	0.806
22	30	22	63.1	0.47	0.35	22^o	> 1000	60.6	37.3	0.834
23	30	22	63.1	0.47	0.35	60^o	> 1000	61.3	40.4	0.794

*: clay-clay test. w$_i$(%): initial water content at the beginning of consolidation, w$_f$(%): final water content at the end of shearing. N$_f$(−): Number of cycle to failure, e_0(-): void ratio before shearing.

(undrained shear strength in direct shear, Fig. 4.4). Additionally, the monotonic program can be considered as a reference, to better understand the cyclic behavior of clay-clay and clay-structure interface. After the consolidation (or consolidation+heating) phase, for monotonic tests different deformation rates were applied ($\dot{P}_d =$ 0.01, 0.02%/min). Based on ASTM 1998; the relative lateral displacement, is defined as the changes in horizontal displacement, ΔW(mm) divided by the initial length of the sample ($l_0 = 60$ mm).

The cyclic program consisted of two parts. The first part, cyclic clay-clay test was performed to investigate the differences in the cyclic behavior between clay-clay and clay-structure interface. The second part was dedicated to the cyclic clay-structure interface tests at different temperatures. For cyclic tests, the shear stress was increased

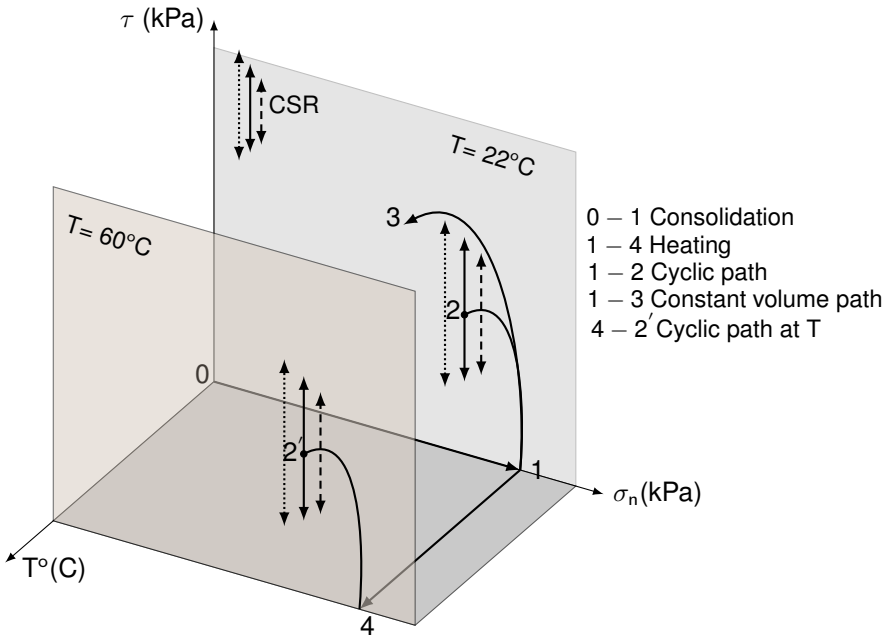

Figure 4.4: Cyclic thermo-mechanical path.

to the average value (τ_a, path 1-2 in Fig. 4.4) and then the shear cycles fluctuated in a regular manner between $\tau_a + \tau_{cy}$ and $\tau_a - \tau_{cy}$ with a frequency of 0.005 Hz. The cycles were continued until a relative lateral displacement of 10% was reached. Failure was defined when the relative lateral displacement reached 10%. The volume of the sample was kept constant throughout the tests. Two types of tests were performed, the first one consisted of a constant average shear stress ratio τ_a/S_u^{Ds} (ASR) while varying the cyclic shear stress ratio τ_{cy}/S_u^{Ds} (CSR). The second type was performed with a constant cyclic stress ratio τ_{cy}/S_u^{Ds} but the average stress ratio τ_a/S_u^{Ds} was changed. The objective of the first type was to investigate the effect of cyclic shear stress and the second one was the effect of average shear stress on the cyclic behavior of clay-structure interface. The cyclic stress ratio τ_{cy}/S_u^{Ds} between 0.35 and 0.57 and the average stress ratio τ_a/S_u^{Ds} between 0.38 and 0.47 were chosen.

4.3 Experimental results

4.3.1 Monotonic CVEU clay-clay and clay-structure interface tests

To determine the undrained shear strength in direct shear (S_u^{Ds}) test and to investigate the cyclic behavior of clay-clay and clay-structure interface, monotonic clay-clay and clay-structure tests were performed. The comparison of the results obtained during the monotonic tests of the clay-clay and clay-structure constant-volume equivalent-undrained (CVEU) shear tests highlighted some significant differences (Fig. 4.5).

The peak shear stress for the clay-structure tests are around 1-1.5% of relative

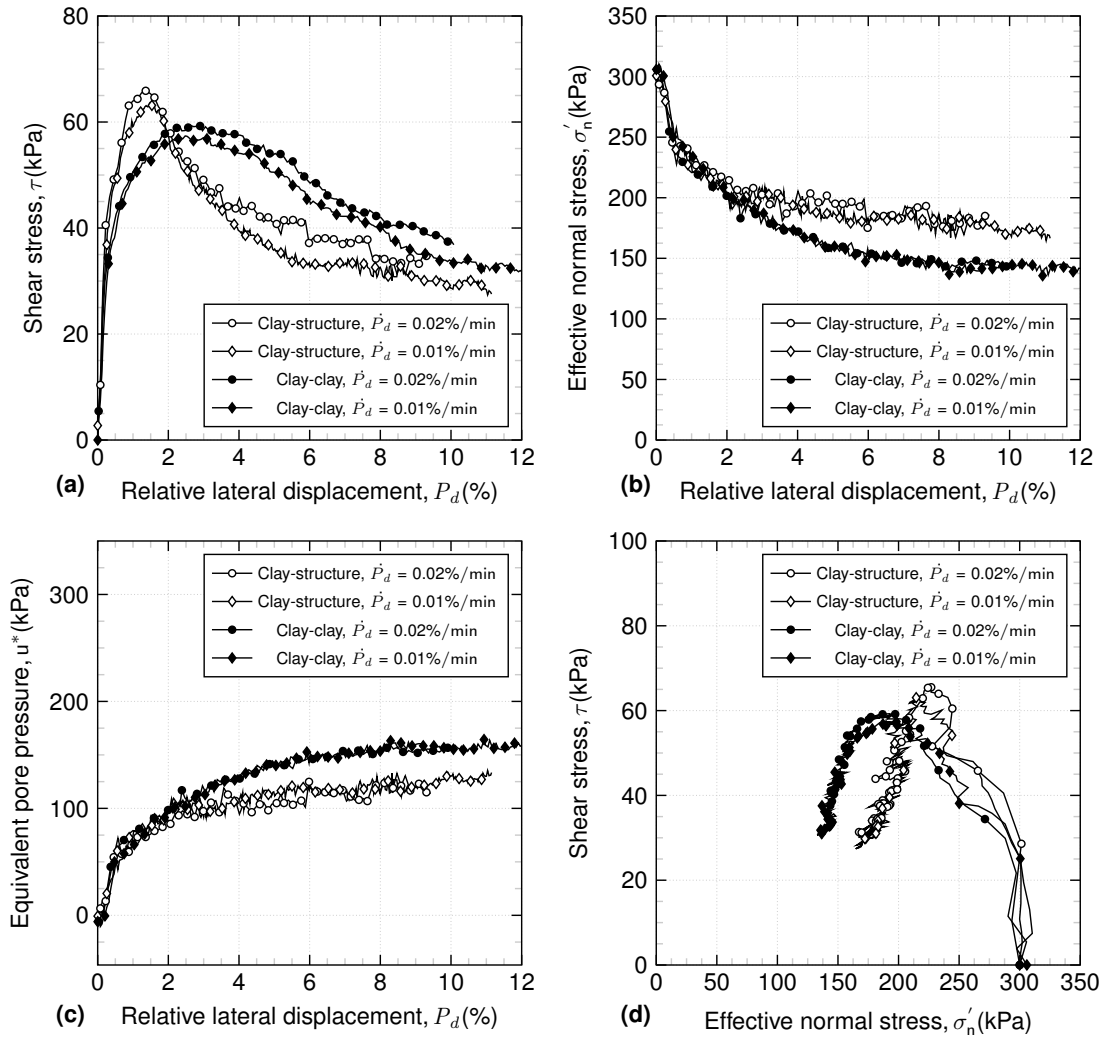

Figure 4.5: Monotonic constant-volume equivalent-undrained (CVEU) clay-clay and clay-structure interface tests.

lateral displacement, while for the clay-clay tests the peak occurs in larger relative lateral displacements (2-3%). Afterwards the strain softening for clay-structure tests occurred at smaller relative lateral displacements (2%) compared to the clay-clay tests which started from 4% and continued until the end of the test. These observations confirmed that the shear occurred in the interface zone.

Fig. 4.5(b) shows the variation in the effective normal stress with relative lateral displacement. Due to the normally consolidated state of the soil and to keep the volume of the sample constant, the effective normal stress decreased with shearing for both clay-clay and clay-structure tests. In the clay-clay case the effective normal stress started to decrease from the beginning of the test and after a relative lateral displacement of 6% it remained unchanged. For the clay-structure tests the effective normal stress ($\sigma_n^{'}$) up to a relative lateral displacement of 2.5% was completely superimposed on the clay-clay behavior. From 2.5 to 12% $\sigma_n^{'}$ decreased more for clay-clay compared to

clay-structure interface. This can be explained by the thickness of the shear band and different shearing modes at the shearing plane between clay-clay and clay-structure samples. Several studies confirmed that the volumetric response (normal stress/pore water pressure variations in CVEU concept) is strongly influenced by different shearing modes at the interface zone (mode I, II and III) (Littleton 1976; Lupinl et al. 2009; Tsubakihara et al. 1993). Mode I is a complete shear in the soil mass, mode II is the sliding at the interface and mode III is a combination between mode I and II. Tsubakihara et al. 1993 performed clay-clay and clay-steel interface tests with different roughness. They mentioned for $R_{max} = 20\mu m$ (the same roughness of the steel plate used in this study), the shearing mode can be considered as type III. In mode III, a combination of mode I and II, partially sliding at the interface occurs. In some parts of shearing plane, clogging of clay particles between asperities takes place and on the other parts full sliding is dominant. The same trends as Fig. 4.5(b) can be observed for the equivalent pore water pressure (Fig. 4.5(c)). From 2.5 to 12% of relative lateral displacement, the equivalent pore water pressure that was generated for clay-clay was higher than the clay-structure tests. The thickness of clay-clay shear band is greater than clay-structure samples and furthermore, the shearing mode for clay-structure interface tests up to 2.5% of P_d is mode I while from 2 to 2-12% is mode II which can explain the observed behavior. For the Mohr-coulomb plane, Fig. 4.5(d) shows the reduction of effective normal stress with increasing the shear stress for both clay-clay and clay-structure interface CVEU tests.

4.3.2 Cyclic behavior at different temperatures

In this section, first, the typical results that can be obtained in one-way CVEU cyclic interface tests are discussed. Then, a comparison between clay-clay and clay-structure cyclic behavior is presented. Finally, the effect of cyclic and and average stress ratio variations under non-isothermal conditions on shear strength is discussed in detail.

4.3.2.1 Typical cyclic results

Fig. 4.6 shows the typical results of one of the one-way cyclic clay-structure interface tests that was performed (τ_a/S_u^{Ds} =0.41, τ_{cy}/S_u^{Ds} =0.54). The shear stress varied between two values of $\tau_a + \tau_{cyc}$= 60 kPa and $\tau_a - \tau_{cyc}$= -8 kPa (Fig. 4.6(a)). Cycle numbers 1 and 45 are shown in the figure to better illustrate the permanent deformation accumulation during the test. The relative lateral displacement (δ) raised with increasing number of cycles until a certain value that corresponding to the failure (Fig. 4.6(b)).

It appears that the first cycle caused a permanent strain of 0.5% and started to

increase progressively with the number of cycles toward the failure point (Fig. 4.6(c)). The rate of strain accumulation with the number of cycles increased progressively until failure. Finally the failure occurred at around 1.28%. To keep the volume of the clay sample constant during the cyclic shearing phase, the effective normal stress was not constant during the test (Fig. 4.6(d)). Due to the normally consolidated state of the clay in this study, the general trend of effective normal stress was decreasing. Mortezaie and Vucetic 2013 found the same decreasing trend of the effective normal stress by cyclic testing of kaolinite in simple shear device. For each cycle, the effective normal stress during shear load on (from -8 to 60 kPa) increased and during shear load off (from 60 to -8 kPa) decreased. The increase in the equivalent pore water pressure due to the first cycle was almost 127 kPa, which is 40% of the initial effective normal stress ($\sigma_{n0}^{'}$ = 300 kPa) that was applied (Fig. 4.6(e)). After the first cycle, the equivalent pore water pressure (u^*) increased with an almost constant slope. In the degradation index method proposed by Idriss et al. 1978; the degradation index is calculated as the ratio between the strain of cycle 1 and N (Eq. 3.1). In this study, this concept was slightly modified in the context to take into account the fact that the relative lateral displacement of the first cycles did not start from the same point compared to the works using this method (Idriss et al. 1978; Zhou and Gong 2001), as follows:

$$\delta^* = \frac{P_{d(cy1)} + (1 - P_{d(cy1)})}{P_{d(cyN)} + (1 - P_{d(cy1)})} = \frac{1}{P_{d(cyN)} + (1 - P_{d(cy1)})} \tag{4.3}$$

where $P_{d(cy1)}$ and $P_{d(cyN)}$ are the cyclic relative lateral displacement at cycles 1 and N. A constant value $(1-P_{d(cy1)})$ is added to both cyclic relative lateral displacements to shift the $P_{d(cy1)}$ so that it starts from 1. Fig. 4.6(f) shows the degradation index vs. the number of cycles. The slope of this curve in a log-log curve is the t parameter. Finally Fig. 4.6(g) shows the Mohr-Coulomb plane of the cyclic test. The above-mentioned types of results are used in the next sections to present the cyclic behavior of clay-clay and clay-structure interface.

4.3.2.2 Cyclic behavior of clay-clay vs. clay-structure interface

To investigate the cyclic behavior difference of clay-clay and clay-structure interface, CVEU cyclic clay-clay and clay-structure interface tests were performed. Both tests were performed with the same average and cyclic stress ratios (τ_a/S_u^{Ds} = 0.41 and τ_{cy}/S_u^{Ds} = 0.47) (Fig. 4.7).

For the same average stress ratio (ASR) and cyclic stress ratio (CSR), the number of cycles to failure for the clay-structure was l85 while for the clay-clay case 370 cycles were necessary to reach failure (Fig. 4.7(a)). The accumulated relative lateral displacement

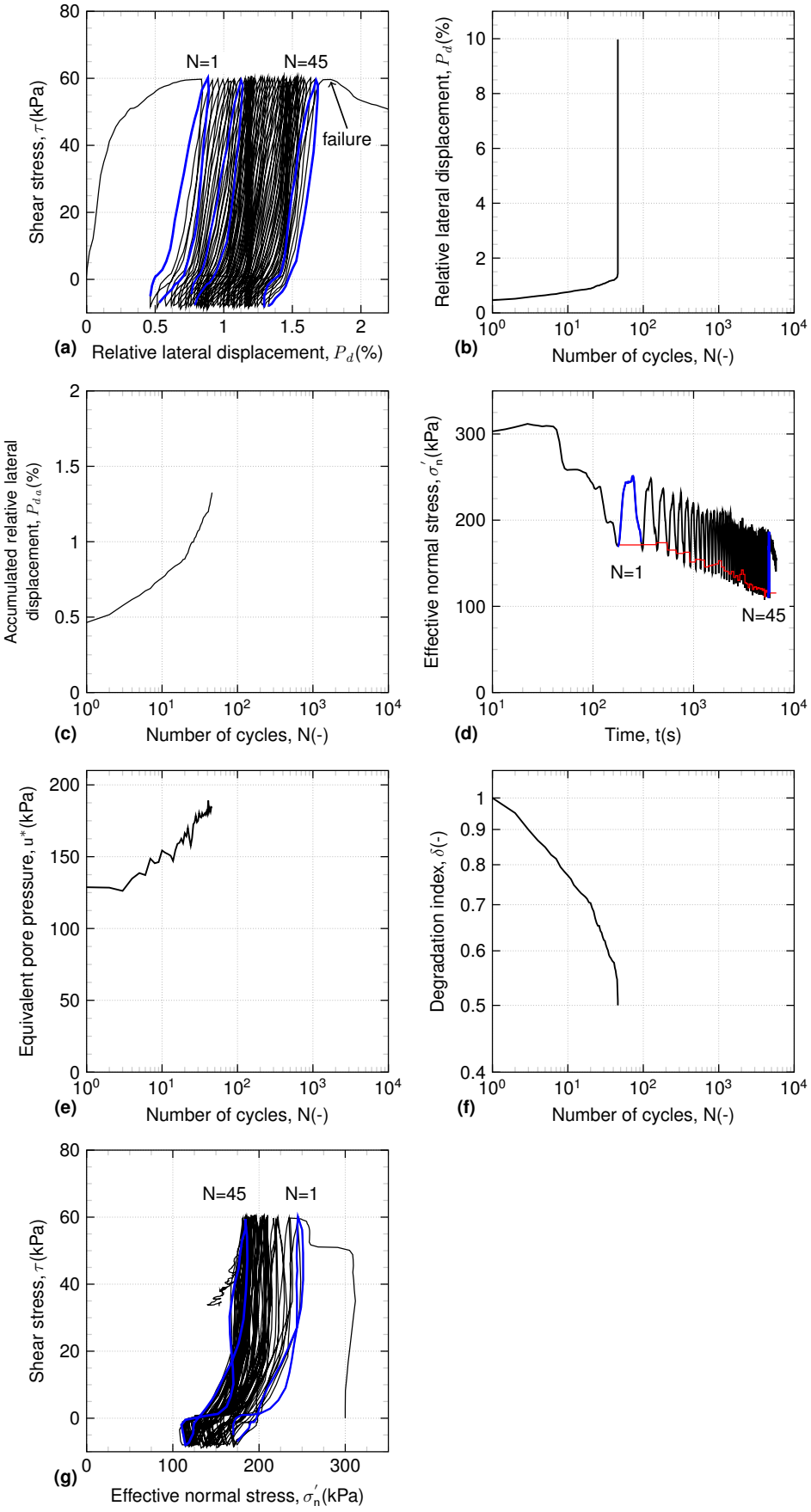

Figure 4.6: Behavior of clay-structure interface under cyclic loading.

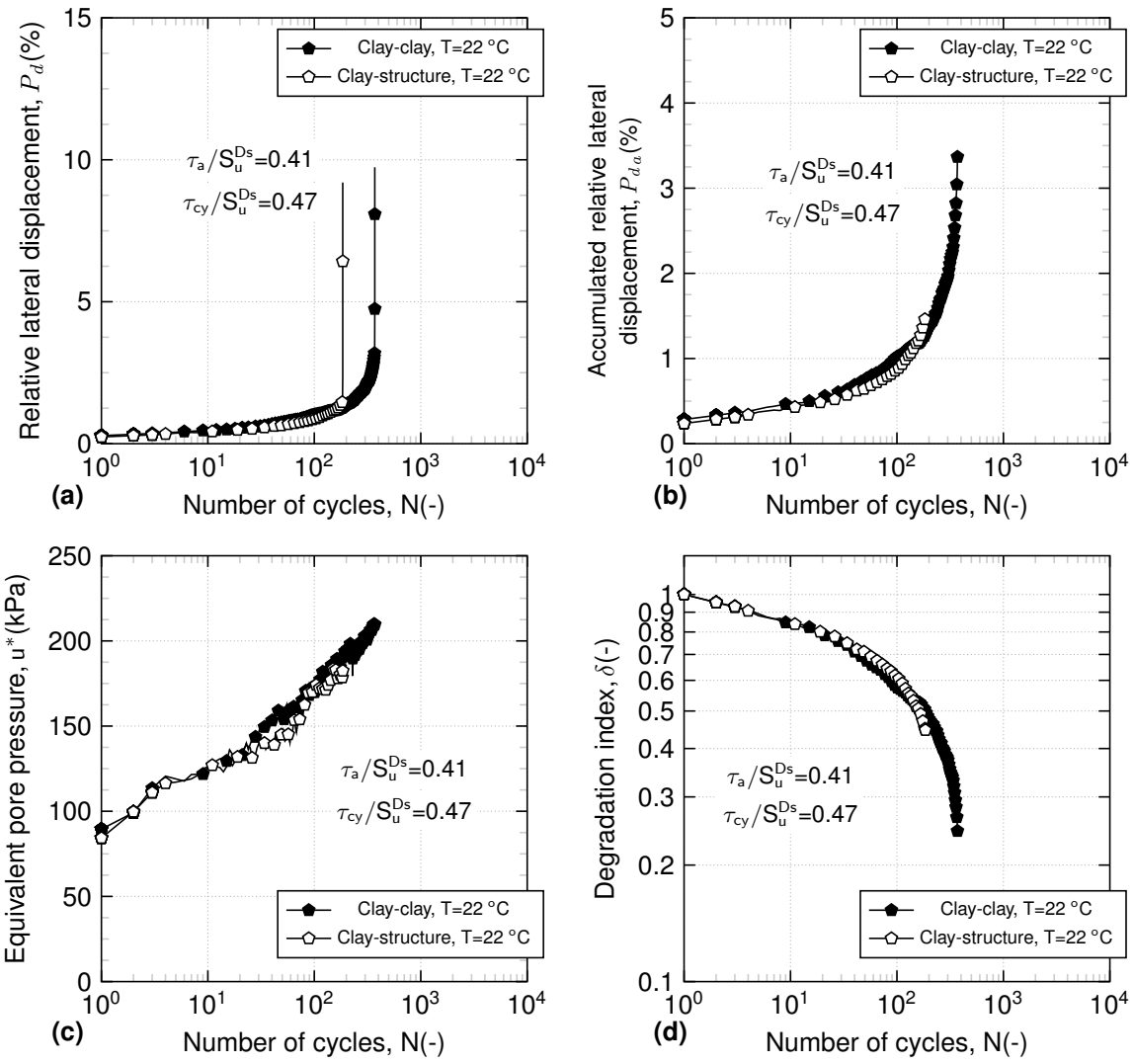

Figure 4.7: Clay-clay vs. clay-structure interface cyclic response.

(P_{da}) for both cases started from the same point (0.12%) and increased progressively with number of cycles (Fig. 4.7(b)). The strain accumulation for both tests followed the same trend but the P_d corresponding to the failure for clay-structure (1.5%) was less than clay-clay case (3.4%). It can be noticed that, lower excess pore water pressure was generated for clay-structure interface test at the end of cycling (Fig. 4.7(c)). Similar to the accumulated relative lateral displacement, the pore water pressure u^* trend for both cases is consistent. As it was observed in the monotonic part, the equivalent pore water pressure (u^*) of clay-clay and clay-structure were superimposed below 2% of P_d (Fig. 4.5(c)). Due to the fact the accumulated relative lateral displacement (P_{da}) of cyclic clay-structure interface is less than 2%, the identical curves for u^* was observed. For the degradation index the same scenario was repeated. Both tests followed the same trend, but due to the higher number of cycles to failure for the clay-clay test, the degradation index decreased more for clay-clay test than for clay-structure interface

test. The main difference between the cyclic behavior of clay-structure interface and that of clay-clay is the number of cycles to failure, which is lower for the interface case.

4.3.2.3 Effect of cyclic stress ratio (CSR) variations at different temperatures

After the consolidation, a heating phase with a rate of 5 $^oC/hr$, was applied to the clay-structure interface. The thermal consolidation curve of the clay-structure interface is shown in Fig. 4.8(a). Heating from 22 to 60 ^{o}C caused 0.15 mm of settlement. After reaching the desired temperature (60 ^{o}C), the slope of the thermal consolidation decreased (Fig. 4.8(a)). The thermal vertical strain with heating from 22 to 60 was 0.88% (Fig. 4.8(b)).

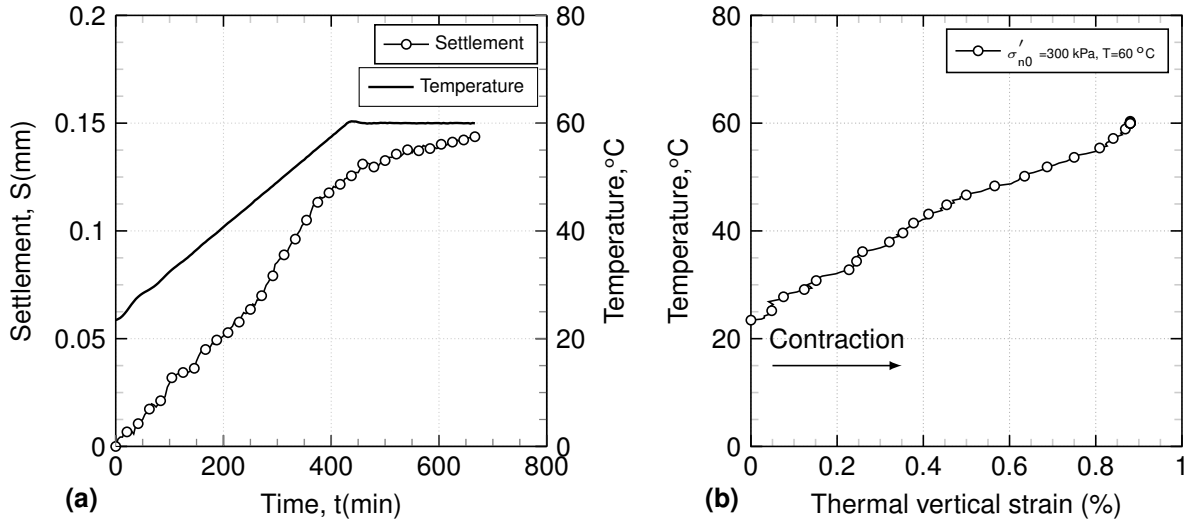

Figure 4.8: (a) Thermal consolidation of clay-structure interface with a heating from 22 to 60 ^{o}C; (b) Thermal vertical strain of clay-structure interface from 22 to 60 ^{o}C.

For the effect of cyclic stress ratio (CSR) variations at different temperatures, two series of tests with an average shear stress of $\tau_a/S_u^{Ds} = 0.41$ (Fig. 4.9) and 0.47 (Fig. 4.10) were performed. For $\tau_a/S_u^{Ds} = 0.41$, the cyclic stress ratio (CSR) varied from 0.35 to 0.57 at different temperatures (22 and 60 ^{o}C).

Reduction of CSR from 0.57 to 0.35, increased the number of cycles to failure from 39 to 4200 cycles (Fig. 4.9(a)). The number of cycles to failure upon cycling at elevated temperatures for all of the different CSR values increased by 2.5-4 times. The accumulated relative lateral displacement (P_{da}) evolution versus the number of cycles is depicted in Fig. 4.9(b). The CSR reduction from 0.57 to 0.35 decreased the relative lateral displacement of the first cycle from 0.48 to 0.12%. Heating reduced the ($P_{da(cy1)}$) for $\tau_{cy}/S_u^{Ds} = 0.57$ from 0.42 to 0.13% which is a reduction of 69%. The equivalent pore water pressure u^*, of the first cycle was larger when CSR was higher (Fig. 4.9(c)). Heated samples have lower equivalent pore water pressure u^*, than unheated ones.

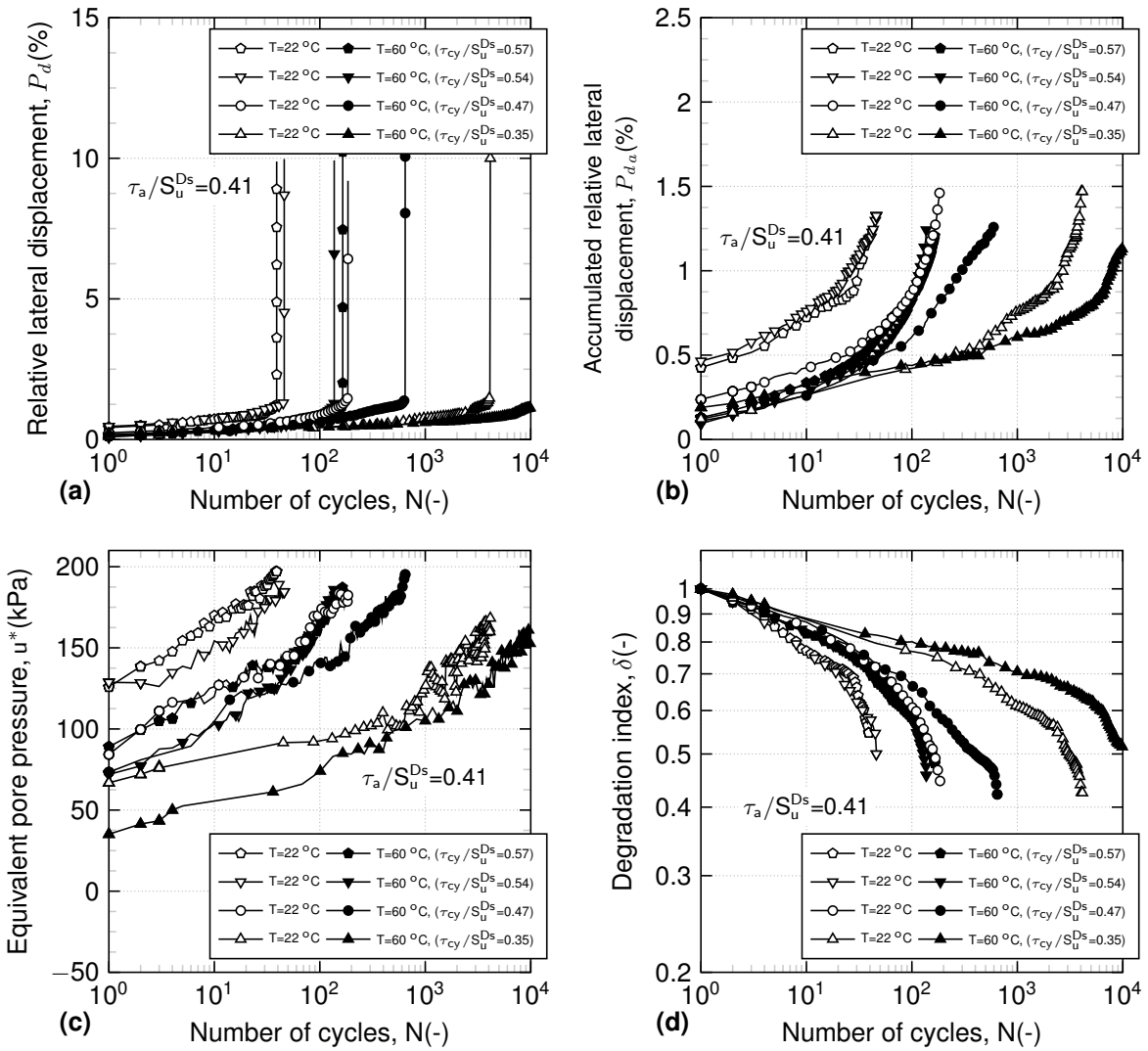

Figure 4.9: Effect of cyclic shear stress variation at different temperatures for τ_a/S_u^{Ds} = 0.41 and τ_{cy}/S_u^{Ds} =0.35 to 0.47 for clay-structure interface tests. (a) Shear strain vs. number of cycles; (b) permanent shear strain vs. number of cycles; (c) equivalent pore water pressure vs. number of cycles; (d) degradation index vs. number of cycles.

Higher CSR values, raised the degradation index rate (Fig. 4.9(d)). For CSR value of 0.35 the degradation index of 0.6 was obtained in around 1000 cycles, while for a CSR value of 0.47, the same degradation index could be obtained with only 100 cycles. Considering the effect of temperature, as in the previous observations the degradation index decreased for heated samples and they showed less tendency to degrade compared to unheated samples. The degradation index of 0.6 for the test with CSR of 0.53 at 22 ^{o}C was obtained in 35 cycles while for the heated sample, it was obtained in 100 cycles.

The second series of tests was performed with an average shear stress of τ_a/S_u^{Ds} = 0.47 (Fig. 4.10) and two different CSR$_s$ of 0.47 and 0.35. The tests with lower CSR

values (0.35), were stopped after almost 2000 cycles. The test with $\tau_{cy}/S_u^{Ds} = 0.47$ was performed twice to verify the repeatability of the tests (Fig. 4.10(a)).

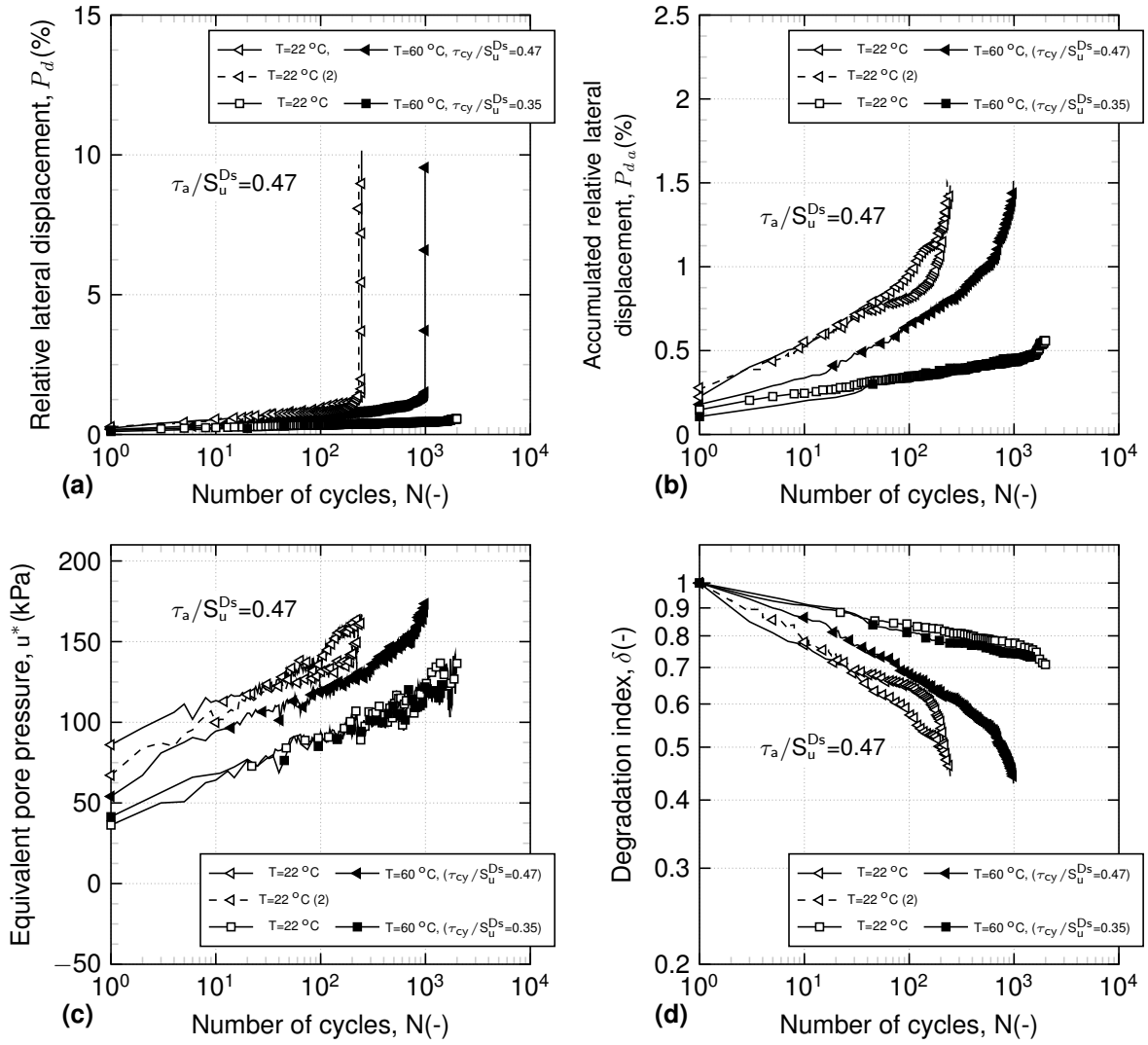

Figure 4.10: Effect of cyclic shear stress variation at different temperatures for $\tau_a/S_u^{Ds} = 0.47$ and τ_{cy}/S_u^{Ds} =0.35 and 0.47 for clay-structure interface tests. (a) Shear strain vs. number of cycles; (b) permanent shear strain vs. number of cycles; (c) equivalent pore water pressure vs. number of cycles; (d) degradation index vs. number of cycles.

The accumulated relative lateral displacement of the first cycles ($P_{da(cy1)}$) for the CSR values of 0.47 and 0.35 were 0.25 and 0.13% respectively (Fig. 4.10(b)). The heated samples showed a lower ($P_{da(cy1)}$) and the rate of strain accumulation was less than that of the unheated samples (Fig. 4.10(b)). For the CSR of 0.47 the pore water pressure u^*, for cycle 1 was 65-88 kPa, while for CSR=0.35 it was 37 kPa (Fig. 4.10(c)). Fig. 4.10(d) shows the degradation index with the number of cycles. For heated samples with a CSR of 0.47, in 100 cycles, the degradation index was 0.68, while at 22 ^{o}C it was 0.6-0.65.

4.3.2.4 Effect of average stress ratio (ASR) variations at different temperatures

For the effect of average stress variations τ_a/S_u^{Ds} (ASR), two series of tests with CSR values of 0.54 and 0.47 were performed. Fig. 4.11 shows the results of the test with a CSR of 0.54. The number of cycles to failure reduced from 65 to 46 with decreasing

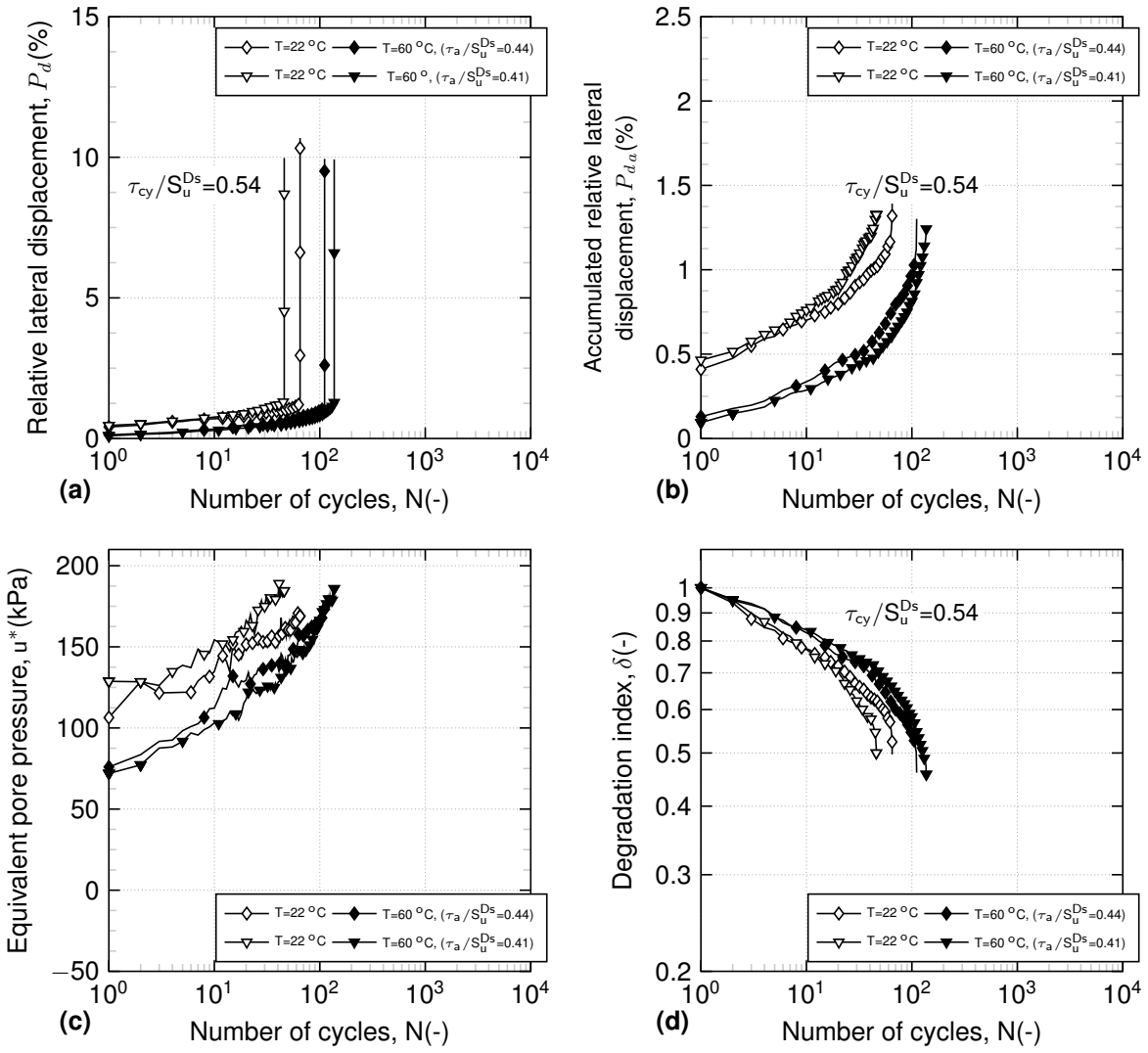

Figure 4.11: Effect of average shear stress variation at different temperatures for $\tau_{cy}/S_u^{Ds} = 0.54$ and τ_a/S_u^{Ds} =0.41 and 0.44 for clay-structure interface tests. (a) Shear strain vs. number of cycles; (b) permanent shear strain vs. number of cycles; (c) equivalent pore water pressure vs. number of cycles; (d) degradation index vs. number of cycles.

the average shear stress ratio from 0.44 to 0.41 (Fig. 4.11(a)). Increased number of cycles to failure by 2-2.5 times was the consequence of the heating from 22 to 60 ^{o}C. Fig. 4.11(b) illustrates the accumulated relative lateral displacement (P_{da}) as a function of number of cycles. For both ASR values of 0.44 and 0.41 at 22 ^{o}C, the (P_{da}) corresponding to the first cycle started from almost 0.45%. However, for heated samples these values decreased to 0.13%. Fig. 4.11(c) shows the value of u^* with

the number of cycles. The test with higher ASR generated lower u^* values at 22 ^{o}C. For heated samples the generated u^* was less than unheated samples. Taking into account the results of the test with ASR of 0.41, the heated sample had a u^* of 100 kPa at 10 cycles while for unheated sample at the same cycle the u^* was around 150 kPa. The degradation evolution during the cycles was presented in Fig. 4.11(d). The degradation index of 0.5 was in 65 cycles for the ASR of 0.41 while for an ASR of 0.44, it was obtained in around 111 cycles. Heating caused a lower degradation index in heated samples compared with that in unheated samples. For the unheated sample with an ASR of 0.41 at 10 cycles, the degradation index was 0.76, while for the heated sample, it was 0.82.

Fig. 4.12 shows the results of the second series of tests with a CSR of 0.47. The average shear stress varies between 0.38 and 0.47.

The results clearly indicated that, by reducing the ASR from 0.47 to 0.38, the number of cycles to failure decreased from 246 to 57 at 22^{o}C. The heating tended to increase the number of cycles to failure. For an ASR of 0.41 the number of cycles to failure was increased from 185 to 645 cycles for a temperature increase from 22 to 60 ^{o}C. For ASR values of 0.47, 0.41 and 0.38, the $P_{da(cy1)}$ started from almost 0.25% (Fig. 4.12(b)). However for heated samples these values decreased to 0.12%. Fig. 4.12(c) shows u^* with number of cycles. For ASR of 0.47 at 10 cycles the unheated sample u^* was 114 kPa while for heated sample was around 95 kPa. For heated samples the u^* trend was lower than unheated samples. The degradation index of 0.5 was obtained in 45 cycles for an ASR of 0.38, while for an ASR of 0.41, it was obtained in around 150 cycles (Fig. 4.12(d)). The degradation of the heated samples was less than that of the unheated ones. For the unheated sample with an ASR of 0.38 at 10 cycles, the degradation index was 0.77, while for the heated sample, it was 0.88.

4.4 Discussion

The recorded results are discussed in this section to clarify (i) the effect of mechanical monotonic and cyclic loads on clay-clay and clay-structure interface, (ii) the effect of cyclic and average stress variations at different temperatures and (iii) the thermal effects on strain accumulation, equivalent pore water pressure generation and degradation of clay-structure interface.

Fig. 4.13 presents the monotonic and cyclic constant-volume equivalent-undrained (CVEU) test comparison of the clay-clay and the clay-structure interface.

The strain softening in the monotonic test for clay-clay starts around 2.5% while for the clay-structure interface test, it is in lower relative lateral displacements (0.8%). The cyclic solicitations cannot go beyond the monotonic shear stress-strain curve. In

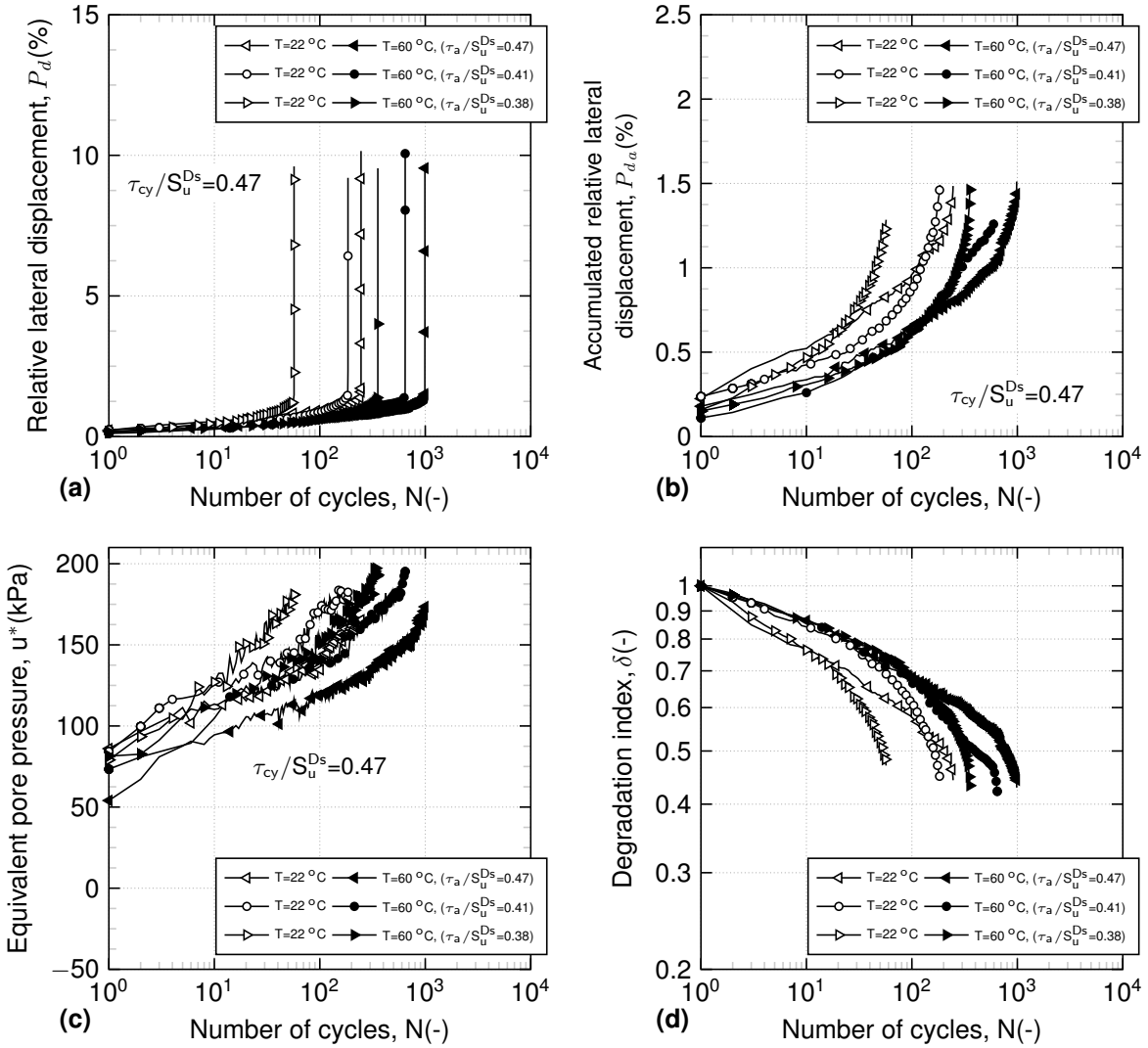

Figure 4.12: Effect of average shear stress variation at different temperatures for $\tau_{cy}/S_u^{Ds} = 0.47$ and τ_a/S_u^{Ds} =0.38 to 0.47 for clay-structure interface tests. (a) Shear strain vs. number of cycles; (b) permanent shear strain vs. number of cycles; (c) equivalent pore water pressure vs. number of cycles; (d) degradation index vs. number of cycles.

other words, when the strain softening started, the capacity for further cycles decreased and due to the fact that the monotonic shear stress is the allowable mobilized shear stress, the cyclic loads cannot exceed the yield limit. The last cycles close to the failure for clay-clay case is around 3-3.5% while for clay-structure test it is about 1.3-1.5%. Therefore, the virgin monotonic curve influences the cyclic behavior of both tests and the reason for lower number of cycles at failure for the clay-structure tests compared with that of the clay-clay test may be due to the difference between the strain softening in the two cases. Andersen 2009 performed post-cycle shear tests after some certain cycles on a clay sample (clay-clay) in simple shear device, to investigate the effect of cyclic loads on static shear strength. The results showed that the post-cyclic shear

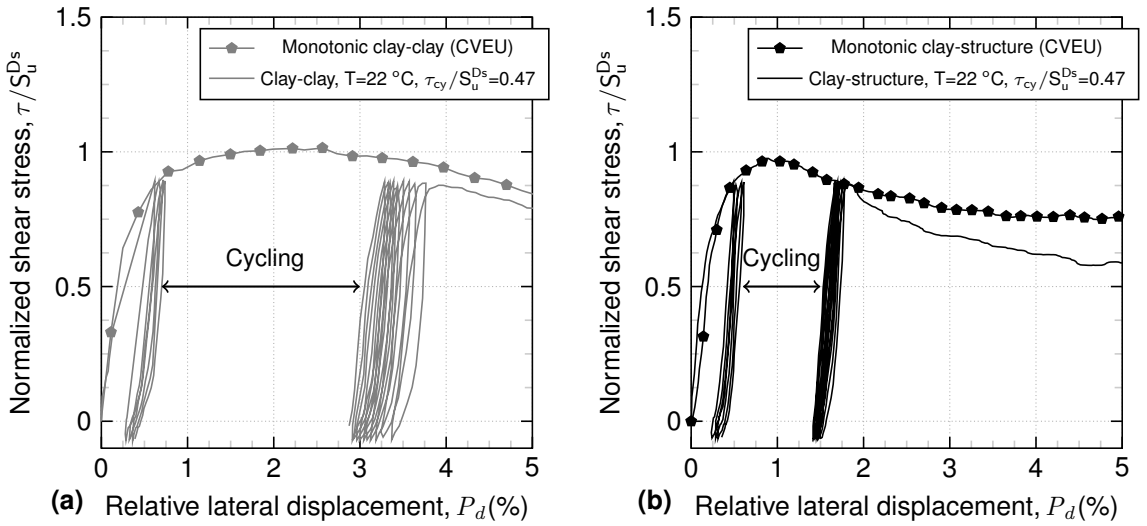

Figure 4.13: Monotonic and cyclic strain-softening comparison in (a) clay-clay test and (b) clay-structure interface test.

strength rapidly converged with the virgin monotonic stress-strain curve. The post-cyclic static shear strength of the clay was governed by the virgin monotonic stressstrain curve and the permanent shear strain that was developed during cyclic loading which is in consistent with the observations in this study. To draw conclusions about the observed cyclic behavior difference between clay-clay and clay-structure interface tests, precautions should be taken in practical design calculations for the interface behavior of geostructures subjected to mechanical cyclic loads.

Fig. 4.14 shows the difference between cyclic loops (N=1, 10 and 100) of the clay-clay and the clay-structure interface tests. The relative lateral displacement at the beginning of the cycles is subtracted, and they all started from zero. The slope of the clay-structure loading-unloading hysteresis is higher than that of the clay-clay case for the cycles mentioned. For N=1 the area encompassed by the clay-structure is smaller than clay-clay case which implies that the energy dissipated in clay-clay case is more than clay-structure interface. Despite the steeper loading-unloading hysteresis loops for clay-structure interface compared to that of the clay-clay, the number of cycles to failure for the clay-structure case is lower than that for the clay-clay case, which confirms the pronounced difference of both cases in terms of shearing plane and strain softening.

Fig. 4.15 shows the cyclic loops for an ASR of 0.41 and CSR_s of 0.57, 0.47 and 0.35 at different temperatures. The cyclic loops of N=1 and 10 for a CSR of 0.57 are compared with their counterparts at different temperatures in Fig. 4.15(a) and Fig. 4.15(b). The cyclic hysteresis at higher temperatures for N=1 and 10 at 60 ^{o}C are steeper compared to those of the unheated samples which may be due to the denser state of the heated samples. It is also observed that the areas encompassed by the hysteresis

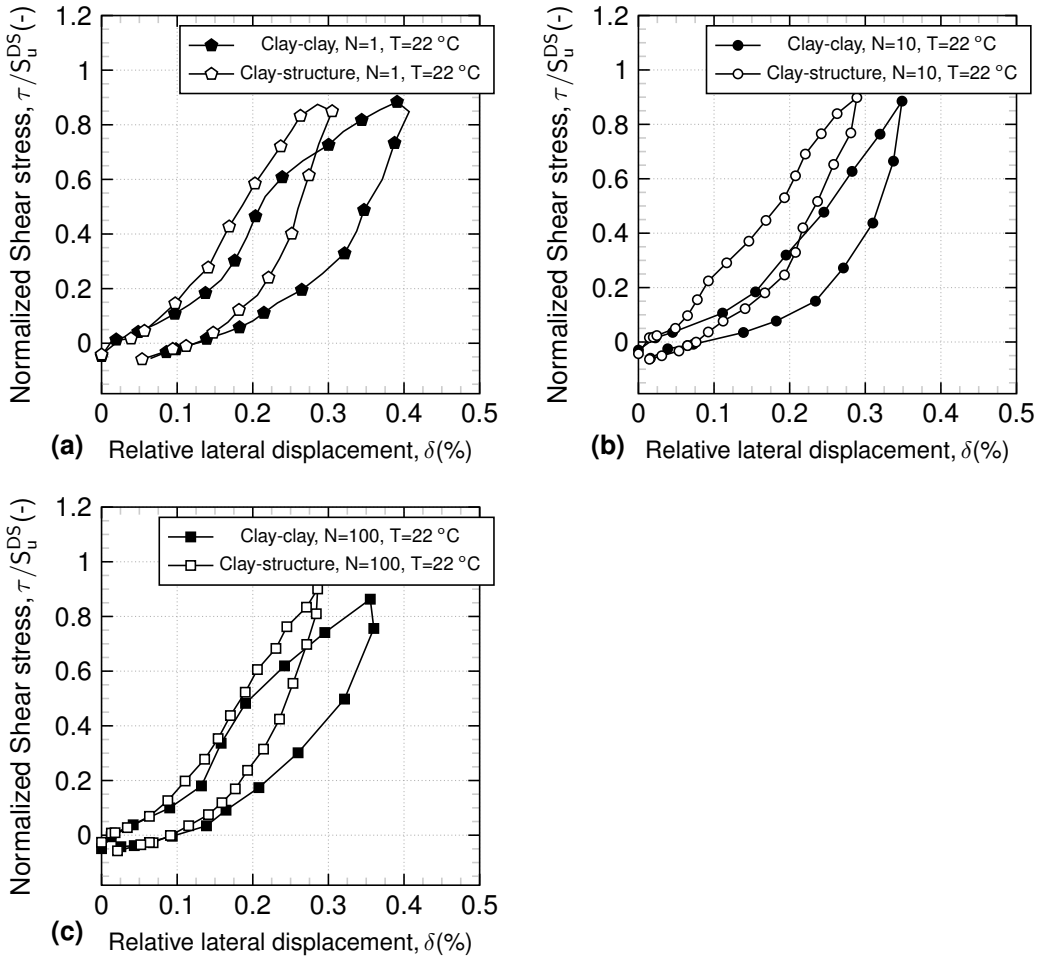

Figure 4.14: Cyclic loops comparison for clay-clay and clay-structure tests at 22 ^{o}C (a) N=1 (b) N=10 (c) N=100. $P_d^*(\%)$= shear strain from the beginning of cycle N.

loop in heated samples are smaller than those in unheated samples in clay-structure interface tests, implying that less energy is dissipated in heated samples. Cekerevac and Laloui 2010 by performing temperature-controlled undrained cyclic triaxial tests on kaolin have reported that, the cyclic hysteresis loops at higher temperatures are more regular and straighter, with steeper loading-unloading curves compared with those of the heated samples which, is consistent with responses observed in this study. The effect of temperature on hysteresis loops has been reported by Xiong et al. 2018 for saturated soft clay in dynamic triaxial cyclic tests. They observed that, with increasing temperature from 25 to 65 ^{o}C, the accumulative plastic strain under 10000 cycles decreased from 0.5% to 0.15% ($p^{'}$ = 50, q_{cyc} = 10 kPa). They compared hysteresis loops of certain cycles, at 25, 45 and 65 ^{o} C and reported that, the shear strain of each cycle at 65 ^{o}C is less than those at 45 and 25 ^{o}C, which is consistent with the results observed in this study. The reason for the densification of the soil may be the thermoplastic strain generated during the heating process which causes the soil to be thermally overconsolidated. For a CSR of 0.47, the effect of temperature on

cyclic loops is less pronounced (Figs. 4.15(c), 4.15(d), 4.15(e)). For a CSR of 0.35, there is almost no noticeable difference among N=10, 100 and 1000 hysteresis loops at different temperatures compared to those at other CSR values (Figs. 4.15(f), 4.15(g) and 4.15(h)).

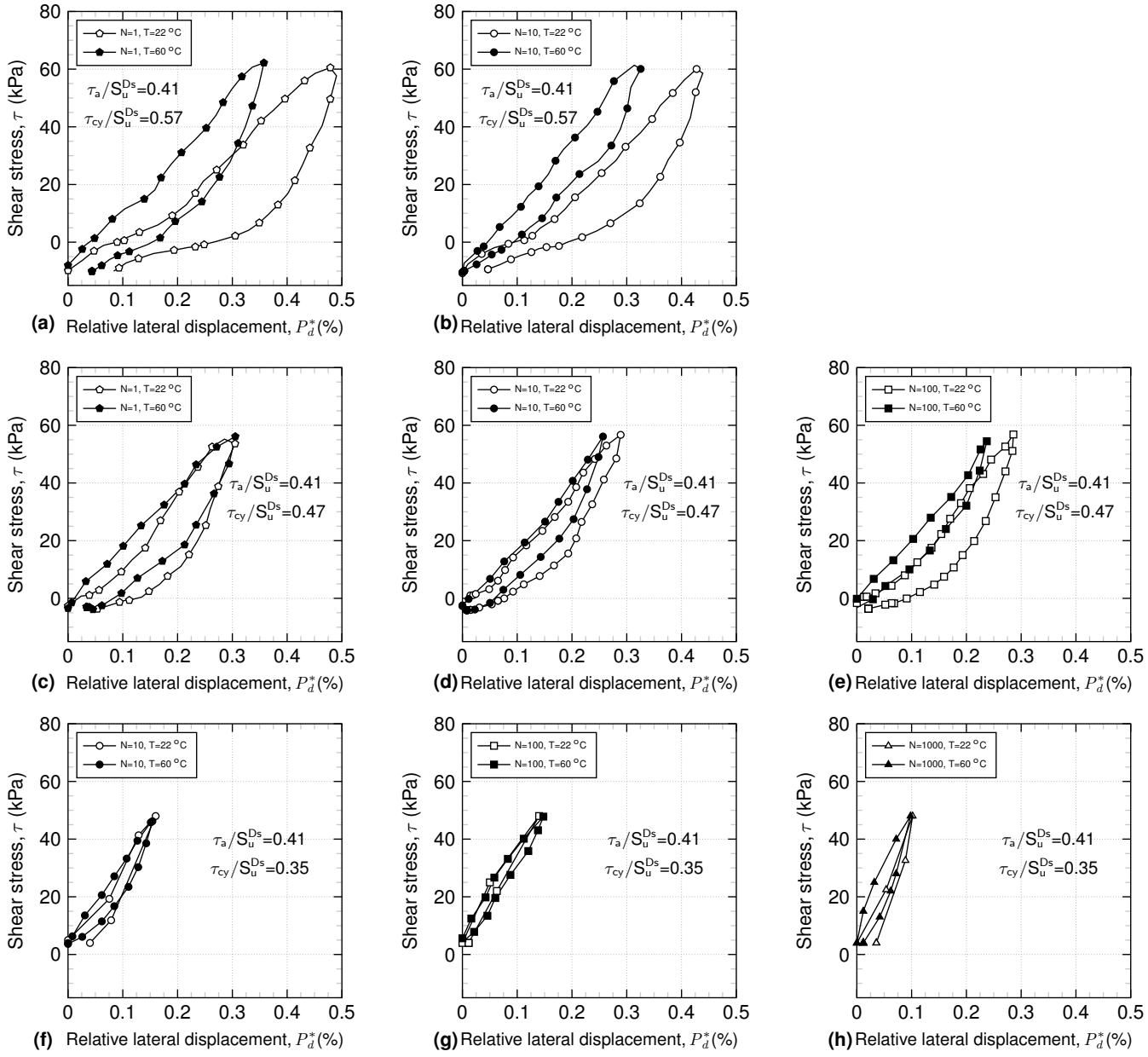

Figure 4.15: Cyclic loops at different temperatures $P_d^*(\%)$= relative lateral displacement from the beginning of cycle N.

The reduction in the CSR value ceases the effect of temperature on cyclic hysteresis loops and the difference between the heated and unheated loops becomes relatively insignificant. This may be due to the fact that, in lower CSR values the cyclic loads are in plastic shakedown but at higher CSR values, the cyclic loads reach the ratcheting

response; therefore, the effect of temperature is more pronounced. Based on the three different CSR values compared in Fig. 4.15, it can be observed that at a CSR less than 0.47 (τ_{cy}/S_u^{Ds}), the effect of temperature on cyclic characteristics of clay-structure interface is negligible. Mortezaie and Vucetic 2016 by conducting cyclic CVEU simple shear tests on kaolinite have observed that beyond a threshold of cyclic shear strain of $\gamma_{td} = 0.012$ and 0.014%, the degradation rate and pore water pressure generation is not evolved with further cycling.

The values of the degradation parameter t in Fig. 4.16 are the slopes of the lines fitted through the logarithm of number of cycles versus logarithm of degradation index data points for cyclic tests. At 22 ^{o}C with increasing CSR from 0.35 to 0.57, the degradation parameter increases from 0.064 to 0.115 but for tests at 60 ^{o}C the degradation parameter increases from 0.049 to 0.097 for the same range of CSR. The degradation parameters for heated samples are lower than the tests at 22^{o}C which can be due to the denser state of the samples that reduces the rate of degradation. The degradation rate for the CSR range between 0.35 to 0.57 decreases about 16% for a temperature increase from 20 to 60^{o}C. On the basis of CVEU simple shear tests on kaolinite (clay-clay type), Mortezaie and Vucetic 2013 have reported that, in the cyclic strain range of 0.1-0.5% , with an vertical stress increase from 220 to 680 kPa, degradation parameter reduces by 20-38%, which can be comparable to the decrease have been obtained by heating in this study. The thermal overconsolidation phenomena, play the same role as mechanical loading.

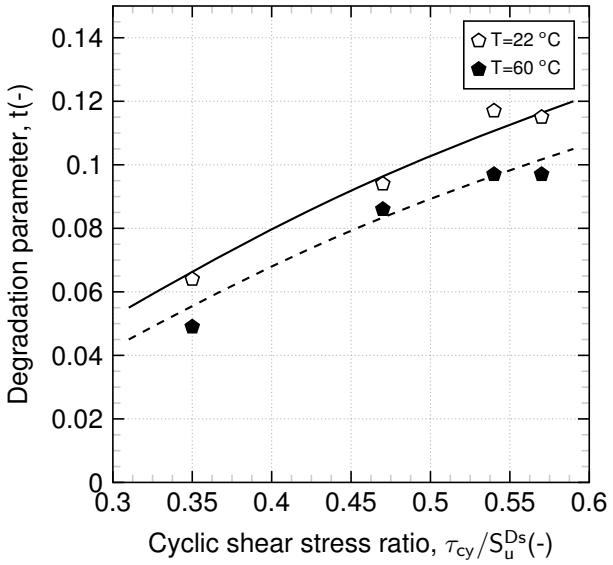

Figure 4.16: Evolution of degradation parameter (t), with cyclic stress ratio variation at different temperatures (22 and 60 ^{o}C).

Fig. 4.17(a) shows the variation in the number of cycles to reach different values of relative lateral displacements (P_d= 0.5, 0.7, 1, 10%) with CSR (τ_{cy}/S_u^{Ds}) variations

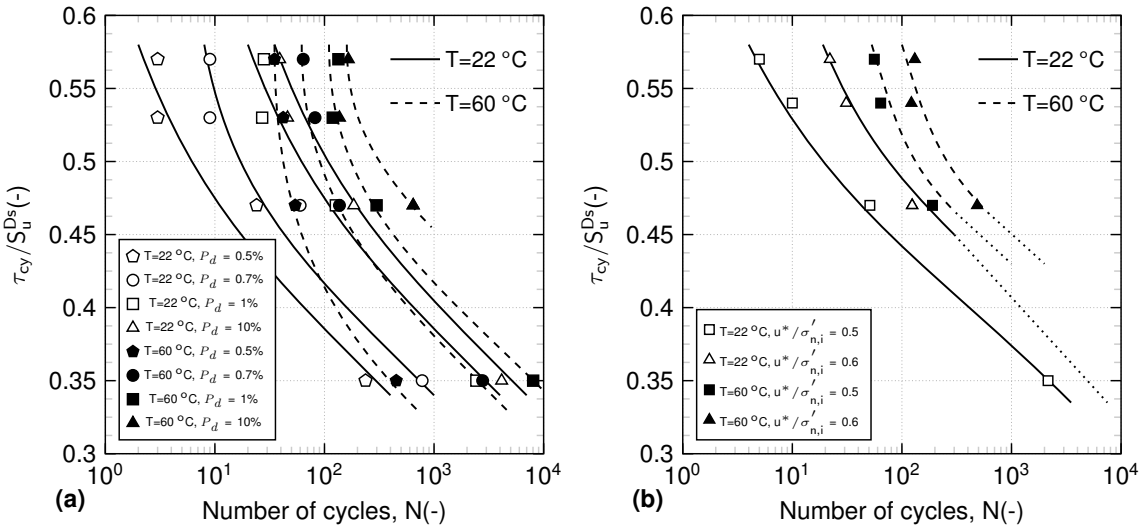

Figure 4.17: (a) τ_{cy}/S_u^{Ds} vs number of cycles curve for different relative lateral displacements; (b) $u^*/\sigma'_{n,i}$ vs number of cycles curve for certain values of normalized equivalent pore water pressure.

at 22 and 60 ^{o}C. With decreasing the CSR$_s$ from 0.57 to 0.35 the number of cycles to reach 0.5% of relative lateral displacement increases from 3 to 125 cycles at 22 ^{o}C. However for the heated samples to reach the same P_d, with the same reduction in the CSR the number of cycles increases from 35 to 452. With decreasing CSR values, the effect of temperature becomes less noticeable. For the CSR of 0.57 at 60^o to reach 0.5% of P_d, the number of cycles is increased by 4-7 times compared to that at 22^o while with decreasing the CSR to 0.35 this ratio becomes 2-4 times. Fig. 4.17(b) shows the variation of number of cycles to reach different values of normalized pore water pressure ($u^*/\sigma'_{n,i}$ =0.5, 0.6) with CSR variations. The number of cycles to reach $u^*/\sigma'_{n,i}$ =0.5 is increasing from 5 to 1500 cycles with decreasing the CSR from 0.57 to 0.35 at 22 ^{o}C. To reach the same normalized pore water pressure (0.5) for heated samples the number of cycles increases by 4-6 times.

4.5 Conclusions

This study presents an investigation of the effect of cyclic parameter variations on clay-structure interface behavior at different temperatures (22 and 60 ^{o}C). Constant-volume equivalent-undrained (CVEU) monotonic and cyclic clay-clay and clay-structure tests were performed. The strain accumulation, equivalent excess pore water pressure, degradation index and stressstrain hysteresis loops are presented and discussed. The following conclusions are obtained:

• In monotonic CVEU tests, the shear behavior of the clay-structure is different from the clay-clay one. The peak, strain softening and effective stress reduction differences confirm that the shear occurs in the interface zone.

The virgin monotonic behavior of the clay-clay and clay-structure interface, shows the limit which the cyclic loads can not go beyond.

• The results clearly show the difference between cyclic behavior of the clay-clay and clay-structure interface tests. The number of cycles to failure for clay-structure test is lower than that for the clay-clay one due to the difference in their strain softening mode.

• In cyclic behavior of interface, decreasing the cyclic stress ratio (CSR) increases the number of cycles to failure and decreases the equivalent pore water pressure and degradation index.

• The temperature increase from 22 to 60 ^{o}C, substantially increases the number of cycles to failure. For almost all of the cyclic clay-structure interface tests, the relative lateral displacement and equivalent pore water pressure corresponding to the first cycle decrease after heating. Drained heating of the normally consolidated kaolin, causes thermal overconsolidation and makes the sample denser, which may be one of the reasons for the increase in the number of cycles to failure. The denser state of the heated samples compared to the unheated samples reduces the rate of degradation.

• Reducing the average shear stress, decreases the number of cycles to failure. The samples are subjected to higher negative shear stresses and therefore, the resistance against cycles are reduced.

• Normally consolidated kaolin clay with the characteristics in this study subjected to cyclic stresses mentioned in this study by heating from 22 to 60 ^{o}C, shows higher number of cycles to failure.

Further investigations should be carried out to investigate the effect of monotonic and cyclic temperature variations on the one-way and two-way cyclic behavior of normally consolidated and overconsolidated clay-clay and clay-structure interface.

Chapter 5

Non-isothermal soil-structure interface model based on critical state theory

Abstract

In energy geostructures, the soil-structure interface is subjected to mechanical loads and thermal variations. In this study a non-isothermal soil-structure interface model based on critical state theory is developed from a granular soil-structure interface constitutive model at isothermal conditions. The non-isothermal model takes into account the effect of temperature on the void ratio of interface prior to shearing. The model is capable to capture the effect of temperature on soil-structure interface under constant normal load and constant normal stiffness conditions for both sandy and clayey interfaces. The additional parameters have physical meanings and can be determined from classical laboratory tests. The formulation is in good agreement with the experimental results and the main trends are properly reproduced.

Keywords: non-isothermal model, constant normal stiffness (CNS), soil-structure interface, temperature, critical state theory.

Résumé

Dans les géostructures énergétiques, l'interface sol-structure est soumise à des charges mécaniques et à des variations thermiques. Dans cette étude, un modèle d'interface sol-structure non isotherme basé sur la théorie de l'état critique est développé à partir d'un modèle constitutif d'interface sol-structure granulaire dans des conditions isothermes. Le modèle non isotherme prend en compte l'effet de la température sur le taux de vide de l'interface avant le cisaillement. Le modèle est capable de saisir l'effet de la température sur l'interface sol-structure dans des conditions de charge normale constante et de rigidité normale constante pour les interfaces sableuses et argileuses. Les

paramètres supplémentaires ont des significations physiques et peuvent être déterminés à partir d'essais classiques en laboratoire. La formulation est en bon accord avec les résultats expérimentaux et les principales tendances sont correctement reproduites.
Mots clés: modèle non isotherme, rigidité normale constante (CNS), interface sol-structure, température, théorie de l'état critique.

5.1 Introduction

The increasing demand for energy in recent years has lead to the utilization of new technologies to exploit renewable energies. One of these developed technologies is thermally active energy geostructures. Conventional geostructures, such as piles and diaphragm walls, are converted to energy geostructures by attaching heat exchanger tubes to their reinforcement cages. Thermally active energy geostructures make heat exchange with the surrounding soil possible by circulating a heat-carrying fluid in the exchanger loops. The thermo-mechanical solicitations impact different parts of the structure such as the concrete body, the soil-structure interface and the surrounding soil. The interface zone consists of a thin layer of soil adjacent to the structure in which normal and tangential stresses are acting on this thin layer. In energy geostructures, the interface zone will be exposed to thermo-mechanical loads. Several studies have shown a significant change in mobilized shaft friction with temperature variations in full scale energy foundations at soil-structure interface zone (Laloui et al. 2006, Bourne-Webb et al. 2009, Murphy et al. 2015, Faizal et al. 2018). Therefore, the design and maintenance of energy geostructures requires additional precautions to take into account the effect of temperature variations on the mechanical behavior of soil-structure interface. In this context it is noteworthy to propose a constitutive model for sandy and clayey interfaces in non-isothermal conditions.

There are several constitutive models in the literature proposed for the thermo-mechanical behavior of soils (Hueckel and Borsetto 1990; Graham, Graham, Tanaka, Crilly and Alfaro 2001; Hueckel et al. 2009; Laloui and François 2009; Tang and Cui 2009; Hamidi and Khazaei 2010; Yao and Zhou 2013). Moreover, most of the interface constitutive models proposed in the literature were developed for granular interfaces in isothermal conditions (Shahrour and Rezaie 1997, Ghionna and Mortara 2002a, Fakharian and Evgin 2000, De Gennaro and Frank 2002, Mortara et al. 2002, Liu et al. 2006, Lashkari 2013). Suryatriyastuti et al. 2014 proposed a t-z cyclic function to take into account the effect of thermal cycles on soil-pile interactions for cohesionless soils. However, for fine grained soil-structure interfaces, very few studies can be found in the literature (Stutz and Mašín 2017), and there is almost no constitutive model that takes into account the effect of temperature.

In this context, the aim of this study is to define an approach capable of capturing the major fundamental features of the soil-structure interface regarding the effect of temperature. To this end, the paper will focus on two aspects:
• How can the effect of temperature on the mechanical properties of the soil-structure interface be taken into account in the model?
• How can the model be efficient for both sand/clay-structure interfaces under constant normal load (CNL) and constant normal stiffness (CNS) conditions?

This paper is divided into three sections. The first one gives a review of the main characteristics of the thermo-mechanical behavior of soil and the soil-structure interface that must be reproduced by the new model. The second part introduces the theoretical framework chosen for the interface behavior and the new formulation developed to capture the effect of temperature on the interface and finally, the model performance is examined.

5.2 Thermo-mechanical behavior of soil and the soil-structure interface

The key features of the thermo-mechanical behavior of soil are first presented. Then, the experimental results concerning the effect of temperature on the mechanical properties of the soil-structure interface are discussed to highlight important features that should be taken into account by the interface constitutive model in non-isothermal conditions.

5.2.1 Features of the thermo-mechanical behavior of soil

Several authors confirmed that the effect of temperature on the mechanical behavior of soils is affected by the thermal and stress history (Campanella and Mitchell 1968, Hueckel and Baldi 1990, Kuntiwattanakul et al. 1995, Burghignoli et al. 2000, Cui et al. 2000, Delage et al. 2000, Cekerevac and Laloui 2004, Abuel-Naga et al. 2006). For overconsolidated clays, a temperature increase induces a reversible thermal dilation and consequently decreases the shear strength of the soil. For normally consolidated clays, the deformation upon heating is contractive and irreversible, and thus, the shear strength of the soil increases with temperature. In normally consolidated clays, the contraction upon heating mainly is the void ratio decrease, which is commonly called the thermal overconsolidation effect. One of the main parameters that is influenced by the temperature variation is the preconsolidation pressure which decreases with temperature increase. Most of the abovementioned models implemented the effect of temperature on the preconsolidation pressure in thermoelastoplastic models.

5.2.2 Features of thermo-mechanical behavior of soil-structure interface

Some experimental studies have been performed on the effect of temperature on the mechanical behavior of the soil-structure interface in direct shear tests (Di Donna et al. 2015; Yavari et al. 2016; Li et al. 2018; Maghsoodi et al. 2019a; Maghsoodi et al. 2019b; Maghsoodi et al. 2020; Yazdani et al. 2019) and centrifuge models (McCartney and Rosenberg 2011). Among these studies, the experimental results of Maghsoodi et al. 2020 are presented in the following. Fig. 5.1 shows the constant normal load (CNL) and constant normal stiffness (CNS) test results of a normally consolidated kaolin clay-structure interface for two different normal stresses, 100 and 300 kPa, at 22 and 60 ^{o}C.

The stress-strain behavior of normally consolidated clay-structure interface exhibited a clear peak under CNL and CNS conditions. For both CNL and CNS tests, the peak shear stress of kaolin clay-structure interface increased with heating from 22 to 60 ^{o}C, but at critical state (large displacements) the effect of temperature was negligible (Fig. 5.1(a) and (b)). The shear stress in CNS tests is decreased compared to CNL results. The thermal overconsolidation effect during heating reduced the contraction of the interface during shear. Fig. 5.1(c) and (d) show the volumetric behavior for both CNL and CNS tests. Due to the increase of stiffness the volumetric contraction of CNS tests is less than CNL tests. Fig. 5.1(e) and (f) shows the evolution of normal stress during shear. For CNL tests as it was expected, the normal stress remains unchanged but on the other side, in CNS tests, to keep the ratio $d\sigma/dv = K$ constant, the normal stress decreased during shearing. In the mentioned studies, authors found that the shear strength of clay-structure interface increases with temperature but the shear strength of sand-structure interface remains unchanged. They concluded that the reason of this increase in the clay-structure interface could be the thermally overconsolidation effect that happened during the heating phase on a normally consolidated clay. These features are demonstrated by data from Maghsoodi et al. 2020. Fig. 5.2(a) shows the thermal vertical strain for kaolin clay-structure interface under 300 kPa during the heating phase and after consolidation (Maghsoodi et al. 2020). Heating from 22 to 60 ^{o}C caused a thermal vertical strain of 0.85% for the clay-structure interface. Fig. 5.2(b) shows the evolution of void ratio during shear for clay-structure interface tests performed under 100 kPa at 22 and 60 ^{o}C (Maghsoodi et al. 2020). The initial void ratio for heated sample is reduced but at the critical state both void ratios are superposed which can explain the identical shear behavior of interface at large displacements (Fig. 5.1(a) and (b)).

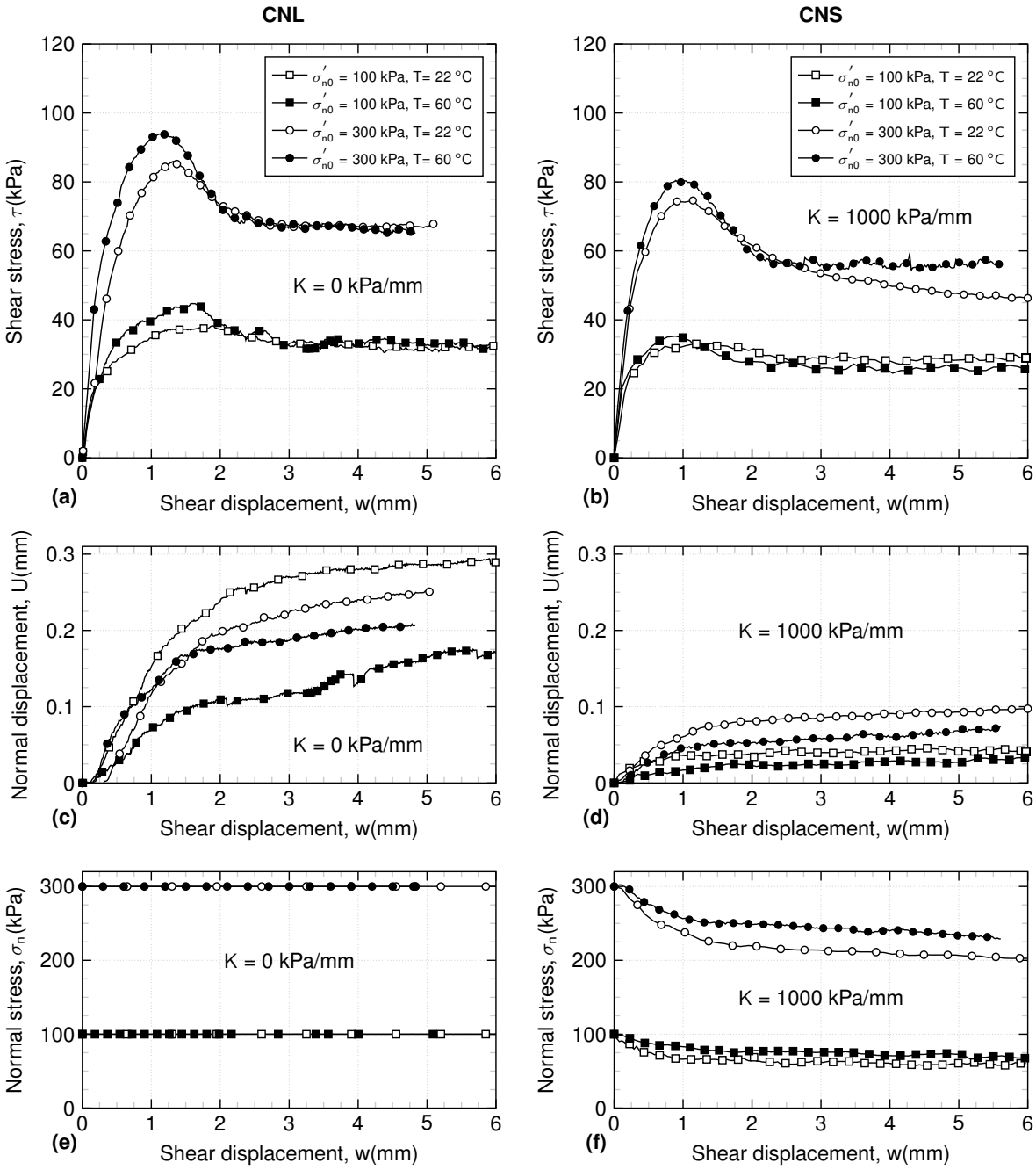

Figure 5.1: CNL (K=0 kPa/mm) and CNS (K=1000 kPa/mm) clay-structure interface results for 100 and 300 kPa at 22 and 60 °C (Maghsoodi et al. 2019b).

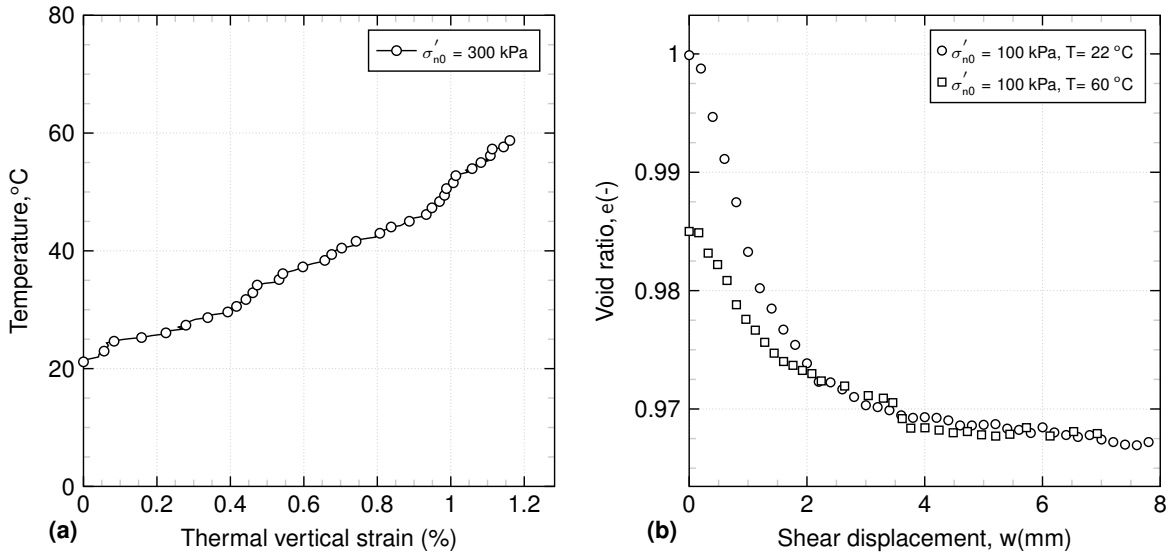

Figure 5.2: (a) Thermal vertical strain vs. temperature for clay-structure interface under 300 kPa. (b) The void ratio evolution during shearing under 100 kPa at 22 and 60 ^{o}C.

5.2.3 Summary

The model should be able to capture the effect of temperature on the soil-structure interface, and should require a limited number of parameters to account for the maximum features of soil-structure interface. Important features that should be captured by the model are as follows:

• The void ratio reduction upon heating for normally consolidated clay-structure interfaces.

• The stress-strain behavior of normally consolidated clay-structure interface under CNL and CNS conditions.

• The volumetric behavior of clay-structure interface at different temperatures during shear for both CNL and CNS conditions.

• The evolution of normal stress during shear for CNL and CNS results.

5.3 Development of a constitutive model for soil-structure interface

5.3.1 Isothermal soil-structure interface constitutive model

Several constitutive models have been proposed for soil-structure interface behavior (Desai et al. 1985; Shahrour and Rezaie 1997; Ghionna and Mortara 2002a; Fakharian and Evgin 2000; De Gennaro and Frank 2002; Mortara et al. 2002; Boulon et al. 2003; Liu et al. 2006; DAguiar et al. 2011; Lashkari 2013; Saberi et al. 2016; Stutz, Mašín

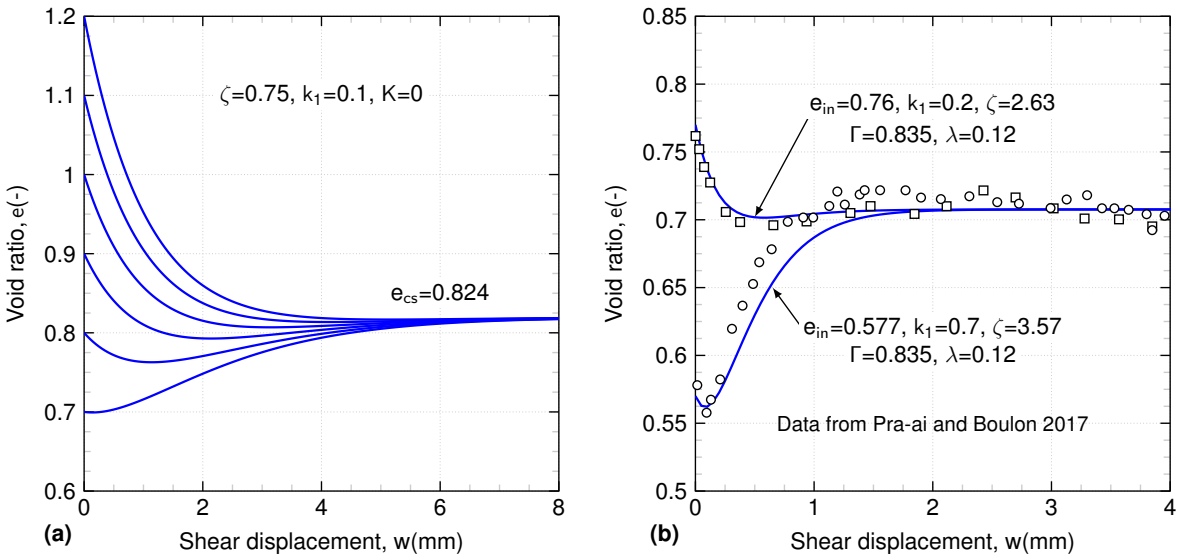

Figure 5.3: Evolution of void ratio during shearing using Eq. 1: (a) different initial void ratios (e_{in} = 0.70, 0.9, 1.0, 1.1, and 1.2) evolution towards the critical state void ratio (e_{cs} = 0.824); (b) Void ratio evolution for a loose and dense Fontainebleau sand-interface test performed by Pra-ai and Boulon 2017.

and Wuttke 2016) and some of them are based on critical state theory (Liu et al. 2006; Lashkari 2017). The objective of this study is to develop an interface model capable of reproducing several features for soil-structure interface mechanical behavior at non-isothermal conditions. To do so, a model which is principally based on void ratio evolution can be used to take into account the effect of temperature on the initial void ratio of interface. generally implementing additional variables (e.g. temperature) in a constitutive model, incorporates more parameters. However, increasing the number of parameters, causes more complexity. Therefore, models with minimum number of parameters that have physical meanings obtained from classical laboratory tests on one hand and be able to capture the maximum number of features on the other hand are required. The model should be flexible for both CNL and CNS conditions and should be feasible and adoptable to implement.

Among the presented models for soil structure interface in the literature, the critical state interface model proposed by Lashkari 2017 is based on void ratio evolution during shear. The model is straightforward in application and has parameters that all have physical meanings. Therefore this model fits well with the mentioned requirements and it has been selected. The model is adopted as the base for developing a new constitutive model for non-isothermal conditions.

5.3.1.1 Modeling formulation

The concept of critical state is based on the theory that at large shear deformations, soil continues to shear without any changes in volumetric and stress conditions. The

void ratio at this large shear deformations is critical state void ratio. The critical void ratio, e_{cs}, is affected by the confining pressure such that it decreases with the increase of confining stress. The behavior of soil at any state thus depends on its distance between the current state and the critical state, which can be defined by a state parameter for sandy soil (Liu et al. 2006).

The constitutive formulation that have been used in Lashkari 2017 have been presented briefly in Table 5.1. Lashkari 2017 proposed the following function for the evolution of the interface void ratio with shear strain:

$$e = e(e_{in}, e_{cs}, \epsilon) = e_{cs}[1 - exp(-\xi\epsilon)] + e_{in}exp(-\xi\epsilon) - \frac{k_1}{1 + K/k_2}(\epsilon)exp(-\xi\epsilon) \quad (5.1)$$

The current void ratio (e) is a function of initial (e_{in}), critical state void ratio (e_{cs}) and shear strain (ϵ). The deformation (ϵ) is defined as the shear displacement divided by initial length of the sample ($\Delta w/l_0$). The parameter ξ controls the rate of void ratio evolution with shear strain (ϵ). K is the normal stiffness acting on the interface. The parameters k_1 and k_2 are non-negative interface parameters. Fig. 5.3(a) shows the Eq. 5.1 for different initial void ratios (0.7-1.2). For the dense samples the $e_{in} < e_{cs}$ and for loose samples $e_{in} > e_{cs}$. The dense sample with $e_{in} = 0.70$ exhibits an initial contraction which after phase transformation, it converts to dilation. In the medium-loose sample with $e_{in} = 0.9$, a greater initial contraction happens which is followed by a dilation. Finally, the soils with $e_{in} = 0.9$, 1.0, 1.1, and 1.2 contract till the shearing ceases. Different void ratios converge towards a single state which is the critical state void ratio. The void ratio evolution equation (Eq. 5.1) have been checked by using data from Pra-ai and Boulon 2017 for Fontainebleau sand-steel interface shear tests (Fig. 5.3(b)). For loose and dense samples the relative density (ID) was 30% and 90%. The initial void ratio of loose and dense samples were $e_{in} = 0.760$ and 0.577. The ξ parameter was calculated to be 2.63 for the loose sand-structure interface which it was calculated to be 3.57 for dense sample. As it was observed for equation (Eq. 5.1), the loose sample contracted till the end of shearing on the contrary the dense sample exhibited a slight contraction followed by a dilation. Both loose and dense sand void ratios reached an asymptotic value at larger shear displacements. The evolution of void ratio experimentally was observed and validated by the equation for sand-structure interface tests.

Another important aspect of the reference interface model is the ability of the model to reproduce the interface behavior under constant normal stiffness (CNS) conditions. The normal stress evolution in CNS conditions depends on the volumetric behavior and consequently the void ratio changes of the interface. The free contractive or dilative

Table 5.1: Constitutive equations of Lashkari 2017 model.

Description	Constitutive equation	Parameters	Eq. N
Void ratio evolution	$e_{cs}[1-exp(-\xi\epsilon)]+e_{in}exp(-\xi\epsilon)-\frac{k_1}{1+K/k_2}\epsilon exp(-\xi\epsilon)$	$e, e_{in}, e_{cs}, \epsilon, \xi$	**1**
Normal stress evolution	$\delta\sigma_n^{'}=K\delta v$	$K, \delta v$	**2**
Normal stress evolution	$\delta\sigma_n^{'}=-K\delta v=\frac{-Kt\delta e}{1+e}$	K, t, e	**3**
Critical state void ratio	$e_{cs}=\Gamma-\lambda ln(\sigma_n^{'}/p_{ref})$	Γ, λ	**4**
State parameter	$\psi=e-e_{cs}$	e, e_{cs}	**5**
Shear stress evolution	$\tau=\frac{\epsilon}{\frac{1}{\mu}+\frac{\epsilon}{M\sigma_n[1+N\langle-\psi\rangle]}}$	$M, \mu, \sigma_n, N, \psi$	**6**

volumetric evolution of the interface upon shearing is prevented by the surrounding soil stiffness. The dilative response is counteracted by an increase of normal stress. On the contrary the contractive response is accompanied by a reduction of normal stress. Interface and surrounding soil interaction can be expressed as:

$$\delta\sigma_n^{'}=-K.\delta v \tag{5.2}$$

Where $\delta\sigma_n$(kPa) is the normal stress difference, K(kPa/mm) is the stiffness of the adjacent soil and δv(mm) is the normal displacement difference of the interface. Considering the thickness of the interface (t), the void ratio evolution of the interface related to the normal stress changes can be obtained by the following equation:

$$\delta\sigma_n^{'}=-K\delta v=\frac{-Kt\delta e}{1+e} \tag{5.3}$$

where t is the interface thickness. Several studies have proposed that in granular interface, the thickness of interface is around 5 to 10 times of the D_{50}(mm) of the soil (Boulon and Foray 1986; Fakharian and Evgin 1997; DeJong et al. 2003). Pra-ai and Boulon 2017 have reported that the soil-structure interface zone cannot explicitly be separated from the surrounding soil. The shearing behavior of interface is different from the surrounding soil. Boulon 1989 considered the interface direct shear samples composed of two parts; the active part which is in contact with the structural element and the passive part which mainly is subjected to an oedometric loading. The active part is influenced by the interface thickness.

Evolution of void ratio, normal stress, interface state parameter, and mobilized shear strength strongly depends on the critical state void ratio (e_{cs}). This parameter can be determined with the Critical State Line (CSL) in the e-$ln\sigma$ plane as follows:

$$e_{cs} = \Gamma - \lambda ln(\sigma_n^{'}/p_{ref}) \tag{5.4}$$

where Γ and λ are interface parameters, and p_{ref} = 100 kPa is a normalizing reference pressure.

The difference between initial and critical void ratio is defined as the state parameter (DeJong et al. 2003; Liu et al. 2006). The interface state parameter ψ can be defined as:

$$\psi = e - e_{cs} \tag{5.5}$$

The dense interfaces have their particularities: (i) reveal a clear peak in shear stress-strain response; (ii) contract at the beginning, then phase transformation occurs then followed by a dilation. The dilation is caused by the void ratio increase from initial value to the critical one ($\psi < 0$). For the loose interfaces: (i) no peak is observed in shear stress-strain response; (ii) contracts throughout the shearing and the void ratio is descending ($\psi > 0$).

Lashkari 2017 assumed that the shear stress-strain-strength of soil-structure interface is mobilized through the following semi-hyperbolic equation:

$$\tau = \frac{\epsilon}{\frac{1}{\mu} + \frac{\epsilon}{M\sigma_n[1+N\langle -\psi \rangle]}} \tag{5.6}$$

where M is slope of the critical state line in the $\tau - \sigma$ plane, and N is an interface parameter which impacts the peak shear stress of the interface. In Eq. 5.6. μ is interface elastic shear modulus.

5.3.2 Extension of the constitutive model towards non-isothermal conditions

As it was discussed in the thermo-mechanical behavior of soil-structure interface, for normally consolidated clays, heating causes a contraction and makes the soil thermally overconsolidated. The model should be capable to evaluate the initial void ratio of the clay after heating, for this, the equation for the reduction of the void ratio upon heating was proposed and implemented in the model. In the new formulation the effect of temperature on initial void ratio is implemented in Eq. 5.1. The slope of void ratio reduction with temperature (α) has been evaluated for normally consolidated clay-structure interface (Fig. 5.4). Using the following equation the initial void ratio at any

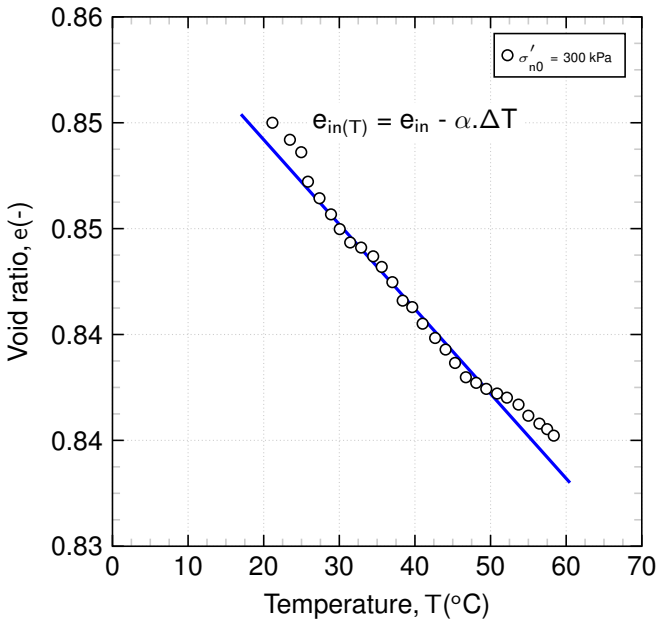

Figure 5.4: Void ratio reduction during heating kaolin clay-interface test. Experimental data by Maghsoodi et al. 2020.

temperature is:

$$e_{in(T)} = e_{in} - \alpha.(T - T_0) \tag{5.7}$$

where $e_{in(T)}$ is the initial void ratio at temperature T. The parameter α is a material dependent parameter which is influenced by physical, thermal and mineralogical characteristics of the soil. Using this parameter and knowing the initial void ratio, by implementing Eq. 5.10 in Eq. 5.1 the evolution of void ratio during shear at any temperature is:

$$e = e_{cs}[1 - exp(-\xi w)] + (e_{in} - \alpha.\Delta T)exp(-\xi w) - \frac{k_1}{1 + K/k_2} w exp(-\xi w) \tag{5.8}$$

The reference model, can reproduce the behavior of loose interfaces also. For loose interfaces the volumetric behavior is contractive and no peak shear stress is expected. For the clay-structure interface tests at different temperatures, several authors reported a clear peak in shear stress-displacement curve in spite of normally consolidated state of the clay which contracted till the end of the shear (Yavari et al. 2016; Maghsoodi et al. 2020 and Yazdani et al. 2019). In the developed model the capability of reproducing this feature should be implemented. Therefore, the shear stress-strain equation was modified as follows:

$$\tau = \frac{w}{\frac{1}{k_t} + \frac{w}{((tan\phi + \frac{c}{\sigma_0^{'}})(\sigma_n^{\beta}))[1+N\langle -\psi \rangle].exp(-(w/N)^{k_2})\xi + \beta}} \tag{5.9}$$

In this equation, due to the strong dependence of clay-structure interface behavior to the adhesion of the interface (cohesion between soil and structure), instead of using M as a frictional parameter, adhesion (cohesion between soil and structure) (C) and friction angle (ϕ) have been introduced into the model. In the model of Lashkari 2017; the shear stress-strain equation, the parameters and their values have been used for sand-structure interface. For this type of interface, the ratio between τ/σ_n is relatively high compared to clay-structure interface response. Due to this fact an additional parameter has been used as the exponent of the σ_n named β which reduces the effect of normal stress. The additional term at the right hand of the equation allows to have a clear peak in shear stress-strain curve in spite of normally consolidated state of the clay-structure interface.

The initial slope of the elastic part can be presented as follows:

$$kt = kt_0(\frac{\sigma_n^{'}}{p_{ref}})^n \tag{5.10}$$

where kt_0 (kPa/mm) is the initial slope of the elastic part of the stress-displacement curve. $\sigma_n^{'}$ (kPa) is the current normal stress and p_{ref} is a reference pressure (100 kPa) and n (-) is the non-linear exponent.

5.3.2.1 Parameter definitions

The non-isothermal model has 12 parameters (Table 5.2). In the τ vs. w plane, k_{t0} is the initial slope of the elastic part of the stress-displacement curve (Fig. 5.5(a)). In the Mohr-Coulomb plane, C and ϕ are the intercept and the slope of the failure line (Fig. 5.5(b)). Γ and λ are, respectively, the intercept and slope of the CSL in the e vs. $\ln(\sigma_n^{'}/P_{ref})$ plane (Fig. 5.5(c)). In contractive regimes (loose sand, normally consolidated clay), the volumetric curve is decreasing towards the critical state. The point corresponding to the part where the volumetric curve starts the critical state phase corresponds to the w_1, which is used to determine the ξ parameter. In dilative regimes (dense sand, overconsolidated clay), the volumetric curve, exhibits a phase transformation and inflection point (Fig. 5.5(d)). The phase transformation point is the first derivative of $de/dw = 0$ and the inflection point is the second derivative of $d^2e/dw^2 = 0$. The shear strains correspond to these points, w_2 and w_3 plays a major role to determine the ξ parameter. ξ can be evaluated for contractive and dilative

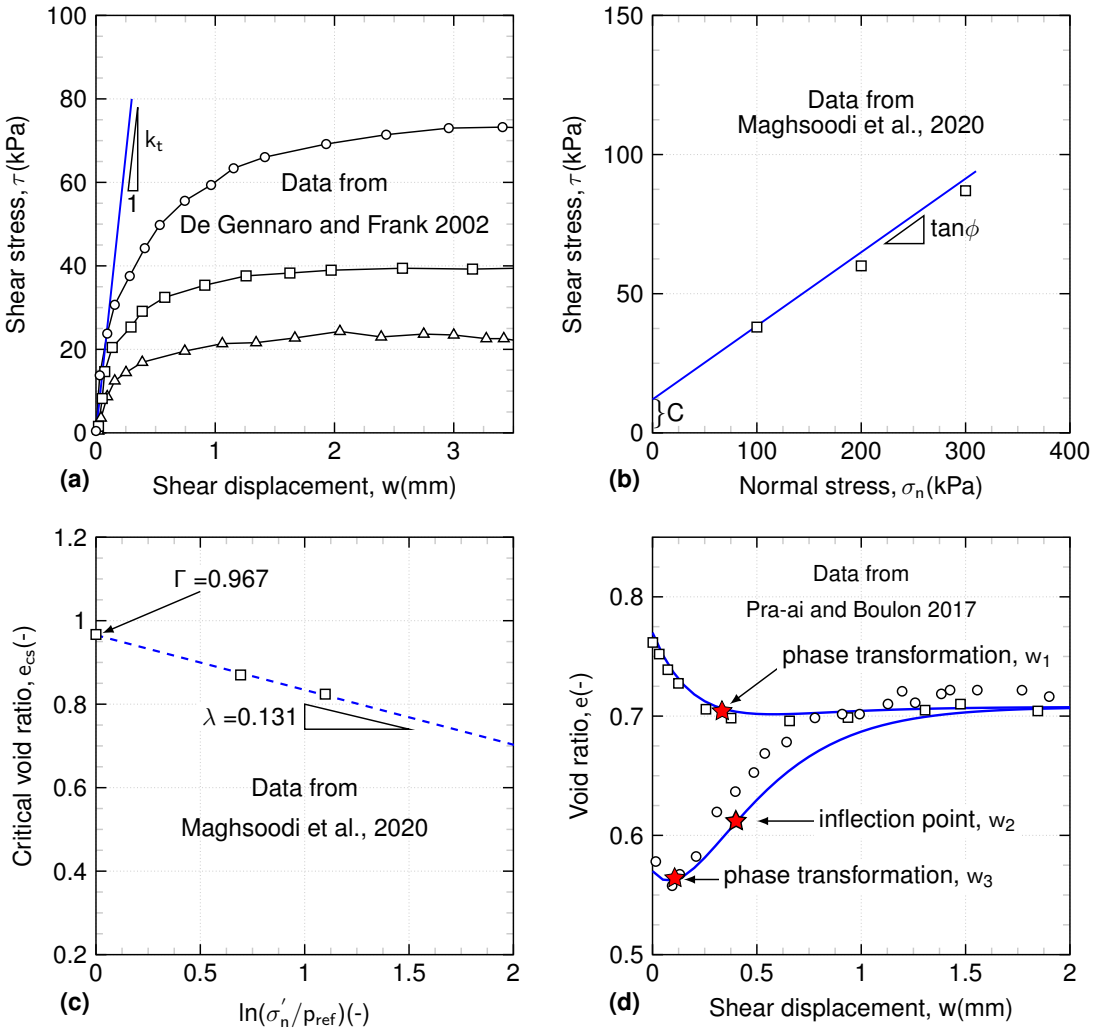

Figure 5.5: Model parameter definitions.

interfaces using the following equations respectively:

$$\xi = \frac{1}{w_1} \tag{5.11}$$

$$\xi = \frac{1}{w_2 - w_3} \tag{5.12}$$

ξ controls the rate of the void ratio evolution during shearing. N impacts the peak shear stress and the strain-softening after it. It can be obtained by calibration against experimental results. In dense regimes the initial contraction amplitude is influenced by k_1 (mm^{-1}). k_2 (kPa/mm) modifies the form of the shear stress curve. By model calibration against experimental data, both k_1 and k_2 can be determined.

Table 5.2: Model parameters of this study.

Interface type	Reference	kt $\frac{kPa}{mm}$	δ (^{o})	Γ (-)	λ (-)	ξ^* (-)	N (-)	K $\frac{kPa}{mm}$	k_1 (-)	k_2 $\frac{kPa}{mm}$	t (mm)	T (^oC)	C (kPa)	β (-)
Fontainebleau sand-structure	Maghsoodi et al. 2020 (CNL)	208	40	0.835	0.040	1.58	2.2	0	0.6	0.11	1.15	22	0	0.900
Fontainebleau sand-structure	Maghsoodi et al. 2020 (CNS)	208	40	0.695	0.040	1.58	2.2	5000	5800	0.22	1.15	22	0	0.935
Fontainebleau sand-steel	De Gennaro and Frank 2002 (CNL)	208	40	0.815	0.040	1.58	1.7	0	0.21	0.11	5.9	22	0	0.910
Silica sand-steel	Fakharian and Evgin 2000 (CNL)	280	40	0.985	0.140	1.58	1	0	0.51	0.51	3	22	0	0.900
Silica sand-steel	Fakharian and Evgin 2000 (CNS)	280	40	0.955	0.140	1.58	1	400	300	0.51	3	22	0	0.940
kaolin clay-structure	Maghsoodi et al. 2020 (CNL)	170	14	0.967	0.131	0.5	1.85	0	0.003	2.9	11	22	12	0.975
kaolin clay-structure	Maghsoodi et al. 2020 (CNS)	170	14	0.990	0.142	0.7	1.85	1000	0.003	2	11	22	12	0.965
illite clay-concrete	Di Donna et al. 2015 (CNL)	300	25	0.870	0.140	0.8	1.85	0	0.003	0.7	10	22	7	0.980
illite clay-concrete	Di Donna et al. 2015 (CNL)	300	25	0.870	0.140	0.83	10.85	0	0.003	0.7	10	60	7	0.980
kaolin clay-concrete	Yazdani et al. 2019 (CNL)	110	11	0.927	0.131	0.42	7.85	0	0.003	4	9.5	24	23	0.952
kaolin clay-concrete	Yazdani et al. 2019 (CNL)	110	11	0.927	0.131	0.45	7.85	0	0.003	4	9.5	34	23	0.952

5.3.2.2 Parametric study

The parametric study allows to determine the effect of each parameter variation. The parametric study is presented in Fig. 5.6. The parametric study condition is the normal stress of 300 kPa, $\Gamma = 0.967$ and a initial void ratio of $e_{in} = 0.85$ at $T = 22^{o}$C which corresponds to a normally consolidated kaolin clay-structure interface. Increasing the k_t from 170 to 680 kPa, increases the elastic slope of shear stress-strain curve, the peak shear stress and very slightly the residual shear stress (Fig. 5.6(a)). Increasing N from 1.85 to 4.85, changes the shape of stress-displacement curve. With increasing N, the peak shear stress increases and simultaneously it moves towards larger shear displacements. The influences of Γ and λ on the model performance are, studied in Fig. 5.6(c) and (d). Increase in Γ decreases the contraction of the normally consolidated clay-structure interface but on the contrary the increase of λ, amplifies the contraction during shear. Increasing the ξ, from 0.5 to 0.9, increases the rate of volumetric contraction towards the critical state condition (Fig. 5.6(e)). The model response under variation of ξ in Fig. 5.6(f) indicates that an increase in ξ increases the peak shear strength without any influence on the residual strength. Variation of k_2, from 1.9 to 3.9, increases the peak shear stress and exhibits a strain softening after the peak. in shear stress-displacement curve (Fig. 5.6(g)). β, raises the shear stress-displacement curves obtained under same normal stress. For example under $\sigma_n = 300$ kPa, $\Gamma = 0.967$ and a initial void ratio of $e_{in} = 0.85$, β increase from 0.85 to 0.98, increases both peak and residual shear strength of the interface.

5.4 The model performance

In the following section, the model performance facing sand/clay-structure interface tests under CNL and CNS conditions at different is examined. The characteristics of the sands and clays that are used for model performance are provided in Table 5.3 and Table 5.4.

5.4.1 Sand-structure interface at isothermal conditions

Maghsoodi et al. 2020 performed Fontainebleau sand-steel interface direct shear tests at different temperatures (22 and 60 ^{o}C). The sand was prepared with a relative density of 90% (e_0=0.557). Due to the fact that the effect of temperature on mechanical properties of the sand was negligible, here just the results at 22 ^{o}C are presented. The shear stress-displacement curve of the sand-structure interface exhibited a clear due to the dense state of the sand samples. The volumetric behavior of the interface consisted of a contraction then dilation. Using the values in the Table 5.2 the modeling results

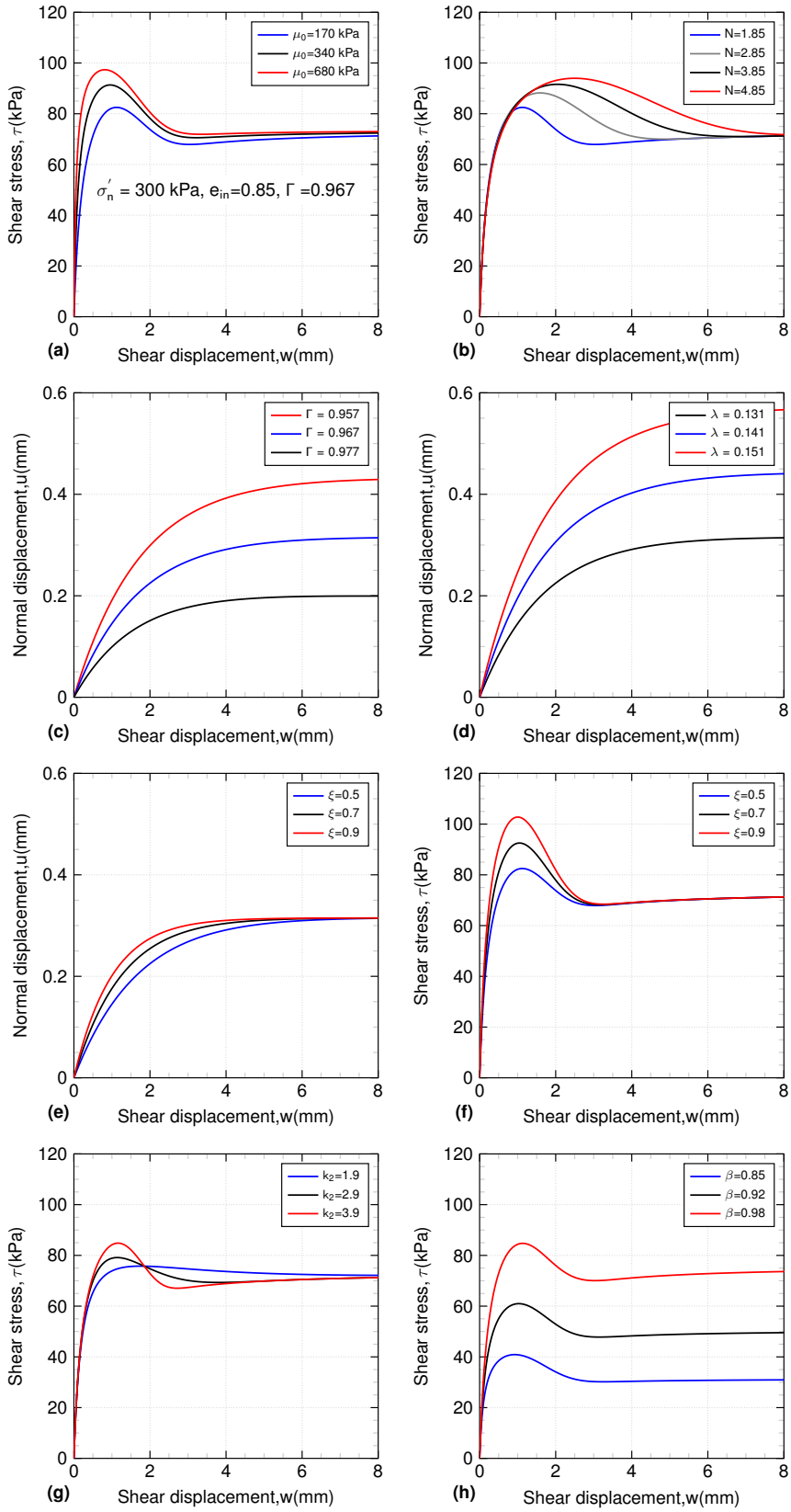

Figure 5.6: model performance and parametric study: (a) variation of shear stress-displacement response with different kt_0, (b) variation of shear stress-displacement response with different N, (c) normal displacement response to different Γ values (d) normal displacement response to different λ values (e) normal displacement response to different ξ values, (f) variation of shear stress-displacement response with different ξ, (g) variation of shear stress-displacement response with different k_2 and (h) variation of shear stress-displacement response with different β

Table 5.3: Physical properties of sands in this study

Interface type	D_{50} (mm)	ρ_s (Mg/m^3)	γ_{dmax} (kN/m^3)	γ_{dmin} (kN/m^3)	e_{max}	e_{min}	$C_u = D_{60}/D_{10}$
Fontaine bleau sand-structure	0.23	2.65	17.2	14.2	0.866	0.545	1.72
Fontaine bleau sand-structure De Gennaro	0.23	2.67	17.2	13.8	0.94	0.54	1.78
Silica sand-structure Fakharian	0.6	2.7	16.35	13.33	1.024	0.651	-

Table 5.4: Physical properties of clays in this study

Interface type	LL (%)	PL (%)	I_p (%)	ρ_s (Mg/m^3)	λ (W/mK)	C (J/m^3K)	k (m/s)
Kaolin clay-structure	57	33	24	2.60	1.5	3.3	10^{-8}
Illite clay-concrete	53.4	30	23.4	2.65	-	-	2.85×10^{-11}
Kaolin clay-concrete	45	25	20	2.62	-	-	-

are in good agreement with experimental results (Fig. 5.7). Based on direct shear tests the friction angle was 40^o with a cohesion of 0, the Γ was found to be 0.835 and $\lambda = 0.040$. Based on experimental observation $w_{p1} = 0.37$ and $w_{p2} = 1$ therefore ξ was found to be 1.58. Due to trial and error N found to be 2.2, the K is 0, k_1 was found to be 0.6 and k_2 0.11. The thickness of the interface, t was 1.15 mm ($5 \times D_{50}(0.23mm)$) and the β parameter was 0.9 for this kind of soil. To find N, it is enough to find the peak shear stress strain and strain corresponding to the after softening phase (near critical state part), the difference between these values corresponds to N. Fig. 5.8 shows the results for CNS sand-structure interface direct shear tests. In experimental part increasing the stiffness increased the shear stress for CNS tests. Using the values in Table 5.2, the modeling results are in reasonable agreement with experimental results for CNS tests.

De Gennaro and Frank 2002 performed interface direct shear tests on a loose Fontainebleau sand and a rough metal plate. The physical characteristics of this sand are summarized in Table 5.3. Loose sand samples have been reconstituted pouring dry sand inside a square shear box 60 mm x 60 mm. Following this procedure the relative density ID equal to 0.46 ($e_0 = 0.753$) have been obtained. Three different normal stresses (25, 50 and 100 kPa) were applied on interface samples. For tests at 25 and

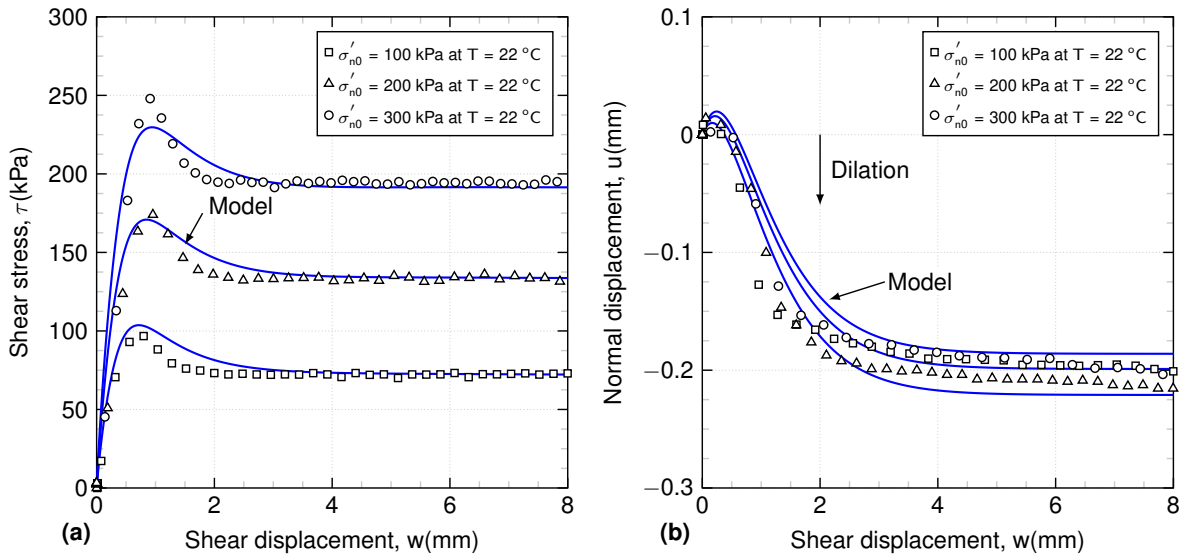

Figure 5.7: Model performance against CNL Fontainebleau sand-structure interface test results under 100, 200 and 300 kPa of normal stress at 22 ^{o}C. (a) shear stress vs. shear displacement; and (b) normal displacement vs. shear displacement (experimental data by Maghsoodi et al. 2020).

50 kPa the interface dilated but for the test at 100 kPa the volumetric behavior was contractive. Based on results reported by De Gennaro and Frank 2002 the friction angle was 40^o and the cohesion was 0. The Γ was found to be 0.815 and $\lambda = 0.040$. $w_{p1} = 0.37$ and $w_{p2} = 1$ therefore ξ was 1.58. Same as Fontainebleau results reported by Maghsoodi et al. 2020 N found to be 2.2, the K was 0, k_1 was equal to 0.21 and $k_2 = 0.11$. The thickness of the interface, t was 1.15 mm and the β parameter was 0.91. Using the values in Table 5.2, the modeling results duplicated satisfactorily the experimental results for CNL tests (Fig. 5.9).

Fakharian and Evgin 2000 performed constant normal load and constant normal stiffness simple shear interface tests between samples of Silica sand and steel plates with different roughness using a Cyclic 3-Dimensional Simple Shear Interface apparatus. The physical characteristics of the Silica sand is summarized in Table 5.3. The sand has been prepared with a relative density of 0.88. The tests were performed with different stiffness values $K = 0$, 400 and 800 kPa/mm with an initial normal stress of 100 kPa (Fig. 5.10). Imposing the stiffness caused the variation of the normal stress acting on the interface. Due to the dense state of the material, the soil dilated at the interface and caused an increase of the normal stress. The first test with $K = 0$ (CNL) was used for the model calibration, and the other results were predicted using this test. With a $D_{50} = 0.6(mm)$, the interface thickness was calculated to be 3 (mm). The friction angle of 40 ^{o}C was used in the model. After model calibration for $\sigma_n = 100$ kPa, the parameters were used for model prediction of constant normal stiffness tests ($K = 400, 800$ kPa/mm). The results of the simulations presented in Fig. 5.10. The

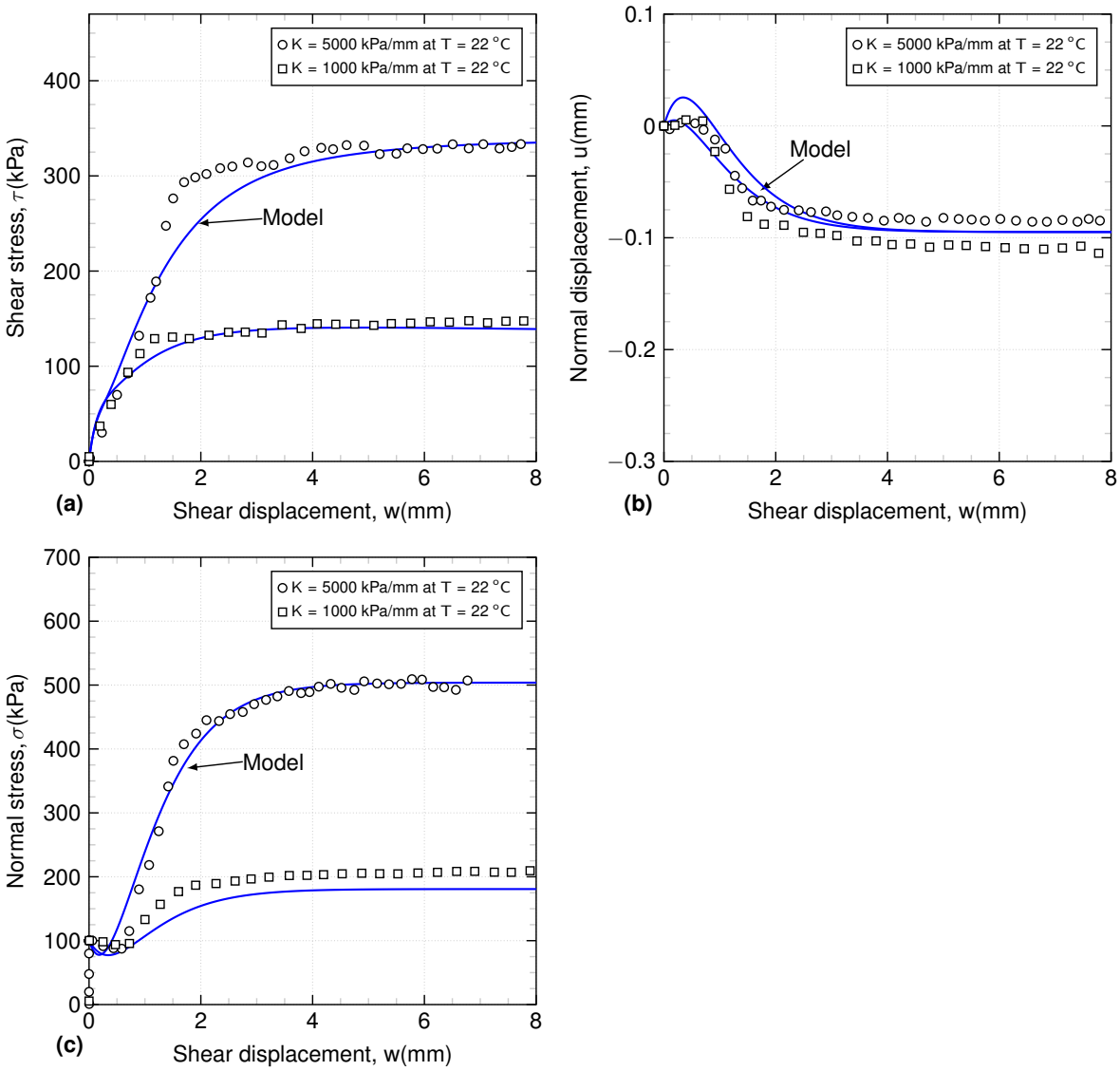

Figure 5.8: Model performance against CNS ($K = 1000, 5000$ kPa/mm) Fontainebleau sand-structure interface test results under 100 kPa of normal stress at 22 ^{o}C. (a) shear stress vs. shear displacement; and (b) normal displacement vs. shear displacement (experimental data by Maghsoodi et al. 2020).

model predictions showed a reasonable replication of experimental results.

5.4.2 Clay-structure interface at non-isothermal conditions

Maghsoodi et al. 2020 performed kaolin clay-steel interface direct shear tests at different temperatures (22 and 60 ^{o}C). The kaolin clay prepared with water content of 63 % and after homogenization consolidated inside the shear box. After consolidation phase CNL and CNS tests were performed. The kaolin clay was in a normally consolidated state and after heating a thermally overconsolidation effect was observed which decreased the void ratio of the clay prior to shearing. This void ratio decrease, made the soil denser and the soil showed a higher peak shear stress compared to unheated samples.

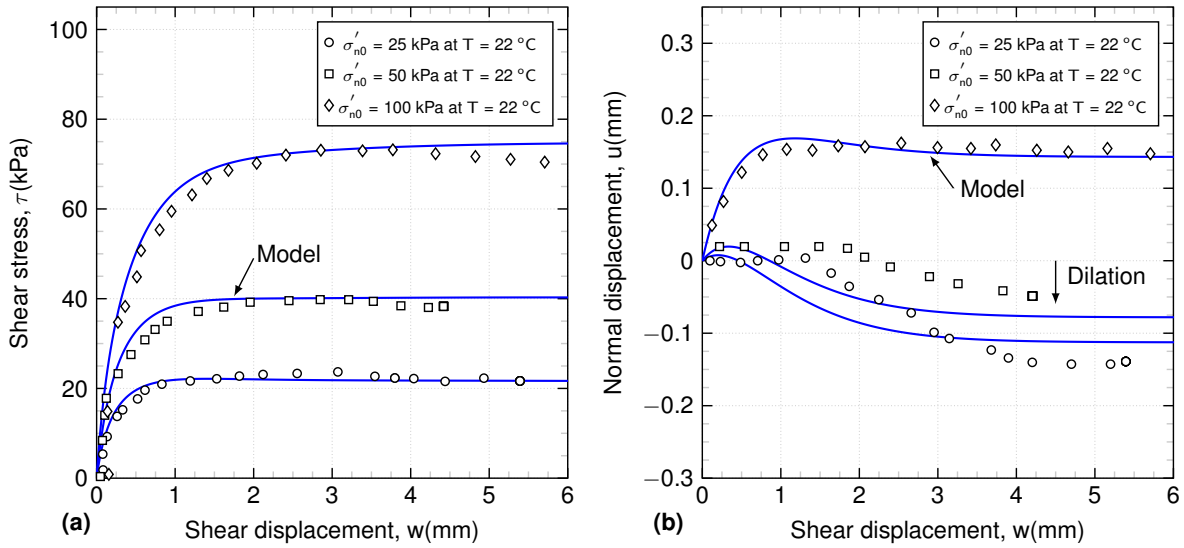

Figure 5.9: The interface model predictions against experimental data for four constant normal stress tests (K = 0) on interfaces between Fontainebleau sand and steel: (a) shear stress vs. shear displacement; and (b) normal displacement vs. shear displacement (experimental data by De Gennaro and Frank 2002).

This feature was captured by the model with a good agreement.

The model simulations and corresponding experimental data are shown in Fig. 5.11. A remarkable peak is discernible in the behavior of all samples that is captured in numerical simulations. It can be seen that the predicted results are satisfactory. For CNS tests, using the parameters in Table 5.4, the modeling results are in a very good agreement with experimental data (Fig. 5.12). In CNS tests, the difference between peak shear stress at different temperatures is lower than CNL case due to the effect of stiffness (Fig. 5.12(a)). The volumetric behavior during shear for both modeling and experimental results can be observed in Fig. 5.12(b). Due to the normally consolidated state of the kaolin clay in the interface, the normal stress is reductive to respect the stiffness. The modeling results for normal stress evolution during shear at different temperatures versus experimental results is illustrated in Fig. 5.12(c).

Di Donna et al. 2015 carried out interface direct shear tests on illite clay-concrete interface at different temperatures (22 and 50 ^{o}C) under three different normal stress (50, 100 and 150 kPa). The illite clay was prepared with target void ratio of e = 1.21 and a target dry density of 1.2 g/cm^3 with a water content of 46%. Concerning the experimental results that they have obtained it can be observed that, temperature increase, increased both peak and residual shear stress of the clay-concrete interface. The temperature increase affected the adhesion between the clay and the concrete which increased from 7 to 20 kPa with a temperature increase from 20 to 50 ^{o}C. The authors have explained the increase of shear strength by the thermal contraction

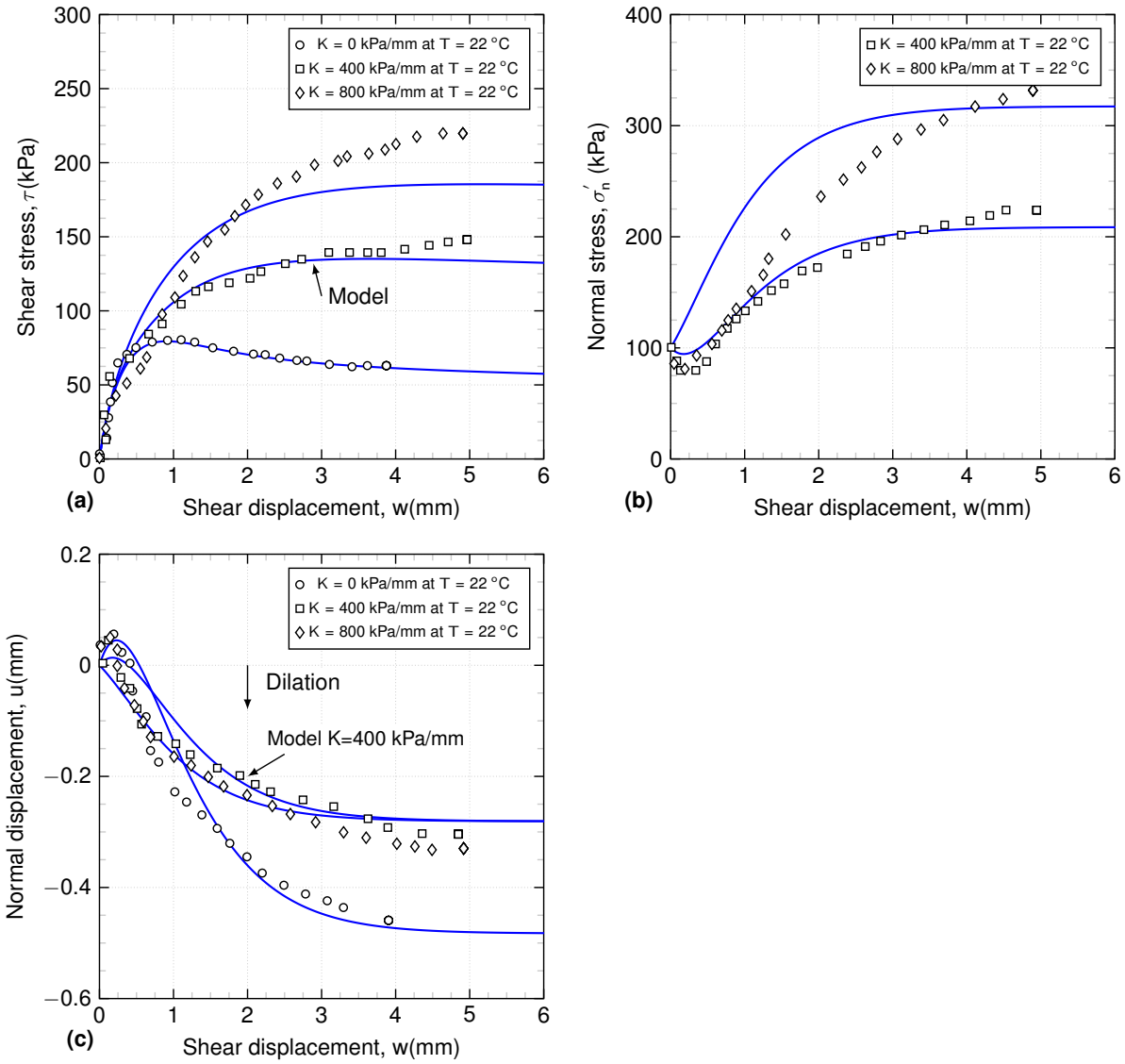

Figure 5.10: The interface model predictions against experimental data for four constant normal stress tests (K = 0) on interfaces between Fontainebleau sand and steel: (a) shear stress vs. shear displacement; and (b) normal displacement vs. shear displacement (experimental data by Fakharian and Evgin 2000).

that happened during the heating phase. The peak shear stress for illite clay-concrete interface is as clear as previous case (Maghsoodi et al. 2020). Therefore the shape of stress-displacement curves that should be reproduced by the model is different from other cases. As it was indicated in their study, the friction angle of the illite clay-concrete was 25 ^{o}, the Γ was 0.870, the $\lambda = 0.140$, the ξ was found to be 0.8, $N = 1.85$, k1=0.003, k2=0.7 and C=7 while beta=0.98. Therefore, the model predictions using the values Table 5.2 are presented in Fig. 5.13. The calibration tests were performed for $\sigma_n = 50$ kPa, and predictions were carried out for other stresses.

Yazdani et al. 2019 performed kaolin clay-concrete interface tests at different tem-

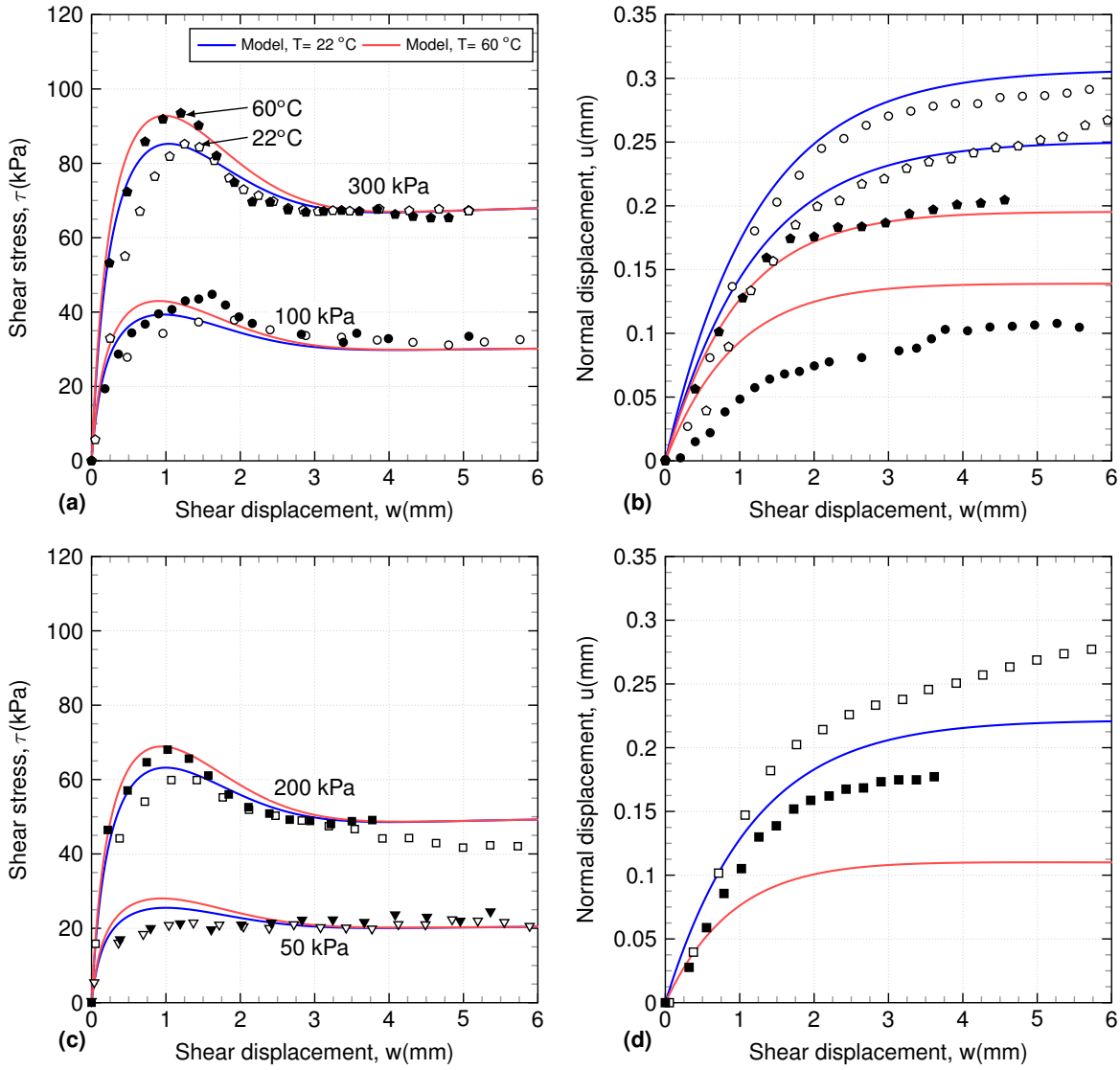

Figure 5.11: The interface model predictions against experimental data for four constant normal stress tests (K = 0) on interfaces between kaolin clay and steel: (a)(c) shear stress vs. shear displacement; and (b)(d) normal displacement vs. shear displacement (experimental data by Maghsoodi et al. 2020).

peratures (24 and 34 °C). The normally consolidated clay-concrete interfaces were tested under 3 different normal stresses (150, 225, 300 kPa). The temperature increase, increased the peak and residual shear strength of the interface. Under higher normal stresses the effect of temperature on the shear stress of the interface was more pronounced. Using the values in Table 5.2, the model capacity to reproduce the interface behavior is presented in Fig. 5.14. The model results are in good agreement with experimental data. The calibration of the model for the tests at 150 kPa have been performed and the prediction capacity is examined for other stresses.

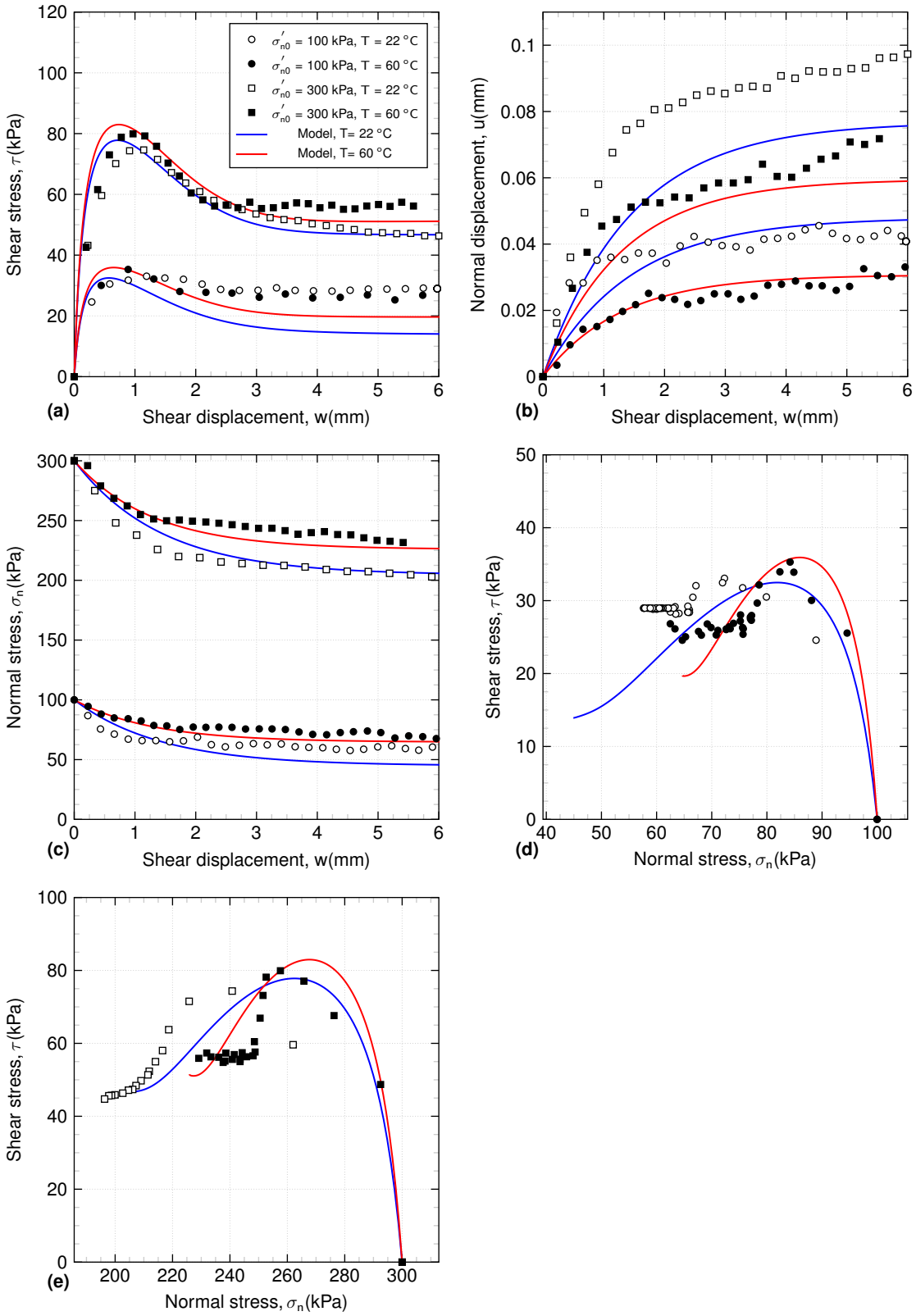

Figure 5.12: The interface model predictions against experimental data for four constant normal stiffness tests (K = 1000 kPa/mm) on interfaces between kaolin clay and steel: (a) shear stress vs. shear displacement; and (b) normal displacement vs. shear displacement (experimental data by Maghsoodi et al. 2020)

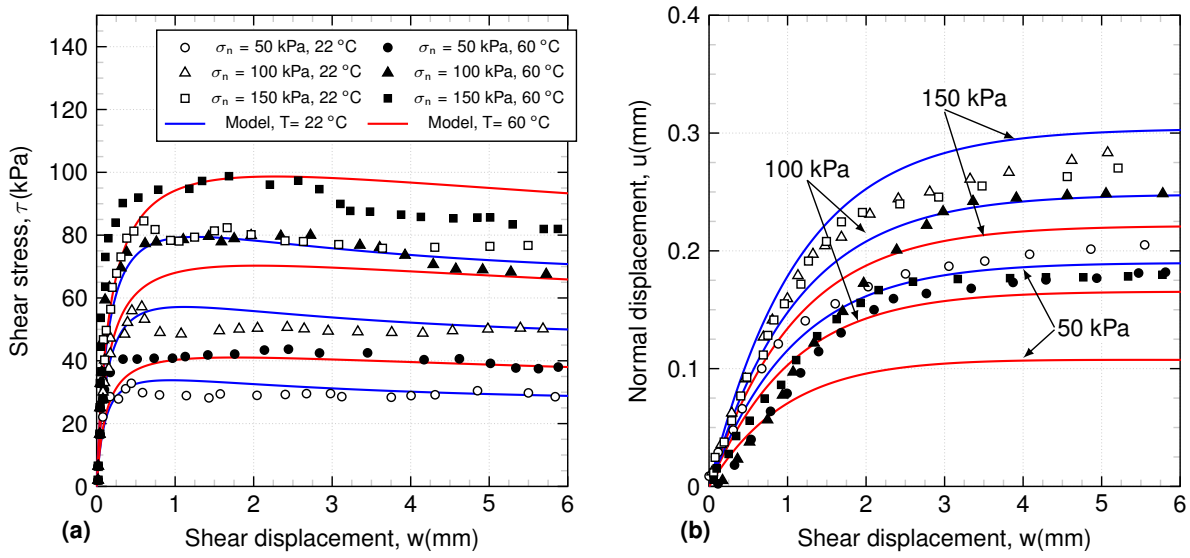

Figure 5.13: The interface model predictions against experimental data for four constant normal stress tests (K = 0) on interfaces between illite clay and concerete: (a) shear stress vs. shear displacement; and (b) normal displacement vs. shear displacement (experimental data by Di Donna et al. 2015).

5.5 Discussion and conclusions

The main objective of this study was to develop an approach to model the impact of temperature on the behavior of soil-structure interfaces. The developed non-isothermal model is based on the critical state concept, and it is an extension of a constitutive model for granular soil-structure interfaces under isothermal conditions. The extended model is capable of reproducing the experimental results of sand/clay-structure interfaces at different temperatures under both constant normal load (CNL) and constant normal stiffness (CNS) conditions. The following remarks can be made:

• The experimental evidence confirmed the thermal independence of the mechanical behavior of the sand-structure interface under CNL and CNS conditions (Di Donna et al. (2015); Yavari et al. (2016); Maghsoodi et al. (2020)). The modeling performance with respect to different CNL and CNS results is satisfactory, and the main features of the sand-structure behavior are reproduced. For CNL tests, the peak shear stress and dilatancy behavior of the sand-structure interface are reproduced by the model. For CNS tests, the model was capable of reproducing the shear stress-displacement response of the sand-structure without showing any clear peak. The normal stress variations have been modeled correctly, and the volumetric behavior has also been reproduced.

• The void ratio evolution of the normally consolidated clay-structure interface during shearing is contractive, similar to what can be observed in loose sand-structure interfaces. However, the shear stress-displacement response exhibits a well-defined

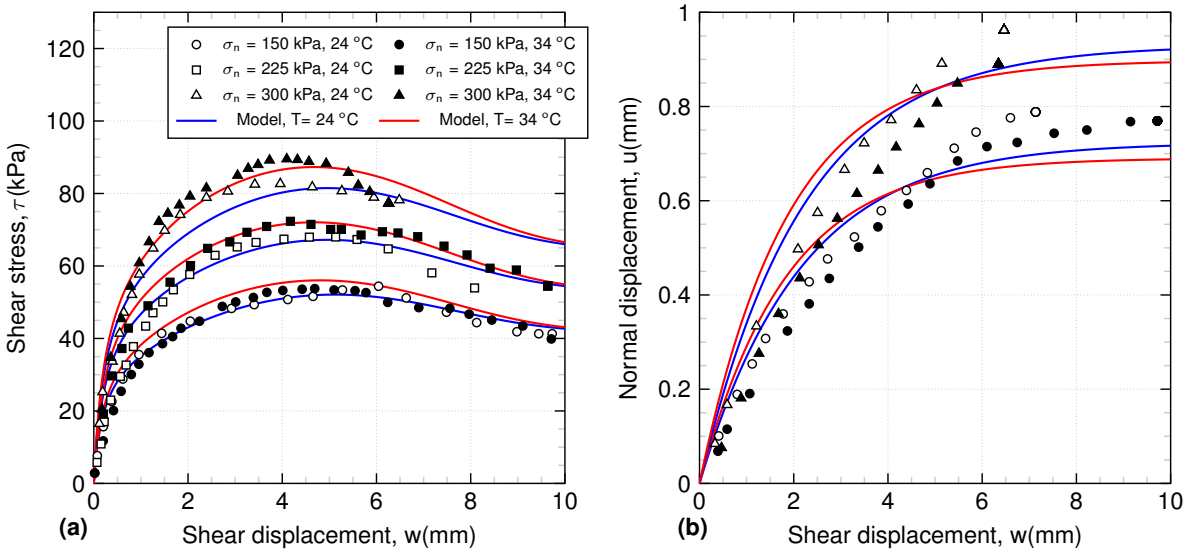

Figure 5.14: The interface model predictions against experimental data for four constant normal stress tests (K = 0) on interfaces between illite clay and concerete: (a) shear stress vs. shear displacement; and (b) normal displacement vs. shear displacement (experimental data by Yazdani et al. 2019).

peak. Several authors have confirmed this behavior, and they have explained that the combination of complex shearing modes (I, II and III) may be the reason for these observations (Tsubakihara and Kishida (1993), Lemos and Vaughan (2000)). The model was developed such that it could capture the peak shear stress of the clay interface.

• Several experimental investigations confirmed the shear strength dependence of clayey interfaces on thermal variations (Di Donna et al. (2015); Yavari et al. (2016); Maghsoodi et al. (2020)). A new formulation was developed to account for the effect of temperature on the behavior of clay-structure interfaces. The consequent effect of the void ratio evolution appeared to be an increase in the peak shear stress-displacement response. The extended model formulation was flexible enough to capture these features.

• The other important aspect of the model was the difference between the CNL and CNS soil-structure interface responses. Regarding the sand-structure interface parameters, the thickness of the interface (t) was found to be approximately 5-10 times D_{50}, which was experimentally observed by several authors (DeJong et al. 2003, Sadrekarimi and Olson 2010, Martinez et al. 2015). However, the clay-structure interface thickness is difficult to determine experimentally. For kaolin clay samples that have been tested in a modified triaxial cell using digital image correlation techniques, the thickness of the shear band was observed to be several millimeters (5-15 mm) (Thakur 2007, Gylland et al. 2014, Thakur et al. 2018). In our extended non-isothermal model, the interface thickness (t) for the clay-structure interface was found to be on same order of magni-

tude as that in the literature. This fact was applied in the modeling results in that for clay-structure interface tests, the thickness of the interface was greater than that in sand-structure interface tests.

• Regarding the model parameters, they can be determined using a temperature-controlled direct shear device. The critical state parameters (Γ and λ) can be estimated from a consolidation test. The void ratio of the clay before and after heating is also straightforward to determine. The mechanical characteristics (δ and C) can be found by performing shear tests under different normal stresses using the direct shear device. These parameters have physical meanings, which makes it easier to find their influence on the modeling performance.

• The overconsolidated clay-structure interface behavior at different temperatures could not be reproduced by the model due to the lack of experimental results in the literature. Therefore, first, experimental tests on the overconsolidated clay-structure interface behavior at different temperatures should be performed, and then, the results can be used for further development of the model. The void ratio evolution in overconsolidated clays is similar to that in dense sand-structure interfaces. Therefore, to introduce the effect of temperature on an overconsolidated clay-structure interface, formulation modification of the void ratio evolution should be implemented. Another important concern of the soil-structure interface behavior is the effect of roughness, which would require further extension of the model.

Conclusions and perspectives

Conclusions

Conventional geostructures like piles and diaphragm walls can be converted to energy geostructures by attaching heat exchanger tubes to their reinforcement cage. In recent years several studies have been conducted on the thermo-mechanical behavior of these thermally-active geostructures in full, small or laboratory scale. Indeed, beside supporting mechanical loads, the presence of thermal loads due to daily and seasonally fluctuations can make the behavior of these energy geostructures more complex. The aim of this study was to deepen the understanding regarding the behavior of sand/clay-structure contact under complex thermo-mechanical loads. A temperature-controlled direct shear device to perform monotonic and cyclic constant normal load or constant normal stiffness tests was developed.

Concerning the monotonic part of the study constant normal load (CNL) and constant normal stiffness (CNS) tests were performed on Fontainebleau sand/kaolin clay-steel interface at different temperatures (5, 22 and 60 ^{o}C) to study the thermal effects on friction angle and adhesion of interface. The results showed that the mechanical properties of sand were independent of temperature (22 and 60 ^oC) for both sand and sand-structure tests. Different stiffness values were applied under constant normal stiffness (CNS) conditions at different temperatures, and it was observed that such as CNL tests, the temperature does not change the interface behavior under CNS condition. Additionally the same interface friction angle was obtained in both CNL and CNS tests for sand-structure interface tests. In kaolin clay, temperature does not affect the friction angle and the main effect was the increase of the cohesion or adhesion. For clay tests, due to thermal contraction of kaolin during heating, the soil becomes denser and showed a higher shear strength. It was found that temperature increases the cohesion of clay samples. In clay-structure contact, due to difference in the nature of materials (clay vs. metal) the adhesion was not as much as clay case, therefore the shear strength increase with temperature increase, was not as much as clay case. In CNS tests on clay-structure interface, the soil exposed to higher temperatures, showed less contraction during shearing, and consequently less normal stress decreased due to

the denser state of the heated clay-structure samples prior to shearing. Therefore, in the interface the soil becomes denser with heating and the shear strength increases slightly.

After performing the monotonic part, the mechanical cyclic behavior of interface was investigated. The concept of constant-volume equivalent-undrained was used in the cyclic tests. One-way cyclic clay-structure interface tests at different temperatures with different cyclic and average stress ratios were performed. In monotonic CVEU tests, the shear behavior of clay-structure was different with clay-clay one. The lower friction angle of clay-structure compare to clay-clay and the shear behavior difference, confirmed that the shear happened in the interface zone. The results clearly showed the difference between cyclic clay-clay and clay-structure interface tests. The number of cycles to failure for clay-structure test was lower than clay-clay. In cyclic behavior of interface, decreasing the cyclic stress ratio increased the number of cycles to failure and decreased the equivalent pore water pressure. Temperature increase from 22 to 60 ^{o}C also increased the number of cycles to failure substantially. For cyclic clay-structure interface tests almost for all of the tests, after heating the shear strain and equivalent pore water pressure correspond to the first cycle decreased. Drained heating normally consolidated kaolin, caused thermal overconsolidation and made the sample denser, which can be one of the reasons for the increase of number of cycles to failure. The denser state of heated samples reduced the rate of degradation. Reducing the average shear stress, decreased the number of cycles to failure. The samples are applied to higher negative shear stresses and therefore, the resistance against cycles are reduced. Finally normally consolidated kaolin clay subjected to the cyclic stresses of this study by heating from 22 to 60 ^{o}C, shows higher number of cycles to failure.

Based on experimental results obtained for monotonic and cyclic part, the necessity to propose a non-isothermal interface constitutive model was observed. Therefore, in the third part of the study, a non-isothermal model which was an extension of a constitutive model for granular soil-structure interface under isothermal conditions was developed. Due to the direct effect of temperature on void ratio, the model was developed based on critical state theory. Due to the thermally independence mechanical response of sand-structure interface, the model parameters for sand-structure interface tests were calibrated for isothermal conditions. The model was capable to reproduce the experimental results of sand/clay-structure interfaces at different temperatures under both constant normal load and constant normal stiffness conditions. The exhibition of peak in stress-strain response of normally consolidated clay-structure interface was reproduced pertinently by the model.

Perspectives

For further investigations into the thermo-mechanical behavior of soil-structure interfaces several aspects can be discussed. Regarding the monotonic behavior of clay-structure interface, there is a lack of experimental data on the overconsolidated clay-structure interface at different temperatures. This aspect can provide a further insight into the clay-structure interface behavior at non-isothermal conditions. Concerning the complex shearing modes that exists in the clay-structure contact, using more complex technologies as X-ray tomography or digital image correlations can provide further insight into the shear mechanism at the interface on one hand and the effect of temperature on it on the other hand. Regarding the cyclic behavior of interface the cyclic behavior of overconsolidated clay-structure interface tests at different temperatures can give a vision into into the cyclic behavior of clay-structure interface behavior at non-isothermal conditions. The cyclic temperatures effects on the soil-structure interface can be noteworthy for further investigations. With respect to the non-isothermal modeling of interfaces, providing experimental data on overconsolidated soils can be used for subsequent calibration of the model. Proposing non-isothermal interface models for cyclic thermo-mechanical loads can be an interesting subject to study.

Bibliography

Abuel-Naga, H., Bergado, D., Bouazza, A. and Ramana, G. (2007). Volume change behaviour of saturated clays under drained heating conditions: experimental results and constitutive modeling, *Canadian Geotechnical Journal* **44**(8): 942–956.

Abuel-Naga, H., Bergado, D., Ramana, G., Grino, L., Rujivipat, P. and Thet, Y. (2006). Experimental evaluation of engineering behavior of soft bangkok clay under elevated temperature, *Journal of geotechnical and geoenvironmental engineering* **132**(7): 902–910.

Abuel-Naga, H. M., Bergado, D. T. and Lim, B. F. (2007). Effect of temperature on shear strength and yielding behavior of soft bangkok clay, *Soils and Foundations* **47**(3): 423–436.

Akrouch, G. A., Sánchez, M. and Briaud, J.-L. (2014). Thermo-mechanical behavior of energy piles in high plasticity clays, *Acta Geotechnica* **9**(3): 399–412.

Andersen, K. H. (2009). Bearing capacity under cyclic loadingoffshore, along the coast, and on land. the 21st bjerrum lecture presented in oslo, 23 november 2007, *Canadian Geotechnical Journal* **46**(5): 513–535.

Andersen, K. H., Rosenbrand, W. F., Brown, S. F. and Pool, J. H. (1980). Cyclic and static laboratory tests on drammen clay, *Journal of the Soil Mechanics and Foundations Division* **106**(5): 499–529.

Ansal, A. M. and Erken, A. (1989). Undrained behavior of clay under cyclic shear stresses, *Journal of Geotechnical Engineering* **115**(7): 968–983.

ASTM (1998). Standard test method for direct shear test of soils under consolidated drained conditions, *ASTM standard D3080-98, West Conshohocken, USA* .

Baldi, G., Hueckel, T. and Pellegrini, R. (1988). Thermal volume changes of the mineral–water system in low-porosity clay soils, *Canadian geotechnical journal* **25**(4): 807–825.

Been, K., Jefferies, M. and Hachey, J. (1991). The critical state of sands, *Geotechnique* **41**(3): 365–381.

Bfer, G. (1985). An isoparametric joint/interface element for finite element analysis, *International journal for numerical methods in engineering* **21**(4): 585–600.

Boukelia, A., Eslami, H., Rosin-Paumier, S. and Masrouri, F. (2017). Effect of temperature and initial state on variation of thermal parameters of fine compacted soils, *European Journal of Environmental and Civil Engineering* pp. 1–14.

Boulon, M. (1989). Basic features of soil structure interface behaviour, *Computers and Geotechnics* **7**(1-2): 115–131.

Boulon, M. and Foray, P. (1986). Physical and numerical simulation of lateral shaft friction along offshore piles in sand, *Proceedings of the 3rd International Conference on Numerical methods in Offshore piling, Nantes, France*, pp. 127–147.

Boulon, M., Garnica, P. and Vermeer, P. (1995). Soil-structure interaction: Fem computations, *Studies in Applied Mechanics* **42**: 147–147.

Boulon, M., Ghionna, V. N. and Mortara, G. (2003). A strain-hardening elastoplastic model for sand-structure interface under monotonic and cyclic loading, *Mathematical and computer modelling* **37**(5-6): 623–630.

Boulon, M. and Jarzebowski, A. (1991). Rate-type and elastoplastic approaches for soil-structure interface bahaviour: A comparison, *International conference on computer methods and advances in geomechanics. 7*, pp. 305–310.

Boulon, M. and Nova, R. (1990). Modelling of soil-structure interface behaviour a comparison between elastoplastic and rate type laws, *Computers and Geotechnics* **9**(1-2): 21–46.

Bourne-Webb, P., Amatya, B., Soga, K., Amis, T., Davidson, C. and Payne, P. (2009). Energy pile test at lambeth college, london: geotechnical and thermodynamic aspects of pile response to heat cycles, *Géotechnique* **59**(3): 237–248.

Brandl, H. (2006). Energy foundations and other thermo-active ground structures, *Géotechnique* **56**(2): 81–122.

Brown, S., Lashine, A. and Hyde, A. (1975). Repeated load triaxial testing of a silty clay, *Geotechnique* **25**(1): 95–114.

Brumund, W. and Leonards, G. (1973). Experimental study of static and dynamic friction between sand and typical constuction materials, *Journal of Testing and Evaluation* **1**(2): 162–165.

Burghignoli, A., Desideri, A. and Miliziano, S. (2000). A laboratory study on the thermomechanical behaviour of clayey soils, *Canadian Geotechnical Journal* **37**(4): 764–780.

Campanella, R. G. and Mitchell, J. K. (1968). Influence of temperature variations on soil behavior, *Journal of Soil Mechanics and Foundations Division* **94**(SM3): 709–734.

Cekerevac, C. and Laloui, L. (2004). Experimental study of thermal effects on the mechanical behaviour of a clay, *International journal for numerical and analytical methods in geomechanics* **28**(3): 209–228.

Cekerevac, C. and Laloui, L. (2010). Experimental analysis of the cyclic behaviour of kaolin at high temperature, *Géotechnique* **60**(8): 651.

Cfms, S. (2017). Recommandations pour la conception, le dimensionnement et la mise en oeuvre des géostructures thermiques, *Revue Française de Géotechnique* **149**: 120.

Chiu, S.-L. (1996). Behaviour of normally consolidated clay at elevated temperature.

Clough, G. W. and Duncan, J. M. (1971). Finite element analyses of retaining wall behavior, *Journal of Soil Mechanics & Foundations Div* .

Coyle, H. M. and Sulaiman, I. H. (1967). Skin friction for steel piles in sand, *Journal of Soil Mechanics & Foundations Div* **92**(SM5, Proc Paper 490).

Cui, Y. J., Sultan, N. and Delage, P. (2000). A thermomechanical model for saturated clays, *Canadian Geotechnical Journal* **37**(3): 607–620.

DAguiar, S. C., Modaressi-Farahmand-Razavi, A., Dos Santos, J. A. and Lopez-Caballero, F. (2011). Elastoplastic constitutive modelling of soil–structure interfaces under monotonic and cyclic loading, *Computers and Geotechnics* **38**(4): 430–447.

Das, B. M. (2015). *Principles of foundation engineering*, Cengage learning.

De Gennaro, V. and Frank, R. (2002). Elasto-plastic analysis of the interface behaviour between granular media and structure, *Computers and Geotechnics* **29**(7): 547–572.

De Wit, C. and Arens, P. (1950). Moisture content and density of some caly minerals and some remarks on the hydration pattern of clay, *Transactions of the International Congress of Soil Science, Amsterdam, 1950*, pp. 3–3.

DeJong, J. T., Randolph, M. F. and White, D. J. (2003). Interface load transfer degradation during cyclic loading: a microscale investigation, *Soils and foundations* **43**(4): 81–93.

DeJong, J. T. and Westgate, Z. J. (2009). Role of initial state, material properties, and confinement condition on local and global soil-structure interface behavior, *Journal of Geotechnical and Geoenvironmental Engineering* **135**(11): 1646–1660.

Dejong, J. T., White, D. J. and Randolph, M. F. (2006). Microscale observation and modeling of soil-structure interface behavior using particle image velocimetry, *Soils and foundations* **46**(1): 15–28.

Delage, P., Sultan, N. and Cui, Y. J. (2000). On the thermal consolidation of boom clay, *Canadian Geotechnical Journal* **37**(2): 343–354.

Desai, C., Drumm, E. and Zaman, M. (1985). Cyclic testing and modeling of interfaces, *Journal of Geotechnical Engineering* **111**(6): 793–815.

Desai, C. and Nagaraj, B. (1988). Modeling for cyclic normal and shear behavior of interfaces, *Journal of engineering mechanics* **114**(7): 1198–1217.

Desai, C. S. and Ma, Y. (1992). Modelling of joints and interfaces using the disturbed-state concept, *International Journal for Numerical and Analytical Methods in Geomechanics* **16**(9): 623–653.

Desai, C. S. and Zhang, W. (1998). Computational aspects of disturbed state constitutive models, *Computer methods in applied mechanics and engineering* **151**(3-4): 361–376.

Di Donna, A. (2014). *Thermo-mechanical aspects of energy piles*, PhD thesis, École polytechnique fédérale de Lausanne, Switzerland.

Di Donna, A., Ferrari, A. and Laloui, L. (2015). Experimental investigations of the soil–concrete interface: physical mechanisms, cyclic mobilization, and behaviour at different temperatures, *Canadian Geotechnical Journal* **53**(4): 659–672.

Dyvik, R., Berre, T., Lacasse, S. and Raadim, B. (1987). Comparison of truly undrained and constant volume direct simple shear tests, *Geotechnique* **37**(1): 3–10.

Eid, H. T., Amarasinghe, R. S., Rabie, K. H. and Wijewickreme, D. (2015). Residual shear strength of fine-grained soils and soil–solid interfaces at low effective normal stresses, *Canadian Geotechnical Journal* **52**(2): 198–210.

Eslami, H., Rosin-Paumier, S., Abdallah, A. and Masrouri, F. (2017). Pressuremeter test parameters of a compacted illitic soil under thermal cycling, *Acta Geotechnica* **12**(5): 1105–1118.

Evans, M. and Fennick, T. (1995). Geosynthetic/soil interface friction angles using a rotation shear device, *Geotechnical Testing Journal* **18**(2): 271–275.

Evgin, E. and Fakharian, K. (1997). Effect of stress paths on the behaviour of sand steel interfaces, *Canadian geotechnical journal* **33**(6): 853–865.

Faizal, M., Bouazza, A., Haberfield, C. and McCartney, J. S. (2018). Axial and radial thermal responses of a field-scale energy pile under monotonic and cyclic temperature changes, *Journal of Geotechnical and Geoenvironmental Engineering* **144**(10): 04018072.

Fakharian, K. (1996). *Three-dimensional monotonic and cyclic behaviour of sand-steel interfaces: Testing and modelling.*, PhD thesis, University of Ottawa, Canada.

Fakharian, K. and Evgin, E. (1997). Cyclic simple-shear behavior of sand-steel interfaces under constant normal stiffness condition, *Journal of Geotechnical and Geoenvironmental Engineering* **123**(12): 1096–1105.

Fakharian, K. and Evgin, E. (2000). Elasto-plastic modelling of stress-path-dependent behaviour of interfaces, *International Journal for Numerical and Analytical Methods in Geomechanics* **24**(2): 183–199.

Finn, F. (1952). The effect of temperature on the consolidation characteristics of remolded clay, *Symposium on Consolidation Testing of Soils*, ASTM International.

Fioravante, V. (2002). On the shaft friction modelling of non-displacement piles in sand, *Soils and foundations* **42**(2): 23–33.

Fioravante, V., Ghionna, V. N., Pedroni, S. and Porcino, D. (1999). A constant normal stiffness direct shear box for soil-solid interface tests, *Rivista Italiana di geotecnica* **33**(3): 7–22.

Foray, P., Balachowski, L. and Rault, G. (1998). Scale effect in shaft friction due to the localisation of deformations, *Centrifuge 98*, pp. 211–216.

Ghaaowd, I., Takai, A., Katsumi, T. and McCartney, J. S. (2015). Pore water pressure prediction for undrained heating of soils, *Environmental Geotechnics* **4**(2): 70–78.

Ghahremannejad, B. (2003). *Thermo-mechanical behaviour of two reconstituted clays*, PhD thesis, University of Sydney, Austraila.

Ghionna, V. N. and Mortara, G. (2002a). An elastoplastic model for sand - structure interface behaviour.

Ghionna, V. N. and Mortara, G. (2002b). An elastoplastic model for sand–structure interface behaviour, *Géotechnique* **52**(1): 41–50.

Gibson, R. and Henkel, D. (1954). Influence of duration of tests at constant rate of strain on measured drained strength, *Géotechnique* **4**(1): 6–15.

Gómez, J. E., Filz, G. M. and Ebeling, R. M. (2003). Extended hyperbolic model for sand-to-concrete interfaces, *Journal of Geotechnical and Geoenvironmental Engineering* **129**(11): 993–1000.

Goodman, R. E. (1989). *Introduction to rock mechanics*, Vol. 2, Wiley New York.

Graham, J., Graham, J., Tanaka, N., Crilly, T. and Alfaro, M. (2001). Modified Cam-Clay modeling of temperature effects in clays Modified Cam-Clay modelling of temperature effects in clays, (October 2016).

Graham, J., Tanaka, N., Crilly, T. and Alfaro, M. (2001). Modified cam-clay modelling of temperature effects in clays, *Canadian geotechnical journal* **38**(3): 608–621.

Gylland, A. S., Jostad, H. P. and Nordal, S. (2014). Experimental study of strain localization in sensitive clays, *Acta Geotechnica* **9**(2): 227–240.

Hamid, T. B. and Miller, G. A. (2009). Shear strength of unsaturated soil interfaces, *Canadian Geotechnical Journal* **46**(5): 595–606.

Hamid, T. and Miller, G. (2005). Elastoplastic constitutive model for unsaturated soil–steel interface, *Abousleiman, Chen, Ulm (eds.) Poromechanics-Giot Centennial (1905-2005)* .

Hamidi, a. and Khazaei, C. (2010). A thermo-mechanical constitutive model for saturated clays, *International Journal of Geotechnical Engineering* **4**: 445–459.

Hanzawa, H., Nutt, N., Lunne, T., Tang, Y. and Long, M. (2007). A comparative study between the ngi direct simple shear apparatus and the mikasa direct shear apparatus, *Soils and foundations* **47**(1): 47–58.

Head, K. H. et al. (1998). *Manual of soil laboratory testing. Volume 3: effective stress tests.*, number Ed. 2, John Wiley & Sons.

Hebeler, G., Martinez, A. and Frost, J. (2016). Shear zone evolution of granular soils in contact with conventional and textured cpt friction sleeves, *KSCE Journal of Civil Engineering* **20**(4): 1267–1282.

Ho, T., Jardine, R. and Anh-Minh, N. (2011). Large-displacement interface shear between steel and granular media, *Géotechnique* **61**(3): 221–234.

Hossain, M. A. and Yin, J.-H. (2012). Influence of grouting pressure on the behavior of an unsaturated soil-cement interface, *Journal of geotechnical and geoenvironmental engineering* **138**(2): 193–202.

Hossain, M. A. and Yin, J.-H. (2015). Dilatancy and strength of an unsaturated soil-cement interface in direct shear tests, *International journal of Geomechanics* **15**(5): 04014081.

Hoteit (1990). *Etude exprimentale du comportement physique et mcanique des interfaces sols-structures*, PhD thesis, Institut National Polytéchnique de Grenoble, France.

Houston, S. L. and Lin, H.-D. (1987). A thermal consolidation model for pelagic clays, *Marine Georesources & Geotechnology* **7**(2): 79–98.

Hu, L. and Pu, J. (2004). Testing and modeling of soil-structure interface, *Journal of Geotechnical and Geoenvironmental Engineering* **130**(8): 851–860.

Hu, L. and Pu, J. L. (2003). Application of damage model for soil–structure interface, *Computers and Geotechnics* **30**(2): 165–183.

Hueckel, T. and Baldi, G. (1990). Thermoplasticity of saturated clays: experimental constitutive study, *Journal of geotechnical engineering* **116**(12): 1778–1796.

Hueckel, T. and Borsetto, M. (1990). Thermoplasticity of saturated soils and shales: constitutive equations, *Journal of Geotechnical Engineering* **116**(12): 1765–1777.

Hueckel, T., François, B. and Laloui, L. (2009). Explaining thermal failure in saturated clays, *Géotechnique* **59**(3): 197–212.

Hueckel, T., Pellegrini, R. and Del Olmo, C. (1998). A constitutive study of thermo-elasto-plasticity of deep carbonatic clays, *International journal for numerical and analytical methods in geomechanics* **22**(7): 549–574.

Hyde, A. F., Yasuhara, K. and Hirao, K. (1993). Stability criteria for marine clay under one-way cyclic loading, *Journal of geotechnical engineering* **119**(11): 1771–1789.

Idriss, I., Dobry, R., Doyle, E., Singh, R. et al. (1976). Behavior of soft clays under earthquake loading conditions, *Offshore Technology Conference*, Offshore Technology Conference.

Idriss, I. M., Dobry, R. and Sing, R. (1978). Nonlinear behavior of soft clays during cyclic loading, *Journal of Geotechnical and Geoenvironmental Engineering* **104**(ASCE 14265).

Jarad, N., Cuisinier, O. and Masrouri, F. (2017). Effect of temperature and strain rate on the consolidation behaviour of compacted clayey soils, *European Journal of Environmental and Civil Engineering* pp. 1–18.

Jardine, R., Lehane, B. and Everton, S. (1993). Friction coefficients for piles in sands and silts, *Offshore site investigation and foundation behaviour*, Springer, pp. 661–677.

Khoury, C. N. and Miller, G. A. (2012). Influence of hydraulic hysteresis on the shear strength of unsaturated soils and interfaces, *Geotechnical Testing Journal* **35**(1): 135–149.

Kishida, H. and Uesugi, M. (1987). Tests of the interface between sand and steel in the simple shear apparatus, *Geotechnique* **37**(1): 45–52.

Kuntiwattanakul, P., Towhata, I., Ohishi, K. and Seko, I. (1995). Temperature effects on undrained shear characteristics of clay, *Soils and Foundations* **35**(1): 147–162.

Lackenby, J., Indraratna, B., McDowell, G. and Christie, D. (2007). Effect of confining pressure on ballast degradation and deformation under cyclic triaxial loading, *Geotechnique* **57**: 527–536.

Laguros (1969). Effect of temperature on some engineering properties of clay soils, *Special Report 103, Washington D.C.* .

Lahoori, M., Jannot, Y., Rosin-Paumier, S., Boukelia, A. and Masrouri, F. (2020). Measurement of the thermal properties of unsaturated compacted soil by the transfer function estimation method, *Applied Thermal Engineering* **167**: 114795.

Laloui, L. and Cekerevac, C. (2003). Thermo-plasticity of clays: an isotropic yield mechanism, *Computers and Geotechnics* **30**(8): 649–660.

Laloui, L. and François, B. (2009). Acmeg-t: soil thermoplasticity model, *Journal of engineering mechanics* **135**(9): 932–944.

Laloui, L., Nuth, M. and Vulliet, L. (2006). Experimental and numerical investigations of the behaviour of a heat exchanger pile, *International Journal for Numerical and Analytical Methods in Geomechanics* **30**(8): 763–781.

Lashkari, A. (2012). A plasticity model for sand-structure interfaces, *Journal of Central South University* **19**(4): 1098–1108.

Lashkari, A. (2013). Prediction of the shaft resistance of nondisplacement piles in sand, *International Journal for Numerical and Analytical Methods in Geomechanics* **37**(8): 904–931.

Lashkari, A. (2017). A simple critical state interface model and its application in prediction of shaft resistance of non-displacement piles in sand, *Computers and Geotechnics* **88**: 95–110.

Lehane, B. and Jardine, R. (1992). Residual strength of bothkennar clay in soil-soil and soil-interface shear, *Géotechnique* **42**(2): 363–367.

Lehane, B., Jardine, R., Bond, A. J. and Frank, R. (1993). Mechanisms of shaft friction in sand from instrumented pile tests, *Journal of Geotechnical Engineering* **119**(1): 19–35.

Lemos, L. (1991). Shear strength of shear surfaces under fast loading, *Proceedings of the Tenth European Conference on Soil Mechanics and Foundation Engineering, Associazione Geotecnica Italiana*, Vol. 1, pp. 137–142.

Lemos, L. J. L. (1986). The effect of rate on residual strength of soil.

Lemos, L. and Vaughan, P. (2000). Clay–interface shear resistance, *Géotechnique* **50**(1): 55–64.

Li, C., Kong, G., Liu, H. and Abuel-Naga, H. (2018). Effect of temperature on behaviour of red clay–structure interface, *Canadian Geotechnical Journal* **56**(1): 126–134.

Li, L.-L., Dan, H.-B. and Wang, L.-Z. (2011). Undrained behavior of natural marine clay under cyclic loading, *Ocean Engineering* **38**(16): 1792–1805.

Littleton, I. (1976). An experimental study of the adhesion between clay and steel, *Journal of terramechanics* **13**(3): 141–152.

Liu, H., Liu, H., Xiao, Y. and McCartney, J. S. (2018). Effects of temperature on the shear strength of saturated sand, *Soils and Foundations* **58**(6): 1326–1338.

Liu, H., Song, E. and Ling, H. I. (2006). Constitutive modeling of soil-structure interface through the concept of critical state soil mechanics, *Mechanics Research Communications* **33**(4): 515–531.

Lupinl, J., Skinner, A. and Vaughan, P. (2009). The drained residual strength of cohesive soils, *Selected papers on geotechnical engineering by PR Vaughan*, Thomas Telford Publishing, pp. 88–120.

Maghsoodi, S., Cuisinier, O. and Masrouri, F. (2019a). Comportement thermo-mécanique de l'interface sable-structure, *17th European Conference on Soil Mechanics and Geotechnical Engineering*.
URL: *https://doi.org/10.32075/17ECSMGE-2019-0274*

Maghsoodi, S., Cuisinier, O. and Masrouri, F. (2019b). Thermo-mechanical behaviour of clay-structure interface, *E3S Web of Conferences*, Vol. 92, EDP Sciences, p. 10002.
URL: *https://doi.org/10.1051/e3sconf/20199210002*

Maghsoodi, S., Cuisinier, O. and Masrouri, F. (2020). Thermal effects on mechanical behaviour of soil–structure interface, *Canadian geotechnical journal* **57**(1): 32–47. **URL:** *https://doi.org/10.1139/cgj-2018-0583*

Martinez, A., Frost, J. D. and Hebeler, G. L. (2015). Experimental study of shear zones formed at sand/steel interfaces in axial and torsional axisymmetric tests, *Geotechnical Testing Journal* **38**(4): 409–426.

Martinez, A. and Stutz, H. H. (2018). Rate effects on the interface shear behaviour of normally and over-consolidated clay, *Géotechnique* .

Matasović, N. and Vucetic, M. (1995). Generalized cyclic-degradation-pore-pressure generation model for clays, *Journal of geotechnical engineering* **121**(1): 33–42.

Matsui, T., Ito, T. and Ohara, H. (1980). Cyclic stress-strain history and shear characteristics of clay, *Journal of the geotechnical Engineering Division* **106**(10): 1101–1120.

McCartney, J. S., Jafari, N. H., Hueckel, T., Sánchez, M. and Vahedifard, F. (2019). Emerging thermal issues in geotechnical engineering, *Geotechnical fundamentals for addressing new world challenges*, Springer, pp. 275–317.

McCartney, J. S. and Rosenberg, J. E. (2011). Impact of heat exchange on side shear in thermo-active foundations, *Geo-Frontiers 2011: Advances in Geotechnical Engineering*, pp. 488–498.

Miller, G. A. and Hamid, T. B. (2006). Interface direct shear testing of unsaturated soil, *Geotechnical Testing Journal* **30**(3): 182–191.

Mitchell, J. K. (1964). Shearing resistance of soils as a rate process, *Journal of Soil Mechanics & Foundations Div* **90**(Proc. Paper 3773).

Mitchell, J. K., Soga, K. et al. (2005). *Fundamentals of soil behavior*, Vol. 3, John Wiley & Sons New York.

Monfared, M., Sulem, J., Delage, P. and Mohajerani, M. (2011). A laboratory investigation on thermal properties of the opalinus claystone, *Rock Mechanics and Rock Engineering* **44**(6): 735.

Monfared, M., Sulem, J., Delage, P. and Mohajerani, M. (2014). Temperature and damage impact on the permeability of opalinus clay, *Rock mechanics and rock engineering* **47**(1): 101–110.

Mooney, R., Keenan, A. and Wood, L. (1952). Adsorption of water vapor by montmorillonite. i. heat of desorption and application of bet theory1, *Journal of the American Chemical Society* **74**(6): 1367–1371.

Morin, R. and Silva, A. J. (1984). The effects of high pressure and high temperature on some physical properties of ocean sediments, *Journal of Geophysical Research: Solid Earth* **89**(B1): 511–526.

Mortara, G. (2001). *An elastoplastic model for sand-structure interface behaviour under monotonic and cyclic loading*, PhD thesis, Technical University of Torino, Italy.

Mortara, G., Boulon, M. and Ghionna, V. N. (2002). A 2-d constitutive model for cyclic interface behaviour, *International journal for numerical and analytical methods in geomechanics* **26**(11): 1071–1096.

Mortara, G., Mangiola, A. and Ghionna, V. N. (2007). Cyclic shear stress degradation and post-cyclic behaviour from sand–steel interface direct shear tests, *Canadian Geotechnical Journal* **44**(7): 739–752.

Mortezaie, A. R. and Vucetic, M. (2013). Effect of frequency and vertical stress on cyclic degradation and pore water pressure in clay in the ngi simple shear device, *Journal of Geotechnical and Geoenvironmental Engineering* **139**(10): 1727–1737.

Mortezaie, A. and Vucetic, M. (2016). Threshold shear strains for cyclic degradation and cyclic pore water pressure generation in two clays, *Journal of Geotechnical and Geoenvironmental Engineering* **142**(5): 04016007.

Moses, G., Rao, S. and Rao, P. (2003). Undrained strength behaviour of a cemented marine clay under monotonic and cyclic loading, *Ocean engineering* **30**(14): 1765–1789.

Murayama (1969). Effect of temperature on the elasticity of clays, *Special Report 103, Washington D.C.* .

Murphy, K. D. and McCartney, J. S. (2014). Thermal borehole shear device, *Geotechnical Testing Journal* **37**(6): 1040–1055.

Murphy, K. D., McCartney, J. S. and Henry, K. S. (2015). Evaluation of thermo-mechanical and thermal behavior of full-scale energy foundations, *Acta Geotechnica* **10**(2): 179–195.

Navayogarajah, N., Desai, C. and Kiousis, P. (1992). Hierarchical single-surface model for static and cyclic behavior of interfaces, *Journal of engineering mechanics* **118**(5): 990–1011.

Nejat, P., Jomehzadeh, F., Taheri, M. M., Gohari, M. and Majid, M. Z. A. (2015). A global review of energy consumption, co2 emissions and policy in the residential

sector (with an overview of the top ten co2 emitting countries), *Renewable and sustainable energy reviews* **43**: 843–862.

Ng, C. W. W., Wang, S. and Zhou, C. (2016). Volume change behaviour of saturated sand under thermal cycles, *Géotechnique Letters* **6**(2): 124–131.

Nova, R. and Wood, D. M. (1979). A constitutive model for sand in triaxial compression, *International journal for numerical and analytical methods in geomechanics* **3**(3): 255–278.

Ohara, S. and Matsuda, H. (1988). Study on the settlement of saturated clay layer induced by cyclic shear, *Soils and Foundations* **28**(3): 103–113.

Plum, R. and Esrig, M. (1969). Effects of temperature on some engineering properties of clay soils, *Special Report* **103**: 231–242.

Porcino, D., Fioravante, V., Ghionna, V. N. and Pedroni, S. (2003). Interface behavior of sands from constant normal stiffness direct shear tests, *Geotechnical Testing Journal* **26**(3): 289–301.

Potyondy, J. G. (1961). Skin friction between various soils and construction materials, *Geotechnique* **11**(4): 339–353.

Poulos, H. and Al-Douri, R. (1992). Influence of soil density on pile skin friction in calcareous sediments, *Proc., 6th ANZ Conf. on Geomech*, pp. 375–380.

Pra-Ai, S. (2013). *Behaviour of soil-structure interfaces subjected to a large number of cycles. Application to piles*, PhD thesis, University of Grenoble-Alpes, France.

Pra-ai, S. and Boulon, M. (2017). Soil–structure cyclic direct shear tests: a new interpretation of the direct shear experiment and its application to a series of cyclic tests, *Acta Geotechnica* **12**(1): 107–127.

Procter, D. C. and Khaffaf, J. H. (1984). Cyclic triaxial tests on remoulded clays, *Journal of Geotechnical Engineering* **110**(10): 1431–1445.

Saberi, M., Annan, C.-D. and Konrad, J.-M. (2017). Constitutive modeling of gravelly soil–structure interface considering particle breakage, *Journal of Engineering Mechanics* **143**(8): 04017044.

Saberi, M., Annan, C.-D. and Konrad, J.-M. (2019). Implementation of a soil-structure interface constitutive model for application in geo-structures, *Soil Dynamics and Earthquake Engineering* **116**: 714–731.

Saberi, M., Annan, C.-D., Konrad, J.-M. and Lashkari, A. (2016). A critical state two-surface plasticity model for gravelly soil-structure interfaces under monotonic and cyclic loading, *Computers and Geotechnics* **80**: 71–82.

Sadrekarimi, A. and Olson, S. M. (2010). Shear band formation observed in ring shear tests on sandy soils, *Journal of geotechnical and geoenvironmental engineering* **136**(2): 366–375.

Seed, H. B. and Chan, C. K. (1966). Clay strength under earthquake loading conditions, *Journal of Soil Mechanics & Foundations Div* **92**(ASCE# 4723 Proceeding).

Shahrour, I. and Rezaie, F. (1997). An elastoplastic constitutive relation for the soil-structure interface under cyclic loading, *Computers and Geotechnics* **21**(1): 21–39.

Shakir, R. R. and Zhu, J. (2009). Behavior of compacted clay-concrete interface, *Frontiers of Architecture and Civil Engineering in China* **3**(1): 85–92.

Sherif, M. A. and Burrous, C. M. (1969). Temperature effects on the unconfined shear strength of saturated, cohesive soil, *Highway Research Board Special Report* (103).

Skempton, A. W. (1985). Residual strength of clays in landslides, folded strata and the laboratory, *Geotechnique* **35**(1): 3–18.

Soltani, J. H. and Soroush, A. (2010). Cyclic behavior of mixed clayey soils.

Soralump, S. and Prasomsri, J. (2015). Cyclic pore water pressure generation and stiffness degradation in compacted clays, *Journal of Geotechnical and Geoenvironmental Engineering* **142**(1): 04015060.

Stutz, H. H. (2016). *Hypoplastic Models for Soil-Structure Interfaces-Modelling and Implementation*, PhD thesis, Kiel University, Germany.

Stutz, H. H., Mašín, D. and Wuttke, F. (2016). Enhancement of a hypoplastic model for granular soil–structure interface behaviour, *Acta Geotechnica* **11**(6): 1249–1261.

Stutz, H. and Mašín, D. (2017). Hypoplastic interface models for fine-grained soils, *International Journal for numerical and analytical methods in geomechanics* **41**(2): 284–303.

Stutz, H., Mašín, D., Wuttke, F. and Prädel, B. (2016). Thermo-mechanical hypoplastic interface model for fine-grained soils, *Proceedings of the 1st International Conference on Energy Geotechnics*, pp. 351–357.

Suryatriyastuti, M., Burlon, S. and Mroueh, H. (2016). On the understanding of cyclic interaction mechanisms in an energy pile group, *International Journal for Numerical and Analytical Methods in Geomechanics* **40**(1): 3–24.

Suryatriyastuti, M., Mroueh, H. and Burlon, S. (2014). A load transfer approach for studying the cyclic behavior of thermo-active piles, *Computers and Geotechnics* **55**: 378–391.

Tabucanon, J. T., Airey, D. W. and Poulos, H. G. (1995). Pile skin friction in sands from constant normal stiffness tests.

Takada, N. (1993). Mikasa's direct shear apparatus, test procedures and results, *Geotechnical Testing Journal* **16**(3): 314–322.

Tan, K. and Vucetic, M. (1989). Behavior of medium and low plasticity clays under cyclic simple shear conditions, *Proceedings of the 4th International Conference on Soil Dynamics and Earthquake Engineering. Mexico City:[sn]*, pp. 131–142.

Tang, A.-M. and Cui, Y.-J. (2009). Modelling the thermo-mechanical volume change behaviour of compacted expansive clays, *arXiv preprint arXiv:0904.3614* .

Taylor, D. W. (1948). *Fundamentals of soil mechanics*, Vol. 66, LWW.

Thakur, V. (2007). Strain localization in sensitive soft clays, *NTNU, Trondheim* .

Thakur, V., Nordal, S., Viggiani, G. and Charrier, P. (2018). Shear bands in undrained plane strain compression of norwegian quick clays, *Canadian Geotechnical Journal* **55**(1): 45–56.

Thian, S. and Lee, C. (2017). Cyclic stress-controlled tests on offshore clay, *Journal of Rock Mechanics and Geotechnical Engineering* **9**(2): 376–381.

Tidfors, M. and Sällfors, G. (1989). Temperature effect on preconsolidation pressure, *Geotechnical Testing Journal* **12**(1): 93–97.

Tika, T. E., Vaughan, P. and Lemos, L. (1996). Fast shearing of pre-existing shear zones in soil, *Geotechnique* **46**(2): 197–233.

Tika, T. M. (1989). *The effect of rate of shear on the residual strength of soil*, PhD thesis, University of London, Imperial College of Science and Technology, UK.

Towhata, I., Kuntiwattanaku, P., Seko, I. and Ohishi, K. (1993). Volume change of clays induced by heating as observed in consolidation tests, *Soils and Foundations* **33**(4): 170–183.

Towhata, I., Kuntiwattanakul, P. and Kobayashi, H. (1993). A preliminary study on heating of clays to examine possible effects of temperature on soil-mechanical properties, *Soils and Foundations* **33**(4): 184–190.

Tsubakihara, Y. and Kishida, H. (1993). Frictional behaviour between normally consolidated clay and steel by two direct shear type apparatuses, *Soils and Foundations* **33**(2): 1–13.

Tsubakihara, Y., Kishida, H. and Nishiyama, T. (1993). Friction between cohesive soils and steel, *Soils and Foundations* **33**(2): 145–156.

Uesugi, M. and Kishida, H. (1986). Frictional resistance at yield between dry sand and mild steel, *Soils and foundations* **26**(4): 139–149.

Uesugi, M., Kishida, H. and Tsubakihara, Y. (1989). Friction between sand and steel under repeated loading, *Soils and foundations* **29**(3): 127–137.

Vucetic, M. and Dobry, R. (1988). Degradation of marine clays under cyclic loading, *Journal of Geotechnical Engineering* **114**(2): 133–149.

Vucetic, M. and Lacasse, S. (1984). Closure to specimen size effect in simple shear test by m. vucetic and s. lacasse (december, 1982), *Journal of Geotechnical Engineering* **110**(3): 447–453.

Wang, J.-h., Liu, Y.-f. and Xing, Y. (1998). Estimation of undrained bearing capacity for offshore soft foundations with cyclic load, *China Ocean Engineering* **12**(2): 213–222.

Wernick, E. (1978). Skin friction of cylindrical anchors in non-cohesive soils, *Symposium on Soil Reinforcing and Stabilising Techniques in Engineering Practice* **42**(42): 201219.

White, D. J. (2002). *An investigation into the behaviour of pressed-in piles*, PhD thesis, University of Cambridge, UK.

Wichtmann, T. (2005). *Explicit accumulation model for non-cohesive soils under cyclic loading*, PhD thesis, Inst. für Grundbau und Bodenmechanik Bochum University, Germany.

Wichtmann, T. (2016). *Soil behaviour under cyclic loading-experimental observations, constitutive description and applications*, Th. Triantafyllidis.

Wichtmann, T., Andersen, K., Sjursen, M. and Berre, T. (2013). Cyclic tests on high-quality undisturbed block samples of soft marine norwegian clay, *Canadian Geotechnical Journal* **50**(4): 400–412.

Wichtmann, T., Niemunis, A. and Triantafyllidis, T. (2005). Strain accumulation in sand due to cyclic loading: drained triaxial tests, *Soil Dynamics and Earthquake Engineering* **25**(12): 967–979.

Xiong, Y.-l., Liu, G.-b., Zheng, R.-y. and Bao, X.-h. (2018). Study on dynamic undrained mechanical behavior of saturated soft clay considering temperature effect, *Soil Dynamics and Earthquake Engineering* **115**: 673–684.

Yao, Y. and Zhou, A. (2013). Non-isothermal unified hardening model: a thermo-elasto-plastic model for clays, *Geotechnique* **63**(15): 1328.

Yasuhara, K., Yamanouchi, T. and Hiaro, K. (1982). Cyclic strength and deformation of normally consolidated clay, *Soils and Foundations* **22**(3): 77–91.

Yavari, N. (2014). *Aspects géotechniques des pieux de fondation énergétiques*, PhD thesis, Université Paris Est, France.

Yavari, N., Tang, A. M., Pereira, J.-M. and Hassen, G. (2016). Effect of temperature on the shear strength of soils and the soil–structure interface, *Canadian Geotechnical Journal* **53**(7): 1186–1194.

Yazdani, S., Helwany, S. and Olgun, G. (2019). Influence of temperature on soil–pile interface shear strength, *Geomechanics for Energy and the Environment* **18**: 69–78.

Yong, R., Taylor, L. and Warkentin, B. P. (1962). Swelling pressures of sodium montmorillonite at depressed temperatures, *Clays and Clay Minerals* **11**(1): 268–281.

Yoshimi, Y. and Kishida, T. (1981). A ring torsion apparatus for evaluating friction between soil and metal surfaces.

Zeghal, M. and Edil, T. B. (2002). Soil structure interaction analysis: modeling the interface, *Canadian Geotechnical Journal* **39**(3): 620–628.

Zhou, J. and Gong, X. (2001). Strain degradation of saturated clay under cyclic loading, *Canadian Geotechnical Journal* **38**(1): 208–212.

Chapter 6

Résumé étendu

6.1 Introduction générale

L'augmentation des émissions de gaz à effet de serre due à la consommation de combustibles fossiles est très préoccupante en raison de leurs impacts négatifs sur l'environnement. Plus de 80 % de la demande énergétique est fournie par les combustibles fossiles et, parmi les différents secteurs, les bâtiments consomment plus de 40 % de la consommation totale d'énergie. Ces dernières années, plusieurs accords et politiques environnementales ont été signés pour diminuer la dépendance aux combustibles fossiles, et augmenter la part des énergies renouvelables telles que l'énergie géothermique, éolienne ou solaire. Plusieurs techniques et technologies ont été développées pour en augmenter l'efficacité énergétique, et exploiter de nouveaux types d'énergies renouvelables. Parmi les différents types de technologies développées, l'énergie géothermique peu profonde a été au centre des attentions ces dernières années ce qui a permis l'émergence des géostructures énergétiques.

Les bâtiments représentent environ 40 % de la consommation mondiale d'énergie dans différents secteurs et jouent un rôle important dans les émissions de CO_2 (Nejat et al. 2015). Plus de 80 % de la consommation d'énergie des ménages est consacrée au chauffage des locaux et de l'eau. Il existe donc un énorme potentiel pour accroître la tendance vers les énergies renouvelables. La majeure partie de cette énorme demande (73 %) est fournie par les combustibles fossiles qui ont des impacts négatifs sur l'environnement. Ces dernières années, l'utilisation des énergies renouvelables, en raison de leur caractère propre, de leur rapport coût-bénéfice et de leur respect de l'environnement, a été au centre des attentions. L'énorme potentiel des sources renouvelables peut compenser une partie de la demande énergétique de différents secteurs, y compris celui des bâtiments. Parmi les différents types d'énergie renouvelable, ces dernières années, l'énergie géothermique peu profonde a été utilisée en raison de sa simplicité d'utilisation, de son fonctionnement rentable et de sa ca-

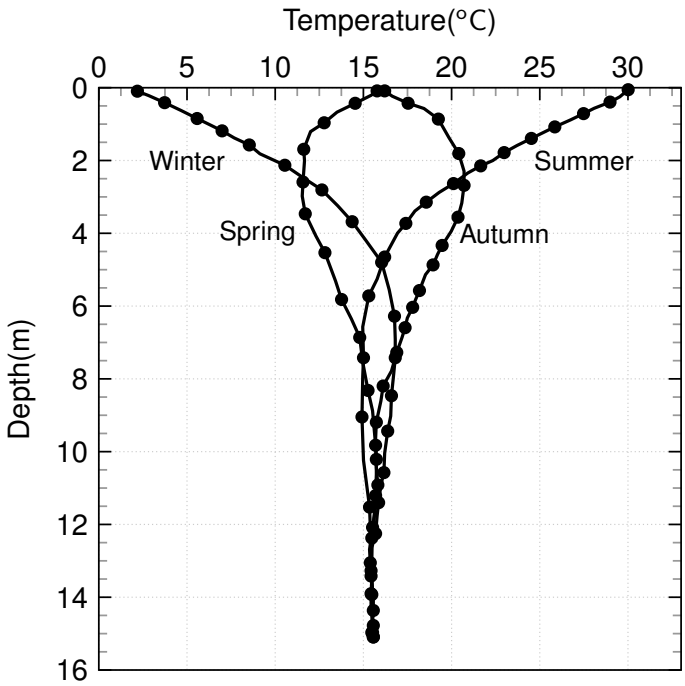

Figure 6.1: Température du sol jusqu'à 15 m de profondeur pendant quatre saisons.

pacité à couvrir une partie des besoins humains (chauffage, électricité, etc.). La désintégration radioactive des matériaux au cœur de la terre peut être à l'origine de l'énergie géothermique. En raison des progrès technologiques, l'exploitation des sources renouvelables est confrontée à de nouvelles avancées et à de nouveaux défis. Parmi ces technologies, l'émergence de la géostructure énergétique a ouvert une nouvelle voie pour exploiter l'énergie géothermique peu profonde. Ces structures exploitent la chaleur du sol en utilisant des tubes échangeurs de chaleur encastrés dans leur cage d'armature. Le faible coût d'exploitation et l'efficacité des structures thermo-actives sont les raisons de l'augmentation des demandes envers ces structures. L'expérience a montré que ces systèmes de chauffage/refroidissement géothermiques à partir de fondations énergétiques et d'autres structures thermo-actives du sol peuvent permettre d'économiser jusqu'à deux tiers des coûts de chauffage conventionnel (Brandl 2006).

La température constante du sol à une profondeur de 10-15 m peut être considérée comme un moyen d'exploiter et d'injecter la chaleur quotidiennement et de façon saisonnière (Brandl 2006) (Fig. 6.1). La chaleur exploitée en hiver est utilisée pour le chauffage et inversement, en été, la chaleur supplémentaire peut être injectée dans le sol à des fins de refroidissement (Fig. 6.2).

Dans les géostructures en contact avec le sol, comme les pieux, les parois moulées, les tunnels et les dalles, avant la phase de bétonnage, des tubes en polyéthylène sont fixés à la cage darmature. Après le bétonnage, et le début de la mise en service de la géostructure, un fluide caloporteur est mis en circulation dans les tubes, ce qui rend

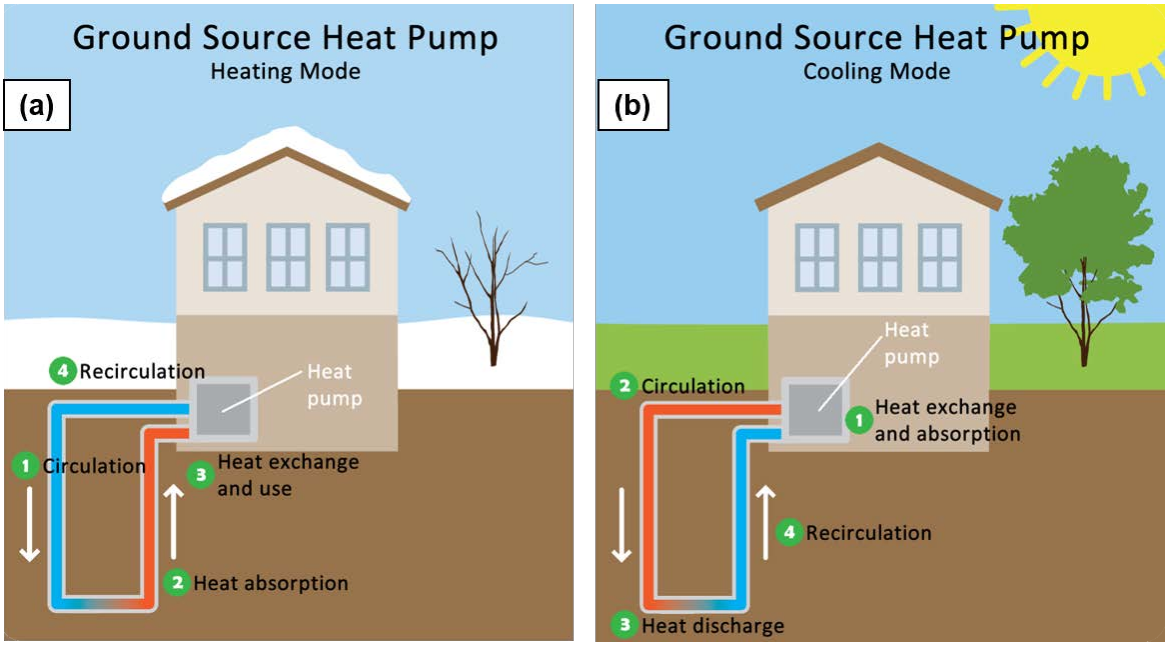

Figure 6.2: Exploitation thermique à l'aide de géostructures énergétiques. (a) Mode chauffage en hiver ; (b) Mode refroidissement en été (www.geoenergymarketing.com).

ainsi possible l'échange de chaleur avec le sol environnant. Les fluctuations quotidiennes et saisonnières du flux de chaleur, entre les tubes de l'échangeur de chaleur et le sol adjacent, peuvent affecter le comportement mécanique du béton, de l'interface sol-structure et du sol environnant. L'interface sol / structure joue un rôle particulièrement important. L'interface sol-structure consiste en une fine couche de sol adjacente à l'élément structurel qui agit comme une zone de transmission pour transférer les charges de la structure vers le sol environnant. L'effet des sollicitations thermo-mécaniques sur l'interface est une question cruciale pour la stabilité de la structure, et cest cet aspect qui est principalement abordé dans cette étude.

Plusieurs aspects thermo-mécaniques de l'interface sol-structure restent sans réponse jusqu'à présent, tels que les effets thermiques sur la réponse monotone de l'interface sol-structure dans des conditions de rigidité normale constante (CNS), le comportement mécanique cyclique de l'argile et de l'interface argile-structure dans des conditions non isothermes et, pour les approches de conception, l'absence de modèle constitutif non isotherme de l'interface sol-structure. Pour résoudre ces problèmes, un dispositif de cisaillement direct à température contrôlée a été développé pour effectuer des essais de cisaillement monotone et cyclique de l'interface sur des interfaces sableuses et argileuses. Plusieurs protocoles expérimentaux ont été mis au point pour réaliser des essais à charge normale constante et à rigidité normale constante. Le plan de la thèse est décrit en détail dans les paragraphes suivants.

Chapitre I : Ce chapitre décrit la définition de la géostructure énergétique, sa

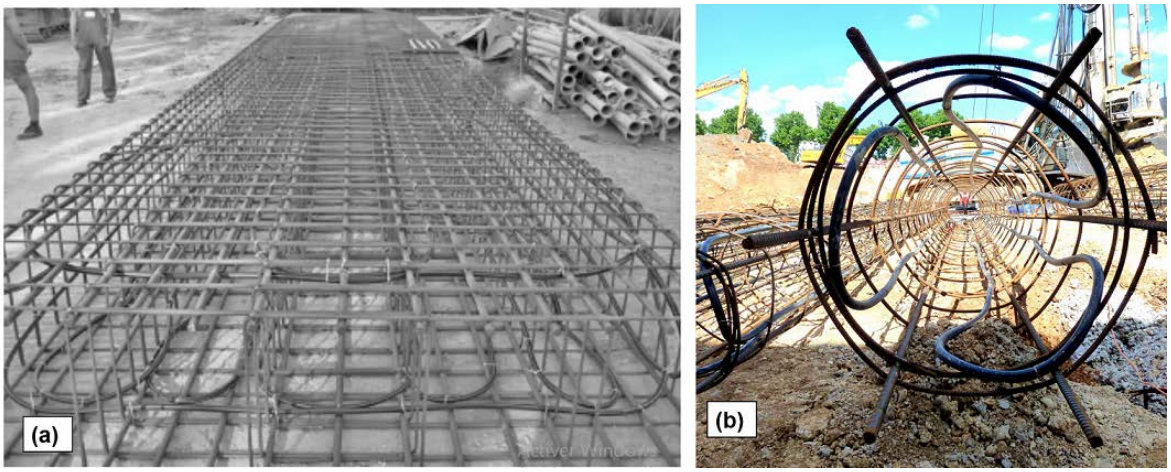

Figure 6.3: Tubes d'échangeur de chaleur fixés à la cage de renforcement de (a) une paroi de membrane (Brandl 2006) ; (b) une pile (Cfms 2017).

construction et les détails de son fonctionnement. Ensuite, le comportement thermo-mécanique des sols, qui est orienté vers les effets thermiques sur les caractéristiques volumétriques, de cisaillement, microscopiques et hydrauliques du sol, est présenté. Ensuite, la définition de l'interface sol-structure, les dispositifs de cisaillement de l'interface, les conditions aux limites et les paramètres importants sont discutés. Ensuite, le comportement cyclique des sols et les interfaces sol-structure sont discutés en détail. Enfin, les remarques finales concernant les points importants qui ont été mentionnés dans la littérature et les aspects manquants de celle-ci sont présentées.

Chapitre II : Une description détaillée du matériel utilisé dans cette étude est présentée. La préparation des échantillons et le programme expérimental sont abordés dans ce chapitre. Les essais de consolidation sur le kaolin pour déterminer le taux de cisaillement ainsi que les développements du protocole expérimental du dispositif sont présentés. La campagne expérimentale pour l'interface sable/argile-structure est ensuite abordée. Les détails du programme cyclique et les méthodes d'exécution sont développées, et enfin les tests de répétabilité sont présentés.

Chapitre III : Dans ce chapitre, les effets thermiques sur le comportement mécanique de l'interface sol-structure sont discutés. Une campagne expérimentale est proposée pour étudier les caractéristiques de cisaillement monotone de l'interface sable/argile-structure dans des conditions non isothermes sous une charge normale constante et des conditions de rigidité normales constantes. Les caractéristiques de cisaillement de l'interface sol-sol et sol-structure à différentes températures ont été étudiées et discutées (22-60 ^{o}C). Les différences de cisaillement à l'interface sol-sol et sol-structure ont également été mises en évidence. Enfin, l'effet de la température sur le déplacement des contraintes de cisaillement et le comportement volumétrique est examiné et des

conclusions sont fournies.

Chapitre IV : ce chapitre est consacré au comportement cyclique unidirectionnel de l'interface argilo-structurelle du kaolin dans des conditions non isothermes. L'objectif de ce chapitre est de comprendre le comportement cyclique de l'interface argile-structure à différentes températures. Le concept de volume constant équivalent non drainé (CVEU) est utilisé pour analyser les essais de cisaillement d'interface. Les essais de cisaillement monotones CVEU sur l'interface argile-argile et argile-structure sont comparés. Ensuite, des essais cycliques à différentes températures sont présentés. L'effet de la température sur l'accumulation de contraintes, la pression d'eau interstitielle équivalente et la dégradation de l'interface est discuté. Enfin, les conclusions de ce chapitre sont présentées.

Chapitre V : Dans ce chapitre, un modèle constitutif pour prendre en compte l'effet de la température sur le comportement mécanique de l'interface sable/argile-structure est développé. Sur la base des observations expérimentales du chapitre III et des études bibliographiques, certains aspects fondamentaux du comportement de l'interface sol-structure dans des conditions de charge normale constante et de rigidité normale constante dans des conditions non isothermes sont identifiés. Ensuite, en utilisant le concept d'état critique pour les modèles constitutifs de l'interface sol-structure, ces caractéristiques sont implémentées dans un modèle étendu pour prendre en compte l'effet de la température sur le comportement mécanique de l'interface sable/argile-structure.

6.2 Matériels et méthodes

La Fig. 6.4 montre le dispositif de cisaillement direct à température contrôlée, la boîte de cisaillement et la plaque d'acier pour modéliser l'interface utilisée dans cette étude. Le dispositif de cisaillement était constitué d'un bâti de chargement qui appliquait la contrainte normale, d'un système pour appliquer la contrainte de cisaillement (en mode de déformation ou de contrainte contrôlée), de capteurs de déplacement vertical et horizontal (Fig. 6.4(a)). Le bâti de charge était capable d'appliquer des forces normales jusqu'à 20 kN. La plage de déplacement en cisaillement était de 0-25 mm. Le dispositif était capable d'appliquer un taux de cisaillement compris entre 0,000001 et 30 mm/min.

Cet assemblage était relié à un système de chauffage/refroidissement qui contrôlait la température d'un fluide. Ce fluide circulait dans la partie inférieure du conteneur de la boîte de cisaillement (Fig. 6.4(b) et (c), partie circulation du fluide). Plusieurs capteurs thermiques ont été placés dans différentes parties du dispositif pour mesurer les températures imposées et obtenues. La boîte de cisaillement était en acier inoxydable (60 x 60 x 35 mm) et se composait des moitiés supérieure et inférieure de la boîte de cisaillement (Fig. 6.4(d)). Une pierre poreuse était placée dans le fond de la moitié inférieure de la boîte de cisaillement. La pierre poreuse supérieure placée à l'intérieur du panneau de chargement directement, en contact direct avec l'échantillon lorsque la contrainte normale est appliquée. Après la préparation de l'échantillon dans la boîte de cisaillement, elle a été placée à l'intérieur du conteneur rempli d'eau (Fig. 6.4(b)). La température de l'eau dans le conteneur a atteint la même température que celle imposée au fluide en circulation. Trois capteurs thermiques, un dans la moitié inférieure, un autre sur la moitié supérieure de la boîte de cisaillement, et le dernier dans le conteneur, contrôlaient la température appliquée.

Dans ce dispositif de cisaillement direct, la contrainte normale σ_n (kPa), le déplacement de cisaillement W (mm), la température du fluide en circulation T (^oC) et la valeur de rigidité K (kPa/mm) ont été appliqués, et le déplacement normal U (mm), la contrainte de cisaillement τ (kPa) et la température de l'échantillon T (^oC) ont été mesurés. Le système était commandé par le logiciel de commande de la boîte de cisaillement qui était capable de sauvegarder la totalité des données générées par le dispositif. Pour réaliser l'interface sol-structure, le sol dans la moitié supérieure de la boîte de cisaillement doit être cisaillé contre une surface structurelle qui est placée dans la moitié inférieure de la boîte de cisaillement. Pour ce faire, un moule d'interface a été conçu, dans lequel une surface structurelle d'une longueur de 80 mm peut être placée (Fig. 6.4(e)). Les échantillons de sol ont été préparés directement dans la moitié supérieure de la boîte de cisaillement.

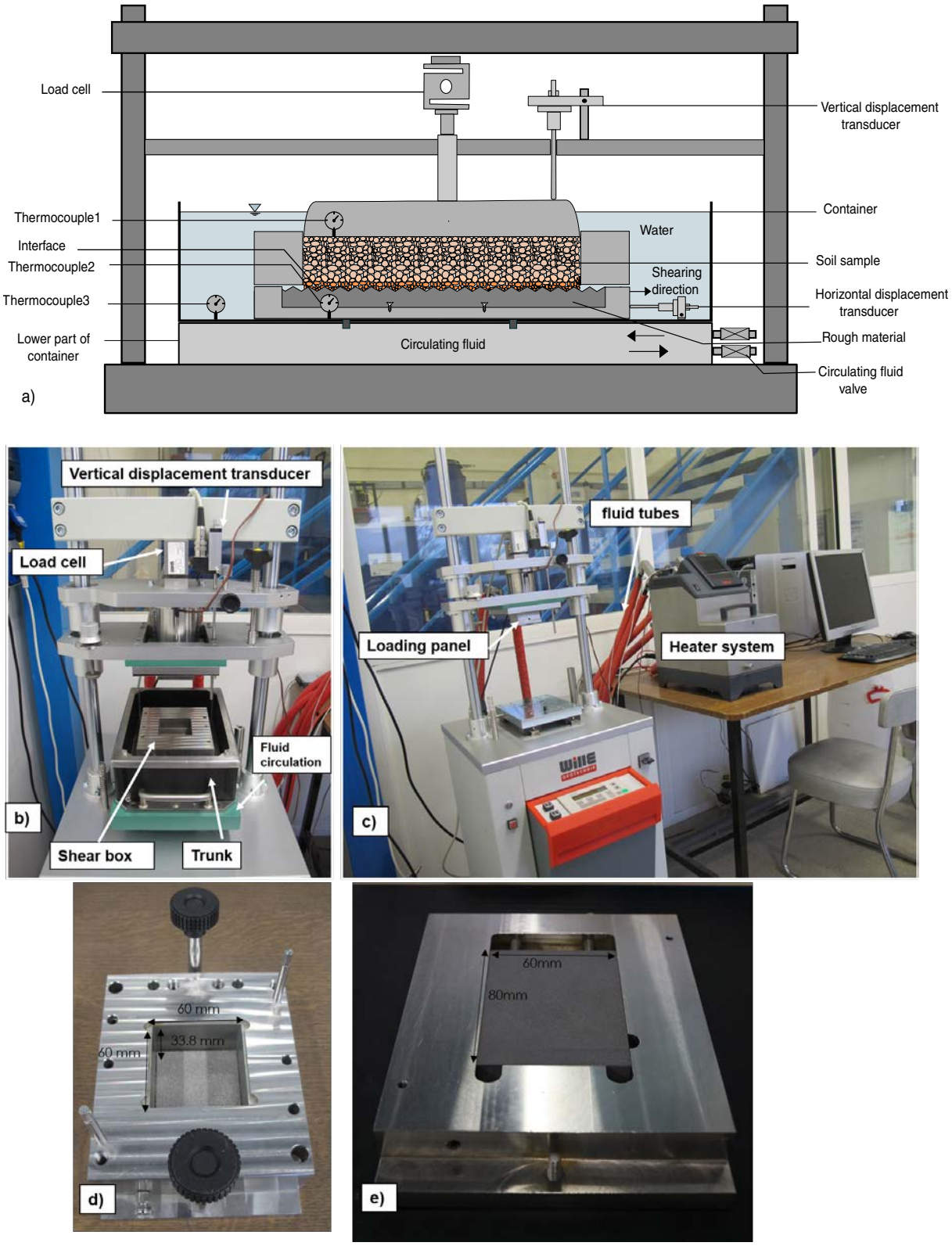

Figure 6.4: Installation expérimentale du dispositif de cisaillement direct à température contrôlée. (a) Vue schématique du dispositif ; (b) différentes parties du dispositif ; (c) système de chauffage et d'enregistrement ; (d) boîte de cisaillement ; (e) surface structurelle placée dans la demi-boîte de cisaillement inférieure conçue.

6.3 L'effet de la température sur le comportement mécanique de l'interface sol-structure

Le comportement mécanique de l'interface sol-structure est d'une grande importance en raison du rôle de l'interface dans la résistance due au frottement et la capacité portante des structures. Dans les structures thermo-actives du fait de la variation de la température, le comportement de l'interface devient plus complexe. L'objectif de ce travail est d'étudier l'effet des variations de température sur le comportement mécanique de l'interface sol-structure. Des essais avec des conditions de charge normale constante (CNL) et de rigidité normale constante (CNS) ont été réalisées dans une boîte de cisaillement direct à différentes températures, 5, 22 et 60 ^{o}C sur des éprouvettes sol-sol et sol-structure. Le sable de Fontainebleau et le kaolin ont été utilisés comme materiaux de référence pour les sols sableux et argileux. Les résultats ont montré que les variations thermiques appliquées ont un effet négligeable sur la résistance au cisaillement des interfaces sable-sable et sable-structure dans les conditions charge normale constante (CNL) et de rigidité normale constante (CNS) et que le comportement du sable peut être considéré comme étant indépendent de la température. Pour étudier l'effet de la rigidité normale sur le comportement mécanique de l'interface sable-structure à 22 C, plusieurs tests expérimentaux ont été réalisés. Les résultats ont montré qu'en augmentant la rigidité, la contrainte normale augmente et, par conséquent, la contrainte de cisaillement augmente aussi. Mais l'angle de frottement de l'interface s'est avéré identique dans les deux conditions charge normale constante (CNL) et de rigidité normale constante (CNS). Dans l'argile étudiée, l'augmentation de la température augmente la résistance au cisaillement en raison de la contraction thermique pendant le chauffage, ce qui augmente la cohésion du sol. Pour les essais argile-argile, l'augmentation de la température de 22 à 60 ^{o}C a fait passer la cohésion du sol de 17 à 23 kPa. L'augmentation de température a eu moins d'impact sur la résistance au cisaillement dans le cas de l'interface argile-structure que dans les échantillons argile. Le principal effet de la température sur l'interface argile-structure était sur la contrainte de cisaillement maximale et la contrainte de cisaillement résiduelle était indépendante de la température. L'augmentation de la température de 22 à 60 ^{o}C a fait passer l'adhérence de l'interface de 12 à 18 kPa. L'adhésion de l'interface argile-structure est inférieure à la cohésion des échantillons d'argile. La Fig. 6.6 montre l'effet de la température sur la cohésion, l'adhérence et l'angle de frottement de différents sols qui ont été étudiés pour des tests de cisaillement direct d'interface à différentes variations de température dans la littérature, ce qui est comparé aux résultats obtenus dans cette étude.

La contrainte de cisaillement en fonction du déplacement en cisaillement pour deux

contraintes normales initiales ($\sigma_{n0}^{'}$=100 et 300 kPa) à 22 et 60 ^{o}C sont présentées dans la figure 6.5(a). à $\sigma_{n0}^{'}$=100 kPa, la contrainte de cisaillement a augmenté avec le déplacement du cisaillement jusqu'à atteindre une valeur de 1 mm (τ = 33 kPa) puis, avec une légère diminution, la contrainte de cisaillement a continué vers l'état critique (τ = 28 kPa). Les courbes pour 22 et 60 ^{o}C ont suivi la même tendance. Les tests à $\sigma_{n0}^{'}$=300 kPa ont montré un pic très net puis ont diminué vers une valeur constante. Comme mentionné pour 100 kPa, sous $\sigma_{n0}^{'}$=300 kPa, les contraintes de cisaillement à 22 et 60 ^{o}C sont similaires. Pour les deux contraintes normales initiales, le kaolin s'est contracté jusqu'à la fin du cisaillement (Fig. 6.5(b)). Pour $\sigma_{n0}^{'}$=100 kPa à 22 ^{o}C, la quantité de déplacement normal à l'état critique était d'environ 0,035 mm. Cette valeur était d'environ 0,02 mm pour des essais à 60 ^{o}C, et les échantillons chauffés présentaient une contraction moindre. Pour $\sigma_{n0}^{'}$=300 kPa à 22 et 60 ^{o}C, la valeur du déplacement normal à l'état critique était de 0,9 et 0,6 mm, respectivement. La figure 6.5(c) présente la variation de la contrainte normale pendant les essais de SNC de l'interface argile-structure. Pour les deux $\sigma_{n0}^{'}$=100 et 300 kPa, les contraintes normales ont diminué pendant le processus de cisaillement. Pour les échantillons exposés à des températures plus élevées, la réduction a été inférieure à celle des échantillons à 22 ^{o}C. Pour les essais à $\sigma_{n0}^{'}$=100 kPa à 22 et 60 ^{o}C, la diminution de contraintes normale était d'environ 42 et 30 kPa respectivement.

La figure 6.5(d) présente les plans de contrainte normale par rapport à la contrainte de cisaillement pour les essais à l'interface argile-structure CNS et CNL. Pour $\sigma_{n0}^{'}$=100 et 300 kPa dans les essais CNS, la contrainte de cisaillement a augmenté avec la diminution de la contrainte normale, et le cisaillement a atteint une valeur maximale puis a diminué. Les échantillons chauffés ont montré une diminution moindre de la contrainte normale. Par exemple, pour $\sigma_{n0}^{'}$=300 kPa, la valeur de cisaillement maximale pour les échantillons chauffés était légèrement supérieure à 22 ^{o}C, et la diminution de la contrainte normale dans l'échantillon chauffé était également inférieure à celle de 22 ^{o}C. L'angle de frottement et l'adhérence de pointe des essais CNS étaient respectivement de 14 ^{o} et 13 kPa.

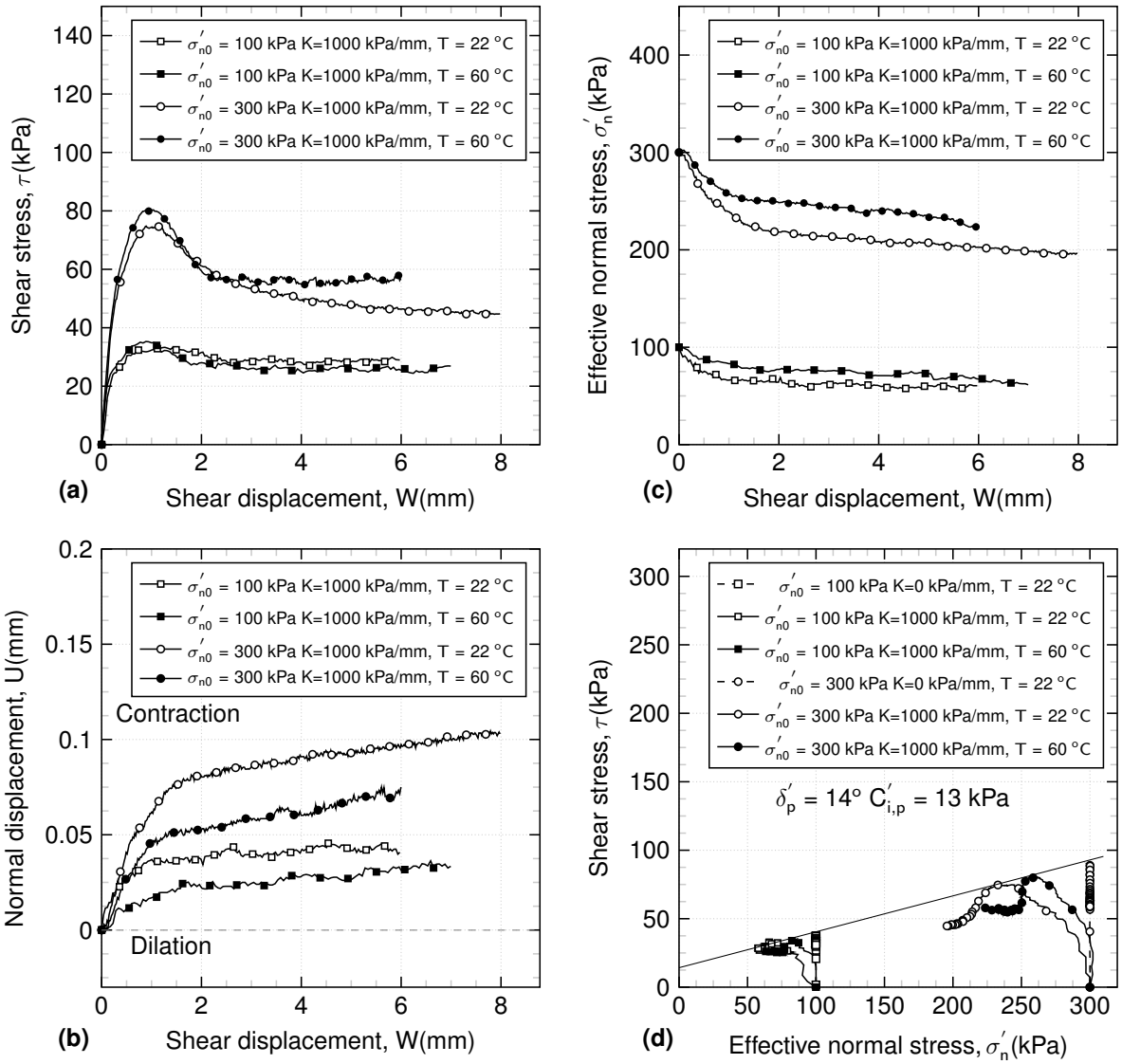

Figure 6.5: Résultats CNS pour l'interface argile-structure à $T = 22\ ^oC$, $T = 60\ ^oC$. (a) contrainte de cisaillement vs. déplacement en cisaillement ; (b) déplacement normal vs. déplacement en cisaillement ; (c) contrainte normale vs. déplacement en cisaillement ; (d) contrainte de cisaillement vs. contrainte normale effective

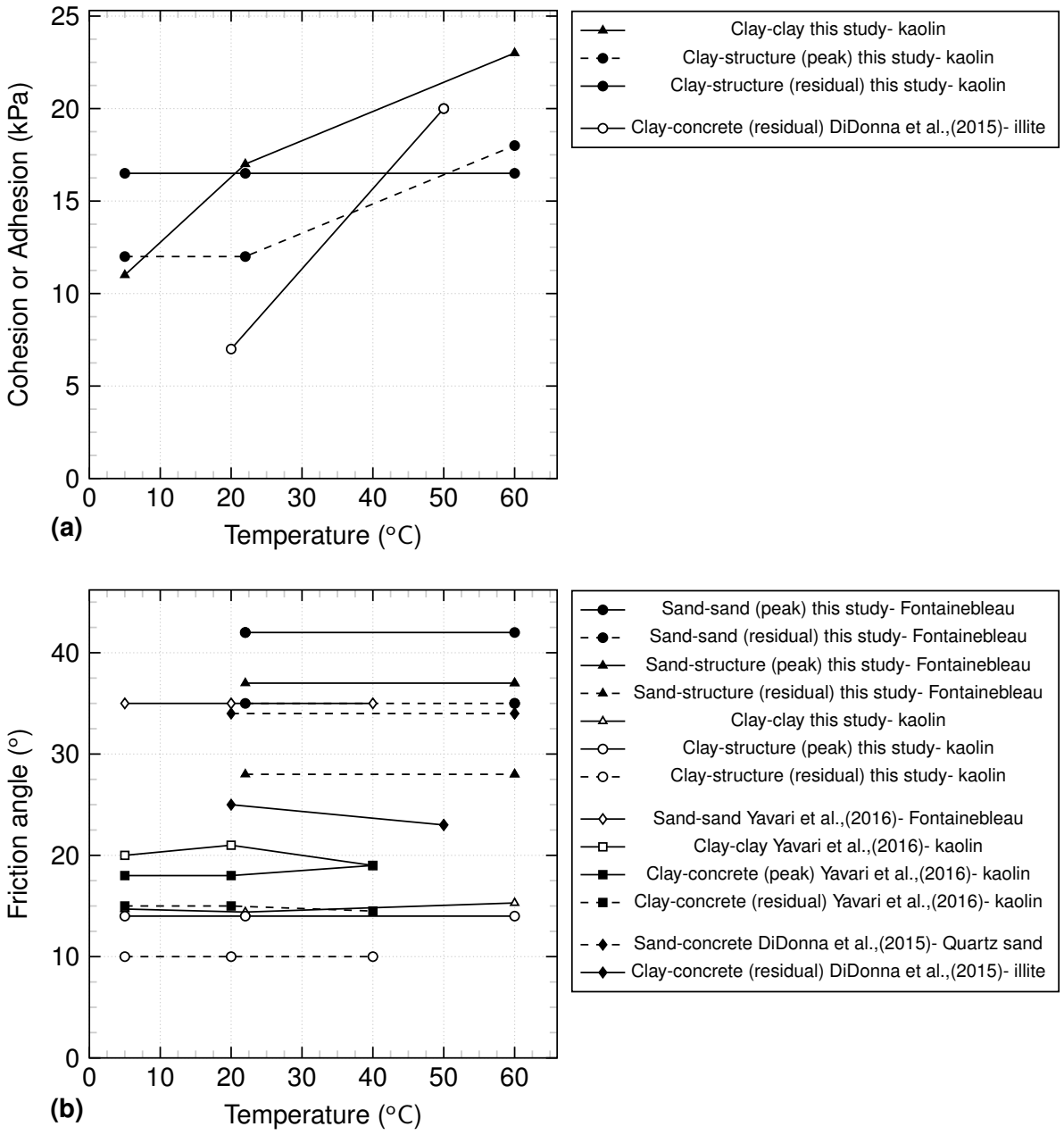

Figure 6.6: Effet de la température sur (a) la cohésion et (b) l'angle de frottement.

6.4 Effet de la température sur le comportement cyclique de l'interface argile-structure

La capacité portante des fondations dépend fortement des charges monotones et cycliques appliquées à l'interface sol-structure. Dans les géostructures énergétiques qui exploitent la chaleur du sol, l'interface est soumise à des charges thermomécaniques cycliques. Des essais de cisaillement direct monotones et cycliques à volume-constant équivalent-nondrainé (CVEU) ont été réalisés sur l'argile et l'interface argile-structure à différentes températures (22 et 60 ^{o}C). Une contrainte verticale effective de 300 kPa a été appliquée aux échantillons et les rapports des contraintes de cisaillement cycliques et moyennes (respectivement τ_{cy}/S_u^{Ds} et τ_a/S_u^{Ds}) ont varié entre 0,35 et 0,57. Le sol testé était un kaolin (PI=24) préparé dans un état normalement consolidé. Les résultats ont montré que le nombre de cycles jusqu'à la rupture pour l'essai d'interface argile-structure était inférieur à l'argile dans la même gamme de contraintes cycliques. Dans les essais cycliques sur l'interface argile-structur, la diminution du rapport de contrainte cyclique (CSR) a augmenté le nombre de cycles jusqu'à la rupture; cependant, la diminution du rapport moyen de contrainte de cisaillement (ASR) a diminué le nombre de cycles jusqu'à la rupture. L'augmentation de la température a diminué le taux d'accumulation de la déformaiton et le nombre de cycles jusqu'à la rupture ont augmenté de 2 à 3 fois.

Les valeurs du paramètre de dégradation t dans la Fig. 6.7 sont le rapport entre le logarithme du nombre de cycles et logarithme de l'indice de dégradation pour les essais cycliques. À 22 ^{o}C avec un CSR croissant de 0,35 à 0,57, le paramètre de dégradation passe de 0,064 à 0,115 mais pour les essais à 60 ^{o}C, le paramètre de dégradation passe de 0,049 à 0,097. Les paramètres de dégradation pour les échantillons chauffés sont inférieurs à ceux des tests à 22^{o}C, ce qui peut être dû à l'état plus dense des échantillons qui réduit le taux de dégradation. Le taux de dégradation pour la gamme de CSR entre 0,35 et 0,57 diminue d'environ 16% pour une augmentation de température de 20 à 60^{o}C. Sur la base d'essais de cisaillement simple de la CVEU sur la kaolinite (type argile-argile), les chercheurs ont rapporté que, dans la plage de déformation cyclique de 0,1-0,5% , avec une augmentation de la contrainte verticale de 220 à 680 kPa, le paramètre de dégradation diminue de 20-38%, ce qui peut être comparable à la diminution obtenue par chauffage dans cette étude. Les phénomènes de surconsolidation thermique jouent le même rôle que la charge mécanique. Le taux de dégradation (paramètre de dégradation, t) a diminué de 16% avec un chauffage de 22 à 60 ^{o}C pour les différents rapports de contrainte cyclique testés.

La figure 6.8(a) montre la variation du nombre de cycles pour atteindre différentes

valeurs de déplacements latéraux relatifs (P_d= 0,5, 0,7, 1, 10%) avec des variations de CSR (τ_{cy}/S_u^{Ds}) à 22 et 60 ^{o}C. En diminuant l'indice CSR de 0,57 à 0,35, le nombre de cycles pour atteindre 0,5 % du déplacement latéral relatif passe de 3 à 125 cycles à 22 ^{o}C. Cependant, pour que les échantillons chauffés atteignent le même P_d, avec la même réduction du CSR, le nombre de cycles passe de 35 à 452. Lorsque les valeurs du CSR diminuent, l'effet de la température devient moins perceptible. Pour que le CSR de 0,57 à 60^o atteigne 0,5% de P_d, le nombre de cycles est multiplié par 4 à 7 par rapport à celui de 22^o, tandis qu'en diminuant le CSR à 0,35, ce rapport devient 2 à 4 fois plus élevé. La figure 6.8(b) montre la variation du nombre de cycles pour atteindre différentes valeurs de pression d'eau interstitielle normalisée ($u^*/\sigma'_{n,i}$ =0,5, 0,6) avec les variations du CSR. Le nombre de cycles pour atteindre $u^*/\sigma'_{n,i}$ =0,5 augmente de 5 à 1500 cycles avec une diminution du CSR de 0,57 à 0,35 à 22 ^{o}C. Pour atteindre la même pression d'eau interstitielle normalisée (0,5) pour les échantillons chauffés, le nombre de cycles augmente de 4 à 6 fois.

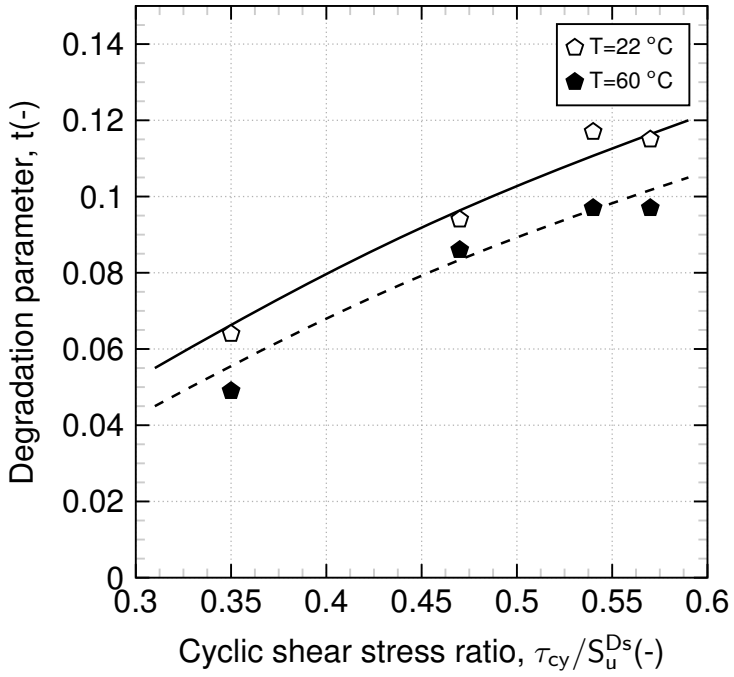

Figure 6.7: Évolution du paramètre de dégradation (t), avec variation cyclique du rapport de contrainte à différentes températures (22 et 60 ^{o}C).

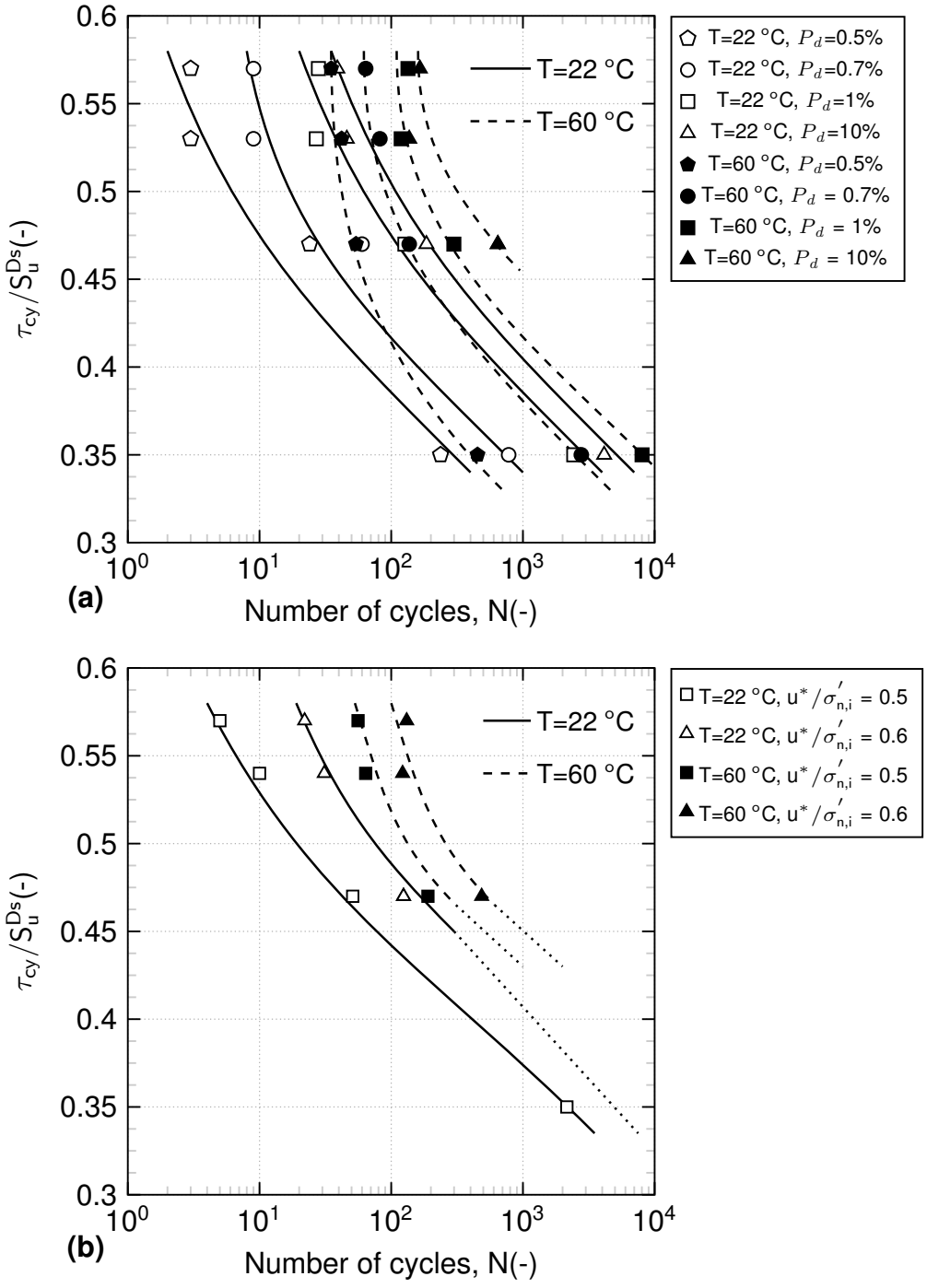

Figure 6.8: (a) τ_{cy}/S_u^{Ds} en fonction de la courbe du nombre de cycles pour différents déplacements latéraux relatifs ; (b) $u^*/\sigma'_{n,i}$ en fonction de la courbe du nombre de cycles pour certaines valeurs de pression d'eau interstitielle équivalente normalisée.

6.5 Modèle d'interface sol-structure non isotherme basé sur la théorie de l'état critique

Dans les géostructures énergétiques, l'interface sol-structure est soumise à des charges mécaniques et à des variations thermiques. Dans cette étude, un modèle d'interface sol-structure non isotherme basé sur la théorie de l'état critique est développé à partir d'un modèle constitutif d'interface sol-structure granulaire dans des conditions isothermes. Le modèle non isotherme prend en compte l'effet de la température sur l'indice des vides de l'interface avant le cisaillement. Le modèle est capable de capturer l'effet de la température sur l'interface sol-structure dans des conditions de charge normale constante et de rigidité normale constante pour les interfaces sableuses et argileuses. Les paramètres supplémentaires ont des significations physiques et peuvent être déterminés à partir d'essais classiques en laboratoire. La formulation est en bon accord avec les résultats expérimentaux et les principales tendances sont correctement reproduites.
Certaines études expérimentales ont été réalisées sur l'effet de la température sur le comportement mécanique de l'interface sol-structure dans des essais de cisaillement direct (Di Donna et al. 2015 ; Yavari et al. 2016 ; Li et al. 2018 ; Maghsoodi et al. 2019a ; Maghsoodi et al. 2019b ; Maghsoodi et al. 2020 ; Yazdani et al. 2019) et des modèles de centrifugeuses (McCartney and Rosenberg 2011). Parmi ces études, les résultats expérimentaux de Maghsoodi et al. 2020 sont présentés ci-après. La figure 5.1 montre les résultats des essais de charge normale constante (CNL) et de rigidité normale constante (CNS) d'une interface kaolin-argile-structure normalement consolidée pour deux contraintes normales différentes, 100 et 300 kPa, à 22 et 60 ^{o}C.

Le concept d'état critique est basé sur la théorie selon laquelle, dans les grandes déformations de cisaillement, le sol continue à se cisailler sans aucune modification des conditions volumétriques et de contrainte. L'indice des vide à ces grandes déformations de cisaillement est le taux de vide à l'état critique. Le rapport de vide critique, e_{cs}, est affecté par la pression de confinement de telle sorte qu'il diminue avec l'augmentation de la contrainte de confinement. Le comportement du sol à n'importe quel état dépend donc de la distance entre l'état actuel et l'état critique, qui peut être défini par un paramètre d'état pour les sols sableux (Liu et al. 2006).

Table 6.1: Paramètres du modèle de cette étude.

Interface type	Reference	kt $\frac{kPa}{mm}$	δ (^{o})	Γ (-)	λ (-)	ξ^* (-)	N (-)	K $\frac{kPa}{mm}$	k_1 (-)	k_2 $\frac{kPa}{mm}$	t (mm)	T (^oC)	C (kPa)	β (-)
Fontainebleau sand-structure	Maghsoodi et al. 2020 (CNL)	208	40	0.835	0.040	1.58	2.2	0	0.6	0.11	1.15	22	0	0.900
Fontainebleau sand-structure	Maghsoodi et al. 2020 (CNS)	208	40	0.695	0.040	1.58	2.2	5000	5800	0.22	1.15	22	0	0.935
Fontainebleau sand-steel	De Gennaro and Frank 2002 (CNL)	208	40	0.815	0.040	1.58	1.7	0	0.21	0.11	5.9	22	0	0.910
Silica sand-steel	Fakharian and Evgin 2000 (CNL)	280	40	0.985	0.140	1.58	1	0	0.51	0.51	3	22	0	0.900
Silica sand-steel	Fakharian and Evgin 2000 (CNS)	280	40	0.955	0.140	1.58	1	400	300	0.51	3	22	0	0.940
kaolin clay-structure	Maghsoodi et al. 2020 (CNL)	170	14	0.967	0.131	0.5	1.85	0	0.003	2.9	11	22	12	0.975
kaolin clay-structure	Maghsoodi et al. 2020 (CNS)	170	14	0.990	0.142	0.7	1.85	1000	0.003	2	11	22	12	0.965
illite clay-concrete	Di Donna et al. 2015 (CNL)	300	25	0.870	0.140	0.8	1.85	0	0.003	0.7	10	22	7	0.980
illite clay-concrete	Di Donna et al. 2015 (CNL)	300	25	0.870	0.140	0.83	10.85	0	0.003	0.7	10	60	7	0.980
kaolin clay-concrete	Yazdani et al. 2019 (CNL)	110	11	0.927	0.131	0.42	7.85	0	0.003	4	9.5	24	23	0.952
kaolin clay-concrete	Yazdani et al. 2019 (CNL)	110	11	0.927	0.131	0.45	7.85	0	0.003	4	9.5	34	23	0.952

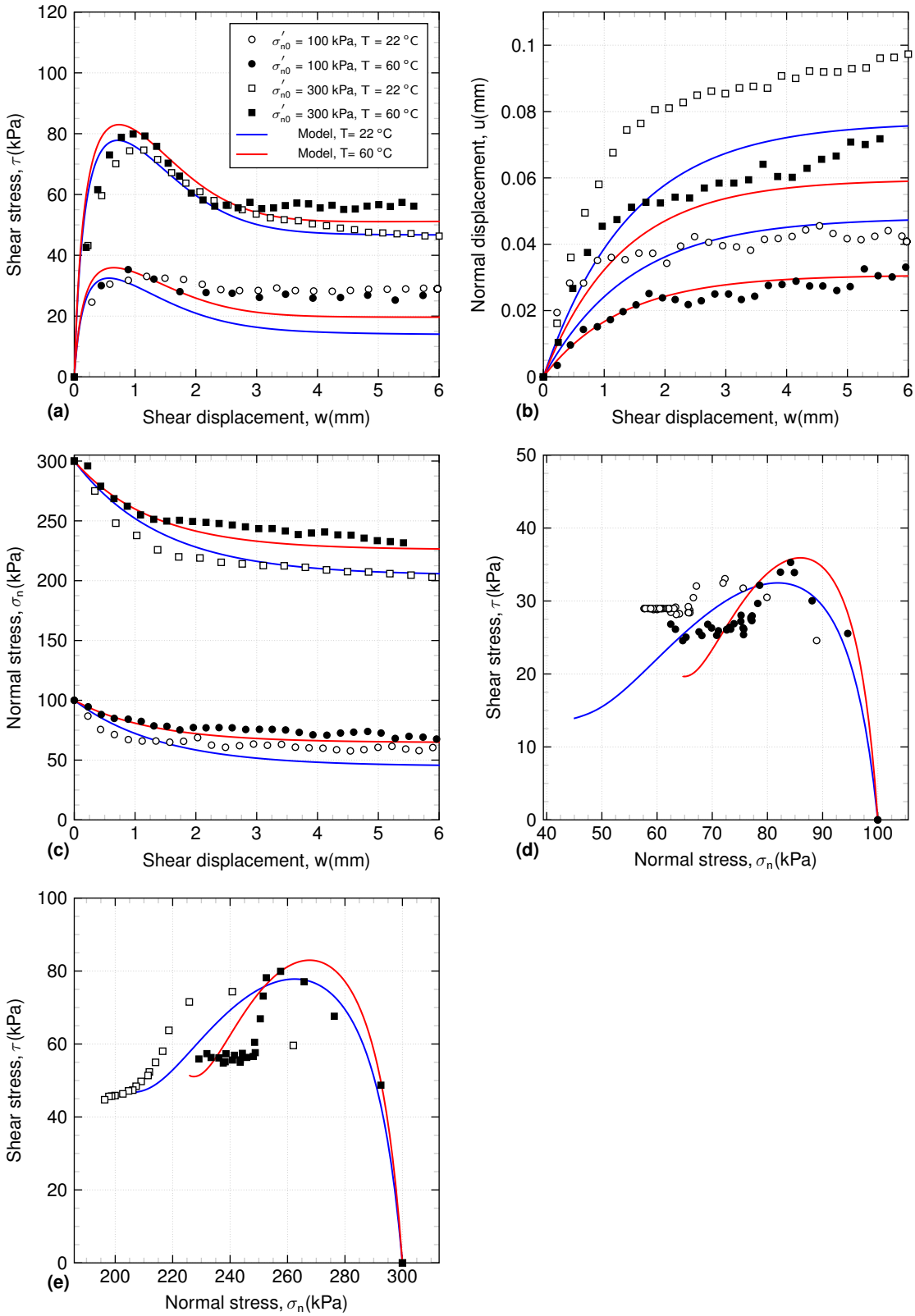

Figure 6.9: Le modèle d'interface prévoit, par rapport aux données expérimentales, quatre essais de rigidité normale constante (K = 1000 kPa/mm) sur les interfaces entre le kaolin argileux et l'acier : (a) contrainte de cisaillement vs. déplacement en cisaillement ; et (b) déplacement normal vs. déplacement en cisaillement (données expérimentales par Maghsoodi et al. 2020)

6.6 Conclusion générale

Les géostructures conventionnelles comme les pieux et les parois moulées peuvent être converties en géostructures énergétiques en fixant des tubes échangeurs de chaleur à leur cage darmature. Ces dernières années, plusieurs études ont été menées sur le comportement thermo-mécanique de ces géostructures thermo-actives en grandeur réelle, à petite échelle ou en laboratoire. En effet, en plus d'être soumis à des charges mécaniques, les fluctuations quotidiennes et saisonnières de température induisent des charges thermiques qui rendent le comportement de ces géostructures énergétiques plus complexe à appréhender. L'objectif de cette étude était d'approfondir la compréhension du comportement du contact sable/argile-structure sous des charges thermo-mécaniques. Un dispositif de cisaillement direct à température contrôlée permettant d'effectuer des essais de charge normale constante monotone et cyclique ou de rigidité normale constante a été mis au point.

En ce qui concerne la partie monotone de l'étude, des essais de charge normale constante (CNL) et de rigidité normale constante (CNS) ont été réalisés sur l'interface sable/argile-kaolin-acier de Fontainebleau à différentes températures (5, 22 et 60 ^{o}C) pour étudier les effets thermiques sur l'angle de frottement et l'adhérence de l'interface. Les résultats ont montré que les propriétés mécaniques du sable étaient indépendantes de la température (22 et 60 ^{o}C) pour les essais sur le sable et la structure du sable. Différentes valeurs de rigidité ont été appliquées dans des conditions de rigidité normale constante (CNS) à différentes températures, et il a été observé que, comme pour les essais CNL, la température ne modifie pas le comportement de l'interface dans des conditions CNS. En outre, le même angle de frottement d'interface a été obtenu dans les essais CNL et CNS pour les essais d'interface sable-structure. Dans la kaolinite, la température n'affecte pas l'angle de frottement. Leffet principal de la température a été l'augmentation de la cohésion, ou de l'adhérence. Pour les essais sur l'argile, en raison de la contraction thermique du kaolin pendant le chauffage, le sol devient plus dense et présente une plus grande résistance au cisaillement., ce qui se traduit par une augmentation de la cohésion des échantillons d'argile. Dans le cas du contact entre l'argile et la structure, en raison de la différence de nature des matériaux (argile vs. métal), l'adhérence n'était pas aussi importante que dans le cas de l'argile, donc l'augmentation de la résistance au cisaillement avec l'augmentation de la température, n'était pas aussi importante que dans le cas de l'argile. Dans les essais CNS sur l'interface argile-structure, le sol exposé à des températures plus élevées, a montré moins de contraction pendant le cisaillement, et par conséquent moins de contrainte normale a diminué en raison de l'état plus dense des échantillons de structure argileuse chauffés avant le cisaillement. Par conséquent, dans l'interface, le sol devient plus dense

avec le chauffage et la résistance au cisaillement augmente légèrement.

Après avoir réalisé la partie monotone, le comportement mécanique cyclique de l'interface a été étudié. Le concept d'équivalent de volume constant non drainé a été utilisé dans les essais cycliques. Des essais cycliques unidirectionnels d'interface argile-structure à différentes températures avec différents rapports de contraintes cycliques et moyennes ont été effectués. Dans les essais CVEU monotones, le comportement en cisaillement de la structure argileuse était différent de celui de l'argile. L'angle de friction plus faible de la structure argileuse par rapport à l'argile et la différence de comportement en cisaillement ont confirmé que le cisaillement s'est produit dans la zone d'interface. Les résultats ont clairement montré la différence entre les tests cycliques d'interface argile-argile et argile-structure. Le nombre de cycles jusqu'à la rupture pour l'essai de la structure argileuse était inférieur à celui de l'argile. Dans le comportement cyclique de l'interface, la diminution du rapport de contrainte cyclique a augmenté le nombre de cycles jusqu'à la rupture et a diminué la pression de pores équivalente. L'augmentation de la température de 22 à 60 ^{o}C a également augmenté considérablement le nombre de cycles jusqu'à la rupture. Pour les essais cycliques d'interface argile-structure, presque pour tous les essais, après chauffage, la contrainte de cisaillement et la pression de pores équivalente correspondent au premier cycle diminué. Le chauffage drainé a induit une consolidation du kaolin. Cette densification est apparue comme pouvant expliquer le nombre supérieur de cycle jusquà la rupture pour la température d'essais la plus grande. L'augmentation de température réduit le taux de dégradation. La réduction de la contrainte de cisaillement moyenne a diminué le nombre de cycles pour atteindre la rupture. Les échantillons sont appliqués à des contraintes de cisaillement négatives plus élevées et donc, la résistance aux cycles est réduite. Enfin, le kaolin normalement consolidé soumis aux contraintes cycliques de cette étude par chauffage de 22 à 60 ^{o}C, montre un nombre plus élevé de cycles jusqu'à la rupture.

Sur la base des résultats expérimentaux obtenus pour la partie monotone et cyclique, la nécessité de proposer un modèle constitutif d'interface non isotherme a été observée. C'est pourquoi, dans la troisième partie de l'étude, un modèle non isotherme qui était une extension d'un modèle constitutif pour l'interface sol-structure granulaire dans des conditions isothermes a été développé. En raison de l'effet direct de la température sur l'indice des vides, le modèle a été développé sur la base de la théorie de l'état critique. En raison de la réponse mécanique indépendante de la température de l'interface sable-structure, les paramètres du modèle pour les essais de l'interface sable-structure ont été calibrés pour des conditions isothermes.

6.7 Perspectives

Pour des études plus approfondies sur le comportement thermo-mécanique des interfaces sol-structure, plusieurs aspects pourraient être abordés. En ce qui concerne le comportement monotone de l'interface argile-structure, il y a un manque de données expérimentales sur l'interface argile-structure surconsolidée à différentes températures. Cet aspect pourrait compléter les données disponibles sur le comportement de l'interface argile-structure dans des conditions non isothermes. Concernant les modes de cisaillement complexes qui existent au contact argile-structure, l'utilisation de technologies dobservation telles que la tomographie à rayons X ou la corrélation d'images pourrait permettre didentifier le mécanisme de cisaillement à l'interface, et sur l'effet de la température. Le comportement cyclique des essais d'interface argile-structure surconsolidée à différentes températures peut donner une vision dans le comportement cyclique de l'interface argile-structure dans des conditions non isothermes. Les effets cycliques des températures sur l'interface sol-structure peuvent être étudiés de manière plus approfondie. En ce qui concerne la modélisation non isotherme des interfaces, la fourniture de données expérimentales sur les sols surconsolidés peut être utilisée pour l'étalonnage ultérieur du modèle. Proposer des modèles d'interface non isothermiques pour les charges thermomécaniques cycliques peut être un sujet d'étude intéressant.